



UNIVERSITY OF
BIRMINGHAM

**Investigating the links between meiotic
chromosome structure and homologous
recombination in *Arabidopsis thaliana***

By

ALLAN WEST

A thesis submitted to
The University of Birmingham
for the degree of
DOCTOR OF PHILOSOPHY

School of Biosciences
University of Birmingham
September 2015

UNIVERSITY OF
BIRMINGHAM

University of Birmingham Research Archive

e-theses repository

This unpublished thesis/dissertation is copyright of the author and/or third parties. The intellectual property rights of the author or third parties in respect of this work are as defined by The Copyright Designs and Patents Act 1988 or as modified by any successor legislation.

Any use made of information contained in this thesis/dissertation must be in accordance with that legislation and must be properly acknowledged. Further distribution or reproduction in any format is prohibited without the permission of the copyright holder.

Abstract

Accurate chromosome segregation during meiosis requires the reciprocal exchange of DNA between homologous chromosomes, via a process called homologous recombination, resulting in the formation of crossovers (COs). This process begins with the formation of programmed DNA double-strand breaks (DSBs). Certain genomic loci, called hotspots, are more likely than others to produce DSBs. This is thought to be determined by various factors, which include post-translational histone modifications, such as H3K4 trimethylation. The histone methyl-transferase AtSDG2 is largely responsible for the deposition of this histone mark. This research shows that CO frequency and distribution are altered in an *Atsdg2* background.

Study of a mutant allele of a gene which codes for a subunit of a histone-acetyl transferase complex, called AtMRG2, revealed a strongly reduced fertility phenotype and failure to produce DSBs. Further study revealed that the defects were due to mutation to the *AtPRD3* gene, known to be essential for DSB formation, and that the mutation to *AtMRG2* was not responsible.

During meiosis, homologous recombination takes place in the context of specific structural arrangement of DNA organised as an array of loops emanating out from a proteinaceous axis, a major component of which is AtASY1. My studies demonstrate that the dynamics of AtASY1 are affected by mutation to AtPCH2, an AAA+ ATPase, and that formation of the synaptonemal complex is perturbed. *Atpch2* mutants initiate DSB formation and CO designation normally, but defects occur in CO maturation, causing a reduced CO frequency and formation of univalent chromosomes at metaphase I.

Finally, the effects of temperature on the structure of meiotic chromosomes and homologous recombination were studied by cytological analysis of Col o and different meiotic mutants subjected to a range of temperatures for the duration of meiosis. I have demonstrated that certain mutations, such as *Atsdg2* and *Atpch2*, confer some resistance to the effects of high (32°C) temperature treatment, which causes various meiotic defects in Col o.

Acknowledgements

I would like to thank my supervisor Chris Franklin for providing me with the opportunity to work on the project and for his support and advice throughout my PhD and undergraduate studies.

I would also like to thank for Eugenio Sanchez-Moran, Kim Osman, James Higgins, Elaine Howell, Stephan Heckmann and Maria Cuacos for their guidance and support, Sue Armstrong for her help with interpreting cytological data and all other members of the Franklin and Franklin-Tong laboratories for their kindness.

I am grateful to Ruth Perry, Steve Price and Lisa Burke for technical assistance and to Karen Staples and Andy Breckles for horticultural expertise. Funding for the project was provided by the Biotechnological and Biological Sciences Research Council (BBSRC).

I would also like to thank my family and friends for all their support.

List of contents

1.1 Overview of meiosis	2
1.2 Overview of chromatin structure.....	8
1.2.1 Histone proteins.....	9
1.2.2 Histone variants	11
1.2.3 Post-translational histone modifications	14
1.3 Meiotic chromosome structure	16
1.3.1. The role of the meiotic axis in imposing homolog bias in DSB repair.....	16
1.3.2 The synaptonemal complex	18
1.3.3. Dynamic organisation of meiotic chromosome components.....	19
1.3.4 Meiotic chromosome cohesion	21
1.4 Homologous recombination.....	23
1.4.1 DSB formation	23
1.4.2 DSB processing.....	24
1.4.3 DNA Strand exchange	26
1.4.4 DSB repair via the non-crossover pathway: Synthesis dependent strand annealing and inter-sister recombination	30
1.4.5 Gene conversion resulting from SDSA	31
1.4.6 Non-homologous end-joining	32
1.4.7 Double Holliday junction formation	32
1.4.8 Crossover resolution – Interfering and non-interfering crossovers	35
1.5 CO Control	38
1.5.1 CO/NCO Decision	38
1.5.2 CO Assurance	39
1.5.3 CO Interference.....	39
1.5.4 CO Homeostasis	42
1.5.5 DSB and CO localisation	42
1.6 Research aims	45
2.1 Plant material.....	48
2.2 Genotyping of <i>Arabidopsis</i> T-DNA insertion mutants.....	48
2.3 Genetic crosses of <i>Arabidopsis</i> lines	48
2.4 DAPI staining of acid-fixed meiocytes.....	49

2.5 Immunolocalisation on acid-fixed material ('Microwave technique')	50
2.6 Spreading immunolocalisation of fresh material and cytological analysis of PMCs	51
2.7 Fluorescence In-Situ Hybridisation (FISH) labelling of meiotic chromosomes	53
2.8 EdU timecourse	54
2.9 Fluorescent tetrad analysis	55
2.10 Temperature experiment	56
2.11 ASY1 immunostaining intensity quantification	57
2.12 RT-PCR	57
2.13 Statistical procedures	58
3.1 Introduction	60
3.2 Results	64
3.2.1 AtSDG2 is required for fertility but is dispensable for meiotic recombination	64
3.2.2 Transcription of <i>AtSDG2</i> and gene expression in an <i>Atsdg2-1</i> background	70
3.2.3 <i>Atsdg2-1</i> PMCs show reduced levels of H3K4Me3	73
3.2.4 Early recombination, axis structure and synaptonemal complex morphogenesis appear unaffected by the <i>Atsdg2-1</i> mutation	75
3.2.5 Crossover numbers are increased in <i>Atsdg2-1</i> compared to Col 0	79
3.2.6 Crossover distribution is altered in <i>Atsdg2-1</i>	82
3.2.7 The increased CO frequency in <i>Atsdg2-1</i> is not due to an increase in class II COs	86
3.2.8 <i>Atsdg2-1</i> PMCs are not defective in H3K56Ac deposition	89
3.2.9 SDG proteins in ASY1 pulldown data	89
3.2.10 SC length is unchanged in <i>Atsdg2-1</i>	89
3.3 Discussion	91
3.3.1 An increased CO frequency in <i>Atsdg2-1</i>	91
3.3.2 Reduced interference in <i>Atsdg2-1</i>	95
3.3.3 Potential meiotic involvement of other SET domain proteins	96
3.3.4 Altered gene regulation in <i>Atsdg2-1</i>	97
3.3.5 A possible DSB repair defect in <i>Atsdg2-1</i>	98
3.3.6 SC length is not significantly different in <i>Atsdg2-1</i>	98
4.1 Introduction	101
4.2 Results	104
4.2.1 Fertility is reduced in <i>Atmrg2-1</i> compared to Col 0	104
4.2.2 <i>Atmrg2-1</i> is defective in CO formation and is asynaptic	107
4.2.3 The recombination defect in <i>mrg2-1</i> is due to a lack of programmed DSBs	114

4.2.4	Loss of AtMRG2 is unlikely to be the cause of the <i>Atmrg2-1</i> meiotic phenotype.....	116
4.2.5	The <i>Atmrg2-1</i> phenotype is likely caused by disruption to <i>AtPRD3</i>	118
4.3	Discussion.....	121
4.3.1	<i>Atmrg2-1</i> mutants show meiotic defects which result from mutation to <i>AtPRD3</i>	121
4.3.2	The meiotic role of <i>AtPRD3</i>	124
4.3.3	The function of AtMRG1/AtMRG2	125
5.1	Introduction	127
5.2	Results	131
5.2.1	<i>Atpch2</i> mutants display reduced fertility.....	131
5.2.2	Crossover formation is defective in <i>Atpch2-1</i>	135
5.2.3	CO patterning is affected by the <i>Atpch2-1</i> mutation.....	140
5.2.4	Chromosomes axis remodelling is defective in <i>Atpch2-1</i>	143
5.2.5	AtPCH2 is required for normal loading of ASY1 onto meiotic chromosomes	147
5.2.6	Meiotic progression in <i>Atpch2-1</i> is delayed	148
5.3	Discussion.....	150
5.3.1	AtPCH2 is required for normal ASY1 dynamics during prophase I	150
5.3.2	AtPCH2 is dispensable for the early stages of recombination and DSB repair	151
5.3.3	CO interference is established in <i>Atpch2-1</i> prior to a CO maturation defect.....	152
5.3.4	Synapsis initiates uni-directionally in <i>Arabidopsis</i>	153
6.1	Introduction.....	156
6.2	Results	161
6.2.1	Col 0	162
6.2.2	<i>Atcdkg</i>	169
6.2.3	<i>Atpch2-1</i>	170
6.2.4	<i>Atsdg2-1</i>	171
6.2.5	<i>Atrbr-2</i>	172
6.3	Discussion.....	179
6.3.1	Synapsis is defective following growth at 32°C.....	179
6.3.2	ASY1 aggregates visible after 32°C treatment	180
6.3.3	<i>Atsdg2-1</i> and <i>Atpch2-1</i> display increased resistance to temperature induced defects.....	183
6.3.4	Temperature induced effects on <i>Atrbr-2</i>	185
7.1	Discussion	187
7.1.1	<i>Atsdg2-1</i> and <i>Atpch2-1</i> meiosis at high temperature.....	187
7.1.2	Future perspectives	189

References	192
Appendix A – FTL analysis raw data	223
Appendix B – ASY1 intensity analysis in Col 0 and <i>Atpch2-1</i> PMCs	224
Appendix C – Cytological atlases of meiosis following temperature treatments.....	228
Appendix D - Primer list	238
Appendix E - FTL interval locations	238
List of publications and presentations.....	239

List of Figures and Tables

Figure 1.1: Overview of <i>Arabidopsis</i> meiosis.....	6
Figure 1.2: Schematic representation of meiotic DSB repair by homologous recombination.....	7
Figure 1.3: Meiotic chromosome structure between leptotene and pachytene.....	8
Figure 1.4: Nucleosome core particle structure.....	10
Figure 1.5: Tethered-loop axis model of DSB formation.....	45
Figure 3.1: Photograph of the <i>Atsdg2-1</i> phenotype.....	66
Figure 3.2: <i>AtSDG2</i> gene schematic showing T-DNA insertions within the two <i>Atsdg2</i> mutants	66
Figure 3.3: Genotyping of <i>Atsdg2-1</i> and <i>Atsdg2-3</i>	66
Figure 3.4: Meiotic atlas of Col 0 and <i>Atsdg2-1</i>	68
Figure 3.5 A: Metaphase I chromosomes in <i>Atsdg2-1</i>	69
Figure 3.5 B: Enlargements of <i>Atsdg2-1</i> bivalents.....	69
Figure 3.5 C: Chiasma frequency in Col 0 and <i>Atsdg2-1</i>	69.
Table 3.1: Summary of RNAseq analysis of SET-domain group genes in <i>Arabidopsis</i>	72
Figure 3.6: Immunolocalisation of ASY1 and H3K4Me3 in Col 0 and <i>Atsdg2-1</i>	74
Figure 3.7: Mean intensity of H3K4Me3 signal in Col 0 and <i>Atsdg2-1</i> PMC nuclei.....	74
Figure 3.8: Immunolocalisation of ASY1 and ZYP1 in Col 0 and <i>Atsdg2-1</i> using SIM.....	76

Figure 3.9: Immunolocalisation of ASY1 and SMC3 in Col o and <i>Atsdg2-1</i>	76
Figure 3.10: Immunolocalisation of ASY1 and RAD51 in Col o and <i>Atsdg2-1</i>	78
Figure 3.11: Immunolocalisation of ASY1 and DMC1 in Col o and <i>Atsdg2-1</i>	78
Figure 3.12: Immunolocalisation of ASY1 and MSH4 in Col o and <i>Atsdg2-1</i>	80
Figure 3.13: Immunolocalisation of ZYP1 and MLH3 in Col o and <i>Atsdg2-1</i>	80
Figure 3.14: Immunolocalisation of ASY1 and HEI10 in Col o and <i>Atsdg2-1</i>	81
Figure 3.15: Cartoon describing FTL analysis.....	84
Figure 3.16: Genetic distance of FTL intervals in Col o and <i>Atsg2-1</i>	85
Table 3.2: Crossover interference ratios of FTL intervals in Col o and <i>Atsdg2-1</i>	85
Figure 3.17: (Top) FISH of 5s and 45s probes in Col o, <i>Atsdg2-1</i> and <i>Atsdg2-1;Atmsh5</i> metaphase I chromosomes. (Bottom) Mean chiasma per PMC.....	87
Figure 3.18: Immunolocalisation of ZYP1 and MUS81 in Col o and <i>Atsdg2-1</i>	88
Figure 3.19: Immunolocalisation of ASY1 and H3K56Ac in Col o and <i>Atsdg2-1</i>	88
Figure 3.20: Mean SC length in Col o and <i>Atsdg2-1</i> pachytene PMCs.....	90
Figure 4.1: Schematic of AtMRG2 and T-DNA insertion sites of <i>Atmrg2-1</i> and <i>Atmrg2-4</i>	106
Figure 4.2: RT-PCR of <i>AtMRG2</i> in Col o and <i>Atmrg2-1</i>	106
Figure 4.3 A: Photograph of <i>Atmrg2-1</i> phenotype compared to Col o.....	106
Figure 4.3 B: Mean silique length in Col o and <i>Atmrg2-1</i>	106
Figure 4.3 C: Mean seeds per silique in Col o and <i>Atmrg2-1</i>	106
Figure 4.4: Meiotic atlas of prophase I in Col o and <i>Atmrg2-1</i>	109
Figure 4.5: Meiotic atlas of post-prophase I in Col o and <i>Atmrg2-1</i>	110
Figure 4.6: FISH of 5s and 45s probes in Col o and <i>Atmrg2-1</i> metaphase I chromosomes.....	111
Figure 4.7: Immunolocalisation of ASY1 and ZYP1 in Col o and <i>Atmrg2-1</i>	112
Figure 4.8: Immunolocalisation of ASY1 and RAD51 in Col o, <i>Atmrg2-1</i> and <i>Atspo11-1-4</i> PMCs.....	113
Figure 4.9: Metaphase I chromosomes in <i>Atmre11</i> and <i>Atmre11;Atmrg2-1</i> , and <i>Atrad51</i> and <i>Atrad51;Atmrg2-1</i>	115
Figure 4.10: Meiotic atlas at <i>Atmrg2-4</i>	117

Figure 4.11: RT-PCR of <i>AtMRG2</i> from Col o and <i>Atmrg2-4</i>	117
Figure 4.12: Immunolocalisation of ASY1 and PRD3 in Col o and <i>Atmrg2-1</i>	120
Figure 4.13: PCR of <i>AtPRD3</i> from Col o and <i>Atmrg2-1</i> DNA.....	120
Figure 4.14: Metaphase I chromosomes in <i>Atspo11-14</i>	123
Figure 5.1: Schematic of AtPCH2 and T-DNA insertion sites of <i>Atpch2-1</i> , <i>Atpch2-1</i> and <i>Atpch2-3</i>	133
Figure 5.2: Photograph of <i>Atpch2-1</i> phenotype compared to Col o.....	133
Figure 5.3: Photographs of siliques from <i>Atpch2</i> mutants compared to Col o.....	133
Figure 5.4: RT-PCR of <i>AtPCH2</i> in <i>Atpch2</i> mutants and Col o.....	134
Figure 5.5: Pollen viability in Col o and <i>Atpch2-1</i> determined by Alexander staining..	134
Figure 5.6: Meiotic atlas of Col o compared to <i>Atpch2-1</i>	137
Figure 5.7: Immunolocalisation of ASY1 and RAD51 in Col o and <i>Atpch2-1</i>	138
Figure 5.8: Immunolocalisation of HEI10 and ZYP1 in Col o and <i>Atpch2-1</i>	139
Figure 5.9: Immunolocalisation of MSH4 and ZYP1 in Col o and <i>Atpch2-1</i>	139
Figure 5.10: Genetic distance of FTL intervals in Col o and <i>Atpch2-1</i>	142
Table 5.1: Crossover interference ratios of FTL intervals in Col o and <i>Atpch2-1</i>	142
Figure 5.11: Immunolocalisation of ASY1 and ZYP1 in Col o and <i>Atpch2-1</i>	145
Figure 5.12: Immunolocalisation to determine ASY1 signal intensity in Col o and <i>Atpch2-1</i>	146
Table 5.2: EdU timecourse of prophase I progression in Col o and <i>Atpch2-1</i>	149
Figure 5.13: EdU labelled PMCs from Col o and <i>Atpch2-1</i> at 32 and 36 hours post-S-phase.....	149
Figure 6.1: Meiotic atlas of Col o PMCs after 20 °C treatment.....	164
Figure 6.2A: Immunolocalisation of ASY1 and ZYP1 in Col o and <i>Atsdg2-1</i> following 20 °C treatment.....	165
Figure 6.2B: Immunolocalisation of ASY1 and ZYP1 in Col o and <i>Atsdg2-1</i> following 32 °C treatment	166
Table 6.1: Summary of temperature induced defects in different genetic backgrounds..	174
Figure 6.3: Synapsed chromosomes in Col o, <i>Atsdg2-1</i> and <i>Atcdkg</i> following treatment at 20, 30 and 32 °C.....	175

Figure 6.4: Metaphase I chromosomes in Col o, <i>Atpch2-1</i> , <i>Atsdg2-1</i> , <i>Atrbr-2</i> and <i>Atcdkg</i> following treatment at 20 and 32°C	176
Figure 6.5: Tetrad PMCs in Col o, <i>Atpch2-1</i> , <i>Atsdg2-1</i> , <i>Atrbr-2</i> and <i>Atcdkg</i> following treatment at 20 and 32°C.....	177
Figure 6.6: Immunolocalisation of ASY1 and ZYP1 in Col o following 32°C treatment.....	178

Chapter 1

Introduction

1.1 Overview of meiosis

Meiosis is the specialized process of cell division responsible for the production of gametes in sexually reproducing organisms (Reviewed for *Arabidopsis* in Osman et al., 2011). Meiosis is distinct from mitosis, as the products of meiosis are not genetically identical. Also unlike mitosis, meiosis is not a cell cycle; the meiotic products are terminally differentiated and will not undergo another round of meiosis. Meiotic cells undergo a single round of DNA replication followed by two rounds of nuclear division, ultimately resulting in four haploid products, all of which are genetically distinct (Figure 1.1). These cells are (or will differentiate into) gametes, which can then fuse with another gamete, combining their two haploid genomes to produce a zygote with a diploid genome. Problems during meiotic divisions can lead to inaccurate segregation of chromosomes, causing aneuploidy (aberrant chromosome numbers) in the gametes. Estimates of aneuploidy rates in human oocytes range from 10% to 60%, the true figure being unknown due to the spontaneous abortion of most aneuploid pregnancies before they reach term (reviewed in Jones, 2008). In humans, aneuploidy causing trisomy of chromosome 21, which still produces viable embryos, leads to Down's syndrome. Other human aneuploid diseases include Edward's syndrome (trisomy 18), Patau syndrome (trisomy 13) and Turner's syndrome (one X chromosome but missing Y). One application of the study of meiosis in plants is focussed on increasing (or redistributing) the associated genetic recombination that takes place, in order to improve plant breeding strategies. These are becoming increasingly important in terms of food security in the light of global population growth, climate change, pest species and crop diseases which continue to cause problems to agriculture, and drought (Baulcombe et al., 2009).

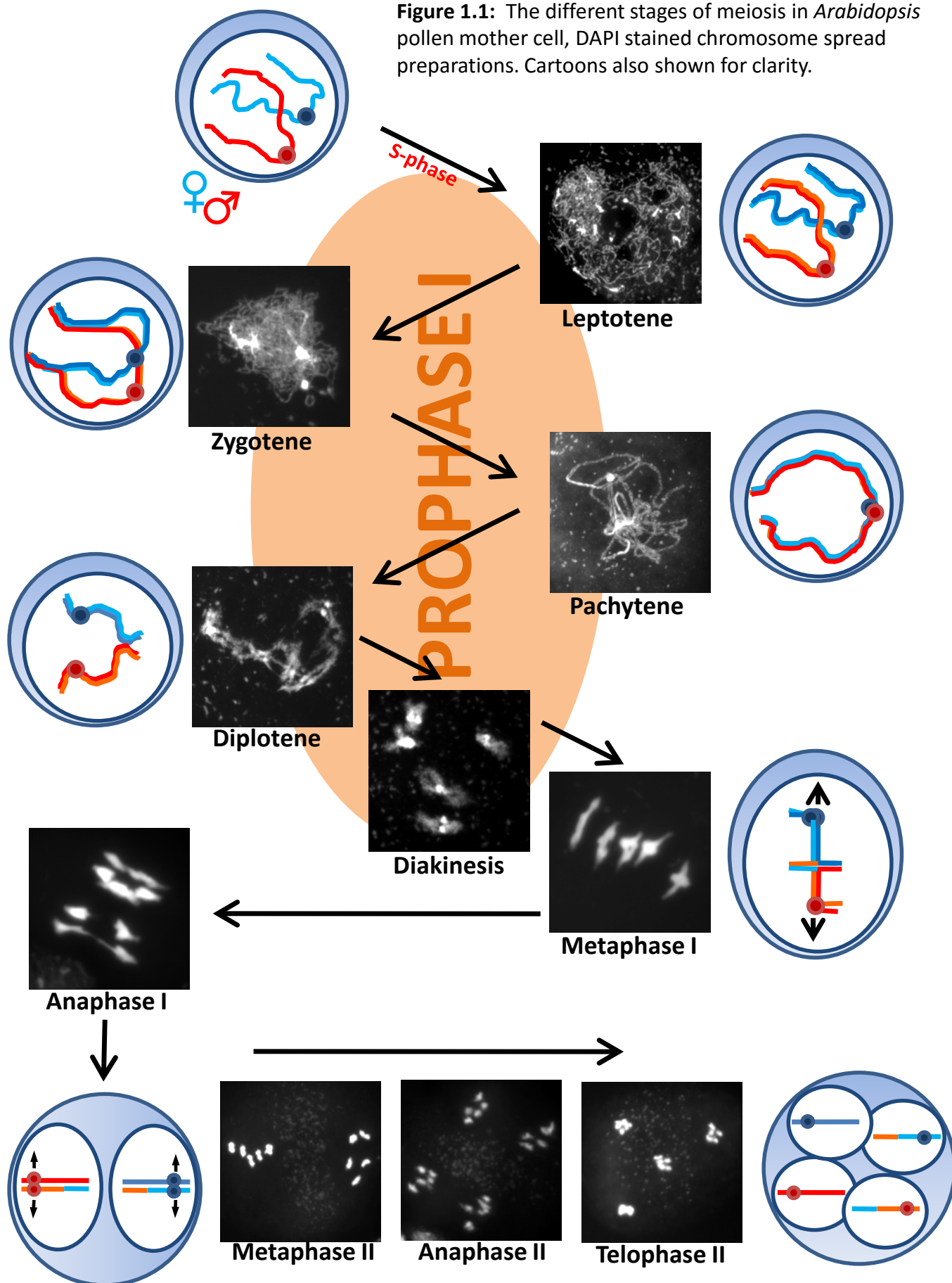
Compared to mitosis, chromosome segregation during meiosis is strikingly different and more complex (reviewed in Zamariola et al., 2014). In mitosis, sister chromatids separate during anaphase (Figure 1.1) and are pulled to opposite poles by spindle fibres. Each cell therefore receives an identical copy of the genome. Accurate and equal segregation of the chromatids is ensured by a cell cycle checkpoint which blocks the onset of anaphase until free kinetochores (found at the centromeres) are bound to the mitotic spindle. The physical tension of these associations ensures that chromosomes align correctly during metaphase. Unlike in mitosis, chromatids in meiotic cells do not separate from their sister in the first round of division. Instead, the two sister chromatids are drawn to the same pole, while the two sister chromatids of the homologous chromosome (originating from the other parent) go to the opposite pole. This is achieved via monopolar kinetochore attachment to the spindle and maintenance of centromere cohesion between sister chromatids. In contrast, mitotic chromosomes, and chromosomes in the second round of meiotic nuclear division, would demonstrate bipolar attachment and a breakdown in cohesion between centromeres. To ensure accurate segregation in the first meiotic division, tension is generated via an alternative mechanism by connections that form between homologous chromosomes during prophase I of meiosis. These connections are called **chiasmata** which are the cytologically visible manifestation of reciprocal exchange between DNA strands of homologous chromosomes, called **homologous recombination**. The genetic products of these exchanges are known as **crossovers** (COs) (Figure 1.2). For segregation to be accurate, at least one CO is required per chromosome, called the obligate CO or obligate chiasma. COs are also responsible for the genetic differences between the haploid products, beyond the random segregation of maternal and paternal chromosomes.

Prophase I is the most time consuming stage of meiosis, during which homologous chromosomes must align themselves with each other and undergo homologous recombination to produce COs. This alignment is achieved with remarkable accuracy despite the genome size, which could be billions of base-pairs long and may contain repetitive sequences throughout. This homology search takes place within a nucleus only ~10µm in diameter, which in humans would be the spatial equivalent of 40km of fine thread packed into a tennis ball (Alberts et al., 2008). The specific mechanisms of this alignment and homology search vary between species (Reviewed in Naranjo, 2012).

Prophase I is divided into five sub-stages (Figure 1.1). In **leptotene** (Greek; *thin threads*) the chromatin associates with a long proteinaceous structure called the **axis**. The chromatin forms looped arrays and joins to the axis at their bases (Figure 1.3). In **zygotene** (*paired threads*), the axes begin to juxtapose with their homologous partners, starting at the telomeres and extending towards the centromere. As they juxtapose, a transverse element protein polymerises between the two axes (Figure 1.3). This process is called **synapsis**. The completion of synapsis along the whole length of each chromosome denotes the onset of **pachytene** (*thick threads*). The proteinaceous structure is called the **synaptonemal complex**, which is tripartite, consisting of the transverse elements, flanked by the two axes, now known as lateral elements. During **diplotene** (*two threads*), the lateral elements dissociate and the two axes separate again, except at the sites of crossover formation. In the final sub-stage of prophase I, **diakinesis** (*moving through*), the chromosomes condense, as bivalents (pairs of homologous chromosomes, held together by chiasmata). The points of crossover are cytologically visible as connections between the homologues (chiasmata). The formation of a crossover in a given locus reduces the likelihood of a crossover forming

in the immediate vicinity, with the chances of another crossover forming increasing with distance from the first. This phenomenon is called **crossover interference**, and like the homology search is still not fully understood (Jones and Franklin, 2006). A separate property of CO formation is **CO localisation**, which in crop cereals such as barley, causes crossovers to form preferentially in the centromere distal regions of the chromosomes, leaving much of the genome untouched by recombination and limiting the amount of variation that can be achieved by crop breeders using traditional crop breeding strategies.

Figure 1.1: The different stages of meiosis in *Arabidopsis* pollen mother cell, DAPI stained chromosome spread preparations. Cartoons also shown for clarity.



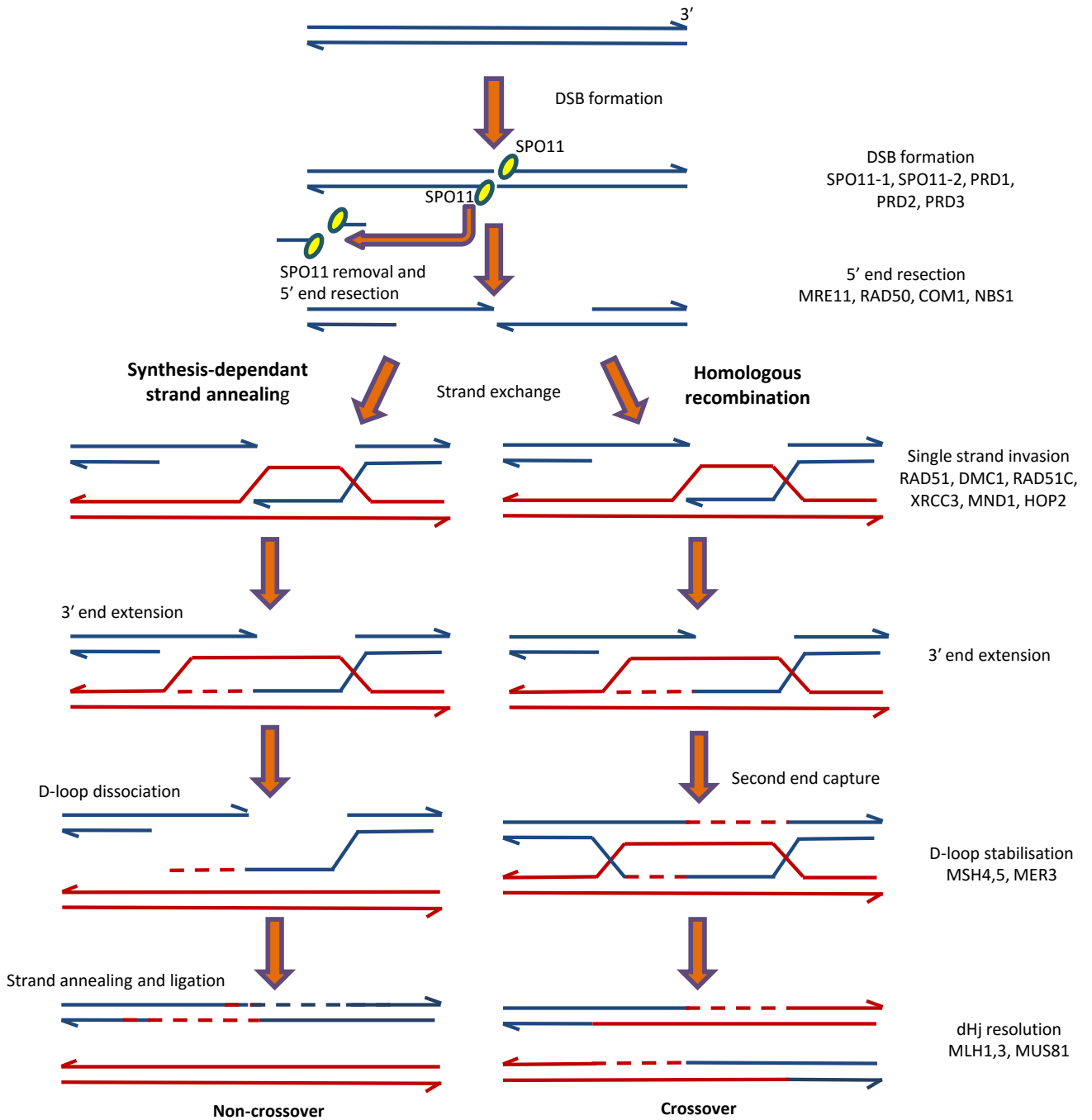


Figure 1.2: Schematic representation of meiotic DSB repair by homologous recombination in *Arabidopsis*.
Based on Osman et al, 2011.

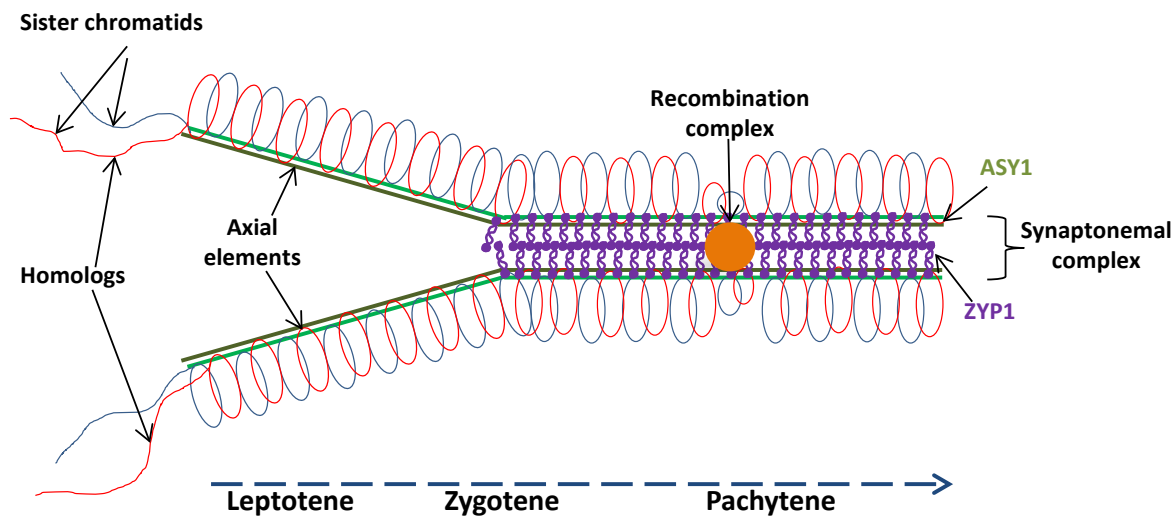


Figure 1.3: Meiotic chromosome structure between leptotene and pachytene. Chromosomes are arranged as looped arrays joined at the loop bases to the proteinaceous axis. The two axes of homologous chromosomes synapse together during zygotene as ZYP1 polymerises between them. Based on Osman et al, 2011.

1.2 Overview of chromatin structure

The whole process of meiotic recombination must be considered not only in terms of the proteins directly involved, but also in terms of chromatin and epi-genetic modifications. Chromatin refers not only to the DNA, but also the proteins with which it associates to achieve a more compact and organised state. This organisation is required in order to keep the right genes accessible or inaccessible for transcription at the correct time and facilitate the level of condensation required for chromosome segregation during mitosis and meiosis. At the most basic level of compaction, DNA wraps around octamers of proteins called histones, to form nucleosome core particles (NCPs)(Figure 1.4)(Luger et al., 1997), first observed with

electron microscopy as a 10nm wide structure resembling 'beads on a string' (Olins and Olins, 1974).

1.2.1 Histone proteins

Each nucleosome consists of an octameric protein complex made up of four pairs of histone proteins; H2A, H2B, H3 and H4. These are approximately 100-140 amino acids long and are known as the core histones. The histone fold domain is common to all four of these proteins, made up of 3 α -helices linked by two β segments (Luger et al, 1997). A fifth histone, called H1, is not included in the octamers and is located between nucleosomes, acting as a 'linker histone' and aiding in the structural organisation of the chromatin (Kasinsky et al., 2001). H1 histones are slightly larger than the core histones, and are ~200-400 amino acids long (Cheema and Ausió, 2015).

The composition of these proteins is rich in basic amino acids, such as lysine and arginine, giving histones an overall positive charge, aiding their strong association with DNA, which being acidic, carries a negative charge. DNA is wrapped around the histone octamers. ~147bp of DNA is wrapped 1.65 times around each octamer, in a left handed superhelical turns (reviewed in Cutter & Hayes, 2015). Particular DNA elements bind to the core histones more strongly than others, such as at AT-rich sequences. These sequences allow greater compression of the minor groove of the double-helix, which increases the binding affinity between the DNA and arginine residues (Rohs et al., 2009). The arrangement of DNA around histone octamers is thought to have an inhibitory effect against DNA binding proteins by physically occluding access to their target DNA sequences, enabling regulatory processes such as transcription, replication and damage repair to proceed uninhibited (Knezetic and Luse, 1986; Lorch et al., 1987; Li and Widom, 2004).

During S-phase, demand for histone proteins is high to support the replicating genome. Histone genes often do not contain introns, and are not poly-adenylated, possibly to minimize post-transcriptional processing and allow rapid translation into proteins (Marzluff et al., 2009).

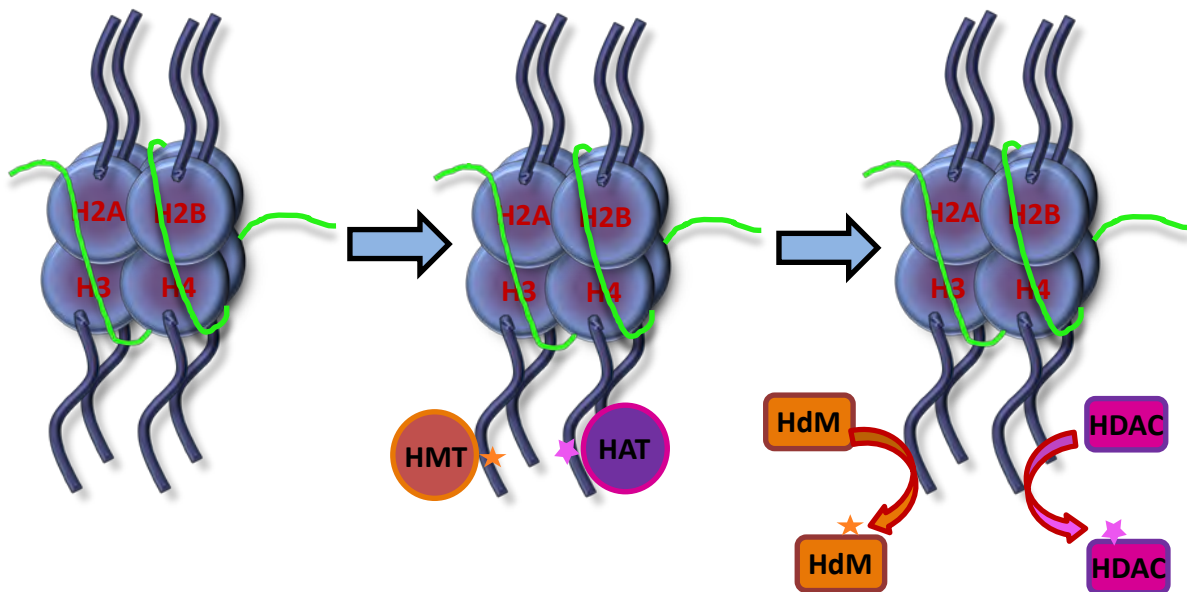


Figure 1.4: Nucleosome core particle structure. These consist of octamers of histones H2A, H2B, H3 and H4. DNA (green) wraps around the nucleosome. The N-terminal tails which protrude from the centre of the octamer are subject to various post-translational modifications. Lysine residues in the tail regions can be methylated by histone methyltransferases (HMTs) or acetylated by histone acetyltransferases (HATs). The modifications can be removed by histone de-methylases (HdMs) and histone deacetylases (HDACs).

The N-terminal domains of the core histones (C-terminal domain for H2A) constitute ~25-30% of their mass and protrude outward from the globular portion of the protein. These tail domains are intrinsically disordered compared to the more structured, globular part of the protein, and are sensitive to proteases and adopt random conformations when not associated with DNA or when free in solution (Cutter and

Hayes, 2015). Histone tail regions are rich in arginine and lysine residues which are subject to a range of post-translational modifications to produce recognition sites for various proteins (Figure 1.4). These modifications, which include methylation and acetylation of lysine residues, can also influence the organisation of the higher-order structure of chromatin, by altering the strength of DNA-histone and histone-histone interactions (discussed below) (Tessarz and Kouzarides, 2014).

The compaction of chromatin is also heavily influenced by a highly diverse family of non-histone proteins called chromatin architectural proteins (Luger and Hansen, 2005). The exact nature of the higher order structure of chromatin, into which the nucleosomes are arranged, is still an area of hot debate. The higher order structure was for a long time described to be a 30nm fibre, which could be arranged in a number of different conformations, but this is increasingly being thought of as an oversimplification of a highly dynamic structure (Woodcock and Ghosh, 2010; Ausió, 2015; Bian and Belmont, 2012). At the nucleus level of chromatin organisation, the genome is arranged into regions of highly condensed **heterochromatin**, which is usually transcriptionally repressed and located at the nuclear periphery, and **euchromatin**, which is more evenly dispersed within the nucleus and is associated with more transcriptionally active regions (Woodcock and Ghosh, 2010).

1.2.2 Histone variants

The genes coding for the histones described so far, often exist as multiple copies within the genome. The histone proteins H2A, H2B, H3 and H4 are therefore better described as protein families, existing in major (canonical) and minor variants. The minor variants are more structurally distinct from the relatively invariant canonical histones,

exhibiting divergence in their tail and histone fold domains and often serving specific functions within the chromatin (reviewed in Cheema & Ausi , 2015). As already mentioned, high expression of the canonical histones is required to support the newly synthesised DNA during S-phase, and this is the only time during the cell cycle when these genes are expressed. In contrast to this, the variant histones can be expressed at any time within the cell cycle, being temporally regulated subject to the requirements of specific cell types or in response to environmental stimuli (Woodcock and Ghosh, 2010; Cheema and Ausi , 2015; Talbert and Henikoff, 2014). In some single celled eukaryotes, the ‘minor variants’ may be the major, or the only histones of a particular histone family (Talbert and Henikoff, 2010). The variant histones have a diverse range of functions including roles in DNA repair (including during meiotic recombination), transcriptional regulation and chromosome segregation.

In *Arabidopsis* there are 13 paralogs of the canonical *H2A* gene for example, H2A 1 - H2A 13, which together would make up the majority of H2A protein within the chromatin (Talbert et al., 2012). These 13 genes also include minor variants of H2A, called H2A.X and H2A.Z, both of which have roles in DNA damage response. In humans the proportion of the H2A complement made up of these variants is highly variable, with H2A.X making up between 2 and 25% of total H2A, depending on cell type, though the reasons for this variability are not clear (Rogakou et al., 1998). H2A.X is subject to a post-translational modification; phosphorylation of a serine residue near the C-terminus, by ATM, ATR and DNA-PK kinases. H2A.X histones with this modification are known as γ H2A.X and have a well characterised involvement in DNA damage signalling in humans (reviewed in Bonner et al., 2008), plants (Lang et al., 2012). Anti- γ H2AX antibodies can be used for the immunolocalisation of DNA

damage sites, which is useful in the study of DSB repair mechanisms, DNA damaging agents, meiosis and telomere integrity (Mahadevaiah et al., 2001).

In both yeast and humans, H2A.Z is found to be enriched near the nucleosome-free transcription start-site regions, and is thought to aid the recruitment of RNA-polymerase II (Talbert and Henikoff, 2010). In *Arabidopsis*, the presence of H2A.Z at promoter regions acts to prevent DNA methylation, an epigenetic modification associated with transcriptional repression, while deposition of H2A.Z is inhibited by DNA methylation, making the two marks antagonistic to each other (Zilberman et al., 2008). In both plants and animals, H2A.Z is thought to be locally removed from chromatin during gene transcription, but is re-deposited when transcription ends (Hardy et al., 2009; Deal et al., 2007). In human cells, unlike in plant cells, H2A.Z is enriched in regions of heterochromatin, possibly due to the lack of transcription taking place there (Hardy et al., 2009). A similar dynamic organisation of H2A.Z containing nucleosomes is seen during the DNA damage response. DNA repair requires the establishment of open/flexible chromatin, facilitated by the deposition of H2A.Z at the sites of DNA damage, but H2A.Z is also quickly removed from those sites to allow the formation of a post-translational histone modification (discussed below), H4 acetylation (Xu et al., 2012b; Gursoy-Yuzugullu et al., 2015). This modification is thought to promote the open chromatin conformation (Xu et al., 2012b). Blocking the removal of H2A.Z causes the chromatin to remain in a hypoacetylated state, and leads to an increase in repair by the error-prone non-homologous end-joining pathway (described later) (Gursoy-Yuzugullu et al., 2015). In *Arabidopsis*, the

deposition of H2A.Z at gene promoters is thought to influence the localisation of recombination hot-spots to these regions, with H2A.Z deposition-deficient mutants displaying reduced CO frequency (Choi et al., 2013).

1.2.3 Post-translational histone modifications

Histones, both canonical and variant, can be subject to post-translational modifications, such as phosphorylation and acetylation (mentioned above), and also methylation, sumoylation and ubiquitination. Some of these modifications, such as acetylation, may alter the net charge of the histone, which may either reduce or strengthen the binding affinity of the associated DNA (reviewed in Tessarz & Kouzarides, 2014). Alternatively, modifications may have a neutral effect on the charge of the histone, as is the case with the addition of methyl groups at lysine residues, and these modifications may instead produce a recognition site for other proteins (Jacobs and Khorasanizadeh, 2002).

Histone acetylation is a modification which unlike methylation, affects the net charge of histones, and is controlled by protein complexes called histone acetyl transferases (HATs), which add acetyl groups to histones, also at lysine residues, and histone de-acetylases (HDACs) which remove the groups (reviewed in de Ruijter et al., 2003). The addition of acetyl groups has a neutralizing effect on the positive charge of the histones, weakening DNAs binding affinity for them, and creating a more open and accessible region of chromatin (Lee et al., 1993). For this reason, DNA sequences being actively transcribed will usually be associated with hyper-acetylated histones. De-acetylation of histones has the reverse effect on DNA binding affinity, producing a more compact and inaccessible state. Hypo-acetylation of histones is more common in regions of heterochromatin.

Methylation of the lysine residues at positions 9 and 27 of histone 3 (H3K9Me/H3K27Me) are usually associated with transcriptionally silent regions of the genome, while methylation of histone H3 at residues 4, 36 and 79 are associated with areas of active transcription (reviewed in Kouzarides, 2007; Wozniak & Strahl, 2014). This is an oversimplification of the true situation though, as H3K9 methylation in mammals can be found at high levels in the coding regions of actively transcribed genes, but is also associated with transcriptional repression when found in gene promoter regions (Vakoc et al., 2005). The inverse of this situation appears to be true for H3K36 methylation (Landry et al., 2003). The level of methylation, mono, di or trimethylation, can produce different effects. In *Arabidopsis*, H3K4Me₂ appears to mark coding regions regardless of whether or not the gene is being transcribed so possibly acting as a marker of potential transcription (Alvarez-Venegas and Avramova, 2005). In *C. elegans*, histone lysine methylation has also been linked to alternative-splicing, as exons which are not destined to be spliced out of the transcript are specifically marked with the H3K36Me₃ modification (Kolasinska-zwierz et al., 2009).

The placement of histone variants and modifications can be maintained during S-phase and the division stages of mitosis and meiosis, making the information heritable across generations. Inheritance of information stored outside of the DNA sequence is called **epigenetic** inheritance. This was demonstrated in mice which were subjected to stress, causing methylation of cytosine bases at particular DNA sequences. Subsequent generations of mice carried the same profile of DNA methylation, regardless of whether they were subjected to the same stresses (Franklin et al., 2010). Similarly, in *Arabidopsis*, UV stress was shown to increase somatic homologous recombination at a reporter gene in treated plants, as well as in the untreated subsequent five generations (Molinier et al., 2006).

Histone variants, post-translational histone modifications and DNA methylation all have a role in dictating the localisation and control of CO formation during meiosis. In yeast, mammals and *Arabidopsis*, recombination hotspots often co-localise with sites of 'open chromatin' markers, such as H2A.Z and H3K4Me3 (Choi et al., 2013; Borde et al., 2009; Brick et al., 2012). These epigenetic effects on meiosis are discussed further in 'DSB and CO localisation' (section 1.5.5) and in Chapter 3.

1.3 Meiotic chromosome structure

1.3.1. The role of the meiotic axis in imposing homolog bias in DSB repair

During leptotene, homologous chromosomes are arranged on a linear, proteinaceous axis. The DNA is arranged on this axis as an array of loops, with an estimated size of around 20kb each, which are joined to the axis at their bases (Figure 1.3) (reviewed in Zickler & Kleckner, 1999; Kleckner, 2006). This organisation appears to be evolutionarily conserved between species, despite variability in loop length and density. These structural properties, together with sister chromatid cohesion (discussed below), keep sister chromatids in close proximity during the recombination process, but use of the homologous chromosome, rather than the sister chromatid, is favoured for use as a template during DSB repair during meiotic recombination. This 'homologue bias' is partly dependent on one of the axis associated proteins called ASY1 in *Arabidopsis*, homologous to Hop1 in yeast and HIM3 in mice (Caryl et al., 2000). ASY1 forms foci early in G2, which progress to form fully linear signals along the chromosome axes by leptotene (Sanchez-Moran et al., 2007). Linear signals of Hop1 are thought to consist of hyper abundant domains separated by regions of lower

abundance (Panizza et al., 2011). A similar pattern is observed in *Arabidopsis* for ASY1 staining (Ferdous et al., 2012). This has since been demonstrated more conclusively by our laboratory using super-resolution light microscopy (Structured Illumination Microscopy; 'SIM') (Lambing et al., 2015). *Atasy1* mutants are asynaptic, and show defective crossover formation (only ~15% of normal levels), but do not show chromosome fragmentation, as would be expected if DSB repair were defective, meaning DSB repair is most likely being achieved using recombination between sister chromatids (Sanchez-Moran et al., 2007). This homologue bias is thought to be established early in meiosis, even before DSB formation (Schwacha and Kleckner, 1997), consistent with when ASY1 begins to localise. DMC1 is also suggested to be involved in this process, mediating the homologue bias in an ASY1 dependent manner, which may stabilize the association of DMC1 with DSB sites (Sanchez-Moran et al., 2007). The specifics of the role of DMC1 in enforcing inter-homolog repair bias are discussed further in section 1.4.3. In *Arabidopsis*, ASY1 requires another axis associated protein called ASY3, homologous to Red1 in yeast, in order to linearize along the axis. The same relationship is observed in budding yeast, where Hop1 requires Red1 in order to localize properly (Smith and Roeder, 1997). ASY3 localises to meiotic axes with a similar pattern of domains of hyper and lower abundance seen in ASY1 (Panizza et al., 2011; Ferdous et al., 2012). ASY1 and ASY3 are likely to form a complex *in vivo*, based on yeast two-hybrid data and co-immunoprecipitation of the homologous proteins in *Brassica oleracea* (Ferdous et al., 2012).

Hop1 and Red1 are required for a large proportion of DSB formation in yeast, while in *Arabidopsis*, *asy3* mutants are reported to show DSB levels at around 70% of wild-type levels, based on γ H2AX staining, though *asy1* mutants did not display a significant difference (Ferdous et al., 2012). The association of Hop1 and Red1

promotes the dimerization and activation of the meiosis-specific kinase, Mek1 (Niu et al., 2005). In addition to its other phosphorylation targets during meiosis, Mek1 has been shown to contribute to the homologue bias via phosphorylation of Rad54, a Rad51 binding partner (Niu et al., 2009). This phosphorylation prevents Rad54-Rad51 complex formation and reduces the recombinase activity of Rad51, thereby allowing more Dmc1-mediated repair. The inter-homolog bias mediated by Mek1 is thought to be counteracted by the meiosis-specific cohesin, Rec8, which promotes inter-sister recombination (Kim et al., 2010). A functional ortholog of Mek1 has not yet been identified in plants.

1.3.2 The synaptonemal complex

As zygotene progresses the SC is formed as Zip1 polymerises between the two axial elements. Zip1 monomers form the transverse filaments which polymerise between the two chromosome axes during synapsis in zygotene (Storlazzi et al., 1996; Börner et al., 2004; Higgins et al., 2005). Zip1 homologues show a large degree of sequence variation, though their structures, which consist of globular domains at both N and C termini separated by a coiled coil domain, are highly conserved (Sym et al., 1993). In budding yeast, mammals and *Arabidopsis*, the formation of the SC is DSB-dependent, while in *C. elegans* and *Drosophila*, the SC forms independently of DSBs (McKim et al., 1998; Dernburg et al., 1998; Baudat et al., 2000; Henderson and Keeney, 2004; Higgins et al., 2005). Fission yeast does not produce an SC, and also lacks interference, suggesting a possible link between these two properties (Kohli and Bähler, 1994). *Arabidopsis* contains two homologues of Zip1 called AtZYP1a and AtZYP1b, both of which are needed for normal fertility (Higgins et al., 2005). Like in yeast, *Atzyp1*

mutants display reduced crossover formation, (~80% WT levels) but their formation is unregulated, so multivalents (chiasmata formed between non-homologous chromosomes resulting from ectopic recombination) and univalents (chromosomes lacking a chiasma) are produced at the end of prophase I (Higgins et al., 2005). In barley, *zyp1* mutants display a similar phenotype to that seen in *Arabidopsis*, with a reduction in CO frequency and defective formation of the SC (Barakate et al., 2014). DSB formation is normal in barley *zyp1* mutants so the reduction in CO frequency is thought to result from defects downstream in the recombination pathway. Rice mutants of the homologous gene, *ZEP1*, display a phenotype distinct from other species studied. Homologous chromosomes in *zep1* mutants still align during prophase I but fail to form an SC and interestingly, were reported to display an increased frequency of COs (Wang et al., 2010). *zep1* mutants suffer from reduced fertility due to effects downstream of meiosis, where ZEP1 is thought to be required for chromosome decondensation following the meiotic divisions, in the early microspores.

The total length of the SC is variable between male and female meiosis in *Arabidopsis*, and correlates with the genetic distance (Drouaud et al., 2007). The level of CO interference (discussed below) was also shown to vary between male and female meiosis.

1.3.3. Dynamic organisation of meiotic chromosome components

In yeast, Hop1 must be phosphorylated at a particular threonine residue, T-318, which activates the meiosis-specific kinase, Mek1 (Niu et al., 2005). Mek1 is responsible for the suppression of inter-sister recombination and promotion of inter-homologue

recombination (Terentyev et al., 2010). The association of Red1 is required for this to occur (Lin et al., 2010). The phosphorylation of Hop1 is carried out by the DNA damage sensor kinases Mec1 and Tel1 (homologues of ATR and ATM respectively, in mammals and *Arabidopsis*), which are activated by Red1 in response to DSB formation (Lin et al., 2010). ATM, ATR and another kinase, DNA-PK (DNA-dependent protein kinase) phosphorylate histone H2A.X at DSB sites, to produce γ H2AX (Burma et al., 2001; Ward and Chen, 2001; Stiff et al., 2004), while Mec1 has also been shown to phosphorylate Zip1, thought to destabilize non-homologous centromere pairing during the early stages of recombination (Falk et al., 2010). SC formation then attenuates the phosphorylation of Hop1 T-318 (Cheng et al., 2013).

In addition to Hop1, Zip1 and H2AX, other chromosome components are phosphorylated during meiosis. A study in mice demonstrated that as well as the axis components HORMAD1 and 2 (related to Hop1) and the SC components SYCP1 and 2 (related to Zip1), meiotic cohesin proteins REC8 and SMC3, are both phosphorylated during meiosis (Fukuda et al., 2012). The same study showed that HORMAD1 and SMC3 are only phosphorylated at the unsynapsed chromosome regions, but not on the synapsed regions, suggesting that meiotic events may be regulated in part, by phosphorylation of these components.

In yeast, Hop1 and Zip1 display a non-uniform distribution along the axis and SC, forming alternating regions of hyper abundance and lower abundance (Börner et al., 2008). A similar pattern of organisation was reported in *Arabidopsis* when viewed with super-resolution microscopy (Lambing et al., 2015). This pattern is influenced by the AAA+ ATPase (ATPases associated with diverse cellular functions), Pch2, which is thought to form a hexameric ring and remodel Hop1 organisation in an ATP dependent manner (Chen et al., 2013). As a result of this remodelling, Hop1 is displaced from the

SC as Zip1 polymerises. In *pch2* mutants, Hop1 persists on the SC and shows a uniform distribution, rather than domains of alternating abundance (Börner et al., 2008). Pch2 is required for efficient inter-homolog DSB repair by stimulating the arrest of defective recombination intermediates and promoting inter-homolog repair bias by acting with Tel1 to stimulate the Hop1-dependent autophosphorylation of the meiotic kinase, Mek1 (Ho and Burgess, 2011; Börner et al., 2008). Pch2 also prevents Hop1 from being phosphorylated in the absence of Red1 (Lo et al., 2014), and is required for the implementation of interference (Joshi et al., 2009). Homologues of Pch2 have been found in yeast, flies, worms, mammals and plants. In rice, the PCH2 homologue, CRC1, co-localises and interacts with the Zip1 homologue ZEP1, but also seems to be required for DSB formation, via an interaction with PAIR1 (Miao et al., 2013).

1.3.4 Meiotic chromosome cohesion

In addition to the organisation of chromosomes in the context of the chromosome axis, cohesion between the sister chromatids must also be regulated. As mentioned earlier, the cohesion between sister chromatids must be maintained through the first meiotic division and released during the second. In fact, sister chromatid cohesion must be lost along the chromosome arms to allow resolution of chiasmata present there, but maintained at the centromere in order to ensure accurate homologue segregation during anaphase I (reviewed in Orr-Weaver, 1999; Lee & Orr-Weaver, 2001). The cohesin complex that holds sister chromatids together during mitosis consists of Smc1, Smc3, Scc1 and Scc3 (in budding yeast). At mitotic anaphase, separase cleaves Scc1 and sister chromatids are pulled to opposite poles by spindle microtubules (Ciosk et al., 1998; Hauf et al., 2001; Uhlmann et al., 1999). In contrast, during meiosis Scc1 is

replaced by a meiosis specific cohesion called Rec8 (Watanabe and Nurse, 1999; Molnar et al., 1995; Klein et al., 1999). The maintenance of centromeric cohesion is enabled by Shugoshin (Sgo1), a protein which protects centromeric Rec8 from cleavage by separase during anaphase I (Kitajima et al., 2004). In mammals, SMC1 and SCC3 are replaced with SMC1 β and STAG3 respectively, leaving only Rec8 as being common to all studied meiotic cohesin complexes, though it appears to behave in different ways depending on the organism (Prieto et al., 2001; Revenkova et al., 2001). In fission yeast, Rec8 forms foci along the chromosomes, from S-phase until metaphase I, particularly at the centromeres, with mutants showing equational separation of sister chromatids in anaphase I (Parisi et al., 1999; Watanabe and Nurse, 1999). In budding yeast, the localisation of Rec8 remains at the centromeric regions until anaphase II, with mutants showing random segregation in anaphase I (Klein et al., 1999). In *Arabidopsis*, mutations to SYN1, homologous to Rec8, cause defective chromosome condensation and cohesion, as well as chromosome fragmentation and polyad formation at metaphase I (Bai et al., 1999; Cai et al., 2003; Bhatt et al., 1999).

Meiotic cohesin physically interacts with components of the axis, affecting the organisation of meiotic chromosomes into looped chromatin domains. This link has been demonstrated to be related to gene transcription. Chromatin-immunoprecipitation sequencing (ChIP-Seq) experiments in yeast, showed that the ring-structured cohesin proteins are enriched at the 3' ends of genes, particularly at the convergence of two genes transcribed toward each other, probably due to the activity of RNA-polymerase II pushing the cohesins along the chromosome (Sun et al., 2015). The meiotic cohesin, Rec8, interacts with Red1 to determine where it binds to the chromosome, and which in turn recruits Hop1. Gene transcription is correlated with the enrichment of the axis proteins (Sun et al., 2015). This causes the

chromosome loop bases to occur at regions surrounding stop codons while gene promoters, and therefore recombination hotspots, remain in the loops (Figure 1.5). This organisation also allows gene transcription to continue, during the organisation of meiotic chromosomes.

1.4 Homologous recombination

1.4.1 DSB formation

Homologous recombination is initiated by the formation of DNA double strand breaks (DSBs), catalysed by the type II topoisomerase related protein, Spo11 (Keeney et al., 1997) (Figure 1.2 and 1.5). Break formation is catalysed by a transesterification reaction between a tyrosine residue of Spo11 to the DNA phosphodiester backbone, resulting in them becoming covalently bound (reviewed in Keeney, 2008). While Spo11 is conserved across kingdoms, the accessory proteins required for its function are not. In budding yeast, at least nine additional proteins are required for meiotic DSB formation (Ski8, Mre11-Rad50-Xrs2 (MRX), Rec102, Rec104, Mer2, Rec114 and Mei4), and ten in fission yeast (Mde2, Rec6, Rec7, Rec8, Rec 10, Rec11, Rec15, Rec24, Rec25 and Rec27) (reviewed in Keeney, 2008). *Arabidopsis* and other plants contain two homologues of Spo11 that are required for DSB formation during meiosis, SPO11-1 and AtSPO11-2, and a third homologue, SPO11-3 which is involved in DNA replication (Stacey et al., 2006; Hartung et al., 2000; Malik et al., 2007). Their function in DSB formation is dependent on the catalytic activity of a specific tyrosine residue (Tyr-103 in SPO11-1, Tyr-124 in SPO11-2). SPO11-1 and SPO11-2 are thought to have arisen from an evolutionarily ancient gene duplication event prior to the evolutionary divergence of plants from other eukaryotes, and SPO11-2 being

subsequently lost in other lineages (Malik et al., 2007). SPO11-1 and SPO11-2, are both required for DSB break formation in *Arabidopsis*, possibly acting as a heterodimer, and accumulate on meiotic chromatin as discrete foci early in G₂, around 1-3 hours post-S-phase, followed by the accumulation of DSBs (Stacey et al., 2006; Sanchez-Moran et al., 2007; Hartung et al., 2007). SPO11-1 and SPO11-2 may function in conjunction with various other proteins as part of a complex (Hartung et al., 2007). At least another three proteins are known to be required for meiotic DSB formation in *Arabidopsis*; PRD1, PRD2 and PRD3, which may act as SPO11-1/2 accessory proteins (De Muyt et al., 2009). SPO11-1 and SPO11-2 will be referred to as SPO11 hereafter for simplicity.

Factors which influence the genomic locations of DSB formation are discussed in the 'DSB and CO localisation' section.

It has been demonstrated in yeast that Spo11 catalysed DSBs are subject to negative feedback mechanisms, which inhibit the continued formation of DSBs in the presence of synapsed chromosomes (Carballo et al., 2013; Thacker et al., 2014). This process also involves the phosphorylation of Rec114 by Mec1/Tel1 in response to DSB formation (Carballo et al., 2013). In the absence of these feedback mechanisms, such as in ZMM mutants which are defective in synapsis, cells experience higher levels of DSB formation (Thacker et al., 2014).

1.4.2 DSB processing

Following DSB formation by Spo11, which remains covalently bound to the break site, Spo11 must be released and the DNA then resected by endonucleases to produce short

stretches of single strand DNA which can invade the homologous chromosome, forming joint molecules (Figure 1.2). This resection is carried out in part by a protein complex made up of Mre11, Rad50 and Xrs2 in yeast (MRX complex) (Mimitou and Symington, 2008; Connelly and Leach, 2002), which works with another complex called Com1/Sae2 in yeast and CtIP in mammals (originally described as a Retinoblastoma binding protein) (Mckee and Kleckner, 1997; Prinz et al., 1997; Fusco et al., 1998). Mre11 and Rad50 are highly conserved and share homology with bacterial nucleases, while Xrs2 is less conserved (Bleuyard and White, 2004). In *Arabidopsis*, NBS1 replaces Xrs2 (MRN complex rather than MRX), which interacts with the COM1 complex, homologous to Com1/Sae2 and CtIP (Uanschou et al., 2007). Mre11, promoted by Sae2, has dsDNA endonuclease activity, and produces ssDNA breaks upstream of the Spo11-induced DSB, before carrying out 3'-5' exonuclease activity toward the DSB (Cannavo and Cejka, 2014). Spo11, attached to a short oligonucleotide, is then released (Neale et al., 2005). Immunoprecipitation and sequencing of these Spo11-bound oligonucleotides can be used to produce the genome-wide DSB maps discussed previously.

More long-range resection of the DNA can then be carried out in a 5' to 3' direction, by Sgs1 (a helicase), and two nucleases, Exo1 and Dna2, to produce a single-strand 3' overhang either side of the break site (Mimitou and Symington, 2008; Zhu et al., 2008). The helicase activity of Sgs2 unwinds DNA double-helices to allow access to Exo1 and Dna2 (Manfrini et al., 2010). This process is not only required for the formation of crossovers, but also for efficient DNA repair following DSB formation by Spo11. If this DSB end processing is inhibited, such as by mutation to AtMRE11 or AtRAD50, extensive DNA fragmentation is observed unless AtSPO11 is also knocked out (Bleuyard et al., 2004; Puizina et al., 2004). A similar phenotype is observed in

AtCOM1 mutants (Uanschou et al., 2007). In yeast and HeLa cells, end resection was recently shown to be inhibited by treatment with caffeine, which cause the degradation of Sae2 and Dna2 (Tsabar et al., 2015a). Part of the following stage in the homologous recombination process, loading of Rad51 onto ssDNA to produce nucleoprotein filaments (discussed below), was also shown to be inhibited by caffeine (Tsabar et al., 2015b).

1.4.3 DNA Strand exchange

The single-strand 3' overhang can now be used to invade the homologous chromosome. This involves a homology search to identify the correct sequence with which to carry out recombination. This process is known to be facilitated by homologues of the bacterial recombinase, RecA, which are required for DSB repair and recombination (Smith et al., 1987; Smith and Wang, 1989). Many eukaryotes possess RecA homologues, called Rad51 and Dmc1. Loss of function mutation to Rad51, like mutation to parts of the MRN/X complex or Com1, leads to DNA fragmentation in meiocytes caused by an inability to repair Spo11 catalysed DSBs, compromised pairing and a complete lack of synapsis (Li et al., 2004; Shinohara et al., 1992). Unlike Rad51, Dmc1 is meiosis specific (Bishop et al., 1992). Perturbing the function of Dmc1 in both yeast and *Arabidopsis* leads to a complete absence of chiasmata and defective synapsis but does not result in chromosome fragmentation, suggesting that it is dispensable for DSB repair but is required for CO formation (Bishop et al., 1992; Couteau et al., 1999). In a *dmc1* mutant background meiotic DNA repair is carried out by Rad51, using the sister chromatid rather than the homologous chromosome (Couteau et al., 1999; Siaud et al., 2004; Sanchez-Moran et al., 2007). *Drosophila* and *C. elegans*, which do not

require the formation of crossovers for synapsis, do not have genes for Dmc1 (reviewed in Ma, 2006). Using immunolocalisation, RAD51 has been observed to localise to the axis as numerous foci in leptotene (~200 in *Arabidopsis*) (Kurzbaue et al., 2012; Franklin et al., 1999). Initially, the number of foci far exceeds the final number of COs, but is reduced as the cell progresses through zygotene into pachytene, when around 50 remain in *Arabidopsis*. These numbers are also consistent with the numbers of early and late ‘recombination nodules’ observed using electron microscopy (reviewed in Zickler & Kleckner, 1999). Early nodules are present at zygotene and are required for accurate pairing of homologous chromosomes and are thought to represent all strand exchange events, while late nodules are less numerous, present later, at pachytene and thought to specifically mark the sites of CO formation.

In *Arabidopsis*, RAD51 has six paralogs, RAD51, RAD51B, RAD51C, RAD51D, XRCC2 and XRCC3, though only RAD51, RAD51C and XRCC3 are likely to be involved in meiosis (reviewed in Ma, 2006; Osman et al., 2011). Disrupting the function of any of these three proteins results in asynapsis and extensive chromosome fragmentation, suggesting they may work as a complex and are essential for carrying out efficient DSB repair (Bleuyard and White, 2004; Abe et al., 2005; Bleuyard et al., 2005; Li et al., 2005). Da Ines, 2013 reported that the RAD51B, RAD51D and XRCC2 paralogs were involved in somatic recombination, and that meiotic CO frequencies were increased in mutants of *rad51b* and *xrcc2* (Da Ines et al., 2013a). However, CO frequency at only a single genetic interval was assayed in this study, so should be interpreted with caution.

The RecA homologues form nucleoprotein filaments with the single-strand resected DNA at the DSB sites, and promote strand invasion and displacement loop (D-loop) formation (Petukhova, 2000). The loading of Rad51 and Dmc1 onto the ssDNA is promoted by several accessory proteins, including BRCA2 in *Arabidopsis* (Seeliger et

al., 2012) and Rpa1, which co-localizes with RAD51 during prophase I in yeast (Gasior et al., 1998), mice (Moens et al., 2007) and humans (Oliver-Bonet et al., 2007). All appear to show localisation of the protein to chromosomes around early leptotene but this localisation diminishes during progression to pachytene. Mutation to one of the five RPA1 paralogs in *Arabidopsis*, causes fertility defects resulting from defective CO formation (Osman et al., 2009). Immunolocalisation in *Arabidopsis* shows RPA1 localisation during prophase I similar to that observed in other organisms. The reduced CO formation in *Atrpa1* mutants was suggested to be due to defects during the second-end capture stage of homologous recombination, based on WT-levels of RAD51 and MSH4 localisation but a strong reduction in MLH1 localisation, which localises to future CO sites (discussed below) (Osman et al., 2009). The lack of chromosomal fragmentation in the mutant shows that DSB repair is still being carried out efficiently, in contrast to the situation observed in rice *rpa1* mutants, where chromosomal fragmentation and sensitivity to DNA damaging agents is observed (Chang et al., 2009).

The nucleoprotein filaments are hypothesized to act as ‘search tentacles’, seeking out homologous sequences between homologous chromosomes to facilitate the single-end invasion stage of recombination (Figure 1.2) (Kim et al., 2010). The heterodimer Hop2-Mnd1 is required as a cofactor for the strand-exchange forming activity of Dmc1, with mutations to either resulting in similar phenotypes to *dmc1* (Chan et al., 2014). Dmc1 colocalizes with Rad51 during zygotene, though it is thought to occupy the opposite side of the DSB and carry out distinct functions that impose the homologue bias during meiotic recombination (Pradillo et al., 2012; Kurzbauer et al., 2012). RecA, Rad51 and Dmc1 have all been demonstrated, *in vitro*, to carry out their homology search by sampling of 8 nucleotide tracts for homology between the invading

nucleoprotein filament and the dsDNA (Qi et al., 2015). Successful pairing of the 9th nucleotide stabilizes the complex and subsequent pairing is carried out in a stepwise manner in nucleotide triplets, due to the way DNA is stretched within the filament. Triplets containing mis-matched base-pairs remain unstable when the pairing is catalysed by RecA or Rad51, but when Dmc1 is used, mis-matched triplets are stabilized (Lee et al., 2015). This difference in the stabilisation properties of the RecA homologs may explain the preference for inter-homolog recombination during meiosis, and for inter-sister recombination in somatic cells. In the absence of Dmc1, any inter-homolog heteroduplex DNA catalysed by Rad51 is likely to be unstable, due to sequence polymorphisms, which would not exist between sister chromatids. During meiosis, Dmc1 is expressed, allowing the stabilisation of heteroduplex DNA, despite these polymorphisms.

In yeast, the strand exchange activity of Rad51 is suppressed by Dmc1 during meiotic recombination (Lao et al., 2013). In yeast and *Arabidopsis*, *rad51* and *dmc1* mutants were complemented with catalytically inactive versions of RAD51 protein which could localize at DSB sites, but was incapable of DSB repair (Cloud et al., 2012; Da Ines et al., 2013b). Both studies found that while the complementation had no effect on the *dmc1* double mutant, which remained sterile, it was able to fully rescue the *rad51* phenotype, indicating that during meiosis, the catalytic activity of DMC1 may be solely responsible for DSB repair, but requiring the presence of RAD51 as an accessory protein in order to carry out its function.

1.4.4 DSB repair via the non-crossover pathway: Synthesis dependent strand annealing and inter-sister recombination

Once a D-loop has been formed via strand invasion by Rad51/Dmc1 nucleoprotein filaments, the 3' end of the invading strand is then extended, using the receiving strand as a template (Figure 1.2). It is thought that it is at this point that the DSB repair pathway is committed to production of either a CO or a non-crossover (NCO) product. A larger number of DSBs are produced than the final number of COs, meaning the majority of DSBs are repaired as NCOs. It is thought that the decision as to which repair pathway a DSB will take, CO or NCO, is made early on in the recombination process, even before stable strand exchange has occurred (Hunter and Kleckner, 2001; Sanchez-Moran et al., 2007; Börner et al., 2004). Though dHjs could theoretically be resolved as either CO or NCO products, most NCOs are thought to be resolved via the synthesis dependant strand annealing pathway (SDSA), where the process does not proceed as far as the formation of a dHj (Allers and Lichten, 2001; McMahon et al., 2007). So far there is no biochemical evidence for SDSA in plants, so the presence of this repair pathway is only inferred from studies in yeast.

The other NCO producing pathway is inter-sister recombination. During meiosis in budding yeast, homologous recombination takes place preferentially using the homologous chromosome, with around 20-30% being repaired using the sister chromatid, though the products of inter-sister recombination are inherently more difficult to detect than for inter-homolog recombination, due to the genetically identical nature of sister chromatids (Goldfarb and Lichten, 2010; Kim et al., 2010). Mek1 was demonstrated to have a role in destabilizing inter-sister joint molecules as well as reducing the rate of inter-sister repair.

1.4.5 Gene conversion resulting from SDSA

Gene conversion is a consequence of recombination which can occur during CO formation and also during SDSA. When homologous sequences containing a polymorphism undergo recombination and form a D-loop, the exchange can produce sequence mismatches in the heteroduplexed region. When the D-loop has been disrupted, depending on which of the strands is used as a repair template, the mismatch will either be reverted to back to the original sequence for that homolog, or it can be repaired using the new sequence, which is a gene conversion event. Gene conversion tracts typically measure ~2kb in yeast (Mancera et al., 2008).

In *Arabidopsis*, a variation of the fluorescent tetrad analysis system (FTL) has been used to study the distribution of NCO products. This system uses a pollen-expressed fluorescent reporter, and a non-fluorescent allele of this reporter found on the homologous chromosome, the fluorescence of which is restored by a gene-conversion event and can be used to measure these at specific loci (The FTL system is described in detail in chapter 3) (Sun et al., 2012). They reported the average gene-conversion frequency per locus per meiosis as 3.5×10^{-4} . This study also showed that like in yeast, some regions are more likely than others to produce NCO products. Another study of gene conversion in *Arabidopsis* performed genetic crosses between Columbia and Landsberg *erecta* ecotypes, then sequenced the F2 plants and their parents, revealing that over 90% of recombination events resulted in a gene-conversion event (Yang et al., 2012). The authors estimated that this could be as high as 99%. The study also found that the average NCO-associated gene conversion tract length was 402bp. A similar study in yeast found that gene conversion tracts in were slightly shorter for NCOs (1.8kb) compared with CO-associated tracts (2.0kb), and that certain genetic intervals are biased towards formation of either COs or NCOs (Mancera et al., 2008).

1.4.6 Non-homologous end-joining

Non-homologous end-joining (NHEJ) is an alternative DSB repair pathway to homologous recombination (reviewed in Fell & Schild-Poulter, 2015). Gene conversion events mean that homologous recombination may not carry out DSB repair entirely free of errors, but insertions or deletions are a rare occurrence and the process is largely faithful to the original sequence, ensured by its use of homologous sequences as a repair template. NHEJ by contrast, does not use a repair template, ligates DNA ends in a sequence-independent manner and is more error-prone than homologous recombination. NHEJ is mediated by Ku70/Ku80 heterodimers, which have a strong binding affinity for unresected DNA DSB ends (Mari et al., 2006). Once bound, the Ku70/Ku80 dimer recruits a complex which includes ligase IV and XRCC4 (Nick McElhinny et al., 2000). In yeast, during G₁, NHEJ is the preferred mode of DSB repair, but in G₂ following DNA synthesis, homologous recombination becomes the preferred method, as the sister chromatid becomes available for use as a repair template (Clerici et al., 2008). Ku proteins are also known to have a role in the protection of telomeres, the linear ends of chromosomes. In *Arabidopsis*, mutation to *KU70* causes hypersensitivity to DNA damaging agents and increased telomere length (Bundock et al., 2002). This is distinct from mammalian cells and yeast, where *Ku* mutants suffer from reduced telomere length (reviewed in Fell and Schild-Poulter, 2015).

1.4.7 Double Holliday junction formation

Recombination intermediates which proceed on the CO-producing pathway of DSB repair begin in the same way as SDSA. Once the invading strand has formed a D-loop

in the homologous chromosome, the 3' end of the invading strand is then extended, using the receiving strand as a template (Figure 1.2). If the structure is not destabilised and resolved via SDSA, the pathway will instead be set on a course which results in the formation of a double Holliday junction (dHJ) (Holliday, 1964). The extension of the 3' end results in a single Holliday junction, and the intermediate structure is stabilised (Figure 1.2). A dHj is formed following a process called second end capture, where the extended 3' ssDNA end associates with the resected 5' end on the other side of the DSB. This requires Msh4, Msh5 and Mer3, all of which are involved in crossover formation in yeast (Hollingsworth et al., 1995; Nakagawa and Kolodner, 2002; Novak et al., 2001; Nakagawa and Ogawa, 1999). The two MSH proteins are homologues of the bacterial MutS protein (**MutS Homologue**) which are required for DNA mis-match repair (MMR) in prokaryotes (Fishel, 2015). Heterodimers of the MSH proteins are thought to stabilize the single end invasion step, while MER3 functions as a DNA helicase, unwinding double stranded DNA and allowing dHj formation (Snowden et al., 2004; Nakagawa and Kolodner, 2002; Mazina et al., 2004). MSH heterodimers have also been shown to bind to dHJs *in vitro* (Snowden et al., 2004; Bocker et al., 1999).

Immunolocalisation in *Arabidopsis* shows that MSH4 is present as numerous foci in leptotene, similar to the number of RAD51 foci, and that the number of foci decreases during zygotene until only a few are left by pachytene (Higgins et al., 2004). Proper MSH4 localisation is dependent on various upstream meiotic proteins, including retinoblastoma related protein (RBR) (Chen et al., 2011). As in yeast, the *Arabidopsis* homologue of MER3 (also known as rock-n-rollers (RCK)) is required for class I crossover formation, with a loss-of-function mutation producing a phenotype similar to that of MSH4, where crossovers are reduced by ~85%, leaving only interference-insensitive crossovers (Mercier et al., 2005; Chen et al., 2005).

In addition to the MutS homologues and Mer3, the Zip proteins (Zip 1,2,3 and 4) are also required for crossover formation, with the 3 types of protein collectively referred to as ZMM proteins (Börner et al., 2004). Mutation to ZMM genes leads to severe reductions in crossover numbers (10-15% of normal levels), while the crossovers that do form occur with a Poisson distribution, suggesting that they are not subject to **crossover interference** (Hollingsworth and Brill, 2004). Interfering crossovers do not form independently of one another, meaning the formation of one reduces the likelihood of another forming in close proximity. The strength of the interference effect diminishes with distance from the site of recombination. Interference is discussed further below.

HEI10, found in plants, mammals and *Sordaria*, is part of the ZMM group of proteins and is part of a family of proteins possessing E3 SUMO/ubiquitin ligase activity, similar to Zip3 found in budding yeast and ZHP-3 found in *C. elegans*, and RNF212 which is found in mammals in addition to HEI10 (Chelysheva et al., 2012; Agarwal and Roeder, 2000; Bhalla et al., 2008; Reynolds et al., 2013). Zip3 acts as a negative regulator of Zip1 polymerisation in budding yeast. The wild-type situation is that synapsis is dependent on earlier inter-homolog interactions, but in a *spo11/zip3* background, the SC is still able to assemble without recombination or pairing (MacQueen and Roeder, 2009). This synapsis was initiated at centromeric regions though, where recombination is unlikely to occur. In mammals, this activity is due to the antagonistic effect which HEI10 has on RNF212, a SUMO-ligase which also has similarities with Zip3 and is required for stabilisation of the MSH4-MSH5 complex and subsequent CO formation (Reynolds et al., 2013; Qiao et al., 2015). In *Arabidopsis*, HEI10 is required for interfering CO formation, but is dispensable for synapsis (Chelysheva et al., 2012), in contrast to yeast Zip3 mutants, which show

aberrant SC formation (Agarwal and Roeder, 2000). The fact that Zip3 appears to work as both a positive and negative regulator of synapsis in yeast is interesting, and has been speculated to either stem from its sumoylation activity, which could be acting on multiple protein targets involved in recombination and synapsis, or in a centromere specific manner for its function as a suppressor of synapsis (MacQueen and Roeder, 2009).

Another of the ZMM proteins found in *Arabidopsis* is an XPF-endonuclease called SHOC1. This protein has a human homologue, and shares a distant similarity to the budding yeast ZMM protein Zip2 (Macaisne et al., 2008). Mutation to SHOC1 causes a phenotype typical of ZMM mutations, where interfering crossover formation is lost (Macaisne et al., 2008). SHOC1 is thought to form a heterodimer with PTD in *Arabidopsis*, to form a complex similar to XPF-ERCC1, which are involved in somatic DNA repair through their recognition of branched DNA structures (Macaisne et al., 2011).

1.4.8 Crossover resolution – Interfering and non-interfering crossovers

A stable dHj can, in theory, be resolved either as a crossover or a non-crossover, depending on which strands are cut in the junction. In reality, all dHjs are thought to be resolved as COs, and most or all NCOs are thought to be generated by SDSA (Allers and Lichten, 2001). DHjs can be resolved as either interfering or non-interfering COs. The **MutL** homologues, Mlh1 and Mlh3, are involved in the late stages of interfering CO formation, acting downstream of the ZMM proteins, which are also specific to interfering CO formation. In prokaryotes, dimers of MutL are recruited to mismatched bases during DNA replication by MutS dimers, the newly synthesised strand

is then cut to remove the offending base, and the correct base can then be inserted in its place (reviewed in Jun et al., 2006). In eukaryotes, MLH complexes, which consist of a dimer of Mlh1 and Mlh3, bind to dHJs and have endonuclease activity on dsDNA (Ranjha et al., 2014). It is this endonuclease activity which is thought to be involved in dHj resolution. In yeast, a RecQ helicase, Sgs1, has been shown to suppress the formation of COs in mitotic cells, resulting from homologous recombination. During meiosis, the helicase activity of Sgs1 unwinds joint molecules at the D-loop stage, to produce NCO products via SDSA (Bachrati et al., 2006; De Muyt et al., 2012; Zakharyevich et al., 2012). In the absence of Sgs1, aberrant joint molecules accumulate, often between non-homologous chromosomes, and are resolved by the structure selective endonucleases, Yen1 and Slx1-Slx4, which would normally play only a minor role in dHj resolution (Zakharyevich et al., 2012; De Muyt et al., 2012). Mms4-Mus81 is another structure-selective endonuclease with a more prominent role in meiosis, resolving ~20% of COs in wild-type yeast (discussed further below). The majority of COs however, are resolved by Mlh1-Mlh3 dimers working together with the Exo1 nuclease, acting on the joint molecules which have not been destabilized by Sgs1 and have progressed to form dHJs. Sgs1 is therefore thought to regulate the NCO/CO decision pathway in early meiosis. Consistent with this, in *Arabidopsis*, MLH1 and MLH3 co-localise at pachytene at the loci where COs will form, producing a similar number of foci as there are COs (~10) (Jackson et al., 2006; Ferdous et al., 2012). Mutation to *MLH3* affects the localisation of MLH1 and these mutants show a 60% reduction in crossover number (Jackson et al., 2006).

The formation of interference-insensitive COs is mediated by Mus81 and Mms4/Eme1, and forms a separate pathway of CO formation (Hollingsworth and Brill, 2004). The Mus81-Eme1 heterodimer is also similar to the Xpf-Ercc1 complex mentioned before

(Kikuchi et al., 2013). Msh4/Msh5 mediate interference-sensitive COs, which are also called type I COs (Higgins et al., 2008b), while the Mus81 mediated, interference-insensitive COs are called type II crossovers (Higgins et al., 2008a). The ratio of type I to type II COs varies between species (Hollingsworth and Brill, 2004). The majority of COs produced in *S. cerevisiae* and *Arabidopsis* are Msh4/Msh5 COs, with a minority being produced by Mus81 (Hollingsworth and Brill, 2004; Higgins et al., 2004). *C. elegans* forms only interfering COs, and the reverse is true for *S. pombe*, where all COs are interference-insensitive (Osman et al., 2003; Hollingsworth and Brill, 2004; Youds et al., 2010).

Crossover interference in *Arabidopsis* does not operate identically in male and female meiosis. Interference has been shown to be increased in female meiocytes, which also show fewer non-interfering, class II crossovers, likely due to differences in the physical length of the meiotic chromosome axes (Basu-Roy et al., 2013). CO interference is discussed further below in **CO Control**.

The stabilizing activities of the ZMM proteins are counteracted by certain helicases which act as anti-recombination factors. These factors are proposed to de-stabilise intermediate joint-molecules prior to dHj formation, promoting NCO formation in competition with Mus81, which would otherwise process these intermediates as non-interfering COs. In *Arabidopsis*, the FANCM helicase acts to limit the formation of interference-insensitive crossovers, with *Atfancm* mutants being reported to display an increased CO frequency resulting specifically from MUS81 catalysed COs (Crismani et al., 2012; Knoll et al., 2012). A similar phenotype is reported for the fission yeast homolog of FANCM (Lorenz et al., 2012). In *Arabidopsis*, FANCM function requires two co-factor proteins MHF1 and MHF2 (Girard et al., 2014). The AAA-ATPase, FIGL-1 is also reported to have a non-interfering CO-limiting function, but while FANCM is

proposed to act upon D-loop intermediates, FIGL-1 is suggested to operate earlier, at the strand invasion stage (Girard et al., 2015).

1.5 CO Control

As has been suggested earlier, COs do not form at random points in the genome. The control over their formation occurs at multiple levels.

1.5.1 CO/NCO Decision

The decision over whether a DSB is processed to form a CO or NCO, is made prior to strand exchange, as has been demonstrated in yeast (reviewed in Bishop & Zickler, 2004). Although it is theoretically possible for dHjs to be resolved as either COs or NCOs, depending on which DNA strands are cut by the endonuclease, the available evidence supports the early decision model and that a very high proportion, probably all meiotic dHjs are processed to form COs (Allers and Lichten, 2001). The decision to form a CO or NCO is subject to influence from the local chromatin architecture and also gender-specific bias. A study in mice showed that a recombination hotspot located centrally on chromosome 1 showed similar patterns of CO/NCO rates between sexes, while a distally located hotspot which produced similar levels of NCO events in both sexes, only produced CO events in males (De Boer et al., 2015).

1.5.2 CO Assurance

CO assurance is the observation that in a typical wild-type meiosis, every chromosome will produce at least one CO, the 'obligate CO', no matter how small that chromosome might be relative to the others or how small the average CO number per chromosome (Jones and Franklin, 2006). This phenomenon ensures accurate chromosomal segregation at anaphase I and requires the establishment of ZMM-containing interference-sensitive recombination complexes and full polymerisation of the SC (Shinohara et al., 2008). An exception to this is seen in fission yeast, which does not produce interfering COs or form an SC (Bahler et al., 1993; Osman et al., 2003). This organism ensures that each chromosome receives at least one CO by producing COs at a high enough frequency (~38 CO per meiosis over 3 chromosomes) to make it highly unlikely that one chromosome would be left with zero COs, despite their random distribution (Berchowitz and Copenhaver, 2010).

1.5.3 CO Interference

As mentioned earlier, CO interference is the phenomenon of a reduced probability of two COs forming in close proximity, in comparison to a Poisson distribution. This is due to the property of interfering CO-designated sites inhibiting the formation of other interfering COs in a distance-dependent manner, meaning the inhibitory signal becomes weaker with increasing physical distance from the CO site.

There is some conflicting evidence as to whether or not interference requires formation of the SC. In *C. elegans*, the SC has been shown to influence interference based on its structure, but also have its structure modified by CO formation (Libuda et al., 2013). By measuring inter-CO distance based on immuno-staining, in WT and *syp1*

RNAi lines, the authors observed a reduction in inter-focus distance in the RNAi lines, and a local expansion in chromatin in the vicinity of COs. This implies that COs are promoted by local chromatin structure, but that CO formation produces a local change in this structure which inhibits the formation of more COs. In contrast to this, cytological examination of yeast meiosis has demonstrated that synapsis initiation complexes, based on measuring foci of Zip2 and Zip3, showed interference operating on their distribution, even the absence of Zip1, which is required for SC formation (Fung et al., 2004). It has also been demonstrated that interference is established early in the recombination pathway, prior to SC formation (Börner et al., 2004). Together with the finding that the CO/NCO repair pathway decision is made prior to strand exchange, including in *zip1* mutants, we can infer that the SC is not required for interference in yeast. In *Arabidopsis*, *Atzyp1* mutants, which cannot form an SC, still produce COs which are subject to interference (Higgins et al., 2005).

Recently, it has been determined that the physical distance between COs is the metric by which interference operates, rather than genomic length, which varies depending on the size of the DNA loops attached to the axis (Zhang et al., 2014b). Another *C. elegans* study showed that mutations which disrupted a meiotic condensin increased the length of the SC and also the number of crossovers (Mets and Meyer, 2009). Similarly, in *Arabidopsis*, SC length is increased in male compared to female meiosis, and displays a concomitant increase in CO frequency (Giraut et al., 2011).

There are several theories on the mechanisms governing interference. One hypothesis, the ‘counting model’, was that crossovers were separated by a specific number of non-crossover events (Stahl et al., 2004). This has been largely disproved by studies showing that a reduction in the number of DSBs does not necessarily lead to a reduction in the number of crossovers (Martini et al., 2006; Rosu et al., 2011; Cole et

al., 2012b), see CO Homeostasis section below). The polymerisation model of interference postulates that interference is imposed by an unknown factor which polymerises out from CO-designated recombination sites preventing other DSB sites from being processed as COs (King and Mortimer, 1990). In this model, the unknown factor could be a protein or an epigenetic modification.

Alternatively, the 'mechanical stress' or 'beam-film' model postulates that the formation of a crossover somehow relieves physical tension in the local vicinity on that chromosome, with that physical tension being transmitted from outside the nucleus (Kleckner et al., 2004). The term 'beam-film' refers to the analogy of a metal beam coated with a ceramic film. Upon heating, the metal would expand, producing cracks in the ceramic film. Each crack would relieve stress in the local vicinity, making the formation of another crack less likely (Kleckner et al., 2004). Study of crossover distribution patterns in yeast, flies, grasshopper and tomato supports this model (Zhang et al., 2014a). Recently the topoisomerase, TOP2 α , which is able to relieve physical stress on chromosomes, has been implicated as being the key protein involved in transmission of the interference signal across the chromosome (Zhang et al., 2014b).

The mechanism which governs CO interference has been shown to be distinct from CO assurance, as one can be disrupted without affecting the other. CO interference is set up earlier than assurance, and seems to require assembly of Msh4/Msh5 containing interference-sensitive recombination complexes, while CO assurance requires ZMM proteins involved later in the CO pathway and full extension of the synaptonemal complex (Bishop and Zickler, 2004; Shinohara et al., 2008).

A whole-genome recombination mapping study in yeast showed that interference does not only act on COs, but also NCOs, providing strong support to the theory that

interference is established very early in the recombination pathway, preceding CO/NCO designation (Mancera et al., 2008).

1.5.4 CO Homeostasis

In *Arabidopsis*, the number of DSBs is around 11 times higher than the final number of COs per cell (Ferdous et al., 2012). CO homeostasis refers to the observation that altering the number of DSBs does not necessarily cause a change in the number of COs, until the DSB number is reduced to around 60% of wild type levels (Henderson and Keeney, 2004). The cell compensates for the reduction in DSB number by maintaining the number of COs at the expense of NCOs. This has been demonstrated in yeast using alleles of *spo11* with varying levels of reduced and increased activity (Henderson and Keeney, 2004; Martini et al., 2006; Cole et al., 2012a), and in *Arabidopsis* using RNAi against *SPO11*, and analysing the effects of differing degrees of *SPO11* knockdown (Roberts, 2009). CO Homeostasis is thought to be linked to interference, as it disappears when interference is absent and displays a stronger or weaker effect as interference increases or decreases (Zhang et al., 2014a).

1.5.5 DSB and CO localisation

The formation of SPO11-catalysed DSBs (and subsequent crossovers) is more common in some genomic regions than others. These areas of high DSB frequency are called recombination ‘hotspots’, while areas of disproportionately low crossover frequency are known as ‘coldspots’, though it should be pointed out that these labels

are probability based, and it is possible for meiotic DSBs to form almost anywhere in the genome (Pan et al., 2011). In mammals, the location of hotspots/coldspots is determined by DNA sequence motifs (Smagulova et al., 2011), as well as nucleosome occupancy and specific modifications to histone proteins.

Genome wide maps of DSB sites have aided in the understanding of recombination hotspots. In yeast, DSB hotspots are known to localise at the nucleosome depleted regions of gene promoters (Pan et al., 2011). In mammals, DSB hotspots are most strongly associated with PRDM9-dependent, meiosis-specific H3K4Me3 sites, which are often found at regions of nucleosome occupancy and overlapping genes, but rarely found at transcriptional start sites, (Smagulova et al., 2011). In the absence of PRDM9, hotspots are re-distributed to PRDM9-independent H3K4Me3 sites, often found at gene promoter regions (Brick et al., 2012). In *Arabidopsis*, DSB hotspots are associated with gene promoter and terminator regions, as well as nucleosome-depleted regions, low levels of DNA methylation, H3K4Me3 and the histone variant H2A.Z (Choi et al., 2013).

Recombination hotspot locations have been demonstrated to be influenced by transcription factor binding. In transcription factor mutants, DSB activity was affected in genes which included binding sites for the affected transcription factors (Mieczkowski et al., 2006; Zhu and Keeney, 2015). This relationship was highly context dependent though, as some genes were subject to increased DSB activity but others showed a reduction and some experienced no effect. Transcription factors did affect the fine-scale localisation of DSBs occurring within the hotspots (Zhu and Keeney, 2015).

As mentioned previously in section 1.3.3, the organisation of chromatin loops onto the meiotic axis is largely determined by the effects of transcription, with Rec8 clustering around the 3' end of actively transcribed genes and determining the site of axis attachment via an interaction with Red1 (Sun et al., 2015). In the context of this small scale, DSBs are known to occur in the loop regions, though the machinery required for DSB formation is localised at the axis. This discrepancy is resolved by the 'tethered loop-axis' model of DSB formation, where future DSB sites in the loops are tethered to the axis for DSB formation and subsequent recombination (Figure 1.5) (Panizza et al., 2011). It is not clear whether Spo11 itself localises to the target site in the loop or to directly to the axis, prior to tethering. The specifics of this model are discussed further in section 3.1.

CO localisation is also in effect at the chromosomal level, causing COs to occur preferentially in certain regions, such as the sub-telomeric or centromere proximal regions. This effect is particularly conspicuous in a number of cereal crop species (reviewed in (Higgins et al., 2014)). This phenomenon has strong implications for crop breeders, who can find it difficult or impossible to use conventional breeding techniques to get desirable alleles into the same line. In species such as wheat, up to one third of genes are found in recombination-poor regions (Erayman et al., 2004), with a similar situation in barley, where around one third of all genes are found in the centromere proximal regions, which only constitute 6.4% of the genetic map (Mayer et al., 2011). The basis of this behaviour is poorly understood.

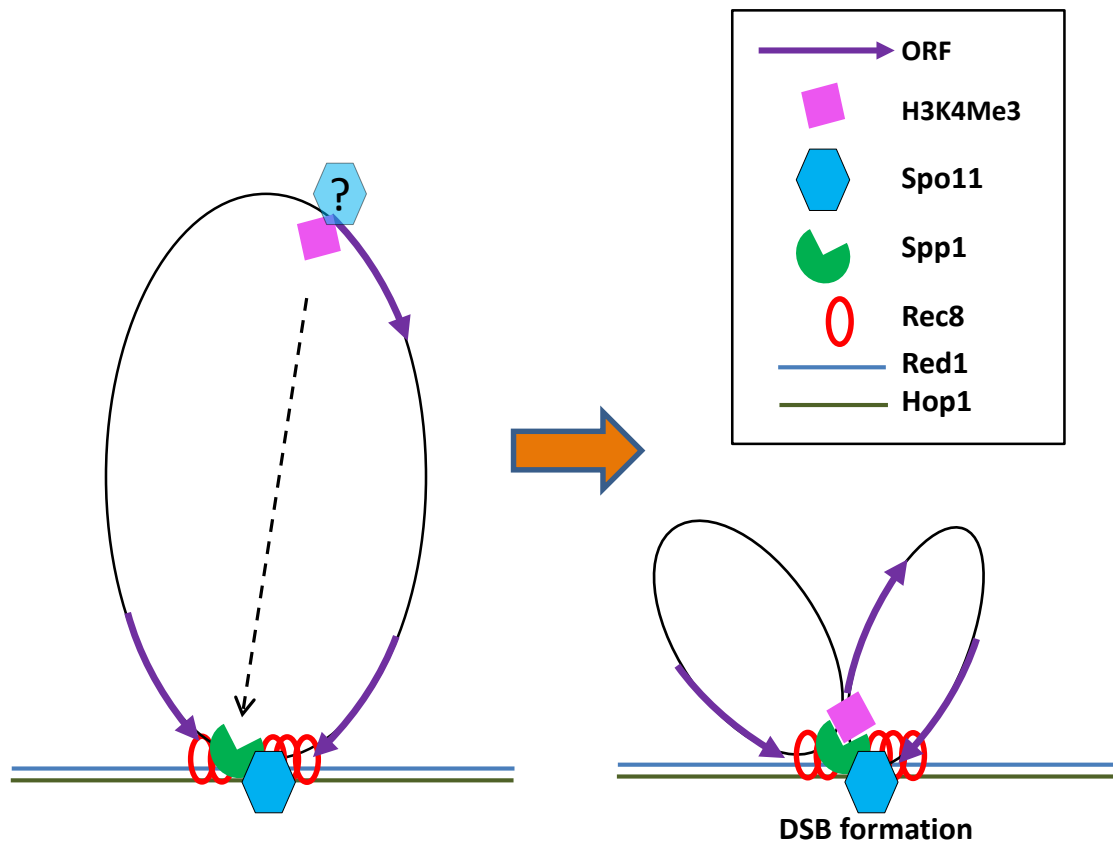


Figure 1.5: Tethered-loop axis model of DSB formation. Spp1 recognises tri-methylated H3K4 histones found at promoter regions and tethers them to the axis where DSBs are formed. Spo11 is shown located on the axis, though it remains possible that it localises to the future DSB site in the loop but remains inactive until brought to the axis. The meiotic cohesin, Rec 8 localises at the 3' end of genes and interacts with Red1 to determine the positioning of the loop module. Based on Sommermeyer et al, 2013.

1.6 Research aims

The aim of the project was to further our understanding of how epi-genetic and chromosome structural factors can influence the distribution and number of COs and how this is modulated by environmental factors using *Arabidopsis* as a model organism.

Initially, two *Arabidopsis* proteins responsible for the deposition of different histone modifications were investigated to establish whether they play a role in meiosis. AtMRG2 possesses a MRG domain, which is associated with complexes that both acetylate and de-acetylate histones, and also a chromo-domain, which is likely to bind to specific histone methylation modifications. Interest in AtMRG2 arose following research by group in Singapore who identified an *Atmrg2*T-DNA mutant with a strong fertility defect and apparently no somatic phenotype. Based on the reduced fertility phenotype of the mutant allele, I investigated it in detail to establish if this was due to a meiotic defect.

The second histone modification protein studied was AtSDG2, a known histone methyl-transferase responsible for the majority of H3K4Me3 deposition in *Arabidopsis* (Guo et al., 2010). AtSDG2 is also known to be required for fertility, though meiosis has not been studied in detail in the *Atsdg2* mutant (Berr et al., 2010).

To further understand how structural reorganization of the chromosomes can influence meiotic recombination I have investigated the function of AtPCH2. This followed on from previous work in our laboratory which established that AtPCH2 and ASY1 co-immunoprecipitate, and revealed meiotic defects in mutants of *Atpch2*. The purpose of the study herein was to investigate at which point in the recombination pathway the protein operates and its influence on the dynamics of the axis protein ASY1

Finally, the impact of the environment was investigated by studying the effects of temperature on the progression of meiosis in wild-type *Arabidopsis* and in mutants with various meiotic defects. Chromosome spread preparations and immunolocalisation of ASY1 and ZYP1 were used to establish at what temperature the chromosomes begin to experience structural defects and DSB repair begins to fail.

Chapter 2

Materials and methods

2.1 Plant material

Mutant lines of *Arabidopsis thaliana* were purchased from the European Arabidopsis Stock Centre (NASC) in Nottingham, UK. Plants were grown in soil based compost under glasshouse conditions with supplementary lighting (400W high pressure sodium bulbs) in a 16 hour light/8 hour dark cycle. Pots were pre-treated with Intercept 70WG (Imidicloprid) according to manufacturer's instructions to control the sciarid fly population.

2.2 Genotyping of *Arabidopsis* T-DNA insertion mutants

~0.2cm² sections of *Arabidopsis* leaf tissue were removed from rosette leaves using sterile 0.5ml microfuge tubes. 50µl of extraction buffer (100mM TRIS-HCl pH9.5, 250mM KCl, 10mM EDTA) was added to tubes and leaf material was then macerated using a sterile filter pipette tip (200µl size). The mixture was then heated to 95°C for 10 minutes in a PCR machine, then placed on ice for 2 minutes. 50µl of dilution buffer (BSA) was added to the tubes and then centrifuged in a mini-centrifuge at 13,000 rpm for 1 minute to pellet cell debris. Samples were then either used immediately or stored at -20°C.

2.3 Genetic crosses of *Arabidopsis* lines

Arabidopsis plants approximately 6-10 inches tall were selected and flower buds chosen which had the stigma and petals just protruding from the bud. Buds from the same inflorescence that were too early or late to fit this category were removed, as were any other siliques or inflorescences on the plant. The selected buds were emasculated

under a stereoscopic microscope using jeweller's forceps to remove the sepals, petals and stamen, leaving only the pistil. Mature anthers from opened flowers of a separate plant were then used to pollenate the stigma of the emasculated bud, by rubbing one against the other. Seeds from the resulting siliques were collected after the siliques turned from green to light brown, after around 2 weeks.

2.4 DAPI staining of acid-fixed meiocytes

Inflorescences of unopened flowers of *Arabidopsis thaliana* were fixed in ice-cold 3:1 fixative (ethanol and glacial acetic acid). The fixative was changed at least 3 times over 2 days. Inflorescences were washed in 500µl citrate buffer (pH 4.5) 3 times for 5 minutes each time. Unopened buds were dissected out with a mounted needle and forceps. 250 µl of a digestive enzyme mixture (0.33% w/v pectolyase, 0.33% w/v cellulase) was added to the buds which were then incubated for 1.5 hours at 37°C in a moist chamber. Digestions were stopped by adding 500µl of cold sterile distilled water and were then kept on ice. Individual buds were transferred to microscope slides with a drop of water and then macerated with a mounted needle and brass rod. 10µl of 60% acetic acid was added to the macerated material and slides were placed on a 45°C hotplate for 30 seconds, and stirred briefly with a mounted needle. Another 10µl of 60% acetic acid was added and slides were left for another 30 seconds. 100µl of cold 3:1 fixative was applied to the slide with a pipette by forming a circle around the drop of acetic acid, as the droplet is repelled by it. Another 100µl was added, this time onto the drop, and the excess was allowed to drain off the slide. Slides were then dried using a hairdryer. Slides were then stained with 7µl DAPI (4',6-diamidino-2-phenylindole)

(10ng/ml in Vectashield) and coverslips placed on top. Slides were then viewed with an epi-fluorescence microscope. This protocol can be found in Armstrong, 2013.

2.5 Immunolocalisation on acid-fixed material ('Microwave technique')

Acid-fixed material was used to prepare slides as described above, minus the addition of DAPI. Slides were placed in a plastic slide rack taking care to leave at least 1cm spacing between slides. ~250ml of citrate buffer (10mM tri-sodium citrate, pH to 7.0 with 1M citric acid) was added to a pipette tip box (enough liquid to cover the level of slides when placed inside) and heated in the microwave for ~3 minutes until just beginning to boil. The rack of slides was then placed in the hot citrate buffer for 45 seconds then transferred to a separate pipette tip box containing PBS with 0.1% Triton X100 at room temperature, and left to cool for 5 minutes. 50µl of blocking solution (1% bovine serum albumin (BSA) in PBS) was then applied to each slide, covered with a piece of Parafilm (~2cm x 3cm) and incubated at room temperature for 20 minutes. Primary antibodies were diluted in blocking solution (two antibodies per slide, mixed together with blocking solution) at ratios from 1:250 to 1:1000 depending on the specific antibodies being used. Parafilm coverslips were removed from slides using tweezers and 50µl of primary antibody solution was applied to each slide and covered with a fresh piece of Parafilm. Slides were then incubated in a humid chamber at 4°C overnight (approximately 15-18 hours). Parafilm coverslips were then removed as before, and slides were washed in PBS containing 0.1% Triton X100, 3 times for 5 minutes per wash. Secondary antibodies conjugated to FITC or Texas Red, were diluted in blocking solution (1:50 ratio for FITC, 1:100 for Texas Red). 50µl of the secondary antibody mix was applied to the slides, and incubated in the dark, at room

temperature for 45 minutes. Slides were washed another 3 times in PBS/Triton before draining and counter-staining with 7µl DAPI in Vectashield (10ng/ml). Coverslips were then placed on top and were viewed with an epi-fluorescence microscope. This protocol can be found in Chelysheva et al., 2013.

2.6 Spreading immunolocalisation of fresh material and cytological analysis of PMCs

Inflorescences were picked from mutant and Columbia ecotype plants of *Arabidopsis thaliana* and were placed in a petri dish on a piece of wet filter paper to prevent drying. Unopened buds from 3-4 inflorescences were selected between 300-500µm for each slide. Buds were placed onto slides in a drop (~10µl) of 0.4% cytohelicase, 1.5% sucrose, 1% polyvinylpyrrolidone and anthers were dissected out under a stereoscopic microscope using a mounted needle and jeweller's forceps. Non-anther material was discarded to reduce background fluorescence. 10µl more cytohelicase was added during to the process to prevent drying, and then again after the dissection before being placed in a moist, 37°C chamber for 10 minutes to digest cell walls. After 10 minutes, anthers were macerated by tapping repeatedly with a brass rod (approximately 3mm diameter). Another 10µl of cytohelicase was applied, followed by 10µl 1% lipsol detergent to degrade cell membranes and aid spreading of the cells. Slides were then placed directly onto a 37°C hotplate for 5 minutes. Material was stirred with a mounted needle for the first 30 seconds and another 10µl lipsol was applied after ~3minutes to prevent drying. Material was then fixed by applying 20µl 4% paraformaldehyde (pH8 and stored at 4°C) under a fume hood, and leaving to dry for at least 2 hours. Paraformaldehyde was made to cover the whole surface of the

material, using a pipette tip. After drying, slides were given a brief rinse in sterile, distilled water (SDW) for ~two seconds, before washing 3 times in phosphate buffered saline (PBS) containing 0.1% Triton X100 for 5 minutes per wash, at room temperature. After washing, 50µl of blocking solution (1% bovine serum albumin (BSA) in PBS) was applied to each slide, covered with a piece of Parafilm (~2cm x 3cm) and incubated at room temperature for 20 minutes. Primary antibodies were diluted in blocking solution (two antibodies per slide, mixed together with blocking solution) at ratios from 1:250 to 1:1000 depending on the specific antibodies being used. Parafilm coverslips were removed from slides using tweezers and 50µl of primary antibody solution was applied to each slide and covered with a fresh piece of Parafilm. Slides were then incubated in a humid chamber at 4°C overnight (approximately 15-18 hours). Parafilm coverslips were then removed as before, and slides were washed in PBS containing 0.1% Triton X100, 3 times for 5 minutes per wash. Secondary antibodies conjugated to FITC or Texas Red, were diluted in blocking solution (1:50 ratio for FITC, 1:100 for Texas Red). 50µl of the secondary antibody mix was applied to the slides, and incubated in the dark, at room temperature for 45 minutes. Slides were washed another 3 times in PBS/Triton before draining and counter-staining with 7µl DAPI in Vectashield (10ng/ml). Coverslips were then placed on top and were viewed with an epi-fluorescence microscope. This protocol can be found in Armstrong and Osman, 2013.

2.7 Fluorescence In-Situ Hybridisation (FISH) labelling of meiotic chromosomes

DAPI stained slides (see above), were selected for FISH following analysis with an epifluorescence microscope. Slides were stood vertically in 100% ethanol for 10 minutes to dissolve the Vectashield under the coverslips, which were then gently removed from the slides. Slides were then washed in 4T (4x SSC (sodium chloride/sodium citrate buffer) and 0.05% Tween 20) for 1 hour, followed by a 10 minute wash in 2x SSC at room temperature. Cell cytoplasm was then digested with pepsin (0.01% pepsin in 0.01M HCl) at 37°C for 90 seconds, then slides were washed in 2x SSC for 10 minutes to remove the debris. Proteins were cross linked by washing in 4% paraformaldehyde (pH8 and stored at 4°C) for 10 minutes. Material was dehydrated with an alcohol series by washing for 2 minutes each in 70%, 90% then 100% ethanol before drying for 15 minutes. 5s and 45s probes were labelled by nick translation (Roche) to incorporated UTP conjugated to either biotin or digoxigenin. Some probes were directly labelled with Spectrum Green at this point. 3µl of each probe (2ng/µl) was mixed with 14µl of hybridisation mix (deionised formamide, 20X SSC and dextran sulphate (average Mw>500,000) to give a total of 20µl per slide. This was applied directly onto slides using a pipette, coverslips were gently placed on top and the edges were sealed with rubber solution. Slides were placed onto a 75°C hotplate for 4 minutes to denature chromosomal and probe DNA. Slides were then placed in a humid box, in the dark at 37°C overnight (approximately 15-18 hours), to allow probes to hybridise to the genomic DNA. Rubber solution was then removed with tweezers and coverslips gently removed before slides were washed in 50% formamide/2x SSC at 45°C, 3 times for 5 minutes each. Slides were then washed in 2x SSC at 45°C for 5 minutes, 4T at 45°C for 5 minutes followed by 4T at room temperature for 5 minutes. Slides were drained but

not allowed to dry before secondary antibodies were applied. Anti-digoxigenin conjugated to fluorescein isothiocyanate (FITC) was prepared in digoxigenin blocking solution (0.25g Boehringer Mannheim DIG nucleic acid blocking reagent in 4x SSC and 0.05% Tween20) (1: 50 ratio). Avidin (a biotin binding protein) conjugated to Cy3 was diluted in milk blocking solution (2.5g skimmed milk powder in 4x SSC and 0.05% Tween20 (1:200 ratio). 80 μ l of the first secondary probe was applied to each slide and covered with a square of Parafilm (approximately 2cm x 3cm) before being incubated at 37°C for 30 minutes in the dark. After this incubation, Parafilm slips were removed and slides washed 3 times in 4T, at room temperature, in the dark for 5 minutes per wash. The second secondary antibody was then applied (unless Spectrum Green was used to directly label one of the primary probes) and incubated in the same manner as the first, followed by 3 more washes in 4T. Slides were then washed through another alcohol series, as described before, and allowed to dry for ~15 minutes. 10 μ l of DAPI in Vectashield was then applied to slides and coverslips placed on top before viewing with an epi-fluorescence microscope. This protocol can be found in Armstrong, 2013.

2.8 EdU timecourse

Plant stems were cut with scissors under water, 5cm from the base of the primary inflorescence. Stems were then transferred into 10mM 5-ethynyl-2'-deoxyuridine (EdU) solution in phosphate-buffered saline (PBS), and left for 2 hours in glasshouse conditions to allow uptake of the EdU into the stem. EdU acts as a thymidine analogue and is incorporated into the DNA of S-phase cells. After the 2 hours, stems were transferred into sterile distilled water and left in glasshouse conditions for 10, 20, 25, 30, 32 or 36 hours, before inflorescences were removed and placed in ice-cold 3:1

fixative (ethanol:acetic acid). Fixative was changed at least 3 times over 2 days, and slides were prepared according to the protocol described above for DAPI staining of meiocytes. Before the addition of DAPI in Vectashield, EdU detection cocktail was prepared using Life Technologies Click-iT EdU Alexa Fluor 488 imaging kit according to manufacturer's instructions. Slides were washed in PBS for 10 minutes, were then drained and 15µl of the reaction cocktail was added to the slides on Parafilm coverslips. Slides were incubated at room temperature for 30 minutes, then coverslips were removed with forceps and slides were washed again in PBS, in the dark, for 10 minutes. Slides were drained and 7µl of DAPI in Vectashield (10ng/ml) was applied and coverslips placed on top. The slides were analysed using an epi-fluorescence microscope by identifying the latest EdU labelled meiotic stage at each given time point. This protocol can be found in Armstrong, 2013a.

2.9 Fluorescent tetrad analysis

Genetic crosses were performed between *Atsdg2-1* heterozygotes, confirmed by PCR-based genotyping, and plants homozygous for *qrt* and three fluorescent, pollen-expressed transgenes (eCFP, DsRED2, eYFP expressed by the LAT52 promoter) (Berchowitz and Copenhaver, 2008). The expression of the transgenes was confirmed cytologically using an Olympus BX-61 epifluorescence microscope. Double heterozygotes for all three fluorescence transgenes and the *Atsdg2-1* mutation were selected for in the progeny of this cross, and seeds collected. The next generation of plants were genotyped by PCR to find plants wild-type and homozygous for the *Atsdg2-1* mutation, then these plants were screened cytologically for *qrt* homozygosity combined with heterozygosity of the three fluorescence transgenes. Pollen was then

collected from these plants, using only flowers 5-30, by tapping open flowers into a 20 μ l droplet of PGM media (17% sucrose, 2mM CaCl₂, 1.625mM boric acid, 0.1% triton X-100) on a microscope slide, for 1 minute to release the pollen into solution. Coverslips were gently placed onto the droplet and slides were viewed immediately and scored accordingly, by eye.

Differences between CO frequency of wild-type and mutant for each interval was tested for statistical significance using a Z-test. The Perkins equation (Perkins, 1949), was used to calculate the genetic distance, in cM, for each interval: Distance = 100 x (Tetratype frequency + 6 x Non-parental-Ditype frequency)/2. The interference ratio (IR) was calculated for each interval, as described by Malkova et al, 2004. Using data from two adjacent intervals, I₁ and I₂, the genetic distance of I₁ is calculated using the Perkins equation, once taking into account only tetrads where there is no CO in I₂ (D₁), and then taking into account only tetrads where there is at least one CO in I₂ (D₂). The interference ratio is defined as IR= D₁/D₂. The genetic distance of I₁ will be reduced in the presence of a CO in I₂ if interference is detected, and IR<1. If no interference is detected, the genetic distance of I₁ will be independent of the presence of a CO in I₂, and IR=1. Statistical significance of differences between IR of wild-type and mutant for each interval, was tested using a Z-test (see Statistical procedures).

Online calculators used for the FTL analysis are available at <http://www.molbio.uoregon.edu/~fstahl>

2.10 Temperature experiment

Plants were grown under standard glasshouse conditions (see above), then transferred to a growth cabinet (Microclima series, Snijders Labs). The growth cabinet was

programmed to maintain a specific temperature (14, 20, 28 or 32°C) at 60% relative humidity, on a 16 hour day/8 hour dark cycle. Lights were set at 50% of maximum brightness (approximately 160 $\mu\text{mol m}^{-2} \text{s}^{-1}$). Plants were kept in the growth chamber for 3 days, then inflorescences were fixed in ice cold 3:1 fixative.

2.11 ASY1 immunostaining intensity quantification

Slides were prepared using previously described protocols for immunolocalisation, using fresh and fixed material (ref), and stained with rat anti-ASY1 antibody (1 in 5000 dilution). 5 μl of 6 μm , 0.3% relative intensity InSpeck Red microspheres (Life Technologies), was applied to slides simultaneously with 7 μl DAPI (10ng/ml in Vectashield) and coverslips placed on top. Meiocytes and microspheres were imaged using specific exposure times. Whole nuclei were analysed for mean signal intensity using Nikon NIS-elements software. Randomly selected, non-overlapping sections of axis, ~2-4 μm in length, were defined as regions of interest and analysed in the same way. Intensities were normalised based on mean intensity of the microspheres. Intensity raw data is shown in grey-scale values.

2.12 RT-PCR

Total RNA was extracted from wild-type (Columbia ecotype) buds of *Arabidopsis thaliana* using an RNeasy plant mini kit (Qiagen) according to manufacturer's instructions. Total cDNA was produced from this RNA by first strand synthesis, using a Superscript II kit (Invitrogen) according to manufacturer's instructions.

2.13 Statistical procedures

Mean ASY1 signal intensities between Col and *pch2-1* were compared using a two-tailed T-test, treated as independent samples. Intensities between synapsed and unsynapsed sections of axis/SC were analysed using a paired T-test.

Map distances calculated using the Perkins equation (see above), were analysed for statistical significance using a Z-test, as were interference ratios. The Z-test compares the proportion of two populations displaying a particular characteristic (below). The genetic distance in Morgans was treated as the proportion displaying the characteristic.

$$\frac{(\bar{p}_1 - \bar{p}_2) - 0}{\sqrt{\bar{p}(1 - \bar{p}) \left(\frac{1}{n_1} + \frac{1}{n_2} \right)}}$$

P_1 is the proportion of the first population (Genetic distance of the interval in Col o expressed in Morgans).

P_2 is the proportion of the second population (Genetic distance of the interval in *sdg2-1*).

n_1 Size of population 1 (Total Col o FTL tetrads analysed)

n_2 Size of population 2 (Total *sdg2-1* FTL tetrads analysed)

Null hypothesis

$H_0: P_1 - P_2 = 0$ (There is no difference in the proportion showing the characteristic between the two populations).

Chapter 3

Loss of AtSDG2 alters crossover frequency and distribution

3.1 Introduction

During meiosis, epigenetic marks, such as post-translational histone modifications or DNA methylation, influence the process of homologous recombination. The H3K4Me3 mark is known to mark recombination hotspot sites in budding yeast and mouse (Borde et al., 2009; Buard et al., 2009). The H3K4Me3 mark is generally associated with actively transcribed genes, open-chromatin and it is thought that at these regions, DNA would be more accessible to the recombination machinery. It is specifically found at the 5' end of genes, just downstream of the transcription start site in yeast (Liu et al., 2005), humans (Barski et al., 2007) and *Arabidopsis* (Choi et al., 2013). In budding yeast the loss of Set1, which contains a SET-domain to catalyse H3K4 methylation, causes a global reduction in meiotic DSB formation (Sollier et al., 2004), while in fission yeast, hotspots are marked with H3K9 acetylation rather than H3K4Me3 (Yamada et al., 2013). In budding yeast, Set1 is the sole H3K4 methyltransferase and is essential for normal levels of DSB formation (Borde et al., 2009; Sommermeyer et al., 2013). H3K4Me3 is also deposited at newly formed DSB sites by Set1 throughout the cell cycle (Faucher and Wellinger, 2010). However, a high-resolution DSB map based on Spo11-oligo sequencing concluded that although the H3K4Me3 mark is indeed correlated with DSB hotspots, they may not be the causative agent, and that nucleosome depleted regions, which are coincident with transcription start sites, showing more predictive power of hotspot localisation (Tischfield and Keeney, 2012).

A component of the Set1 complex, Spp1, binds to H3K4Me3 in the chromatin loop regions and also binds the axis-associated, SPO11 accessory protein, Mer2 (Sommermeyer et al., 2013; Acquaviva et al., 2013). This is consistent with the tethered loop-axis model of DSB formation, which describes why DSB hotspots are located in

the chromatin loops while the DSB machinery is found associated with the axis (Figure 1.5). In this model, Spp1 localises to the axis via an interaction with Mer2, tethering a H3K4Me3 site found in the loop to the axis, thus enabling DSB formation. In the *set1* mutant in budding yeast, DSB formation is reduced but not absent and appears to be promoted instead by H3K79 methylation produced by the histone methyltransferase, Dot1 (Ismail et al. 2014). Dot1 is unusual among histone methyl transferases due to its lack of a SET domain. There is no known Dot1 homolog in *Arabidopsis*.

In mice and humans, PRDM9 (originally named Meisetz), is a meiosis specific H3K4 trimethyltransferase (Hayashi et al., 2005). More recently, PRDM9 has also been shown to tri-methylate H3K36 (Eram et al., 2014). PRDM9 is essential for meiotic progression in mice, and is known to direct hotspot activity to specific genetic motifs, through binding to its zinc-finger domain (Grey et al., 2011). At these sites, PRDM9 produces the H3K4Me3 modification through its SET domain (Hayashi et al., 2005). These sites of H3K4Me3 modified nucleosomes surround a central nucleosome-depleted region (NDR) where both the PRDM9-binding consensus sequence and the recombination hotspot are located (Baker et al., 2014). The nucleosome remodelling which produces this NDR has been demonstrated to result from PRDM9 binding, rather than precede it (Baker et al., 2014). Mutation to the zinc-finger domain alters the proteins DNA-binding specificity and changes hotspot distribution within the genome (Grey et al., 2011). In the absence of PRDM9 in mouse, DSB hotspots move from PRDM9 associated H3K4Me3 sites, usually found in introns and intergenic regions, to PRDM9-independent H3K4Me3 sites, such as promoter regions (Brick et al., 2012). These ectopic sites are repaired inefficiently, resulting in sterility, suggesting that as well as creating a favourable environment for recombination, PRDM9 is also involved in recruitment of the recombination machinery.

The SET domain group (SDG) proteins are a family of histone modifying proteins related to the *Drosophila* SET domain protein groups; **S**uppressor of variegation [Su(var)], **E**nhancer of zeste [E(z)], and **T**rithorax (Trx), which all share the conserved histone modifying domain at their C-termini (Tschiersch et al., 1994). This domain is evolutionarily ancient and is found in all three of life's domains (Eukaryotes, Bacteria, Archaea) and viruses (Ng et al., 2007). The SET domain of the *Drosophila* Su(var)3-9, and their homologues in humans, yeast and plants, methylate the lysine residue of histone H3 at position 9 (H3K9), to impart a repressive chromatin state (Schotta et al., 2002; Rea et al., 2000). E(z) homologues methylate H3K27 and H3K9 to repress homeotic gene expression through its role in the polycomb repressive complex (Cao et al., 2002). Trithorax group (TrxG) proteins methylate H3K4 and H3K36 to overcome repression at actively transcribed genes from the H3K27 methylation modification, produced by polycomb complex group (PcG) proteins (Schuettengruber et al., 2007). The *Arabidopsis* genome contains 47 SET domain group proteins (<http://www.chromdb.org>), 12 of which are trithorax-related *SDG* genes. Only a few of these proteins have been characterised (reviewed in Yu et al. 2009; Liu et al. 2010).

ATX1/SDG27 and ATXR7/SDG25 are involved in suppression of flowering through activation of *FLOWERING LOCUS C (FLC)*, which is important for the winter-annual habit of *Arabidopsis* (Yun et al., 2012). This activation results from their H3K4 methyltransferase activity at this locus (Tamada et al., 2009; Pien et al., 2008). ATX1/SDG27 is also involved in the activation of genes which regulate flower development (Alvarez-Venegas et al., 2003). The PcG histone methyltransferase CLF (CURLYLEAF) is one of several proteins responsible for H3K27 methylation, mutants of which have been shown to have impaired somatic recombination, though meiotic recombination remained unaffected (Chen et al., 2014).

AtSDG2 (AtATXR3 – Arabidopsis Trithorax-Related 3) is a 2335 amino-acid trithorax-group-related histone methyl-transferase, previously reported to be the major H3K4 methyltransferase, capable of mono, di and tri-methylation of this residue (Guo et al., 2010). The protein is highly conserved in a range of plants including monocots, dicots, moss and algae, but has no significant structural similarities to other proteins, other than its SET domain which is found between amino acid residues 1849 and 1989 (Guo et al., 2010). The gene appears to be expressed in most, possibly all, tissues, though it is most highly expressed in flower bud tissue (Guo et al., 2010; Berr et al., 2010). Mutation to this gene causes dwarfism, impaired root growth and development, disrupted auxin signalling and the misregulation of hundreds of genes (Guo et al., 2010; Yao et al., 2013). AtSDG2 is also required for the activation of *FLC*. These defects most likely result from the severe reduction in H3K4Me3 in *Atsdg2* compared to wild-type (Berr et al., 2010). H3K4Me2 is also reduced, though to a lesser extent. *Atsdg2* mutant cells have a reduced G1 phase of their cell cycles, and show defective cell expansion, division and differentiation. The gene is also essential for normal fertility. *Atsdg2* mutants are completely female sterile while male fertility is impaired severely with very few functional pollen grains produced (Berr et al., 2010).

Generally, in plants, CO frequencies are increased in gene-dense regions. Species such as barley, maize, wheat and tomato all display the highest CO frequency in their gene-rich sub-telomeric regions, while CO formation is suppressed in the chromosome central regions, which are more repeat-dense (reviewed in Yelina et al. 2015). In *Arabidopsis*, hotspots are associated with H3K4Me3 as well as the histone H2A variant, H2A.Z, and low DNA methylation (Choi et al., 2013). *Arabidopsis arp6* mutants, which are defective in H2A.Z deposition, show a reduction in CO frequency, while *met1* mutants, which are defective in DNA methylation, show a redistributed CO

pattern. In *met1*, CO frequency unexpectedly decreases in the pericentromeric regions, where loss of DNA methylation might be expected to lead to de-repression of heterochromatin and an increased CO frequency (Yelina et al., 2012; Colome-Tatche et al., 2012; Melamed-Bessudo and Levy, 2012; Mirouze et al., 2012). The number of COs increases in the gene-rich chromosome arm regions, as well as centromere proximal regions, so the overall number of COs remains unchanged. As in budding yeast, *Arabidopsis* recombination hotspots are often found at gene promoter regions (Choi et al., 2013).

I have been investigating the effects of histone methyltransferase gene mutations on the number and distribution of crossovers in *Arabidopsis*. I have so far mainly focussed on *Atsdg2* mutants, where crossovers seem to form at more interstitial points on the chromosome, compared to wild-type. I have also shown that the number of crossovers may be increased, and that the effects of the mutation are restricted to the interference sensitive crossover pathway. These changes do not seem to result from early recombination defects or axis and synaptonemal complex morphogenesis.

3.2 Results

3.2.1 AtSDG2 is required for fertility but is dispensable for meiotic recombination

Arabidopsis lines were obtained from NASC (European Arabidopsis Stock Centre) with T-DNA insertions within the *AtSDG2* (*ATXR3*) gene. Homozygotes of *Atsdg2-1* (WISCDsLox361D10) and *Atsdg2-3* (SALK_021008) (previously described in Berr *et*

al, 2010) show a dwarf phenotype and are sterile, despite being reported to produce ~40% viable pollen (Figure 3.1). Heterozygotes of both lines are indistinguishable from wild-type plants. *Atsdg2-1* and *Atsdg2-3* contain their T-DNA insertions in exons 1 and 4 respectively (Figure 3.2). Homozygous plants also have abnormal root development and show slower vegetative growth compared to Col 0 (Yao *et al*, 2013). It has been previously reported that the *AtSDG2* gene is expressed strongly in bud tissue, based on RT-PCR and *in situ* hybridisation (Berr *et al*, 2010). The increased bud-tissue expression, sterility of the mutants and association of the H3K4Me3 mark at recombination hotspots, together suggested that *Atsdg2* mutants might display meiotic defects and was worth investigating.

Mutants which were homozygous for *Atsdg2-1* and *Atsdg2-3* were confirmed by genotyping (Figure 3.3). DAPI staining was performed on chromosome spread preparations of fixed material from Col 0 and the *Atsdg2-1* mutant (Figure 3.4). Meiotic chromosomes in Col 0 and *Atsdg2-1* meiocytes showed linear chromosome axes at leptotene (Figure 3.4 A and I), which paired along their lengths during zygotene (Figure 3.4 B and J) and displayed fully paired chromosomes at pachytene (Figure 3.4 C and K). Chromosomes began to desynapse and condense at diplotene (Figure 3.4 D and L) and 5 bivalent chromosomes were visible at diakinesis (Figure 3.4 E and M) and metaphase I (Figure 3.4 F and N). Equal chromosome segregation then took place in both meiotic division stages (Figure 3.4 G and O). In Col 0, tetrads were produced with 5 chromosomes per nucleus (Figure H), while in *Atsdg2-1*, many tetrad cells possess only three nuclei (Figure 3.4 P). The frequency of tetrads showing this conformation was previously reported at ~50% (Berr *et al*, 2010) and a roughly similar proportion displayed this phenotype in my studies.



Figure 3.1: The *sdg2-1* homozygote shows a clear dwarf phenotype compared to the *sdg2-1* heterozygote and Col 0 plants. The *sdg2* phenotype is visibly identifiable ~1 week following germination, as leaves are slightly curled.



Figure 3.2: Schematic the *AtSDG2* gene showing positions of T-DNA insertions in the two *sdg2* mutants. Exons are shown as black boxes, untranslated regions in grey.

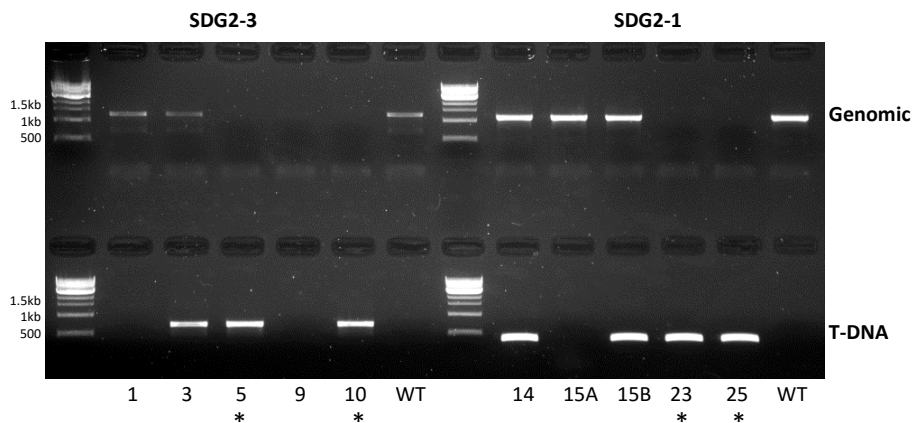


Figure 3.3: Genotyping *sdg2-1* and *sdg2-3* mutants by PCR of genomic DNA and T-DNA. Plant which displayed the *sdg2* phenotype (stars) all successfully amplified a product using the T-DNA specific primer set but failed to amplify the genomic DNA region of *SDG2*.

Metaphase I nuclei in *Atsdg2-1* show that the mutant is not defective in formation of the obligate CO, as no univalent chromosomes were observed in several hundred cells analysed, where univalents would be noticeable (metaphase I onwards) (Figure 3.5). Chromosome fragmentation was observed in only one of the *Atsdg2-1* meiocytes, indicating that DSB repair efficiency may be very mildly affected, though this was the only instance of fragmentation observed after viewing several hundred *Atsdg2-1* metaphase I nuclei (Figure 3.5 A, yellow arrow). Metaphase I chromosomes initially appeared unremarkable, as they do not display any obvious defects, but appeared distinct from Col o upon closer inspection, often showing shapes that may be indicative of an increased number or a redistribution of COs to positions more proximal to the centromere (Figure 3.5 B, red arrows). A chiasma count, suggested a significant difference in chiasma frequency between Col o (9.00 per cell; n=29) and *Atsdg2-1* (10.95; n=20) (T-test $P < 0.001$) (Figure 3.5 C), although some caution is required as FISH probes were not used in this analysis.

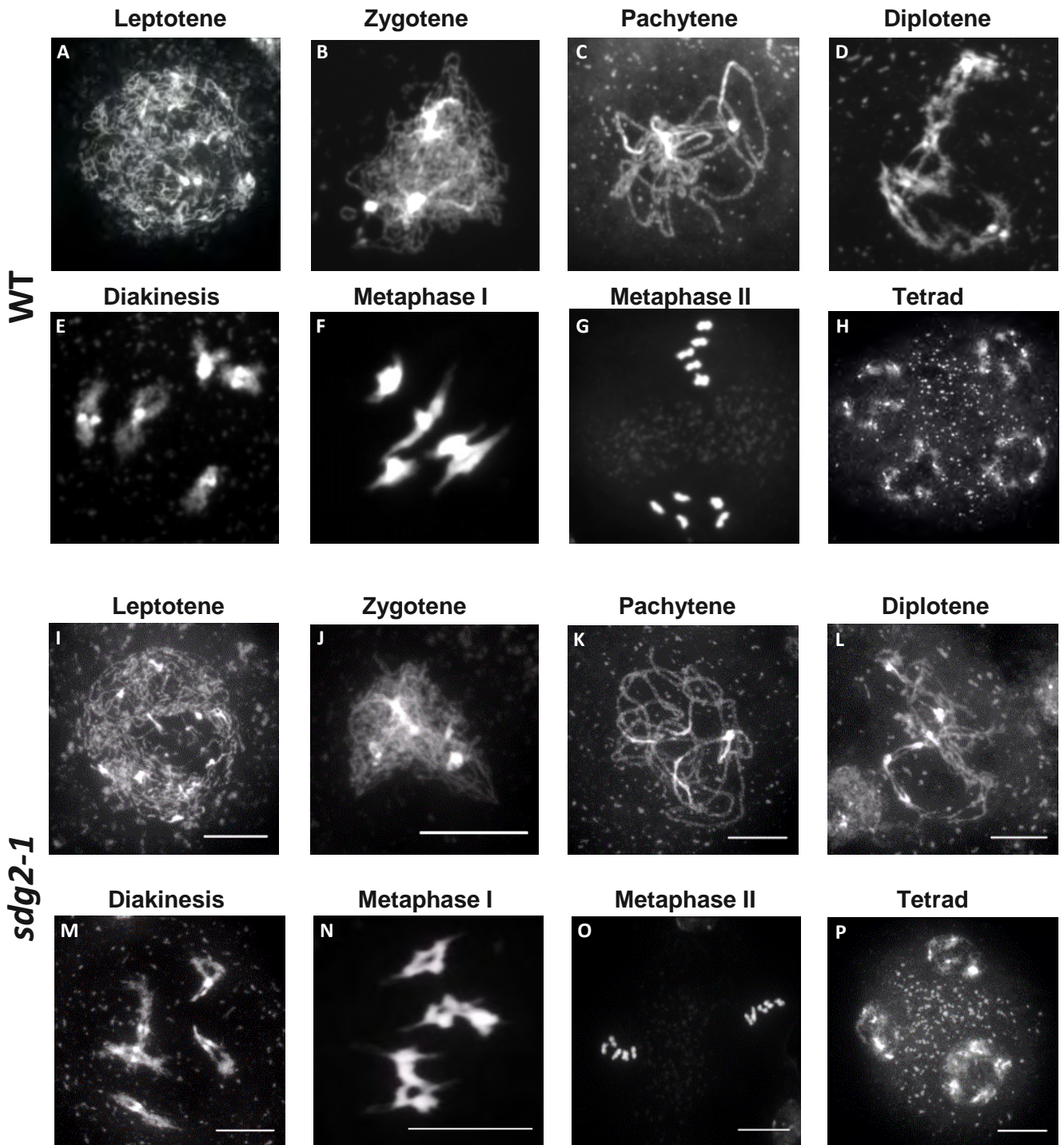
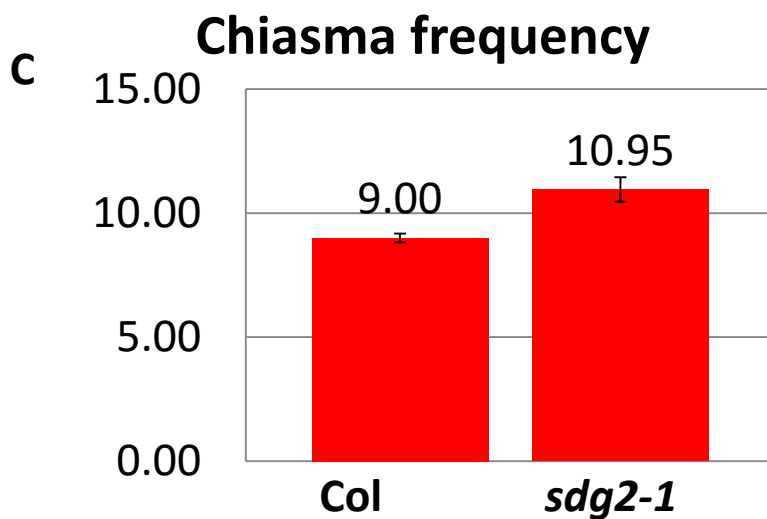
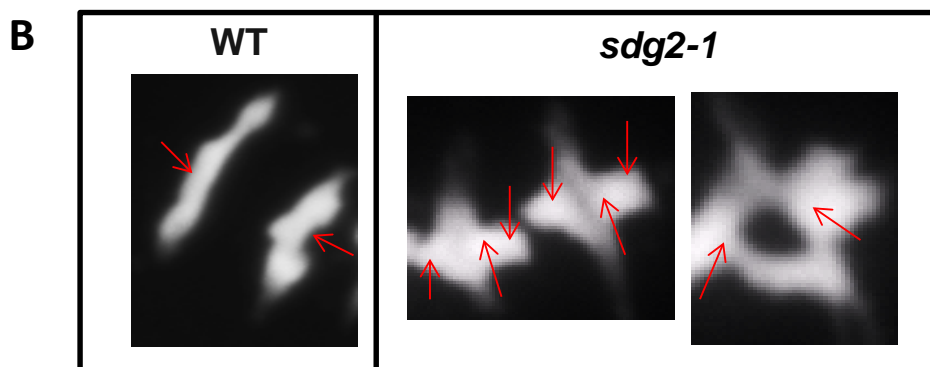
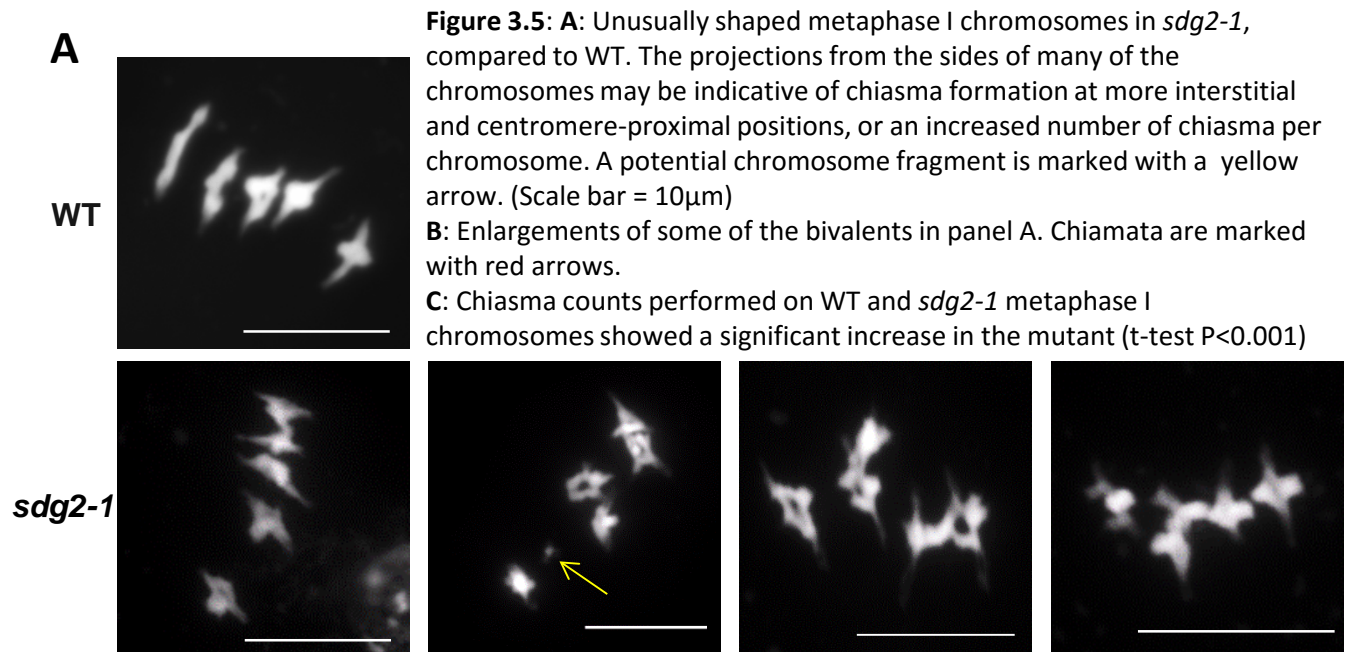


Figure 3.4: Meiosis in *Atsdg2-1* appears to progress in the same way as in wild-type, until the tetrad stage when ~50% of cells display 3 nuclei instead of 4. The shape of the metaphase I chromosomes may be indicative of an altered pattern of crossover formation, either resulting from an increased number of them or a re-distribution. More metaphase I cells are shown in Figure 3.5
Scale bar = 10 μ m



3.2.2 Transcription of *AtSDG2* and gene expression in an *Atsdg2-1* background

A previous study on *Atsdg2-1* performed a microarray analysis of transcripts obtained from young flower buds, identifying 452 genes which were downregulated more than two-fold compared to Col 0, and 273 which were upregulated (Berr et al, 2010). The researchers identified 11 genes involved in gametophyte development which were misregulated in *Atsdg2-1*, along with an additional 7 which were identified by q-PCR. I cross-referenced the list of genes from their microarray experiment, against a list of 115 known meiotic genes (list from Yang et al, 2011 plus meiotic genes identified since publication) to investigate whether any meiotic effects in the mutant might be caused by the altered transcription profile. None of the known meiotic genes were among the list of genes which are misregulated in *Atsdg2-1*. Microarray analysis of *Atsdg2-1* was also performed by Guo et al, 2010, showing 321 genes downregulated by more than four-fold compared to wild-type and 271 genes upregulated. Raw data from this study was unavailable for analysis. The data in this study was generated from transcripts of 12 day old whole seedlings, so may not be as informative for studying a potential meiotic role, as the data from Berr et al, 2010.

The same study by Berr et al, reported that *AtSDG2* was expressed at high levels in anthers and ovules, based on RT-PCR experiments. To see how this up-regulation compared to other SET-domain group genes, I took a list of the 42 known SET genes from The Arabidopsis Information Resource (<https://www.arabidopsis.org>) and then analysed them with Cuffdiff, for differential expression using PMC specific RNAseq data generated by Chen et al., 2010 (Analysis performed by Jianhua Yang, Coventry University). The results of this analysis are shown in Table 3.1. *AtSDG2* does not show

particularly high expression in meiocytes, based on its RPKM (Reads Per Kilobase of transcript per Million mapped reads) value, and the variability between the two replicates suggests that its expression during meiosis may not be significant, in contrast to the findings reported in Berr et al, 2010. *AtASHH3* (*SDG7*), which encodes a H3K36 methyltransferase, appears to show a higher expression, relative to the other genes in this family. Previous work involving this mutant showed no obvious developmental phenotype. It should also be noted that although the RPKM of *AtASHH3* (~23) is high relative to the other genes analysed in this set, it would still be considered a low value RPKM. Also, most known meiotic genes, produce low RPKM values, while genes with no meiotic involvement may still produce high RPKM values, and high variability between experimental replicates for *AtSDG18* and *AtSDG13* (*AtSUVRI*) means that these values may not be significant (Jianhau Yang, personal communication).

	Gene	RPKM		Significant?
		E1	E2	
AT1G02580	MEA	0.168619	0.118236	0
AT1G05830	ATX2	4.73107	5.56675	0
AT1G17770	SUVH7	0.029262	0.020518	0
AT1G04050	SUVR1	10.957	14.7144	1
AT1G26760	SDG35	1.18598	1.51433	0
AT2G05900	SDG11	0.448506	0.314005	0
AT2G19640	ASHR2	1.74843	2.58165	0
AT2G23380	CLF	2.38055	3.35708	0
AT2G33290	SUVH2	0.62114	0.748615	0
AT2G44150	ASHH3	22.7932	23.6536	0
AT2G22740	SUVH6	1.80501	2.44521	0
AT2G24740	SDG21	0.727795	0.629147	0
AT3G04380	SUVR4	1.22829	1.92643	0
AT3G59960	ASHH4	0	0.089771	0
AT3G61740	ATX3	3.28172	5.03709	1
AT4G02020	EZA1	2.443	2.89602	0
AT4G15180	SDG2	2.95525	4.0193	1
AT4G27910	ATX4	2.83831	4.64577	1
AT4G30860	ASHR3	1.68158	2.98419	0
AT4G13460	SDG22	2.96066	3.17674	0
AT5G06620	AT5G06610,AT	3.92175	4.34912	0
AT5G13960	SUVH4	3.33019	4.28977	0
AT5G17240	SDG40	3.52203	3.51777	0
AT5G43990	SDG18	10.7052	13.6073	1
AT5G53430	SDG29	5.53037	6.11699	0
AT5G09790	SDG15	3.14525	4.28682	0
AT5G24330	ATXR6	6.4447	6.41129	0
AT5G42400	ATXR7	0.94561	0.830167	0

Table 3.1: RPKM (Reads Per Kilobase of transcript per Million mapped reads) of known SET-domain group genes in PMC-specific RNAseq data generated by Chen et al, 2010. Results marked with a 1 in the significance column are deemed to show too much variation between experimental replicates (E1 and E2), and are therefore unreliable. SDG2 is indicated by a red arrow, as the subject of this study, ASHH3 is also indicated due to a notably high RPKM.

3.2.3 *Atsdg2-1* PMCs show reduced levels of H3K4Me3

Immunostaining of early prophase I PMCs was performed with antibodies against the meiotic axis component ASY1, which was dual-localised with H3K4Me3, to investigate whether H3K4Me3 levels are reduced in meiocytes in *Atsdg2-1*. Previously published work has shown that in *Atsdg2-1*, H3K4Me3 levels are reduced in root tip cells and whole seedling samples but meiocytes have not been looked at specifically (Guo et al, 2010, Yao et al, 2013). Fluorescent microspheres (InSpeck, Life Technologies) were applied to chromosome spread preparations of fresh material (Lipsol spreading technique, see Materials and Methods) as a control for quantifying mean fluorescence intensity more accurately between sets of slides. Microspheres were imaged from sets of slides for Col o (n=12) and *Atsdg2-1* (n=13), using specific exposure times, ie; all the microspheres on the Col o and *Atsdg2-1* slides were exposed for the same duration. An additional, built-in control for this experiment is the fact that primary and secondary antibody solutions are prepared in single tubes, so all the slides in a set (wild-type control and mutant), are all treated with the same antibody solution, eliminating variability in antibody concentrations. Early prophase I PMCs (based on the appearance of ASY1 staining), were imaged from the same slides for wild-type (n=33) and *Atsdg2-1* (n=29) (Figure 3.6). Signal intensity was quantified for whole nuclei using Nikon NIS-Elements software and adjusted based on the intensity of the fluorescent microspheres (*Atsdg2-1* adjusted to 87% of original value). *Atsdg2-1* PMCs showed a significant reduction in H3K4Me3 signal to 68% of the mean level seen in Col o (Two-tailed T-test $p < 0.0001$) (Figure 3.7). This indicates that other histone methyltransferases responsible for making the H3K4Me3 modification are not able to fully compensate for the loss of AtSDG2 during meiosis.

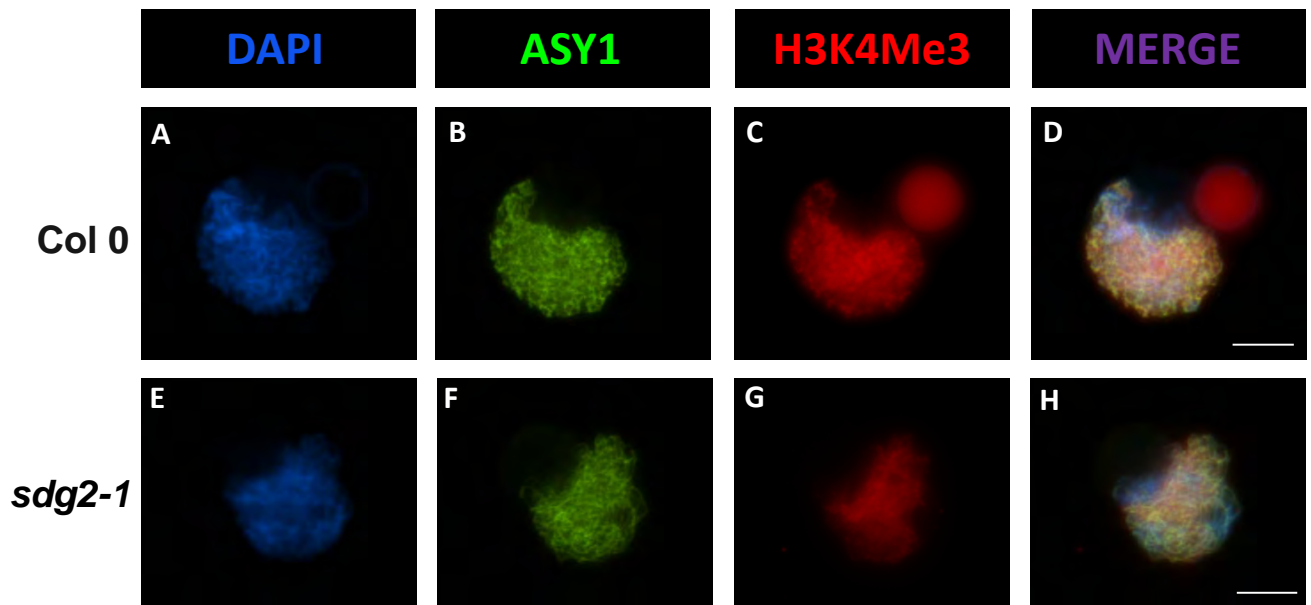


Figure 3.6: Immunolocalisation of ASY1 and H3K4Me3 in Col 0 (A-D) and *sdg2-1* (E-H) leptotene meiocytes. One of the red fluorescent microspheres used as a control for measuring fluorescence intensity is visible next to the Col 0 cell. Scale bar = 5 μ m

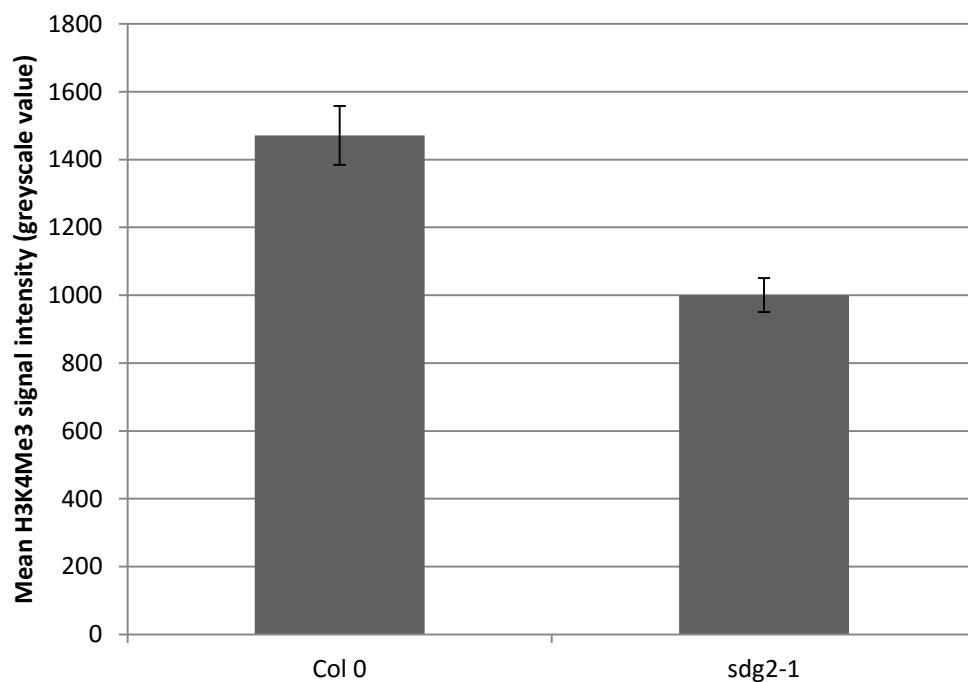


Figure 3.7: Mean intensity of the H3K4Me3 signal in Col 0 and *sdg2-1* nuclei, measured in greyscale units.

3.2.4 Early recombination, axis structure and synaptonemal complex morphogenesis appear unaffected by the *Atsdg2-1* mutation

Dual-immunostaining of the axis protein ASY1 and the synaptonemal complex transverse filament protein ZYP1, was performed to investigate the structure of the axis and synaptonemal complex in Col o and *Atsdg2-1* PMCs, using lipsol-spread preparations of fresh bud tissue. Slides were analysed using SIM (structured illumination microscopy)(Applied Precision OMX Blaze, University of Dundee). At zygotene stage, Col o PMCs show bright, linear ASY1 staining in the unsynapsed regions of chromosome axis, arranged in alternating domains of hyper and lower abundance (Figure 3.8 A and C). This signal becomes less bright and more diffuse in the synapsed regions of the chromosomes. The synapsed chromosome regions are stained with ZYP1, which also produces a linear signal. Based on ASY1 and ZYP1 staining, axis morphology and synapsis appear wild-type-like in the *Atsdg2-1* mutant (Figure 3.8 B and D). The organisation of ASY1 into alternating domains of hyper abundance and lower abundance appears in *Atsdg2-1* as it does in WT (Figure 3.8 C and D). ASY1 also appears to become less bright and more diffuse in the regions where ZYP1 has polymerised in *Atsdg2-1*. The cohesin protein SMC3 was also dual immunolocalised with ASY1, to further investigate whether any structural differences are present between Col o and *Atsdg2-1*. SMC3 was dual-localised with ASY1, and imaged with a conventional epi-fluorescence microscope (Figure 3.9). In Col o zygotene PMCs, staining of SMC3 overlaps with ASY1 on unsynapsed chromosome regions, and brightness approximately doubles in synapsed regions, as would be expected from two overlapping signals. Analysis of zygotene PMCs from *Atsdg2-1* did not reveal any noticeable differences to wild-type.

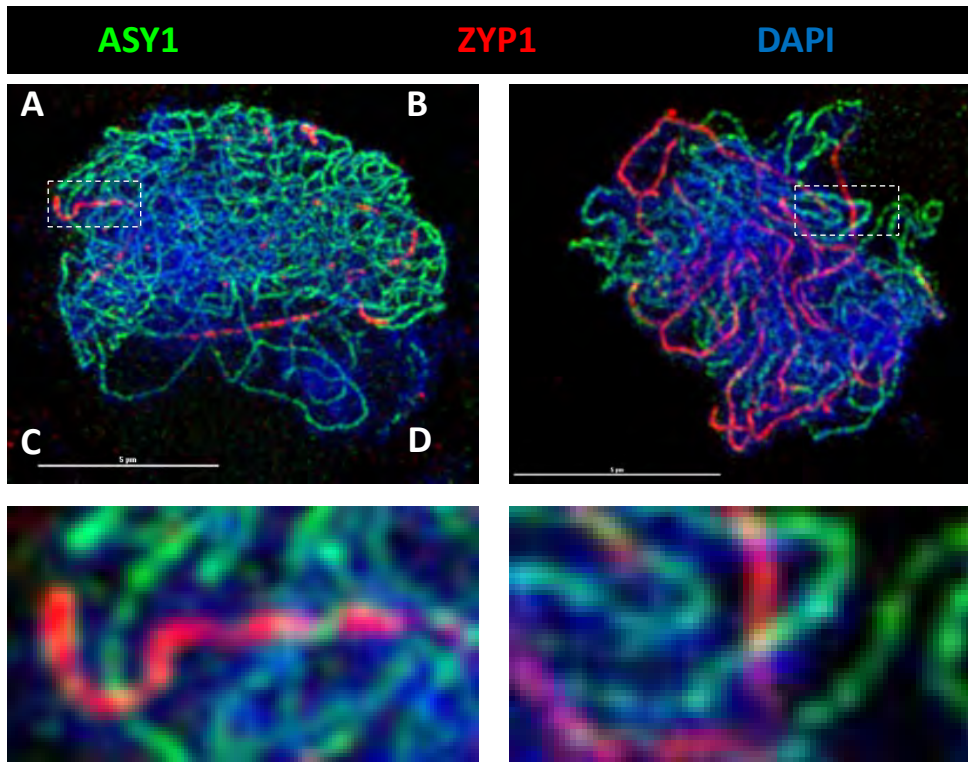


Figure 3.8: Dual immunolocalisation of ASY1 and ZYP1 in Col 0 and *Atsdg2-1* PMCs during zygotene, using SIM super-resolution microscopy. The domains of hyper and lower abundance of ASY1 can be seen in both WT and *Atsdg2-1*. ZYP1 appears to produce a more uniform linear signal, compared to ASY1, and shows no apparent difference between Col 0 and *Atsdg2-1*.

Scale bars = 5 μ m

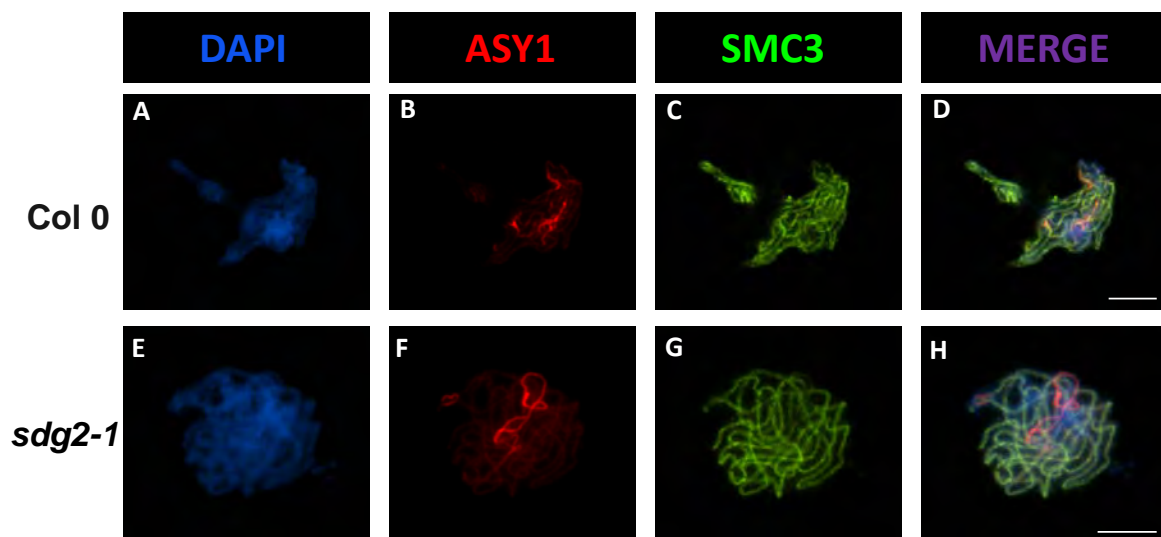


Figure 3.9: Dual-immunolocalisation of ASY1 and SMC3 in Col 0 and *Atsdg2-1* PMCs

Scale bar = 5 μ m

I then decided to investigate whether the early stages of recombination in *Atsdg2-1*, by immunolocalisation of the recombinase enzyme RAD51, which is crucial to the repair of DSBs by recombination (Li et al., 2004). RAD51 was dual immunolocalised with ASY1 and foci were counted in early prophase I PMCs, identified based on the linear appearance of ASY1 staining (Figure 3.10). RAD51 appears to localise in comparable numbers in Col o (139 n=3 SD=4.1) and *Atsdg2-1* (144 n=5 SD=2.4), suggesting that DSBs are formed at similar levels to those in Col o, and that the early stages of recombination proceed as normal in *Atsdg2-1*. The meiosis-specific recombinase DMC1 also localises to *Atsdg2-1* chromosomes in a similar manner to Col o, forming numerous foci in early prophase I (Figure 3.11), as does the MutS homologue MSH4, which is involved the stabilisation of joint-molecules during homologous recombination (Figure 3.12). Together, these results indicate that meiotic recombination events initiate in similar numbers in *Atsdg2-1* and Col o.

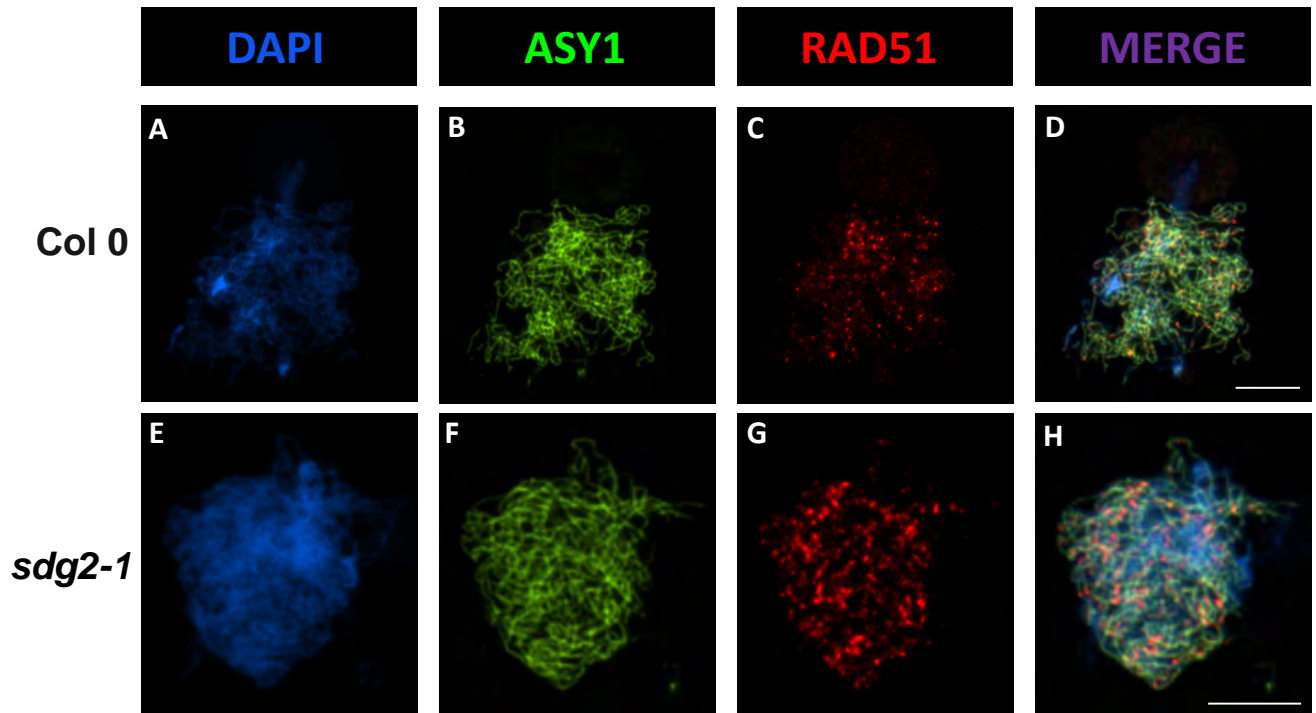


Figure 3.10: Dual-immunolocalisation of ASY1 and RAD51 in Col 0 and *Atsdg2-1* PMCs.

Scale bar = 5 μ m

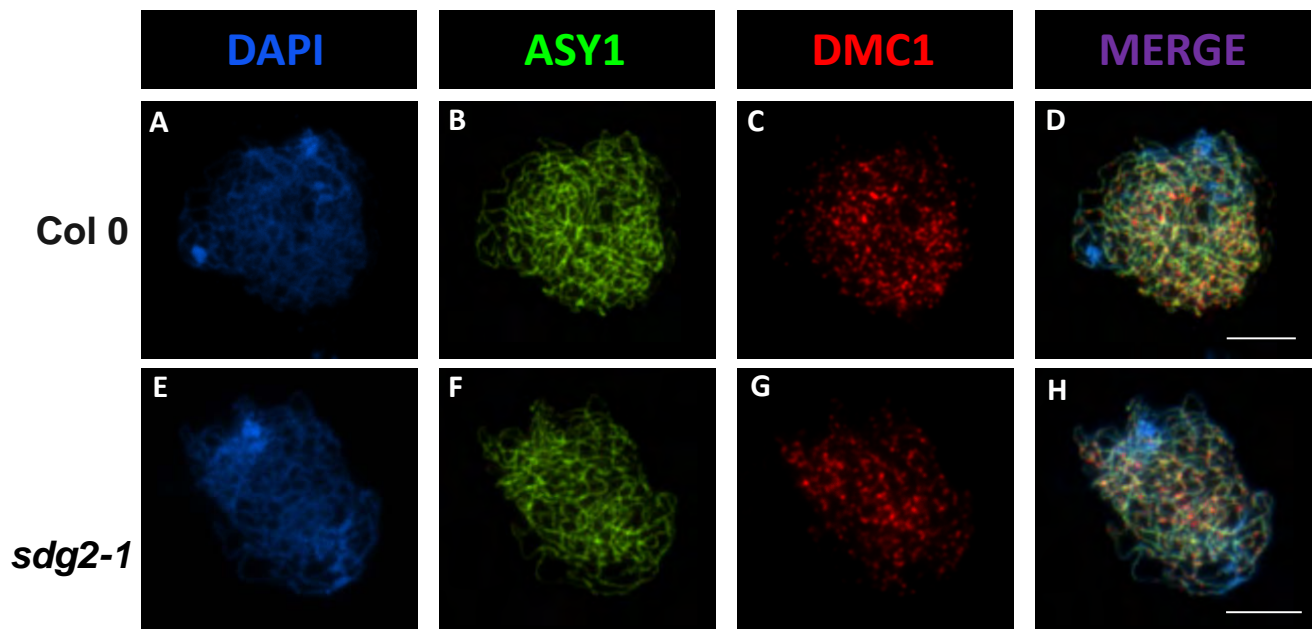


Figure 3.11: Dual-immunolocalisation of ASY1 and DMC1 in Col 0 and *Atsdg2-1* PMCs.

Scale bar = 5 μ m

3.2.5 Crossover numbers are increased in *Atsdg2-1* compared to Col o

Dual immunolocalisation of ZYP1 and MLH1, which marks sites of class I CO formation, was performed to investigate the effect of the *Atsdg2-1* mutation on CO number and any possible effect on CO interference (Figure 3.13). In Col o cells, 9.4 MLH1 foci are reportedly observed on pachytene chromosomes, similar to the average number of COs (Jackson et al., 2006). In this study the counts for Col o, pachytene nuclei showed a mean of 10.0 MLH1 foci (n=6, SD=0.89) while in *Atsdg2-1*, the mean number of MLH1 foci was 13.1 (n=12, SD=0.90). This is consistent with the observed increase in CO frequency based on chiasma counts. HEI10 can also be used to observe the number of interfering CO at an earlier stage than MLH1 (Chelysheva et al., 2012). In *Sordaria macrospora*, HEI10 forms different classes of foci size during leptotene, the larger foci progressing to form COs, while the smaller ones are resolved as NCOs (De Muyt et al., 2014). HEI10 was dual immunolocalised with ASY1 and large HEI10 foci were counted at leptotene (Figure 3.14). Col o meiocytes in early prophase I displayed an average of 9.8 large HEI10 foci (n=8, SD=1.28) while *Atsdg2-1* displayed 12.5 (n=8, SD=1.20). Together these data indicate that in the absence of AtSDG2, the total number of COs is increased, and that this increase is consistent with the observed increase based on chiasma scoring of DAPI stained metaphase I chromosomes.

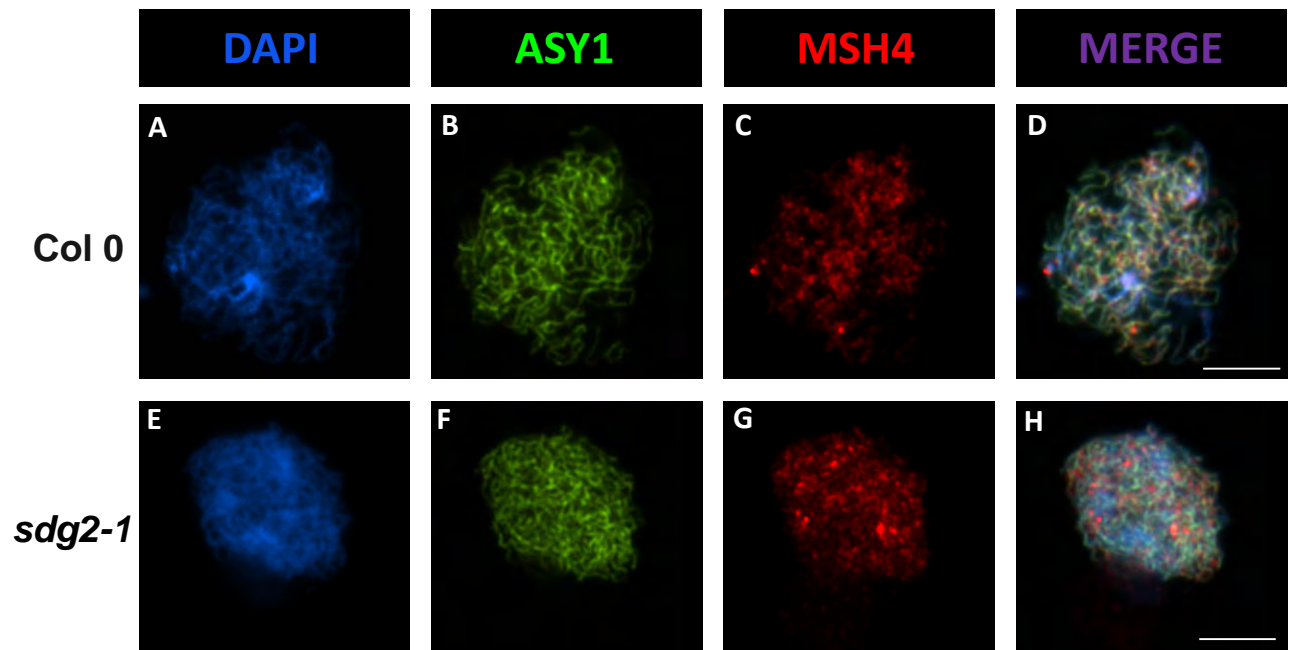


Figure 3.12: Dual-immunolocalisation of ASY1 and MSH4 in Col 0 and *Atsdg2-1* PMCs.
Scale bar = 5 μ m

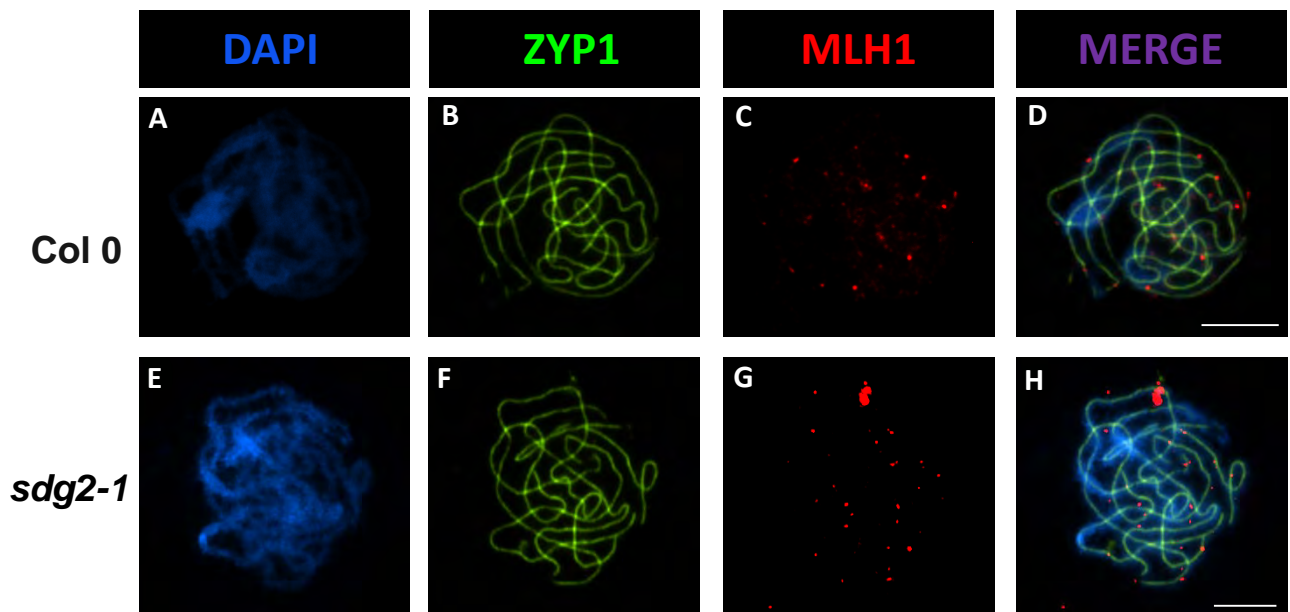


Figure 3.13: Dual-immunolocalisation of ASY1 and MLH1 in Col 0 and *Atsdg2-1* PMCs.
Scale bar = 5 μ m

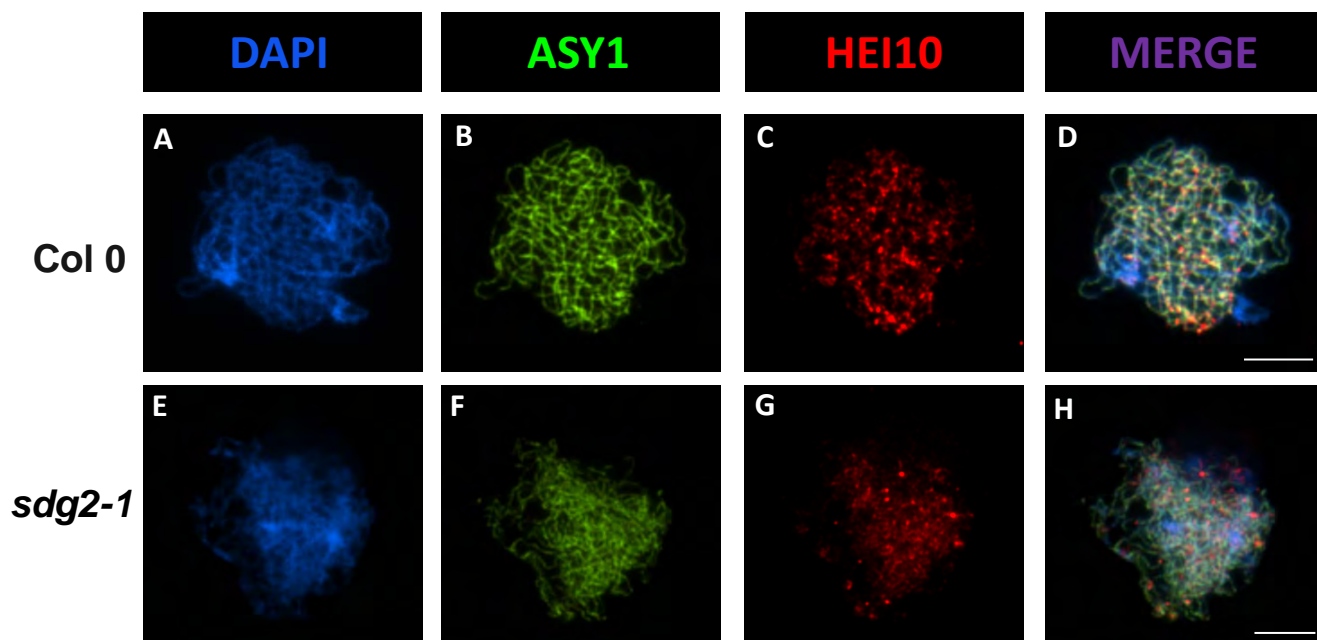


Figure 3.14: Dual-immunolocalisation of ASY1 and HEI10 in Col 0 and *Atsdg2-1* PMCs.

Scale bar = 5 μ m

3.2.6 Crossover distribution is altered in *Atsdg2-1*

I decided to further investigate the possible increase in CO formation in *Atsdg2-1*, using the fluorescent-tagged-line (FTL) system (Berchowitz and Copenhaver, 2008; Francis et al., 2007)(FTL lines provided by G. Copenhaver)(Figure 3.15). Three genetically linked fluorescence transgenes are expressed post-meiotically in pollen (See Appendix E for genomic locations). These fluorescence genes are in a *quartet* (*qrt*) mutant background. The *qrt* mutation prevents the separation of the four meiotic products (pollen grains). Different colour combinations are produced in individual pollen tetrads depending on the position of COs which occur between the transgenic markers. This allows direct visualisation of meiotic CO events for a single meiosis, which occur within the interval. The system was used to analyse the genetic distance between the markers in control Col o plants and in the *Atsdg2-1* background. Six genetic intervals were analysed in *Atsdg2-1* and Col o, in three pairs of connected intervals located on two different chromosomes (2 and 5); I2f-I2g, I5a-I5b and I5c-I5d (see Appendix A for raw data). The total number of tetrads analysed in *Atsdg2* is less than for Col o in all intervals, due to the strong reduction in pollen formation in the mutant, though in total 4 times as many flowers were analysed from *Atsdg2-1* compared to Col o (231 vs 57).

The map distances determined from the FTL analysis are summarised in Figure 3.16. Map distance in I2f did not show any statistical difference between Col o and *Atsdg2* backgrounds (I2f; 6.14cM Col o vs 6.60cM *Atsdg2-1*; Z-test P=0.56) but a significant decrease in genetic distance was observed in *Atsdg2-1* compared to Col o in the adjacent interval, I2g (5.05cM Col o vs 3.60cM *Atsdg2-1* P=0.03). Both pairs of intervals on chromosome 5, I5a, I5b, I5c and I5d all displayed significantly increased genetic distance in *Atsdg2-1* compared to Col o (I5a 25.1cM Col o vs 30.2cM *Atsdg2-*

1. I5b 16.0cM Col o vs 19.8cM *Atsdg2-1*. I5c 6.3cM Col o vs 11.8cM *Atsdg2-1*. I5d 6.8cM vs 11.7cM *Atsdg2-1*, $P < 0.0001$ for all except I5b: $P = 0.0005$).

The FTL system can also be used to measure genetic interference across each interval, by taking into account whether the presence of a CO in the adjacent interval has reduced the probability of one occurring within the interval in question. The interference ratio (IR) is calculated using the Malkova method (Malkova et al., 2004), which essentially uses the Perkins equation (Perkins, 1949) to calculate map distances, when at least one CO is present in the adjacent interval and when there is no CO in the adjacent interval. The ratio between these two map distances is used to estimate the strength of interference originating from one interval, acting on the adjacent interval. When CO formation is entirely independent of the presence of a CO in the adjacent interval, $IR = 1$. As the strength of interference increases, IR decreases, until it reaches 0, in the case of total interference. Positive interference, where the presence of a CO increases the likelihood of another occurring in the adjacent interval, is indicated by IR values higher than 1.

To summarise the data shown in Table 3.1, a small increase in IR was observed in the I2fg interval pair in *Atsdg2-1* compared to Col o, though this was not statistically significant. A significant increase in IR was recorded in *Atsdg2-1* compared to Col o for the I5ab interval pair, indicating a decrease in the level of CO interference. I5cd showed the opposite, with the IR showing a decrease in *Atsdg2-1* compared to Col o, indicating an increase in interference, though both intervals only showed borderline statistical significance ($P = 0.06$ for both intervals).

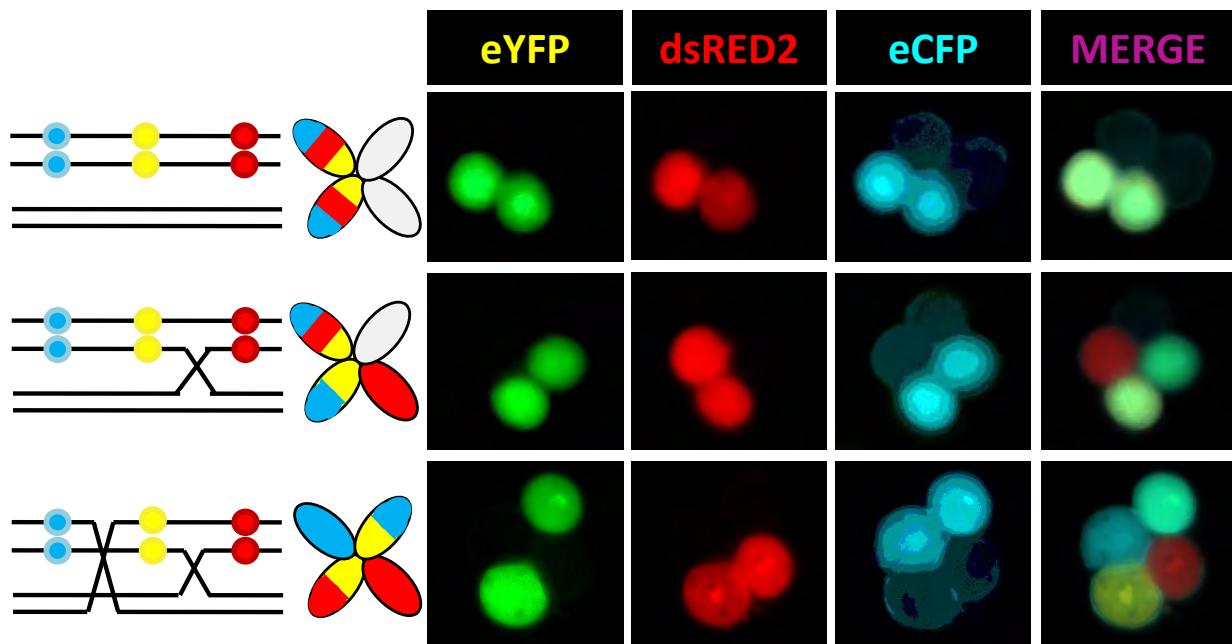
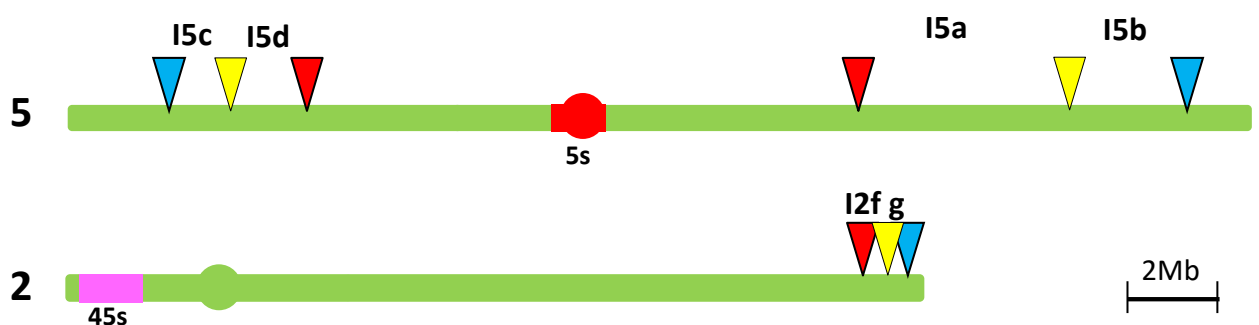


Figure 3.15: Crossover analysis using fluorescently tagged lines. The four pollen products of each meiosis remain connected due to the *quartet* mutation. Crossovers which occur within the genetic interval produce colour patterns other than the parental, non-recombinant pattern (top). (eYFP signal appears green due to the filter used).
 Bottom: The locations of the fluorescent transgene markers used in our study. 5s and 45s rDNA regions are also shown.



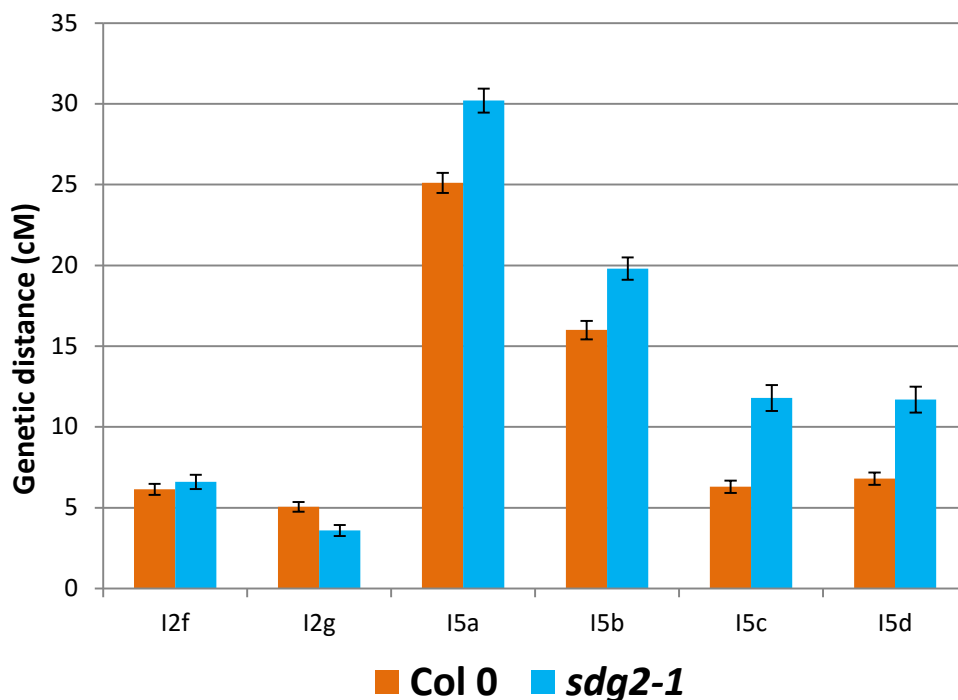


Figure 3.16: Fluorescent tetrad analysis of different intervals within the *Arabidopsis* genome. *sdg2-1* mutants display an increased map distance at 4 out of 6 intervals tested. Error bars = SEM

	I2f	I2g	I5a	I5b	I5c	I5d
Col 0	0.116	0.113	0.345	0.271	0.458	0.461
<i>sdg2-1</i>	0.273 (P=0.29)	0.260 (P=0.31)	0.480 (P=0.004)	0.364 (P<0.001)	0.213 (P=0.06)	0.212 (P=0.06)

Table 3.2: CO interference ratios (IR) for the 6 genetic intervals calculated from FTL data from Col 0 and *sdg2-1*. IR=1 in the absence of interference. Statistical significance was calculated using a Z-test (P values shown in table).

3.2.7 The increased CO frequency in *Atsdg2-1* is not due to an increase in class II COs

Atsdg2-1 was crossed with *Atmsh5*, which is required for the formation of class I COs. Chiasma counts of WT metaphase I cells showed an average chiasma count per cell of 9.00 ($n=29$) (Figure 3.17). *Atsdg2-1/Atmsh5* (1.28 chiasma per cell, $n=53$) and *Atmsh5* (1.21 chiasma per cell, $n=56$) were clearly reduced compared to Col 0, though were not significantly different from each other (T-test; $T_{(109)} = 0.36$, $P = 0.71$) and were similar to previously published work on *Atmsh5* (Higgins, et al. 2008)(Figure 9). A slightly higher variance was observed in *Atsdg2-1/Atmsh5* (1.47) compared to *Atmsh5* (0.68), though this was not statistically significant (ANOVA $P=0.73$).

To address the same question via a different approach, immunostaining experiments with MUS81, which marks the sites of class II, interference-insensitive COs, does not show any clear difference in *Atsdg2-1*, compared to Col 0 which displays 2 MUS81 foci and *Atsdg2-1* displaying only 1 at late pachytene stage (both $n=1$), indicating that the effect on CO distribution may not result from a change in the control of class II CO formation (Figure 3.18), although since $n=1$, repeat experiments would need to be performed before a confident interpretation can be made.

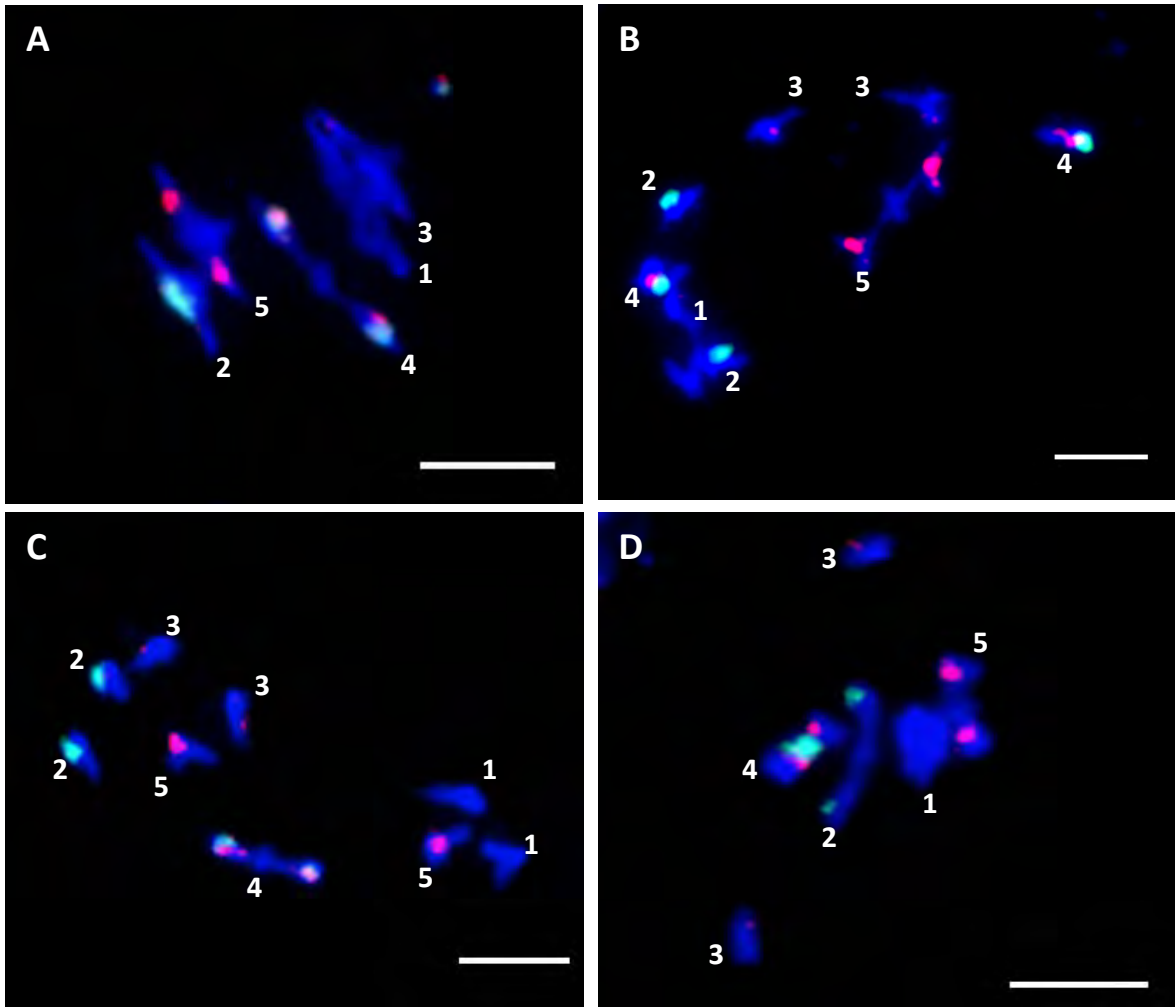
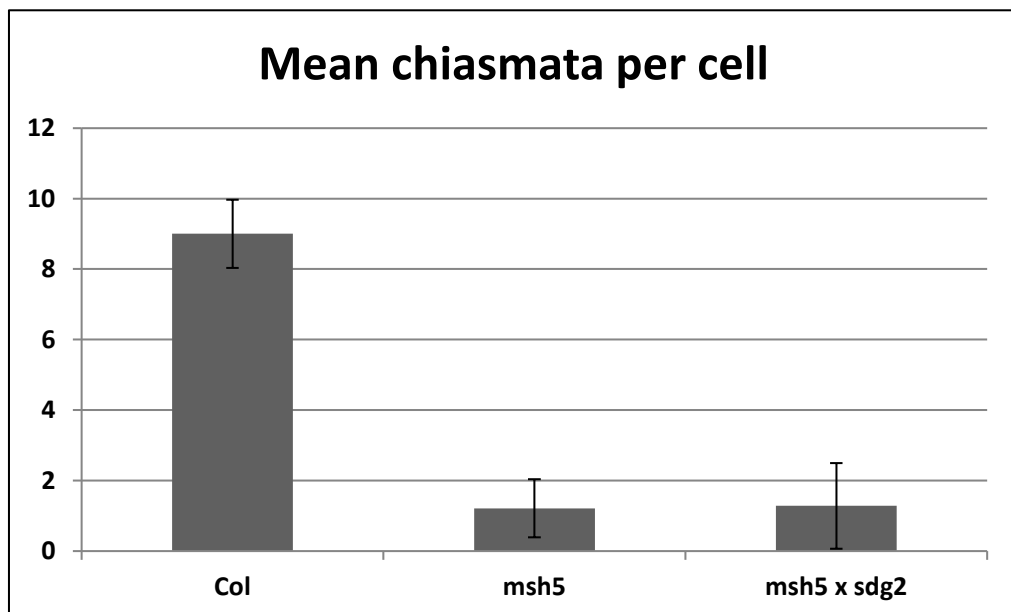


Figure 3.17: FISH of 5s (red) and 45s (green) rDNA probes in DAPI-stained metaphase I PMCs in Col 0 (A), *Atmsh5* (B) and *Atsdg2 x Atmsh5* (C,D) (Above).

Scale bar = 5 μ m

Chiasma frequency of Col 0, *Atmsh5* and *Atsdg2-1 x Atmsh5*. Error bars = standard error (Below).



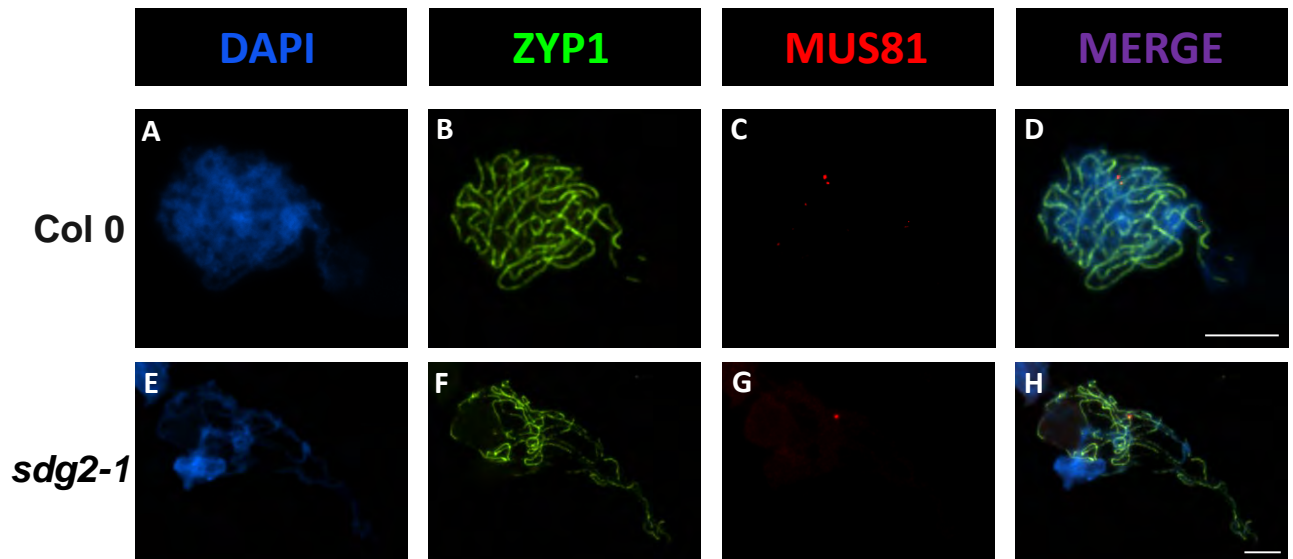


Figure 3.18: Dual-immunolocalisation of ASY1 and MUS81 in Col 0 and *Atsdg2-1* PMCs.
Scale bar = 5 μ m

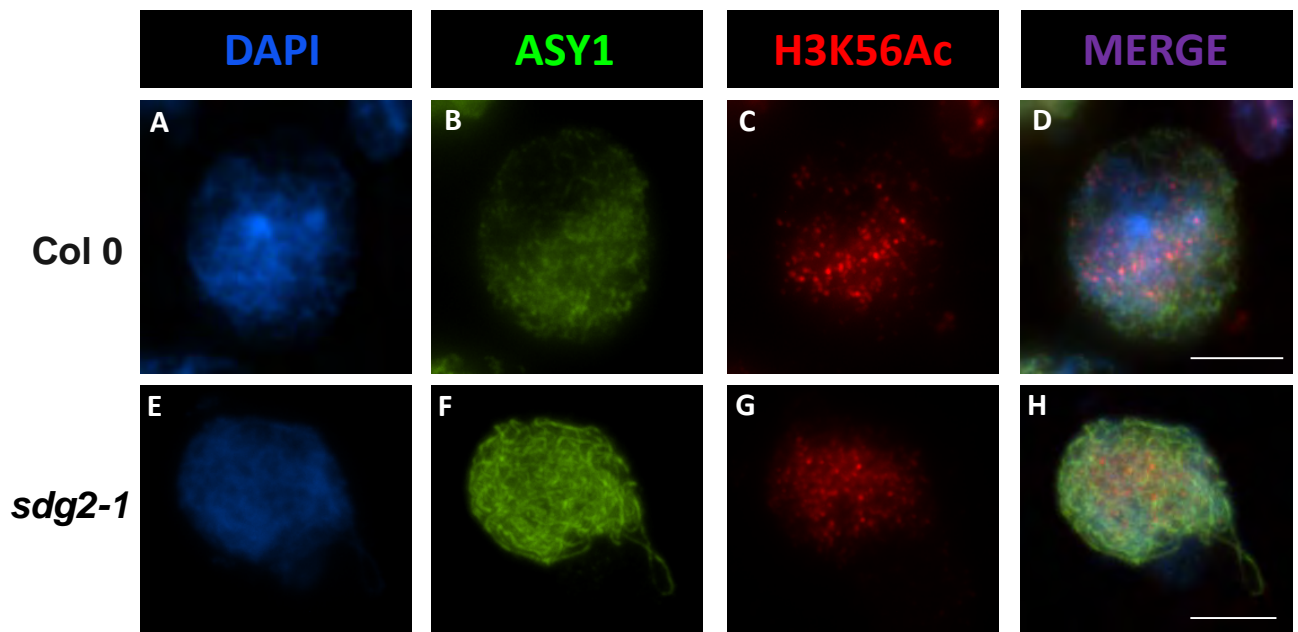


Figure 3.19: Dual-immunolocalisation of ASY1 and H3K56Ac in Col 0 and *Atsdg2-1* PMCs.
Scale bar = 5 μ m

3.2.8 *Atsdg2-1* PMCs are not defective in H3K56Ac deposition

The H3K56Ac histone modification has been shown to be involved in DSB-repair template choice, by promoting repair via the sister chromatid in yeast (Muñoz-Galván et al., 2013). I decided to investigate whether the phenotype of *Atsdg2-1* might be due to the loss of some H3K4Me₃, leading to a loss of other histone modifications. I dual-immunolocalised the H3K56Ac modification with ASY1 to see if any differences were apparent between Col o and *Atsdg2-1*. Initial experiments to investigate the localisation of this mark in early prophase I, did not reveal any clear differences (Figure 3.19). Other histone acetylation antibodies, such as H4K16Ac, will also be investigated, as well a more thorough analysis of H3K56Ac.

3.2.9 SDG proteins in ASY1 pulldown data

Mass spectrometry data of proteins pulled down by immunoprecipitation of ASY1 (K. Osman, J. Yang and F.C.H. Franklin unpublished data, protocol in Osman et al., 2013, contained two SDG proteins. SDG18 (SUVR2) was identified in 3 of 11 pull-down experiments and SDG10 (EZA1, SWN) was identified in 1. SDG18 is a methyltransferase of H3K9, while the target of SDG10 is unknown. AtSDG2 was not identified in this data.

3.2.10 SC length is unchanged in *Atsdg2-1*

The length of the SC has been reported to be correlated with the CO frequency. In *Arabidopsis*, male SCs are physically longer than female, and display a proportional increase in genetic distance (Giraut et al., 2011). With this in mind for the *Atsdg2-1*

mutant, which appears to be displaying an increased CO frequency, I decided to measure the SC length at pachytene, by manually measuring ZYP1/ASY1 immunostained PMCs at the pachytene stage (using NIS-elements software, Nikon). Mean SC length in Col 0 PMCs was 178.32 μ m (n=5, standard error = 8.4) while *Atsdg2-1* was 188.89 μ m (n=6, standard error = 5.97). These values did not show a statistically significant difference (two-tailed T-test, P=0.32).

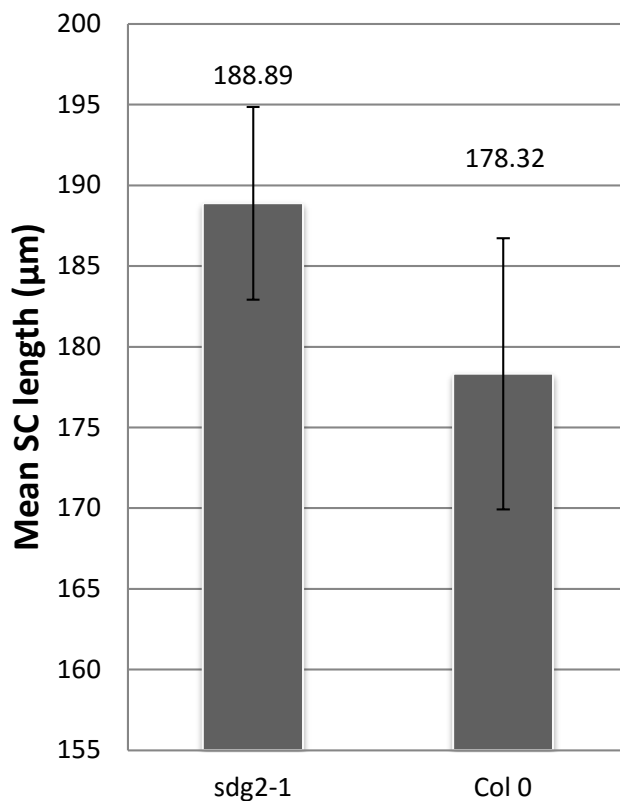


Figure 3.20: Mean SC length measurements from *sdg2-1* (n=6) and Col 0 (n=5), based on measurements made of ZYP1 stained SC in pachytene PMCs. The difference is not significant. T-test, 2-tailed P=0.32

3.3 Discussion

The general finding of this work, that CO frequency is increased in an *Atsdg2* background, is unexpected. The published literature shows that *AtSDG2* displays strong expression in bud tissue, *Atsdg2* mutants are sterile and the H3K4Me3 modification which it produces has a known association with recombination hotspots. These were all indicators that an *Atsdg2* null mutant might suffer some form of meiotic defect. Instead, PMCs of *Atsdg2-1* appear cytologically normal until the tetrad stage, and show subtle changes in crossover frequency, distribution and interference.

3.3.1 An increased CO frequency in *Atsdg2-1*

Several independent lines of evidence from my studies point to an increase in the number of COs in *Atsdg2-1*. The FTL analysis indicates that genetic distance is significantly increased in both pairs of intervals tested on chromosome 5 in *Atsdg2-1* compared to Col 0, while interval I2g shows a significant decrease in *Atsdg2-1* and I2f shows no significant change. This could reflect increases in CO frequency occurring at the chromosome level, affecting different chromosomes in different ways, as was reported for a histone H3 acetylation mutant, which had increased CO frequency in chromosome 4 and decreased CO frequency in chromosomes 1 and 2 (Perrella et al., 2010). Alternatively, changes in CO frequency could be operating on a smaller scale, affecting certain chromosome regions more than others, as was reported for a histone deacetylase (*Sir2*) mutant in yeast (Mieczkowski et al., 2007). It is not possible to differentiate between these two possibilities from the current data, though additional FTL intervals or FISH labelling of PMCs to differentiate between different

chromosomes could help provide an answer. It should also be noted here that a bias of the FTL system is that only viable tetrads are scored, meaning the 3-nuclei/polyad PMCs which presumably mature into 3-pollen 'triads', are not included in the analysis. If these cells experience a stronger effect resulting from the *Atsdg2-1* mutation, which leads to them forming 3 nuclei instead of 4, then the FTL analysis would be based only on the cells experiencing a weaker effect, and could potentially influence the outcome.

An increase in CO numbers in *Atsdg2-1* is evidenced by chiasma counts performed on metaphase I PMCs (Col o 9.00 vs *Atsdg2-1* 10.95), foci counts of MLH1 at pachytene (Col o 10.0 vs *Atsdg2-1* 13.1) and foci counts of large HEI10 foci at leptotene (Col o 9.8 vs *Atsdg2-1* 12.5). These numbers appear to show a general trend of a modest but significant increase in CO frequency, while the unusually shaped metaphase I chromosomes seen in *Atsdg2-1* (Figure 3.5 B), combined with the FTL analysis, support the conclusion that this mutant shows altered CO distribution compared to Col o.

The observed increase in COs seen in *Atsdg2-1* is unexpected, given the involvement of H3K4Me3 in recombination hotspots. Less H3K4Me3 might be expected to result in a reduced number of hotspots, and a concomitant reduction in the CO frequency, but instead, the COs appear to have moved elsewhere in the genome, and occurred more frequently. One possible explanation is that in *Atsdg2-1*, a subset of H3K4Me3 has been lost, and recombination has instead occurred at AtSDG2-independent H3K4Me3 sites, as is the case for PRDM9 (Brick et al, 2012). In this hypothesis, these sites might be distinguished as being recombinationally hot in some other way, such as by an addition or loss of an alternative epigenetic mark, resulting in the observed re-distribution and increase in COs. Several additional epigenetic factors are known to be hotspot associated in *Arabidopsis*, such as DNA methylation, low nucleosome

density and the presence of the histone variant, H2A.Z (Choi et al, 2013). Another issue with my initial hypothesis is the assumption that a reduced number of hotspots would lead to reduced CO frequency. When RNAi is used to generate *spo11* knockdown lines, only the lines which show severely reduced DSB numbers show a reduction in CO numbers, due to CO homeostasis mechanisms (Roberts, 2009).

The changes in CO frequency seen in *Atsdg2-1* could result from defective SPO11 targeting mechanisms. A study of ZMM mutants in yeast, which experience pairing defects, showed that they also experience an increase in DSB formation, due to the presence of unpaired homologs which are thought to control the negative feedback mechanisms normally inhibiting continued DSB formation on paired chromosomes (Thacker et al., 2014). Based on mapping of Spo11-bound oligonucleotides, the study also found that ZMM mutants experienced greater or lesser DSB frequencies in different chromosomal regions, and that not all chromosomes were affected equally. Combined with the findings of PRDM9 studies, the conclusion to this is that Spo11 will continue to produce DSBs until restrained by negative feedback mechanisms, and that in the absence of Spo11 targeting (eg, PRDM9), or H3K4Me3, it will still continue to produce DSBs at alternative sites until negative feedback is implemented. SPO11 targeting may have evolved exclusively in animals, based on the fact that PRDM9 has only been identified in animals, and mutating it leads to the DSB hotspots reverting back to the 'default' H3K4Me3 locations of promoter regions where they would be found in budding yeast and plants (Brick et al., 2012). The loss of some H3K4Me3 in *Atsdg2-1* could potentially be affecting this default mechanism of SPO11 targeting, leading to altered DSB distributions which, if similar to the situation in yeast, might not affect all chromosomes equally, as we see in the FTL analysis. The next question is whether AtSDG2-dependent H3K4 tri-methylation is targeted to particular genomic

loci and if so, how are they determined? If recombination is relocating to alternative H3K4Me3 sites, what makes them alternative? The alternative DSB sites would also not necessarily be H3K4Me3 associated, as in yeast when the H3K4 methyltransferase Set1 is disrupted, and DSB formation instead depends on H3K79 methylation, produced by Dot1 (Ismail et al., 2014).

The decrease in H3K4Me3 levels has been shown to affect the transcription of a large number of genes in *Atsdg2-1* mutants (Berr et al, 2010, Guo et al, 2010). This is likely due to the loss of H3K4Me3 at promoter sites, where it would normally be enriched and is likely to enhance transcription factor binding (Zhang et al., 2009; Vermeulen et al., 2007; Lauberth et al., 2013). It is possible that transcription factor binding normally occludes accessibility to sites which would otherwise be recombination hotspots. The absence of transcription factor binding at these sites in the *Atsdg2-1* background would therefore open these sites up to the recombination machinery, and lead to the observed redistribution and/or increase in CO formation. However, studies which mapped DSB sites in yeast, by sequencing Spo11-bound DNA oligomers, found little change between wild-type and transcription factor mutants (Mieczkowski et al., 2006; Zhu and Keeney, 2015). The study by Zhu and Keeney also examined the relationship between the openness of chromatin, based on nuclease sensitivity, and DSB hotspot activity, but similarly found that although changes occurred between mutants and controls, these did not show a clear correlation. Variations in chromatin openness did often alter the DSB pattern when examined at a fine scale. Although the study found that transcription factor binding motifs, for the two transcription factors studied, showed a strong correlation with hotspot localisation, actual transcription factor binding sites determined with chromatin immunoprecipitation, showed almost no relationship with DSB hotspots. Changes in hotspot activity between mutants and

wild-type were also shown not to correlate with H3K4Me3 levels in this analysis, suggesting that despite the known association between these two factors, quantitative measures of H3K4Me3 does not act as a predictor of DSB frequency at hotspots. If *Arabidopsis* displays similar properties to those observed in yeast in this study, then a simple hypothesis of transcription factor binding differences based on reduced H3K4Me3 levels in *Atsdg2-1*, might not be sufficient to explain the changes in CO distribution recorded in my studies. One major difference between my work and that of Zhu and Keeney, 2015, is that my studies have been focussed on COs, rather than DSB hotspots. Changes in CO number and distribution would not necessarily require any change in DSB hotspot distribution, and while transcription factors might not influence the binding of the DSB producing machinery, they could potentially have some effect on downstream processes, such as the length of DSB-end resection or the binding of CO promoting proteins.

3.3.2 Reduced interference in *Atsdg2-1*

The finding that RAD51 foci counts appear similar between Col o and *Atsdg2-1*, as well as the similar appearance of DMC1 and MSH4 foci, suggests that early recombination events occur in similar numbers in *Atsdg2-1* as they do in Col o. This means that the observed increase in CO number is less likely to be due to an increase in the number of DSBs, which might be considered an unlikely scenario anyway, as experiments using SPO11-RNAi lines have demonstrated CO homeostasis, where moderate decreases in DSB frequency have little effect on the final number of COs (Roberts, 2009). This still holds true for moderate increases in DSB number, when demonstrated in mice possessing additional copies of the *Spo11* gene (Cole et al., 2012a). It seems a more

likely scenario that a slightly higher proportion of recombination events are being designated as COs, which could result from the observed reduction in the level of interference. This hypothesis is supported by the increased interference ratio in two of the three FTL interval-pairs analysed.

The FTL analysis indicates that CO interference is affected differently in each interval pair. The individual intervals of each pair showed similar changes in IR in *Atsdg2-1* compared to Col o. In I2f for example, the IR in *Atsdg2-1* was 0.273, vs 0.116 in Col o. A similar pattern is observed in all 6 intervals tested, whether increasing or decreasing. This is expected, and perhaps only confirms that interference is operating in both directions, from one interval to the adjacent one, more or less equally. A more interesting finding is that each interval pair shows a different outcome, one with increased interference, one with decreased and the other showing little change.

3.3.3 Potential meiotic involvement of other SET domain proteins

The ASY1 immunoprecipitation data revealed that AtSDG10 (EZA1) and AtSDG18 (SUVR2) were identified in the mass spectrometry analysis. *AtSDG18* also showed relatively high RPKM values in the RNAseq data, though the difference between these values categorises them as insignificant. AtSDG18 also contains a zinc-ion binding, Pre-SET domain which could possibly be involved in DNA binding. AtSDG18 would therefore be an interesting candidate for future studies into this area. The absence of AtSDG2 from the ASY1 immunoprecipitation data is not entirely unexpected, and does not necessarily make it any less likely to have a meiotic role, as the interaction between AtSDG2 and its target, histone H3, might be transient.

3.3.4 Altered gene regulation in *Atsdg2-1*

AtSDG2 was not significantly upregulated based on our analysis of PMC-specific RNAseq data, generated by Chen et al, 2010. This was surprising based on previous findings by Berr et al, which reported that *SDG2* is highly upregulated in bud tissue. The immunostaining of H3K4Me₃, while not providing any information regarding the transcriptional expression level of *AtSDG2*, does indicate that perturbing its function causes a reduction in H3K4Me₃ levels in PMCs. It would be interesting in future experiments to transform plants with a meiosis specific promoter driving the expression of RNAi or inactive CRISPR/Cas9 targeted against *AtSDG2* in addition to other H3K4 methyltransferases to investigate the effects of even further loss of this modification during meiosis. Causing further reduction of H3K4Me₃ in the whole organism by performing genetic crosses between different *SET* gene mutants is unlikely to yield viable plants, but could also be attempted. Previous experiments from our lab where T-DNA insertion mutants of the histone methyltransferases, *Atashh2* and *Atashh3*, were crossed together to reduce H3K36Me₃ levels to lower levels than in either individual mutant, yielded plants which suffered severe developmental defects. *Atsdg2-1* already displays a more severe somatic phenotype compared to *Atashh2*.

The absence of transcripts with a known meiotic role in the *Atsdg2-1* microarray analysis performed by Berr et al, 2010, makes the possibility of the observed effects being the result of a misregulation of a different gene, less likely, but still possible since not every gene involved in meiosis has yet been characterised and the complex protein-protein interactions involved in meiosis are far from being fully understood.

3.3.5 A possible DSB repair defect in *Atsdg2-1*

The presence of a single chromosome fragment out of several hundred cells looked at, might not be biologically meaningful, and should not be over-interpreted but could suggest a minor reduction in the efficiency of DNA repair pathways in *Atsdg2-1*. An analysis of a higher number of cells might be needed to confirm this, with just as careful scrutiny looking at Col o cells to see how frequently chromosome fragments would be expected normally.

3.3.6 SC length is not significantly different in *Atsdg2-1*

I hypothesized that the increased CO frequency in *Atsdg2-1* might be reflected in a concomitant increase in SC length. This correlation is observed between male and female meiosis in *Arabidopsis*, where male meiocytes have an increased CO frequency and SC length compared to female meiocytes (Giraut et al., 2011). A similar situation is seen in condensin mutants in *C. elegans* (Mets and Meyer, 2009). The absence of a significant change in SC length in *Atsdg2-1* was unexpected, but not unprecedented. *Atfig1* and *Atfancm* mutants, both of which are reported as having increased CO frequency, also do not show a change in the length of the SC, though these mutants display an increase in the frequency of non-interfering COs, unlike *Atsdg2-1* which increases the frequency of interfering COs (Girard et al., 2015; Crismani et al., 2012). Libuda et al., 2013 demonstrated in *C. elegans*, that each CO is associated with a 0.4-0.5 μ m increase in axis length. Given the variability in my own SC length measurements and the small increase in CO frequency, a similar increase in axis/SC length per CO would be unlikely to be detectable. The same study demonstrated that when SC central element proteins were partially depleted, the CO frequency increased,

suggesting that the SC is restraining CO formation in *C. elegans*. Whether or not AtZYP1 loads onto the SC at wild-type levels in *Atsdg2-1* is unknown but could be measured in future experiments in a similar way to the AtASY1 intensity measurements discussed in Chapter 5. A change in SC length may have supported a model where the altered CO distribution in *Atsdg2-1* results from changes in the axis-loop organisation of chromosomes, such as by changes in loop length or inter-loop base module spacing (Kleckner, 2006). The absence of a significant difference does not entirely rule this possibility out either. A recent yeast study which demonstrated the link between transcription and axis-loop organisation also supports this possibility, as transcription is known to be strongly affected for many genes in *Atsdg2-1* (Sun et al., 2015). This study showed meiotic cohesin (Rec8) is preferentially deposited at the 3' end of genes, due to RNA-polymerase II activity, and that Rec8 dictates the genomic location of Red1 binding. This activity keeps the 3' end of genes recombinationally cold while ensuring that actively transcribed genes and their recombinationally hot promoters remain in the chromatin loops (Figure 1.5). The effects of the *Atsdg2-1* mutation on transcription could therefore be altering the organisation of meiotic chromosomes by this mechanism, and could be responsible for the observed changes in CO distribution.

Chapter 4

Characterisation of an *Atmrg2* allele reveals a defect in *AtPRD3* function

4.1 Introduction

MORF4 (mortality factor on chromosome 4) was originally identified as a cell senescence gene which can induce mortality in certain immortal human cell lines (Bertram et al., 1999). The human MRG-family genes MRG15 and MRGX are highly transcribed in all tissues, with the proteins localized to cell nuclei. MORF4, MRG15 and MRGX are predicted to contain leucine-zipper and helix-loop-helix domains such as those found in transcriptional regulators (Pardo et al., 2002). The amino acid sequence of MRG15 is 96% similar to MORF4 but does not induce cellular senescence when expressed in immortal cell lines. The helix-loop-helix and leucine-zipper domains of MRG15 are required for a direct interaction with the tumour suppressor retinoblastoma (Rb), leading to the activation of the *B-myc* promoter (Leung et al., 2001). Unlike MORF4 or MRGX, MRG15 also contains a chromatin-binding chromo-domain at its N-terminus, similar to that found in retinoblastoma-binding protein-1 (RBP-1) (Bertram et al., 1999). Chromo-domain proteins are chromatin remodelling factors involved in either nucleosome movement or histone modification (reviewed in Jones et al., 2000). Some chromo-domain proteins have been demonstrated to associate with DNA and RNA, but most interact with methylated histone tails (Reviewed in Brehm et al., 2004). In budding yeast, the MRG15 homologue Eaf3 associates with methylated H3K36 (Carrozza et al., 2005; Keogh et al., 2005) with the same modification being recognised by human MRG15 (Zhang et al., 2006). In *Drosophila* the chromo-domain proteins HP1 and Polycomb bind to methylated H3K9 and H3K27 tri-methylation respectively (Bannister et al., 2001; Lachner et al., 2001; Cao et al., 2002).

Homologues of MRG15 have been identified in 18 different species (Bertram and Pereira-Smith, 2001). In addition to their chromatin-binding properties, MRG-family proteins are thought to associate with histone acetyl transferases (HATs) and histone de-acetylases (HDACs)(Carrozza et al., 2005; Joshi and Struhl, 2005; Keogh et al., 2005).

Histone acetylation is a post-translational histone modification known to influence the distribution of DSB hotspots in yeast (Mieczkowski et al., 2007). Mutation to *Sir2*, a histone deacetylase, caused increased DSB frequency in some regions and decreased it in others, affecting the DSB frequencies of 12% of all genes. In *Arabidopsis*, a histone H3 acetylation mutant, *Atmcc1*, was reported to show increased CO frequency and altered CO distribution in chromosome 4 and decreased CO frequency in chromosomes 1 and 2, which also failed to produce the obligate CO in some cells (Perrella et al., 2010).

MRG15 is a known component of both HAT and HDAC complexes and is also involved in cell differentiation and DNA repair by homologous recombination (Pena and Pereira-Smith, 2007; Sy et al., 2009; Hayakawa et al., 2010; Pena et al., 2011). MRG15 has been demonstrated to bind to a protein called PALB2, which is involved in DNA damage repair by acting as an intermediary between BRCA1 and BRCA2, which in turn recruits RAD51 (Hayakawa et al., 2010). The Hayakawa *et al* study knocked down MRG15 expression with siRNA, leading to a reduction in gene conversion rates in HeLa cells, in contrast to an earlier paper which reported a hyper-recombination phenotype when PALB2 was mutated to prevent it binding to MRG15 (Sy et al., 2009). The two results are consistent with it performing distinct, antagonizing functions dependent on its interaction with different binding partners; MRG15 is part of a HDAC complex (Sin3), HAT complex (Tip60) and the BRCA DNA repair complex. It has been

reported elsewhere that acetylation by Tip60 is required to suppress non-homologous end-joining in favour of BRCA1 mediated repair, demonstrating a link between histone acetylation and DNA damage repair pathway choice (Tang et al., 2013).

The *C. elegans* MRG15 homologue, MRG1, is required for primordial germ cell survival and proliferation by silencing X-linked genes in the germ line, through its association with the chromatin of autosomes but not X-chromosomes (Takasaki et al., 2007). This pattern of autosome-only association is also seen in a histone methyl-transferase of H3K36, MES4, which is also involved in X-linked gene silencing, though it does not seem to be required for the localisation of MRG1 (Bender et al., 2008; Takasaki et al., 2007). Mutation to *MRG1* in *C. elegans* has been reported to cause chromosomal fragmentation at diakinesis, leading to germ-line apoptosis (Xu et al., 2012a). This apoptosis is dependent on DNA damage checkpoint genes *CLK2/RAD5* and the pachytene checkpoint gene *PCH2*, indicative of the protein having roles in DNA repair and synapsis. The role of MRG1 in DSB repair is further evidenced by SPO11 dependant RAD51 foci, which persisted for longer than normal in *mrg1* worms, and increased chromosomal fragmentation and germ cell apoptosis upon exposure to γ -radiation in these mutants compared to wild-type. The loss of MRG1 also causes defects in pairing of homologous autosomal chromosomes independent of pairing centres (cis-acting genetic elements that associate with nuclear membrane proteins in prophase I to facilitate pairing), leading to a delay in SC assembly and SC assembly between non-homologous chromosomes (Dombecki et al., 2011).

Preliminary analysis of *Atmrg2-1*, a mutant allele of the *Arabidopsis* MRG15 homologue, *AtMRG2*, revealed reduced fertility (Toshiro Ito, personal communication). As this suggested a possible meiotic defect, I undertook a detailed analysis of meiosis in the mutant. The results of this study are presented below.

Although, this confirmed that the reduced fertility in *Atmrg2-1* was indeed due to a defect in meiosis, it was revealed that this was due to disrupted expression of the closely linked *AtPRD3* gene (De Muylt et al., 2009) rather than a direct consequence of loss of AtMRG2.

4.2 Results

4.2.1 Fertility is reduced in *Atmrg2-1* compared to Col o

AtMRG2 was identified by our collaborators at Temasek Life Sciences laboratory in Singapore, as being upregulated in a microarray screen of a microsporogenesis mutant (SPL/NZZ). The *AtMRG2* gene (Locus: AT1G02740) is one of two MRG-domain encoding genes in *Arabidopsis*. The other, *AtMRG1* (Locus: AT4G37280) encodes a protein which displays 51% amino acid identity with AtMRG2. However mutation of this gene by T-DNA insertion (Salk_144163, Salk_023229 and Salk_089867) does not result in any obvious vegetative or reproductive defects, based on plant morphology (data not shown). *AtMRG2* consists of 10 exons, encoding a 38kDa protein of 327 amino acids which contains a histone binding chromo-domain at its N-terminal region and a conserved MRG-domain at its C-terminal region. Although no link between SPL/NZZ and AtMRG2 was demonstrated, AtMRG2 was investigated further to see if it has a role in fertility and meiosis. *Atmrg2* mutants were grown from a segregating T-DNA insertion line (Salk_035089, hereafter referred to as *Atmrg2-1*), available from NASC (European Arabidopsis Stock Centre). The T-DNA insertion in the *Atmrg2-1* mutant is located in the 4th exon, between the chromo-domain and MRG-domain coding regions (Figure 4.1). Although this mutation abolishes the full length

transcript, the 5' region of the gene which encodes the chromo-domain region, is still transcribed into mRNA, detectable by RT-PCR. No transcript was detected by RT-PCR, using primers spanning the T-DNA insertion (Figure 4.2, see Appendix D for primers) (MRG2 Pre-T-DNA Fw/Rv, MRG2 post-T-DNA Fw/Rv primers, MRG2 Trans-T-DNA region was amplified using Pre-T-DNA Fw primer with post-T-DNA Rv primer).

The *Atmrg2-1* plants grown from heterozygous seeds appeared to show no discernible vegetative phenotype, compared to Col o. However, some of the *Atmrg2-1* plants displayed strongly reduced fertility (Figure 4.3 A), apparent from short silique length (Figure 4.3 B) and low seed production (Figure 4.3 C) (4.9mm mean silique length and 1.7 mean seeds per silique $n=50$) compared with Col o (12.6mm mean silique length and 49.9 mean seeds per silique $n=30$). Genotyping confirmed that only the plants homozygous for the T-DNA insertion displayed the reduced fertility phenotype (using primers SALK_035089 GT_a with b for WT allele; SALK_035089 GT_b with LBb1.3 for mutant allele). Seeds for subsequent sowings were collected from heterozygous plants, and from these sowings homozygous plants were selected based on their clearly reduced silique length.

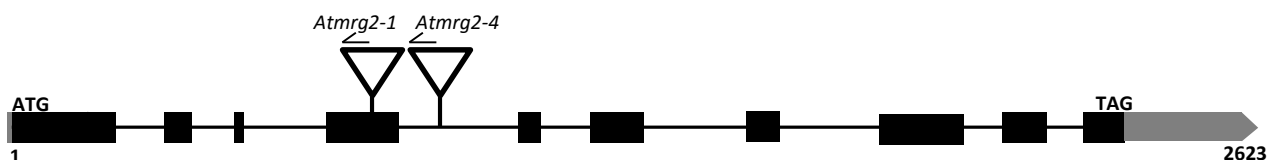


Figure 4.1: Schematic of T-DNA insertion locations within the *AtMRG2* locus for the *Atmrg2-1* and *Atmrg2-4* alleles.

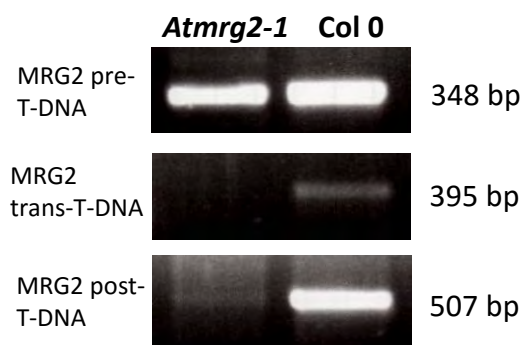


Figure 4.2: RT-PCR of MRG2 pre-T-DNA, trans-T-DNA (primers either side of the predicted T-DNA insertion site), and post-T-DNA. A product for the trans-T-DNA site could only be produced in Col 0, not in *Atmrg2-1*.

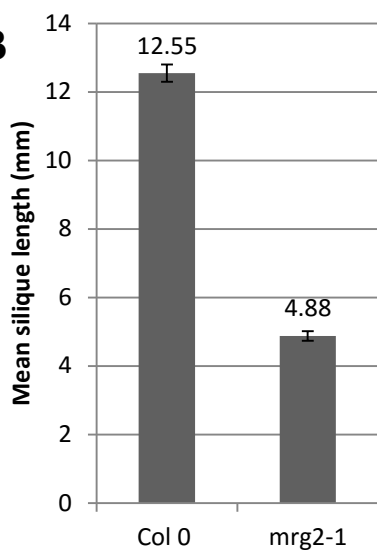
A



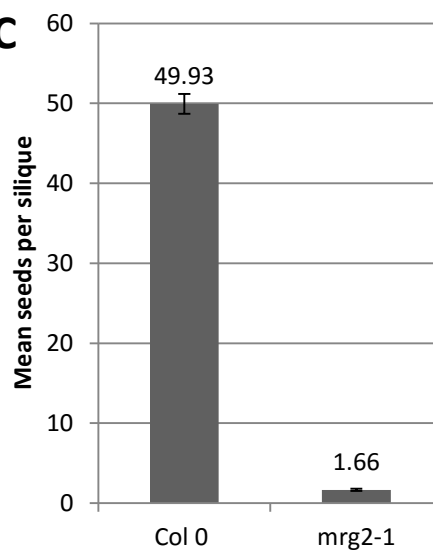
Atmrg2-1 Col 0

Figure 4.3: *Atmrg2-1* shows a clear reduction in fertility compared to Col 0, based on silique length (A and B) and seed count (C). (Error bars in B and C show standard error).

B



C



4.2.2. *Atmrg2-1* is defective in CO formation and is asynaptic

Pollen mother cells (PMCs) from Col o and *Atmrg2-1* plants were analysed cytologically with 4',6-diamidino-2-phenylindole (DAPI) staining of chromosome spread preparations of fixed bud material. Meiotic chromosomes in Col o PMCs showed linear chromosome axes at leptotene (Figure 4.4 A), which paired along their lengths during zygotene (Figure 4.4 B) and displayed fully paired chromosomes at pachytene (Figure 4.4 C). 5 bivalent chromosomes were visible at diakinesis (Figure 4.4 E) and metaphase I (Figure 4.5 A). Accurate segregation was observed in both meiotic division stages (Figure 4.5 B-E), producing tetrads with 5 chromosomes per nucleus (Figure 4.5 F). *Atmrg2-1* PMCs in contrast, never showed any fully paired chromosomes (Figure 4.4 H) and virtually all metaphase I PMCs contained only univalents (Figure 4.5 G). Bivalent chromosomes were observed only twice, out of >100 metaphase I nuclei analysed (Figure 4.6 C-F). Fluorescence in-situ hybridisation (FISH) probes for 5s and 45s rDNA was applied to these chromosomes to allow identification of the individual chromosomes, and confirmed that these chiasmata had occurred between homologous chromosomes. However, chromosome 'stickiness' was often observed in *Atmrg2-1* at metaphase I, which did not appear show any preference for forming between homologous chromosomes (Figure 4.6 G and H). Chromosomes then segregated randomly at each division stage, often producing aneuploid nuclei in the tetrads. Chromosome fragmentation was not observed in the mutants.

To investigate the structure of the meiotic chromosome axis and synaptonemal complex, immunostaining with anti-ASY1 and anti-ZYP1 antibodies was performed in Col o and *Atmrg2-1* meiocytes in early prophase I. ASY1 is a known component of the chromosome axis (Armstrong, 2002), while ZYP1 is the transverse filament protein required for formation of the synaptonemal complex (Higgins et al., 2005). In Col o

plants, ASY1 is present as numerous foci in G2 which form a continuous, linear signal at leptotene. Foci of ZYP1 are present at leptotene, which lengthen into increasingly long stretches during zygotene, forming a continuous signal along the whole length of each chromosome at pachytene (Figure 4.7 A-D). In *Atmrg2-1*, ASY1 appears as it does in Col o, but ZYP1 is usually only observed as foci, and occasionally as short stretches (Figure 4.7 E-H). Full ZYP1 polymerisation was never observed using immunolocalisation (n=10), in addition to no fully paired pachytene chromosomes being observed during extensive analysis of DAPI stained chromosome spread preparations (Figure 4.4), suggesting the *Atmrg2-1* mutant is asynaptic.

To investigate the early stages of recombination, immunolocalisation with ASY1 and RAD51 was performed. RAD51 has been previously used as a marker of DSB sites, as it is an essential component of the DNA damage response (Li et al, 2004). Localisation of RAD51 in Col o shows that the protein localises early in prophase I, forming numerous, axis-associated foci which reduce in number over the course of prophase I (Figure 4.8 A-D). RAD51 foci were also detected in *Atmrg2-1* (Figure 4.8 E-H) suggested that the early stages of recombination were proceeding in the mutant. Surprisingly, a similar pattern of RAD51 localization was observed in an *Atspo11-1-4* (WiscDsLox_461-464J19) line which was used as a control (Figure 4.8 I-L).

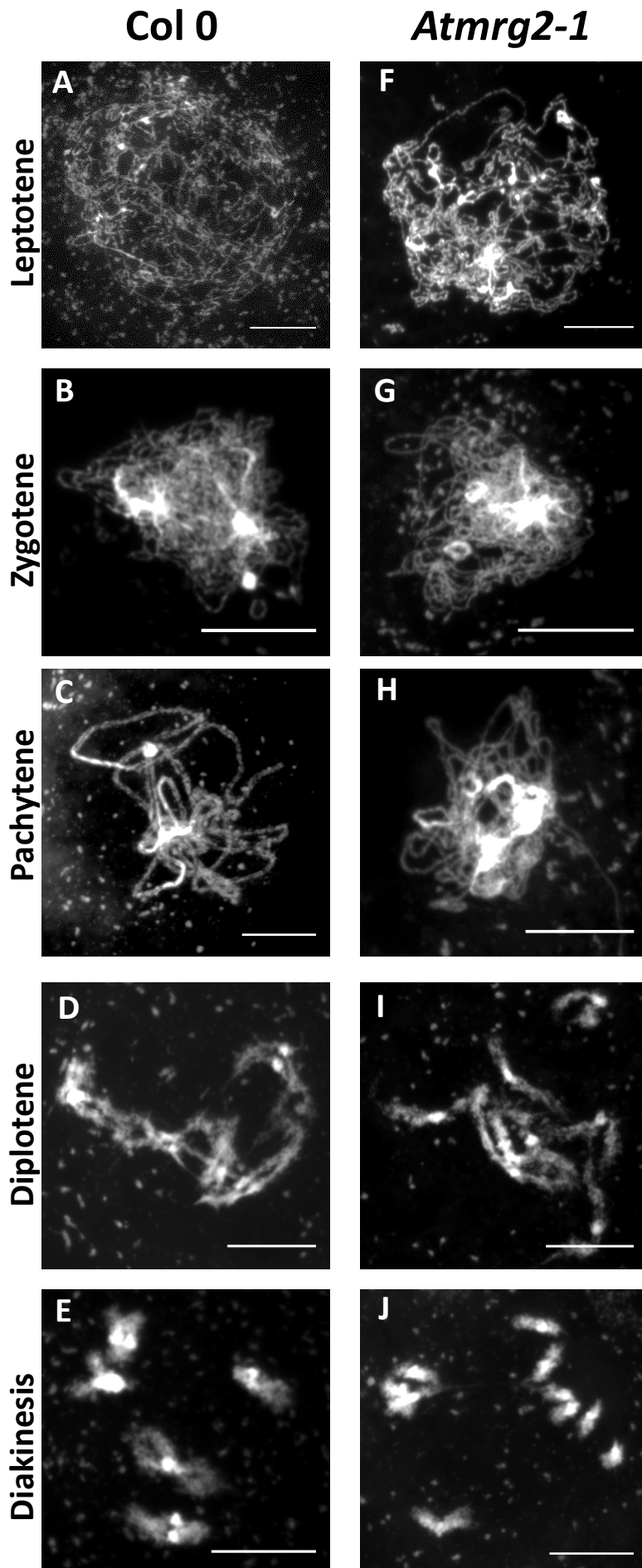


Figure 4.4: Meiotic atlas of prophase I in Col 0 (A-E) and *Atmrg2-1* (F-J) plants. An absence of pairing is seen at mid-prophase I in *Atmrg2-1* (H) compared to Col 0 (C), so proper pachytene nuclei are not observed in *Atmrg2-1*. At diplotene and diakinesis, 5 bivalent structures are observed in Col 0 (D and E), while 10 structures are seen in *Atmrg2-1* (I and J).

Scale bar = 10 μ m

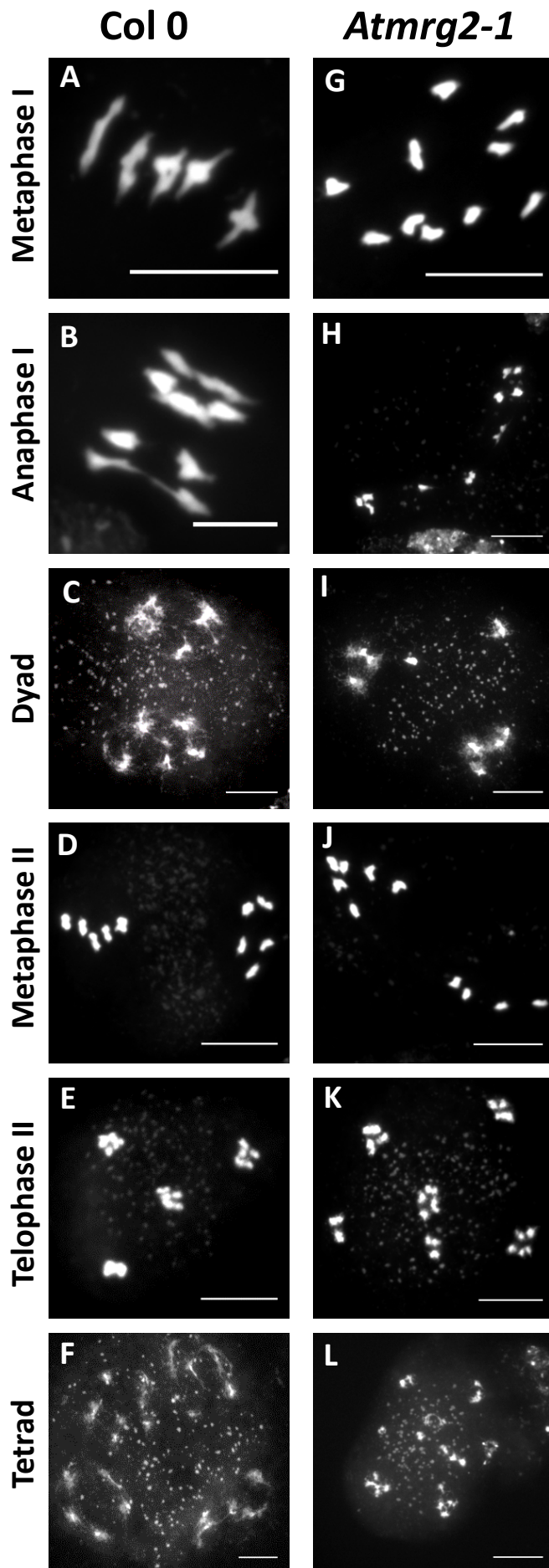


Figure 4.5: Meiotic atlas of the post-prophase I stages in Col 0 (A-F) and *Atmrg2-1* (G-L) plants. 5 bivalent chromosomes, connected by chiasmata are seen in Col 0 at metaphase I (A), while 10 univalents are seen in *Atmrg2-1* (G). The chiasmata ensure accurate segregation at anaphase I in Col 0 (B), while their absence allows random segregation in *Atmrg2-1* (H). At telophase II and tetrad stage in Col 0, 4 nuclei are observed, each containing 5 chromosomes (E and F). *Atmrg2-1* meiocytes at the same stage often form polyads containing variable numbers of chromosomes (K and L). Scale bar = 10 μ m.

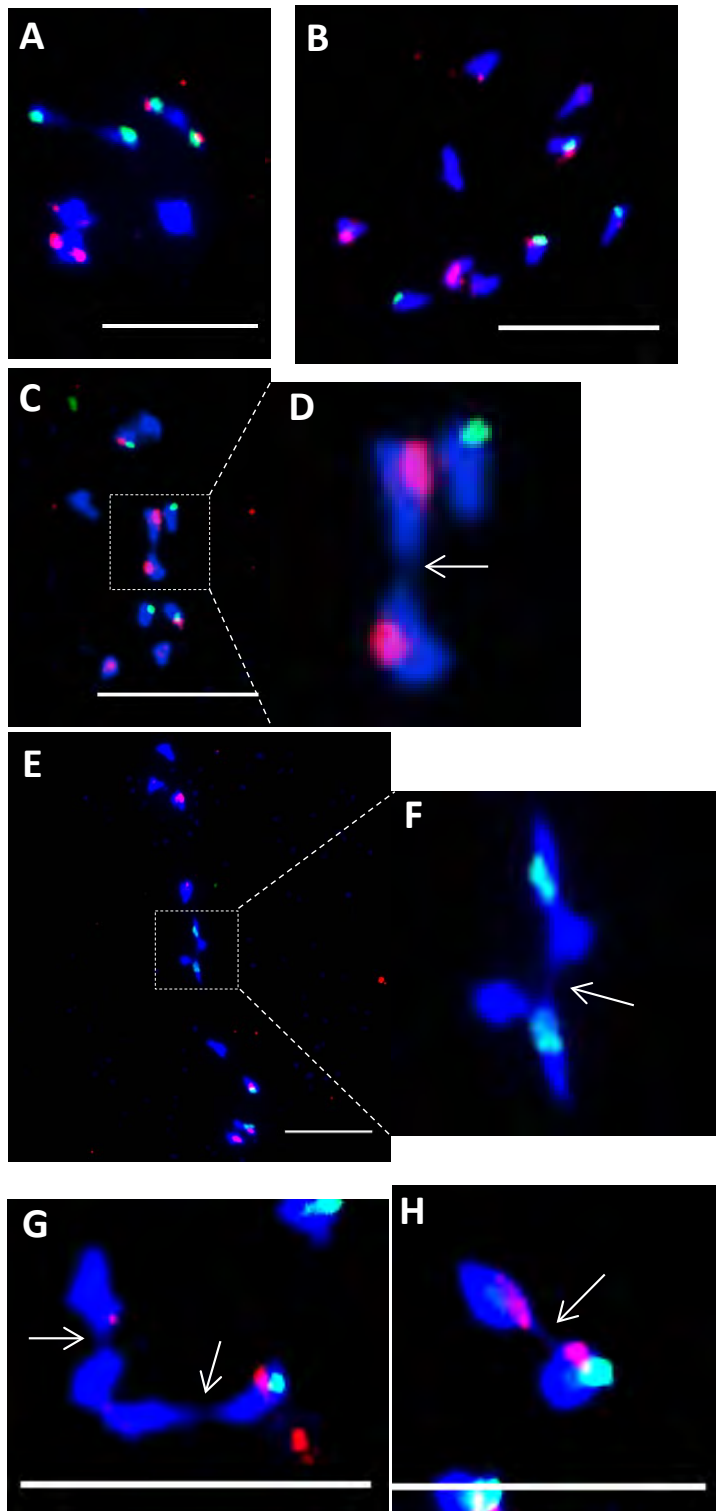


Figure 4.6: Fluorescence in-situ hybridisation of 5s (red) and 45s (green) rDNA probes in Col 0 (A) and *mrg2-1* (B-F) PMCs at metaphase I. The two bivalents observed in *mrg2-1* are magnified in D and F. Examples of chromosome 'stickiness' seen in *mrg2-1* are shown in G and H. Scale bar= 10µm

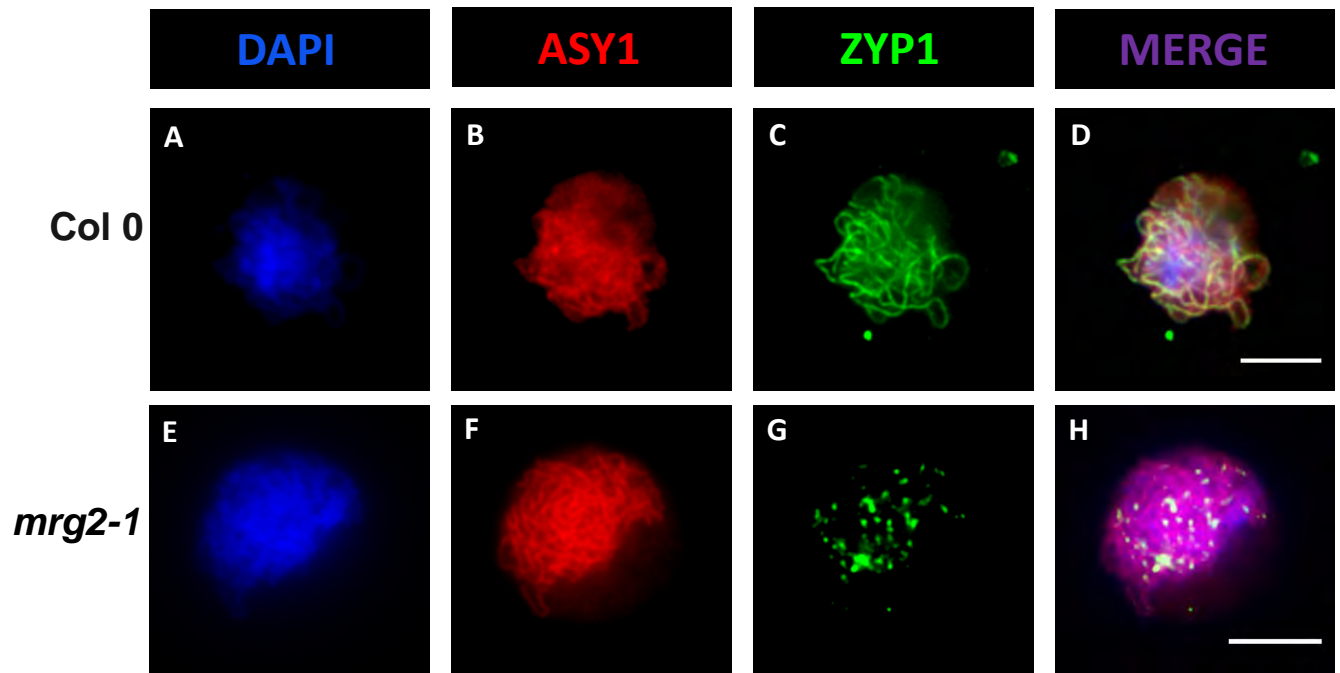


Figure 4.7: Immunolocalisation of ASY1 and ZYP1 in Col 0 and *Atmrg2-1*. *Atmrg2-1* PMCs never show full polymerization of ZYP1, and at most display short stretches of ZYP1.

Scale bar= 5 μ m

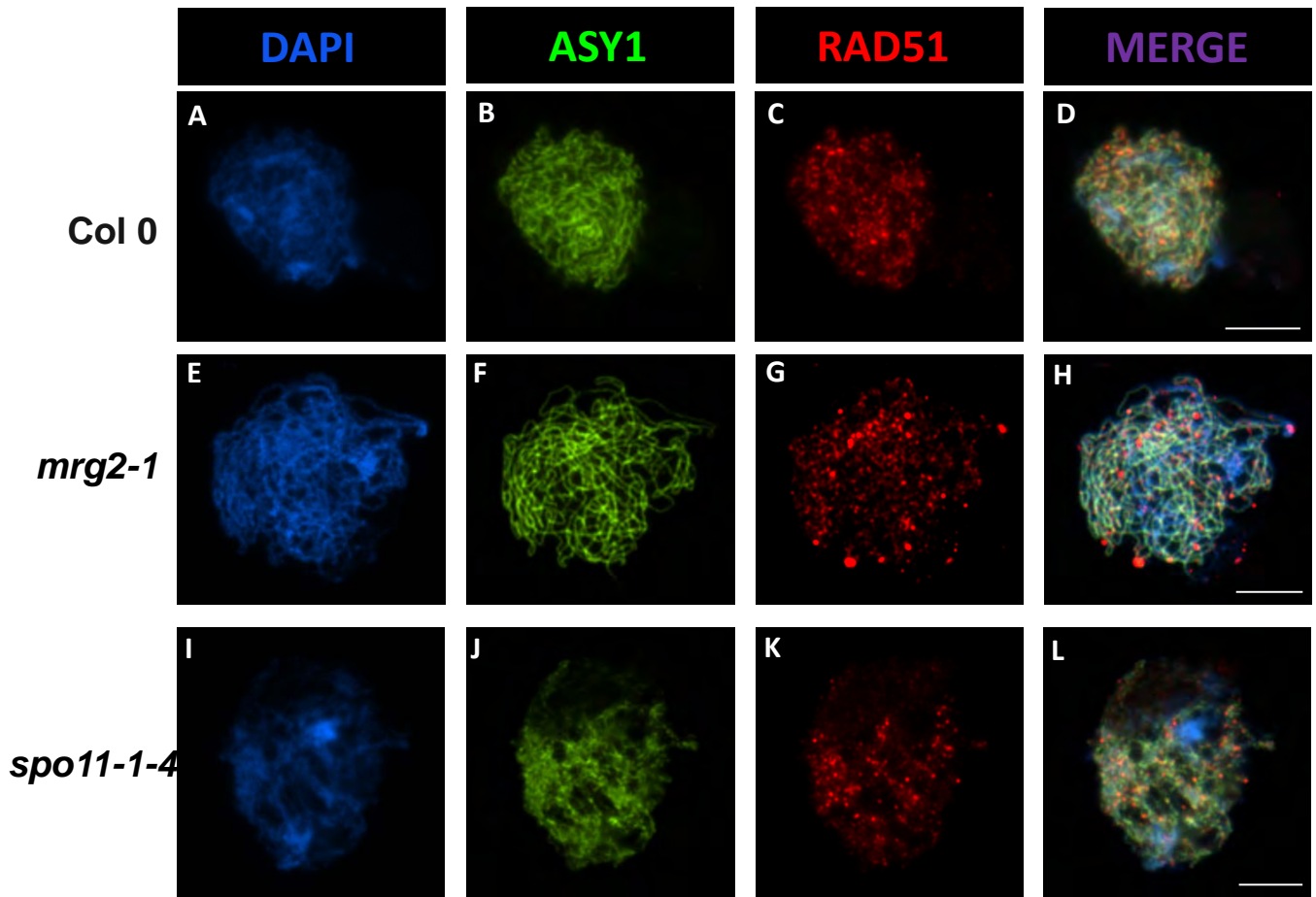


Figure 4.8: Immunolocalisation of ASY1 and RAD51 in Col 0 (A-D), *Atmrg2-1* (E-H) and *Atspo11-1-4* (I-L) PMCs in early prophase I.
Scale bar = 5 μ m

4.2.3 The recombination defect in *Atmrg2-1* is due to a lack of programmed DSBs

In addition to the RAD51 immunolocalisation analysis, I adopted a genetic approach to ascertain whether DSB formation was defective in *Atmrg2-1*. To do this I performed genetic crosses between *Atmrg2-1* and *Atmre11* heterozygotes. The progeny of these crosses were genotyped for both genes and then self-pollinated to acquire plants homozygous for both mutations. MRE11 is required for DSB end-resection during the early stages of homologous recombination and *Atmre11* mutants display extensive chromosome fragmentation at metaphase I, resulting from non-repair of programmed DSBs, seen in Figure 4.9 A and B and previously reported in Puizina et al., 2004 and De Muyt et al., 2009. DAPI stained chromosome spreads of *Atmre11/Atmrg2-1* PMCs did not show extensive fragmentation, and still displayed 10 univalent chromosomes, such as that seen in *Atmrg2-1* (Figure 4.9 C and D). Some chromosome fragments, usually only a single fragment per nucleus, were observed in 4 nuclei out of 20 where fragmentation would be apparent (metaphase I onwards) (Figure 4.9 E and F).

A similar experiment was performed using mutants of the recombinase RAD51. Extensive chromosome fragmentation is also seen in *Atrad51* mutants following metaphase I, comparable to that seen in *Atmre11* (Figure 4.9 G). The RAD51 recombinase operates downstream of MRE11 and is essential for DSB repair by recombination (Li et al, 2004, Da Ines et al, 2013). In the genetic crosses of *Atrad51/Atmrg2-1*, I did not observe extensive fragmentation in double homozygotes, similar to in the *Atmre11/Atmrg2-1* double mutants (Figure 4.9 H and I). Together, these data suggest that there is a strong reduction in the formation of programmed DSBs during meiosis in the *Atmrg2-1* mutant.

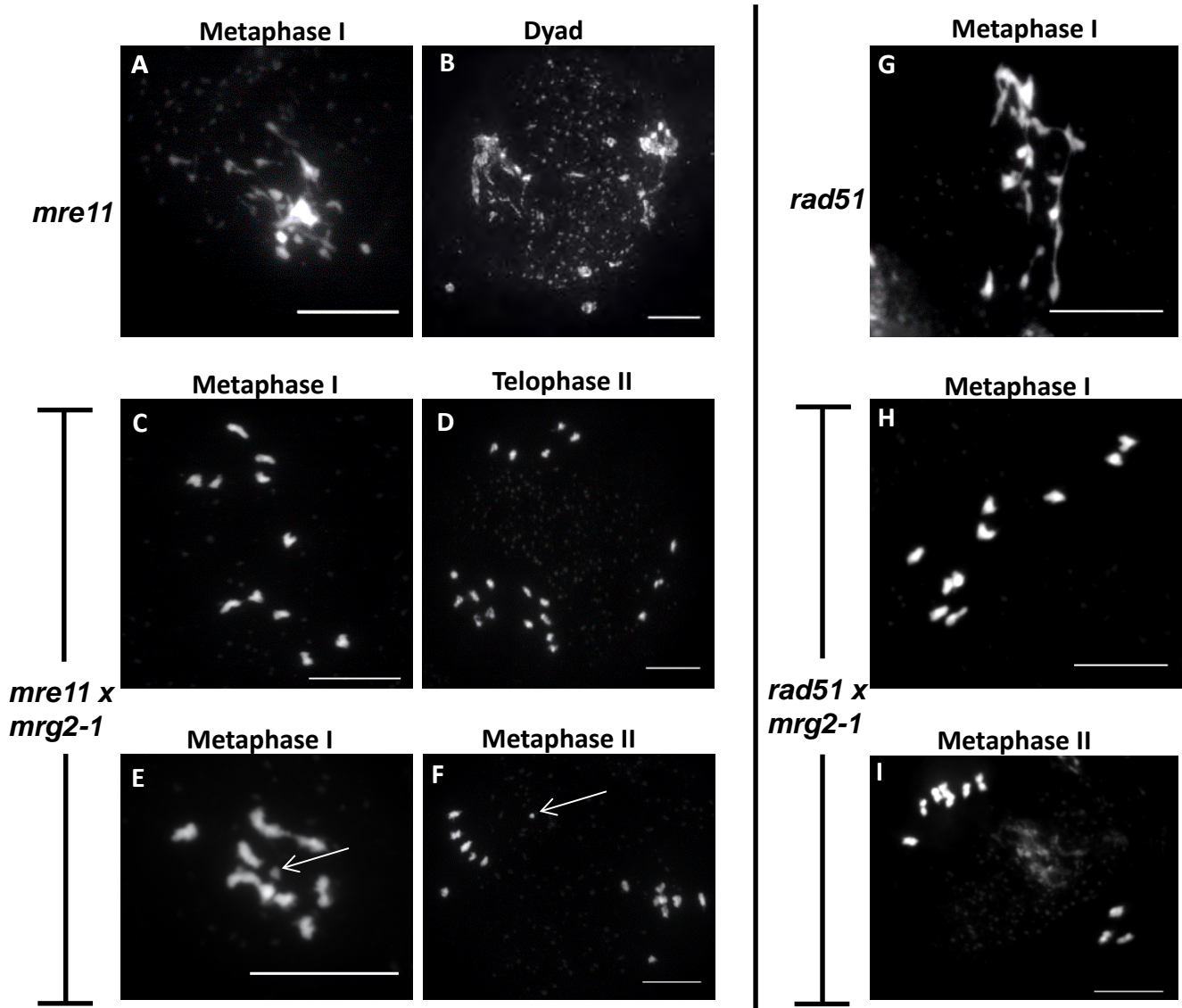


Figure 4.9: DAPI stained meiocytes from *mre11* (A and B) and *rad51* (G), which show extensive chromosome fragmentation. The *mre11/mrg2-1* double homozygous mutant (C to F) does not show extensive fragmentation. The *rad51/mrg2-1* double homozygous mutant also shows an absence of fragmentation (H and I). Low level fragmentation was observed in some *mre11/mrg2-1* cells (arrows, E and F). Scale bar = 10 μ m

4.2.4 Loss of AtMRG2 is unlikely to be the cause of the *Atmrg2-1* meiotic phenotype

To confirm that the observed phenotype in *Atmrg2-1* is due to disruption to the *AtMRG2* gene, I obtained a second allele of *Atmrg2*, which contained a T-DNA insertion at a different site, in intron 4, (SAIL_317_F11, hereafter called *Atmrg2-4*, as alleles 1,2 and 3 are identified in Xu et al., 2014, Figure 4.1) (line available from NASC). Genotyping confirmed homozygosity of the *Atmrg2-4* mutation (SAIL_317_F11 LP/RP for WT product; RP/SAIL LB2 for mutant product), but plants did not display reduced fertility, evident from wild-type like silique length and seed production (data not shown). DAPI stained chromosome spreads of PMCs performed on these lines showed apparently WT-like pairing during prophase I, formation of 5 bivalents at metaphase I and accurate chromosome segregation at the division stages (Figure 4.10). RT-PCR was performed on this line to see whether the *AtMRG2* transcript is still produced in *Atmrg2-4* (Figure 4.11). The RT-PCR showed that a pre-T-DNA section (upstream/5' of the T-DNA insertion site) of the gene could be amplified from Col o cDNA and also from cDNA from two independent *Atmrg2-4* homozygotes, but that a post-T-DNA section (downstream/3' of the insertion site), and the full-length transcript, could only be amplified from Col o, but not from the two *Atmrg2-4* samples. This suggests that *Atmrg2-4* is also an *Atmrg2* null mutant, and that the phenotype observed in *Atmrg2-1* may not be due to disrupted AtMRG2 function.

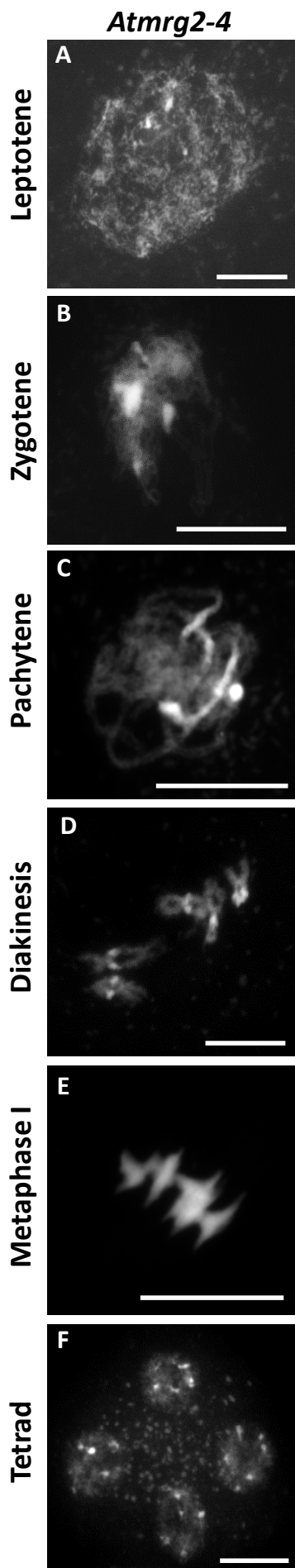


Figure 4.10: *Atmrg2-4*(Sail_317_F11) homozygous line, confirmed by genotyping, does not show the same meiotic phenotype or reduced fertility seen in *Atmrg2-1*. Scale bar = 10 μ m

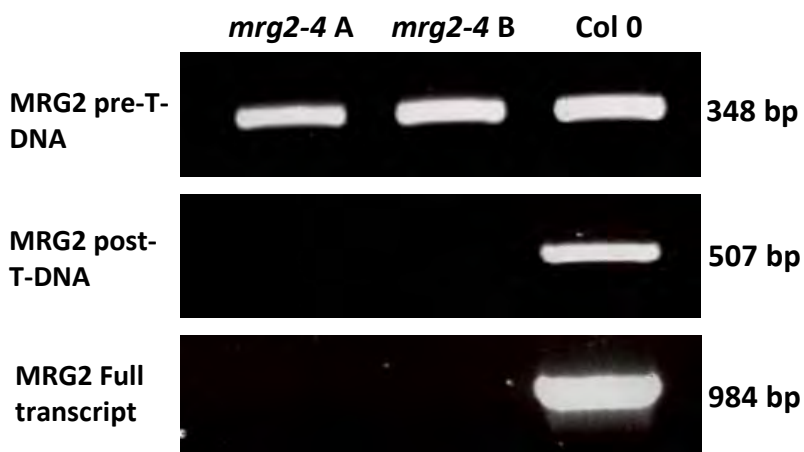


Figure 4.11: RT-PCR of *AtMRG2* transcript using cDNA from Col 0 and *Atmrg2-4*. Full length *AtMRG2* and post-T-DNA *AtMRG2* could not be amplified in this mutant.

4.2.5 The *Atmrg2-1* phenotype is likely caused by disruption to *AtPRD3*

Subsequently, information that pointed to a resolution of these conflicting data was obtained (Aiwu Dong lab, Fudan University, Shanghai, China, personal communication). As part of their study of the *Arabidopsis MRG* gene family, the Fudan group had conducted a transcription profile of *Atmrg2-1* using microarray analysis. This revealed that the meiotic gene *AtPRD3*, which maps near to the *AtMRG2* locus, approximately 350kb away, is down regulated in *Atmrg2-1*. qPCR analysis, carried out by our collaborators in Singapore, demonstrated a reduction in *AtPRD3* expression of between 23 and 63% in *Atmrg2-1* compared to Col o (Toshiro Ito, personal communication). As *AtPRD3* has previously been demonstrated to be essential for DSB formation (De Muyt et al., 2009), I decided to confirm if *AtPRD3* function is compromised in *Atmrg2-1* using immunostaining with anti-PRD3 antibody (Figure 4.12). A clear reduction in *AtPRD3* foci is seen in *Atmrg2-1*, compared to Col o PMCs at the G2/leptotene stage. This result is consistent with the microarray data obtained in Fudan and qPCR data from Singapore.

The reduction in *AtPRD3* expression in *Atmrg2-1* could be due to the loss of *AtMRG2* leading to reduced transcription of the *AtPRD3* gene. However, an alternative hypothesis was that because of the proximity of *AtPRD3* to *AtMRG2* on chromosome 1, the T-DNA insertion in *Atmrg2-1* had not only disrupted the *AtMRG2* locus but had also directly affected that of *AtPRD3*. I therefore investigated whether or not this might be the case using PCR of the *AtPRD3* genomic locus on DNA extracted from *Atmrg2-1* and Col o plants (Primers PRD3 GEN FW/RV). As a control, the *GAPD* housekeeping gene was amplified from Col o DNA and two independent samples of *Atmrg2-1* DNA. Analysis by agarose gel electrophoresis revealed products of the expected size (735 bp) with a similar band intensity in all three reactions, confirming that the DNA extracted

from the three plants was of good quality (Figure 4.13). Subsequent PCR of the full *AtPRD3* genomic locus using Col o DNA produced a product of the expected size (4758 bp), but the same reaction in the two *Atmrg2-1* samples failed to amplify any product. This strongly suggests that the *AtPRD3* locus contains an as-yet-uncharacterised mutation in *Atmrg2-1*.

Finally, a genetic cross was performed between heterozygotes of *Atmrg2-1* and *Atprd3* to obtain a double heterozygote. If *Atmrg2-1* does not contain a functional copy of *AtPRD3*, then the double heterozygote (*Atmrg2-1/+ ; Atprd3/+*) should effectively be homozygous for *Atprd3*, but still heterozygous for *Atmrg2-1*. Production of this double heterozygote was confirmed by genotyping, though only a single plant was obtained, and seed counts and silique measurements were performed to assess fertility. Mean silique length was 4.5mm (n=20), compared to 4.9mm in *Atmrg2-1* and 12.6mm seen in Col o. The mean seed number per silique was 1.2, n=20, compared to 1.7 in *Atmrg2-1* and 49.9 in Col o. This shows that fertility is reduced in the *Atmrg2-1/+ ; Atprd3/+* to levels indistinguishable from *Atmrg2-1* homozygotes, and that *Atmrg2-1* is unlikely to contain a functional copy of *AtPRD3*.

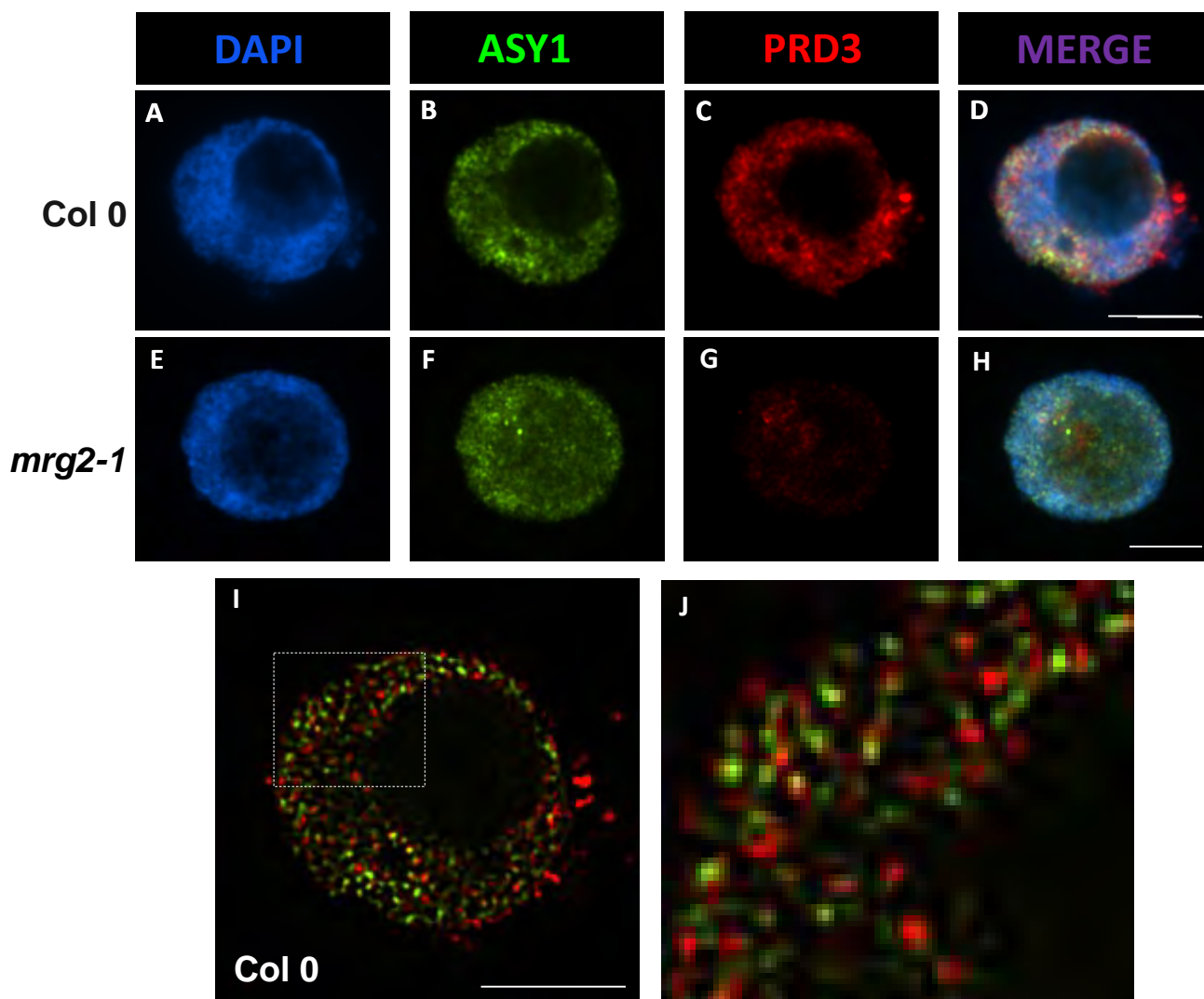


Figure 4.12: Immunolocalisation of ASY1 and PRD3 in Col 0 (A-D) and *Atmrg2-1* (E-H) G2 meiocytes. The Col 0 nucleus shown in A-D is deconvoluted in panel I, with magnification in J showing the adjacent localisation of PRD3 (red) to ASY1 (green). Scale bar = 5 μ m

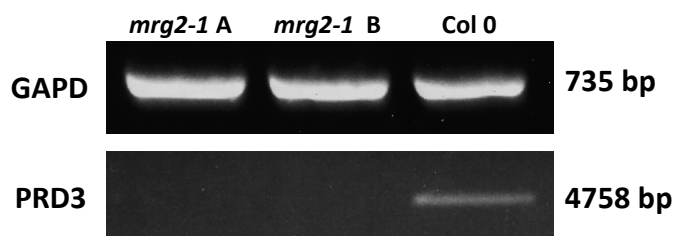


Figure 4.13: PCR of genomic DNA extracted from two homozygous *Atmrg2-1* plants and a control Col 0 plant. Primers for GAPD produced a product of the expected size in all samples. PRD3 genomic locus only produced a product from Col 0 DNA.

4.3 Discussion

The initial aim of this project was to explore the meiotic role of *AtMRG2*, but for reasons which became apparent over the course of my investigations, the emphasis was shifted to explain the cause of the meiotic defects specifically seen in the *Atmrg2-1* allele, which are most likely due to disruption to *AtPRD3*.

4.3.1 *Atmrg2-1* mutants show meiotic defects which result from mutation to *AtPRD3*

DAPI spreading cytology showed that in *Atmrg2-1*, COs form at a highly reduced rate. The two chiasmata which were observed were both between homologous chromosomes, identified by FISH staining of 5s and 45s rDNA, so should probably not be dismissed as random chromosome connections resulting from chromosome 'stickiness'. At least one of these connections (Figure 4.6 D) looked more like a genuine chiasma than the thin chromatin strands seen in chromosome stickiness. Based on this, the meiotic defects observed in *Atmrg2-1* could be consistent with a failure to produce programmed DSBs, such as in *Atspo11* mutants (Hartung et al., 2007; Sanchez-Moran et al., 2007), or a failure to impose CO formation, and carrying out repair by SDSA, or repair via inter-sister-chromatid recombination, such as in *Atdmc1* mutants (Schwacha and Kleckner, 1997; Couteau et al., 1999). However, genetic crossing with *Atmre11* and also with *Atrad51*, demonstrated that the reduction in CO frequency most likely results from a strong reduction in programmed DSB formation, evident from the absence of extensive chromosome fragmentation. The presence of low-level chromosome fragmentation in some nuclei of *Atmre11/Atmrg2-1* is consistent with the rare occurrences of chiasmata, which would require DSB

formation. Chiasmata appeared to be formed at reduced frequency in the *Atspo11-1-1* mutant characterised by Grelon et al., 2001 (8 bivalents in 84 metaphase I cells), though this is a higher frequency than what I have observed in *Atmrg2-1*. It was later shown that this allele is probably 'leaky', as a count of over 300 nuclei from an alternative allele, *Atspo11-1-3*, revealed zero chiasmata (Sanchez-Moran et al., 2007).

The immunolocalisation of the recombinase protein RAD51, suggested that recombination was initiated in *Atmrg2-1*, though similar immunostaining was observed in *Atspo11-1-4* known to be defective in programmed DSB formation. Since numerous studies have shown the absence of RAD51 foci in the absence of DSBs, this data was initially difficult to explain. However, in other on-going work in the laboratory, analysis of PMC chromosome spread preparations of *Atspo11-4* at metaphase I has revealed the presence of occasional chiasmata and chromosome fragmentation (Figure 4.14, courtesy Kim Osman). This suggests that there may be some residual DSB formation. The number of these residual DSBs is unknown, but their presence could offer an explanation as to why RAD51 foci were observed in *Atspo11-1-4* and *Atmrg2-1*. RAD51 foci have been used in various immunolocalisation studies to mark DSB/recombination sites, and shown to be absent in the absence of DSBs, but it is unknown whether the presence of a small number of residual DSBs is enough to activate RAD51 activity, possibly via ATM/ATR kinase mediated DNA damage signalling. If RAD51 is present and activated in the presence of a relatively small number of DSBs, it may still form foci on the meiotic chromatin, not necessarily at end-resected DSB sites, since RAD51 also has double-stranded DNA binding affinity (Sauvageau et al., 2005).

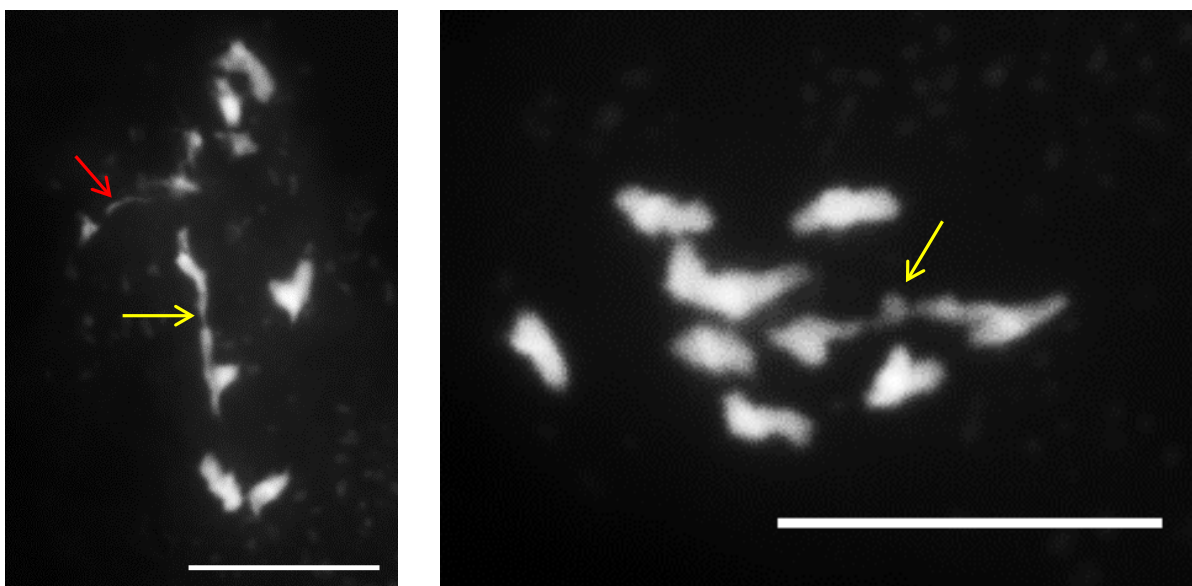
Atspo11-1-4

Figure 4.14: Metaphase I PMCs in *Atspo11-1-4* stained with DAPI. Though rare, bivalent chromosomes (yellow arrows) are sometimes seen in this mutant line, as well as fragmentation (red arrow) (Courtesy of Kim Osman).
Scale bar = 10 μ m

The synaptic defect seen in *Atmrg2-1*, is evident from the failure of ZYP1 to polymerise into anything more than occasional short stretches. This is consistent with observations of *Atprd3*, which also usually shows nothing more than foci of ZYP1 with occasional short stretches (Lambing, 2014).

The PCR data only reveals that full-length *AtPRD3* cannot be amplified from homozygous *Atmrg2-1* genomic DNA, though without further characterisation we can only speculate on the nature of this mutation. One possibility is a second T-DNA insertion site. PCR using the T-DNA left border primer with each of the full-length *AtPRD3* primers failed to amplify a product (data not shown). FISH experiments using a T-DNA probe were also attempted but were unsuccessful. A second possibility is a more conventional genetic mutation such as a frameshift mutation resulting from an IN/DEL or a nonsense point mutation. This possibility seems less likely though, as the

mutation would have to occur within the primer sequence in order to explain the PCR result.

In addition to the inability to PCR *AtPRD3* in *Atmrg2-1*, the immunolocalisation of AtPRD3 in Col 0 and *Atmrg2-1* shows a clear difference in signal strength at the G2 stage, further demonstrating reduced expression of AtPRD3 in *Atmrg2-1*. Lastly, the genetic cross between *Atmrg2-1* and *Atprd3* generated a double heterozygote which displayed the reduced fertility phenotype, further confirming that *Atmrg2-1* does not contain a functional copy of *AtPRD3*. The presence of two bivalent chromosomes in over 100 metaphase I cells analysed, suggests that like *Atspo11-1-1* (Grelon et al., 2001) and *Atspo11-1-4*, this allele of *Atprd3* might also be leaky, though to a lesser extent. The chiasma frequency in *Atmrg2-1* is very similar to that of the *Atprd3-4* mutant reported in De Muyt et al, 2009, which had a chiasma frequency of 0.04. The other 4 *Atprd3* alleles were all reported to have a chiasma frequency of zero. It should also be considered possible that the bivalents observed in *Atmrg2-1*, were actually instances of the same sticky connections seen in Figure 4.6 G and H, which had formed between homologs by coincidence and possessed an atypical ‘chiasma-like’ appearance. Chromosome stickiness such as this was also observed by Grelon et al, 2001 in the *Atspo11-1-1* allele, and also in a rice mutant of the *AtPRD3* homolog, *PAIR1* (Nonomura et al., 2004).

4.3.2 The meiotic role of AtPRD3

Based on currently unpublished work within our laboratory, AtPRD3 is likely to be operating as a SPO11 accessory protein, essential for its function in producing DSBs, though each is independent of the other in their localisation (Lambing, 2014). The co-

immunolocalisation of AtPRD3 and ASY1 in Col o, showed that the protein localises as foci in G2, but adjacent to foci/stretches of ASY1 staining (Figure 4.12 I and J). This indicates that AtPRD3 is associated with the axis, and is supported by work from our laboratory demonstrating *in vitro* interactions between the two proteins in a yeast two-hybrid assay (Lambing, 2014) and also *in vivo*, when PRD3 was detected in a pull-down experiment using an anti-ASY1 antibody on *Brassica oleracea* extracts (Osman et al., 2013).

4.3.3 The function of AtMRG1/AtMRG2

Two papers published after our work on *Atmrg2-1* have delineated the function of AtMRG2. Both papers show that AtMRG2 acts redundantly with AtMRG1 to regulate the expression of genes involved in flowering time, and that *Atmrg1/Atmrg2* mutants show a late-flowering phenotype, specifically under long-day conditions (Bu et al., 2014; Xu et al., 2014). Both papers demonstrate that AtMRG1/2 has binding specificity for H3K4Me3 and H3K36Me3 and that it binds to chromatin at the promoter region of FLOWERING LOCUS T (FT). Xu et al, showed that AtMRG1/2 interacts with the histone acetyl-transferases HAM1/2, to acetylate histones at the promoter and exon 1 of the FT locus. Bu et al demonstrated an interaction with the transcriptional activator CONSTANS, and that this interaction helps to promote binding of AtMRG2 to H3K4Me3 and H3K36Me3.

The redundant activity of AtMRG1 and AtMRG2 means that any future experiments into the meiotic role of *AtMRG* genes should investigate the double homozygous mutant, using the *Atmrg2-4* allele.

Chapter 5

Pachytene checkpoint 2 is required for meiotic chromosome remodelling, synapsis and crossover formation

5.1 Introduction

Pch2 (Pachytene Checkpoint 2) is a meiotic protein which provides an interesting link between the remodelling of meiotic chromosome structure and CO patterning. Pch2 is an AAA+ ATPase, homologs of which are conserved between multiple species. Pch2 has been found to have a meiotic role in recombination and chromosome organisation in budding yeast (Börner et al., 2008; Joshi et al., 2009). The axis component Hop1, homologous to AtASY1, and Zip1 the SC central element protein, load onto meiotic chromosomes in a series of domains of hyper and lower abundance. *Pch2* mutants are defective in this domainal organisation, and instead display a uniform, linear staining for each protein from zygotene onwards, although at the earliest stage of prophase I, leptotene, Hop1 still displays wild-type like domainal organisation, suggesting additional Hop1 loading takes place following this stage, onto the domains of low Hop1 abundance (Börner et al., 2008).

Pch2 also has been reported to act as a suppressor of intersister DSB repair, and to indirectly promote inter-homolog repair (Ho and Burgess, 2011; Zanders et al., 2011). Pch2 appears to do this via an interaction with Xrs2, part of the MRX complex involved in DSB processing, which itself interacts with the ATM homolog, Tel1, necessary for Hop1 phosphorylation (Ho and Burgess, 2011). Hop1 phosphorylation is in turn required for recruitment and activation on the meiosis specific kinase, Mek1, which stabilises the phosphorylation of Hop1 in a positive feedback loop (Chuang et al., 2012). This phosphorylation is dependent on the presence of another axis component, Red1 (homologous to AtASY3). In the *red1/pch2* double mutant, Hop1 is still phosphorylated, meaning that one of the functions of Pch2 is to prevent the Red1-independent phosphorylation of Hop1 (Lo et al., 2014).

Pch2 has a role in CO control in yeast, with mutants displaying increased CO frequency on their larger chromosomes, but no effect on a smaller chromosome, loss of the obligate CO and defective CO interference, based on tetrad analysis of specific genetic intervals (Zanders and Alani, 2009). However, another study looking at CO interference found that interference was not affected in *pch2*, based on distribution of Zip3 foci, which mark CO designated sites in early prophase I (Zhang et al., 2014b). A delay is also observed in the production of CO and NCO products in *pch2* mutants (Börner et al., 2008).

Homologs of PCH2 have been identified in multiple model organisms, which display an interesting variety of meiotic defects. In *Drosophila*, PCH2 is required for a delay-causing checkpoint, activated by mutations to recombination and axis component genes, or chromosomal rearrangements (Joyce and McKim, 2009, 2010). In mice the first characterisation of the PCH2 homolog, TRIP13, studied a hypomorphic allele which was able to complete synapsis but activated a DSB-dependent checkpoint which triggers meiotic arrest, due to the presence of unrepaired breaks (Li and Schimenti, 2007). COs are still formed in this mutant and CO marking proteins such as MLH1 appear to localise normally, meaning the unrepaired breaks observed in the study may result from defects in the NCO repair pathway. A subsequent study of a severe TRIP13 allele showed that the mutants were unable to complete synapsis, displayed a reduction in CO frequency and were defective in implementation of an obligate CO (Roig et al., 2010). Looking at a more moderate allele, the same study demonstrated that the TRIP13 hypomorph displays a reduced inter-focus distance between MLH1 foci, reflecting a defect in CO interference. Overall SC length was also slightly reduced in the hypomorphs.

Another study in mice showed that TRIP13 is required for the depletion of HORMAD1 and HORMAD2 from the chromosome axes during SC formation, similar to the situation observed in yeast for Hop1 (Wojtasz et al., 2009). In wild-type mice, HORMAD1/2 showed intense, linear staining of the unsynapsed axes, which increased over the course of zygotene, but showed less intense, more punctate staining in the synapsed chromosome regions. In the TRIP13 hypomorph, HORMAD1/2 staining persists at the same intensity on the synapsed chromosome regions as it does on the unsynapsed axes, indicating that TRIP13 is required for the reorganisation of HORMAD1/2 on synapsed chromosomes.

In *C. elegans*, *pch2* mutants show accelerated synapsis and DSB repair (Deshong et al., 2014). The authors hypothesize that PCH2 therefore works to slow recombination by destabilizing recombination intermediates in order to ensure their fidelity, as a kind of quality control mechanism. Like in other organisms studied, PCH2 was also shown to be required for CO assurance. Immunolocalisation of PCH2 in worms showed that the protein localises to meiotic chromosomes at around the pachytene stage, but then disassociates from chromosomes at late pachytene. This localisation required SYP1, the central element component, and therefore synapsis.

The rice PCH2 homolog, CRC1 (CENTRAL REGION COMPONENT 1), shows similar localisation patterns to *C. elegans*, co-localising with the central element component (ZEP1) over the course of zygotene and pachytene, doing so in a mutually dependent manner, thereby causing the *crc1* mutant to be asynaptic (Miao et al., 2013). CRC1 has an earlier role than this localisation suggests though, and is required the recruitment of the Hop1 homolog, PAIR2 onto meiotic chromosomes, and therefore pairing. An interaction between CRC1 and PAIR1, the rice homolog of PRD3, was also demonstrated *in vitro* and *crc1* mutants are defective in programmed DSB formation.

This requirement for a PCH2 homolog in the initial stage of recombination appears to be unique to rice, and further highlights the diversity of functions of PCH2 orthologs.

Like many other AAA+ ATPase proteins, Pch2 assembles into a hexameric ring with a central pore. Based on an *in vitro* study, the hexamer binds to Hop1, and displaces it from DNA in an ATP dependent manner, supporting the findings from *pch2* mutants that Pch2 is involved in axis remodelling (Chen et al., 2013).

Together, these results suggest that Pch2 somehow links the structural organisation of the axis with how CO localisation is patterned.

Work performed in our lab has identified an *Arabidopsis* homolog of Pch2, from mass spectrometry analysis of *Brassica rapa* proteins co-immunoprecipitated with ASY1 in pull-down experiments (Osman et al., 2013; Nuntasontorn, 2013). Our lab has been working to analyse the function of AtPCH2 in plants for several years, with the bulk of the findings recently published in Lambing et al., 2015. The parts of the project which I was personally involved in are described here, along with analyses which were not described in the article. I have shown that in *Arabidopsis*, PCH2 is involved in meiotic axis remodelling, ensuring formation of the obligate CO, timely and efficient synapsis. CO interference may be established in early prophase I, during CO designation in an *Atpch2* mutant, but downstream defects occur in maturation of these designated sites into COs. I also show that AtPCH2 is required for WT levels of ASY1 deposition onto the meiotic axes.

5.2 Results

5.2.1 *Atpch2* mutants display reduced fertility

3 separate T-DNA insertion lines were identified as potential *Atpch2* mutants, based on their mapped locations within At4g24710. SAIL_1187_Co6 (*Atpch2-1*), SALK_031449 (*Atpch2-2*) and SALK_130138 (*Atpch2-3*) (Figure 5.1 and 5.2). All three lines displayed no obvious vegetative phenotype, but show a reduction in silique length and numerous gaps in the seed sets within (Figure 5.3). RT-PCR was performed on cDNA produced from inflorescences of all three lines to look for the presence of *AtPCH2* transcripts (Figure 5.4). *AtGAPD*, a housekeeping gene, was successfully amplified by RT-PCR from cDNA from all three *Atpch2* mutants and Col o (GAPD Fw/Rv primers). Full-length *AtPCH2* transcript was successfully amplified from Col o but could not be amplified from any of the *Atpch2* mutants. A 320bp sequence at the 5' region of *AtPCH2* could still be amplified in *Atpch2-2* and *Atpch2-3*, as well as Col o, but not in *Atpch2-1*. It is likely that these mutants produce truncated, non-functional transcripts of *AtPCH2*. A 598bp sequence at the 3' region was also amplified in Col o. Amplification of this product failed in both *Atpch2-2* and *Atpch2-3*, though *Atpch2-1* was able to produce a very faint product, perhaps originating from within the T-DNA insertion. Again, this is likely to be a non-functional transcript, or at least produce non-functional protein. Together with a previously described allelism test where *Atpch2-1/Atpch2-2* double heterozygotes displayed the same phenotype as individual homozygotes (Lambing et al., 2015), we conclude that all three lines are *Atpch2* null mutants, and that the disrupted expression of this gene is responsible for the observed reduction in fertility.

To better quantify the observed reduction in fertility, Alexander staining was performed on Col o and *Atpch2-1 plants*. Col o plants displayed pollen viability of 99.3% (n=811), while analysis in *Atpch2-1* revealed a lower level of pollen viability at 90.1% (n=893) (Figure 5.5). This suggested that the fertility defect could be due to a meiotic, rather than a post-meiotic defect.

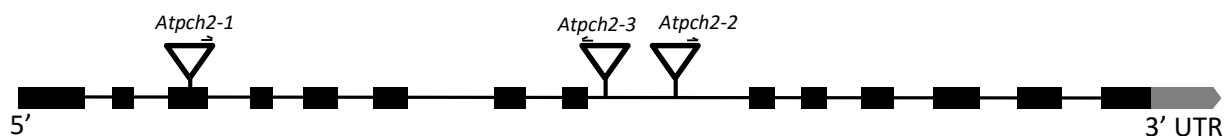


Figure 5.1: Cartoon showing positions of T-DNA insertions in the three *pch2* mutants. Exons are shown as black boxes.



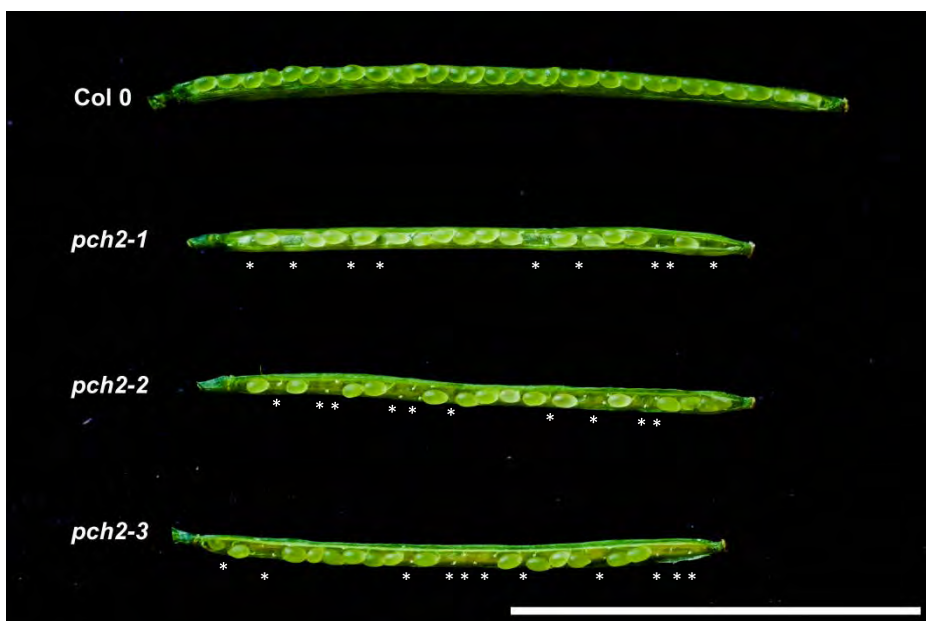
pch2-1

Col 0

Figure 5.2: *pch2-1* and Col 0 *Arabidopsis*. The vegetative phenotype of *pch2-1* is indistinguishable from Col 0, in all but silique length, which shows a small reduction in the mutant.

Figure 5.3: Siliques of all three *pch2* T-DNA insertion mutants show a reduction in silique length and gaps (stars) in the seed set. (Published in Lambing et al, 2015)

Scale bar = 10mm



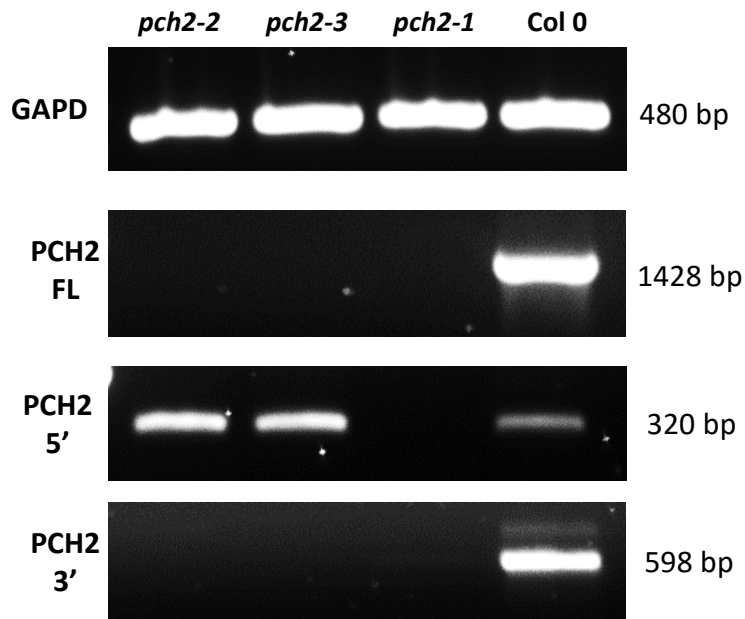


Figure 5.4: RT-PCR of full-length (FL) *PCH2* transcript (1428bp), *PCH2* 3' region (598bp), *PCH2* 5' region (320bp) and GAPD (480bp). The full-length *PCH2* transcript could not be amplified in any of the three T-DNA insertion lines. *pch2-2* and *pch2-3* still produced a product for the *PCH2* 5' region, while *pch2-1* produced a very faint product for the 3' region.

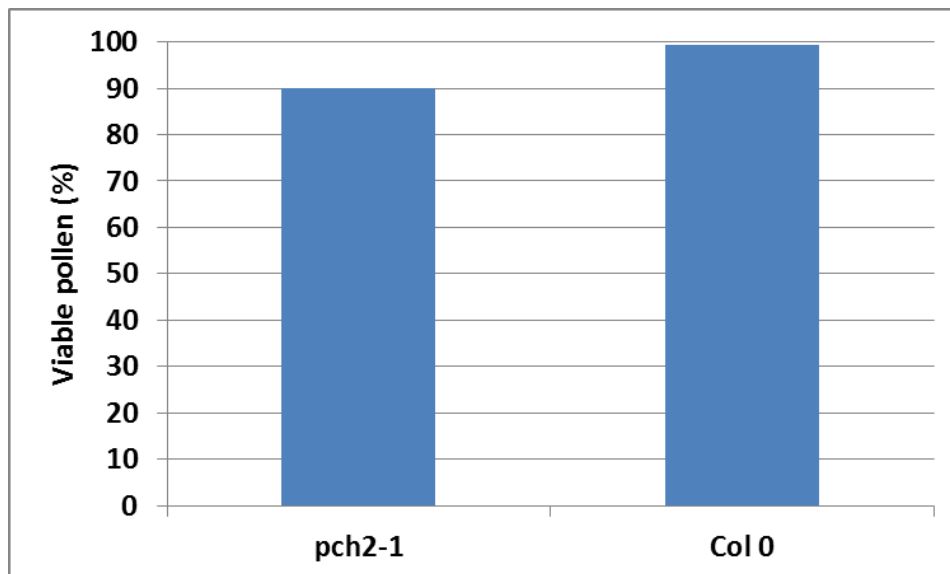


Figure 5.5: Alexander staining of pollen grains in Col 0 (n=811) and *pch2-1* (n=893).

5.2.2 Crossover formation is defective in *Atpch2-1*

DAPI spreading of *Atpch2-1* pollen mother cells (PMCs), compared with those of Col o revealed no discernible difference at the leptotene and zygotene stages (Figure 5.6 A, B, K, L). Col o PMCs then proceed to pachytene stage, where homologous chromosomes are fully synapsed (Figure 5.6 C). Chromosomes in *Atpch2-1* PMCs were never observed to have reached this stage, and at most displayed only partial synapsis (Figure 5.6 M). At metaphase I, in Col o plants, the ten chromosomes are condensed into five bivalent structures of homolog pairs connected by chiasmata (Figure 5.6 F). *Atpch2-1* PMCs often display univalent chromosomes at metaphase I (Figure 5.6 P), and a reduction in mean chiasma frequency, which was previously quantified as being 6.94, versus 9.60 in Col o (Lambing et al., 2015). Chiasma counts in *Atpch2-2* and *Atpch2-3* produced similar results. Following metaphase I, the two division stages of meiosis show accurate chromosome segregation in Col o (Figure 5.6 G-J), but chromosome missegregation is often observed at these stages in *Atpch2-1*, due to the presence of univalent chromosomes, which segregate randomly (Figure 5.6 Q-T).

To investigate whether this reduction in chiasma frequency was a result of impaired programmed DSB formation, dual immunolocalisation was carried out to stain the axis-component ASY1 and the recombinase RAD51, which can be used as an indicator of DSB frequency. Counts of RAD51 foci in early prophase I PMCs shows that Col o nuclei display 146 foci ($n=12$, $P=0.37$ Wilcoxon signed-rank test), at leptotene stage, and that *Atpch2-1* nuclei display a similar number, 144 ($n=12$, $P=0.56$) (Figure 5.7). Other members of our lab working on the project counted similar numbers of DMC1 and MSH4 foci, which were also not significantly different between *Atpch2-1* and Col o (Lambing et al., 2015). These data suggest that the early stages of recombination

proceed as normal, and that the defect in CO formation is a result of a defect occurring downstream in the recombination process.

To test this hypothesis, immunolocalisation was performed using antibodies against proteins which can identify CO-designated recombination sites. MLH1 is involved in the later stages of recombination, in the stabilisation of double Holliday junctions, and specifically marks the sites of interfering COs (Jackson et al., 2006). Dual immunolocalisation of MLH1 and ZYP1 in Col o and *Atpch2-1* PMCs at the pachytene stage showed a reduced number of MLH1 foci in *Atpch2-1* (7.1, n=12) compared to Col o (9.9, n=12) (work carried out by C. Lambing and K. Nuntasontorn, Lambing et al, 2015). These data are consistent with the observed reduction in chiasma frequency in *Atpch2-1*. The E3-ligase HEI10, can also be used to mark the sites of future interfering COs (Chelysheva et al., 2012). HEI10 forms numerous foci at leptotene (~166) which decrease over the course of prophase I, and are no longer detectable at pachytene. Most of these foci are around 175nm in diameter, but a subset are larger in size, >250nm, and are thought to mark future CO sites. In Col o and *Atpch2-1* the mean number of large HEI10 foci in early prophase I was not significantly different (10.6 in Col o, 10.2 in *Atpch2-1*, $P=0.20$). In Col o, the number of these large HEI10 foci remained constant over the course of prophase I, with a mean of 9.9 foci (n=14) at the pachytene stage. In *Atpch2-1*, the number of large HEI10 foci was decreased in late prophase I, to 6.9 (n=27), which is significantly different to Col o ($P<0.001$), and consistent with the chiasma counts and MLH1 immunolocalisation data. These foci appeared to co-localise with synapsis initiation sites and the terminal ends of ZYP1 stretches during prophase I (Figure 5.8, producing a similar pattern to that observed in the MSH4 immunolocalisation in both Col o and *Atpch2-1* (Figure 5.9). A similar pattern was also observed in *Brassica oleracea* (Lambing et al., 2015).

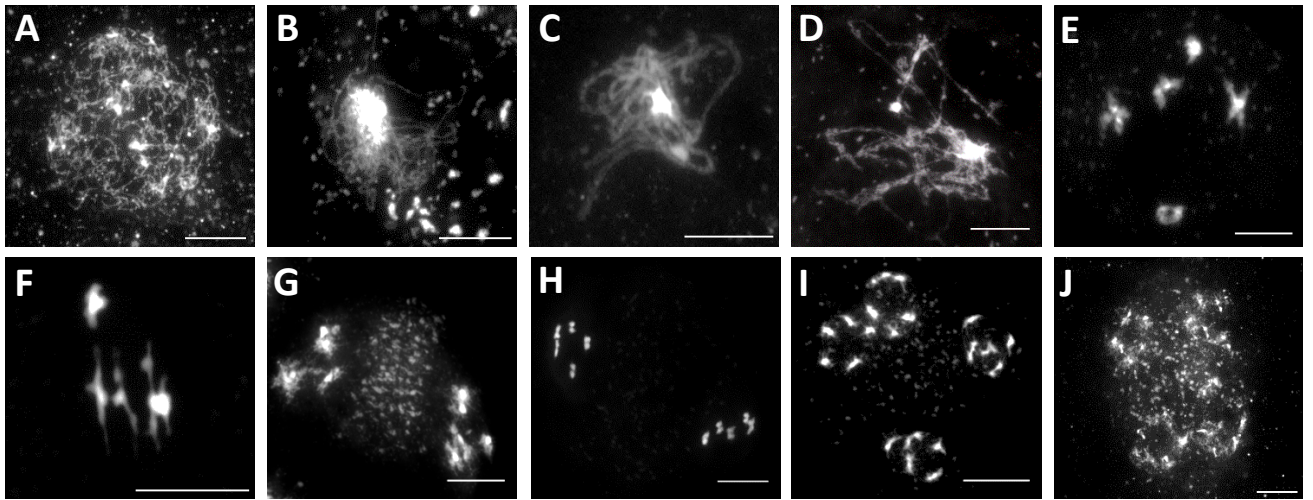
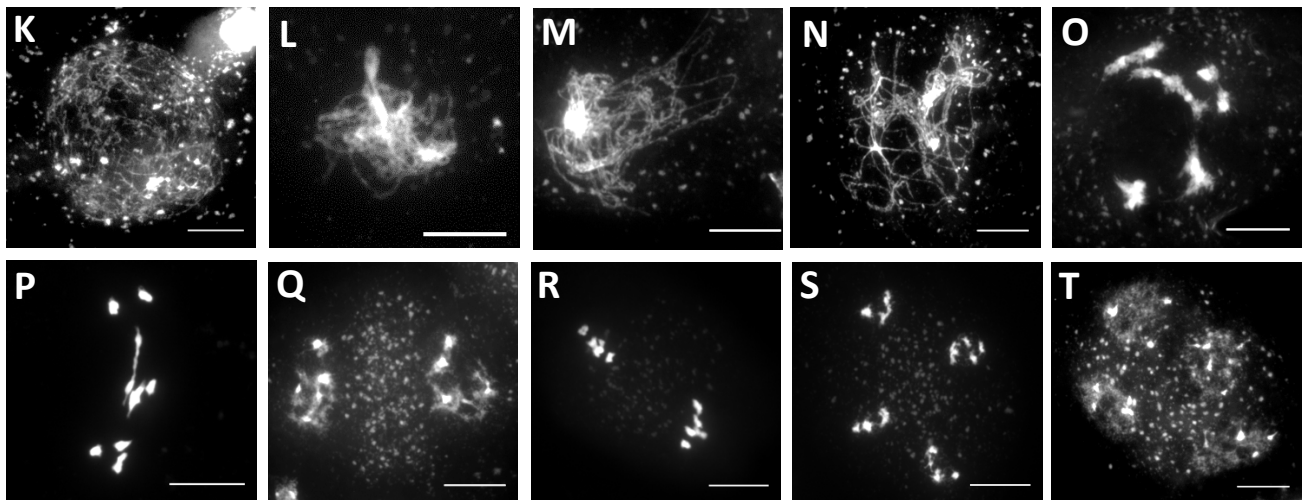
Col 0***pch2-1***

Figure 5.6: Meiotic atlas of Col 0 (A-J) and *pch2-1* (K-T).
Scale bar = 10 μ m

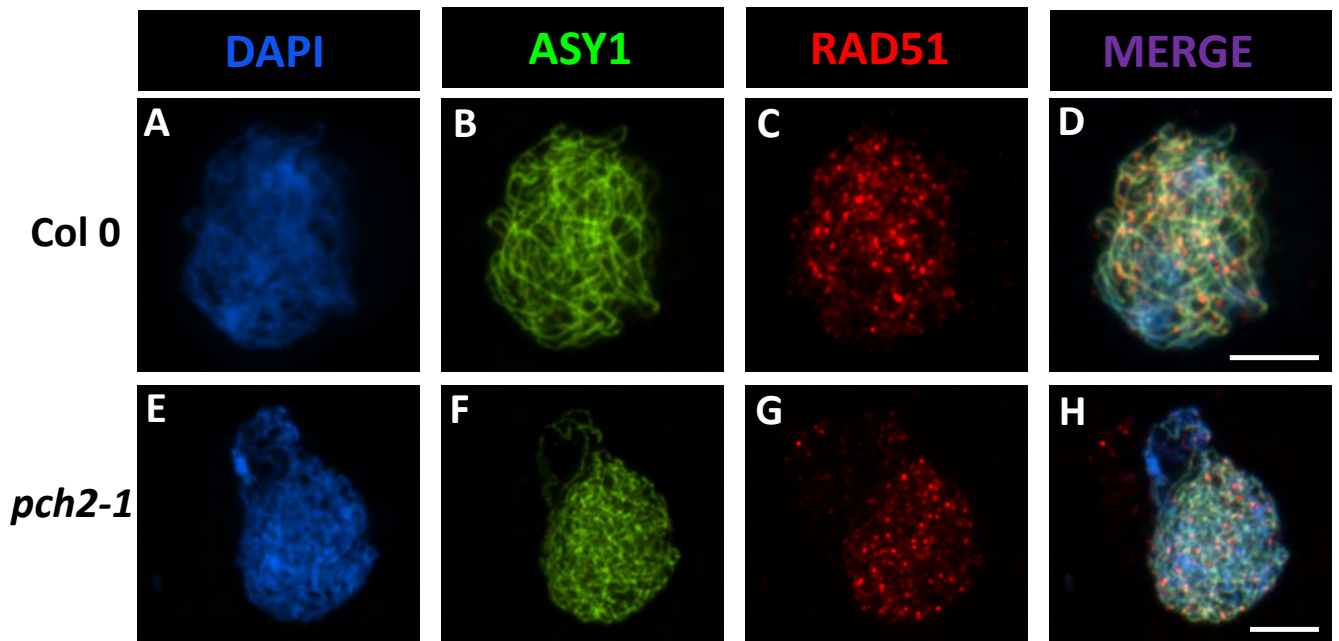


Figure 5.7: RAD51 co-localised with ASY1 in PMCs at leptotene stage. Foci counts show similar numbers in both *Col 0* (147 ± 4 , $n=5$) and *pch2-1* (146 ± 5 , $n=5$). Scale bar = $5\mu\text{m}$

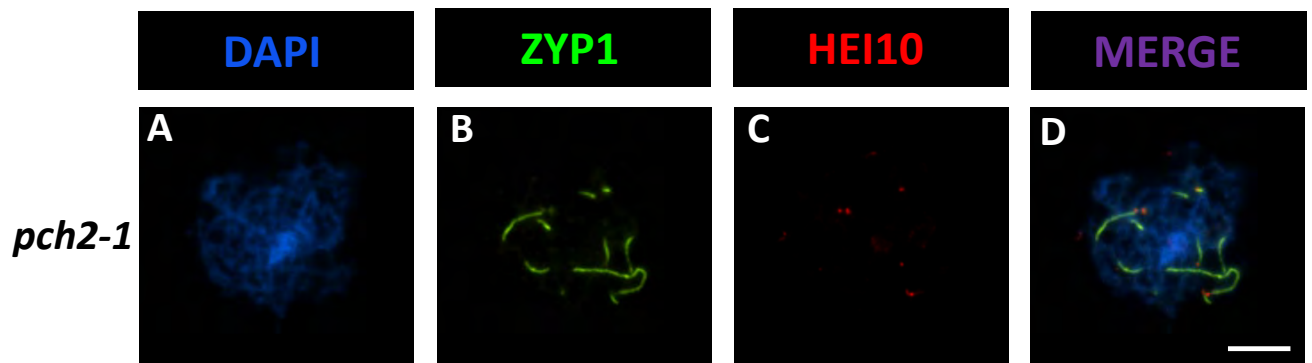


Figure 5.8: ZYP1 colocalised with HEI10 in *pch2-1* PMCs in prophase I. HEI10 foci colocalise with the terminal ends of the ZYP1 stretches.
Scale bar = 5 μ m

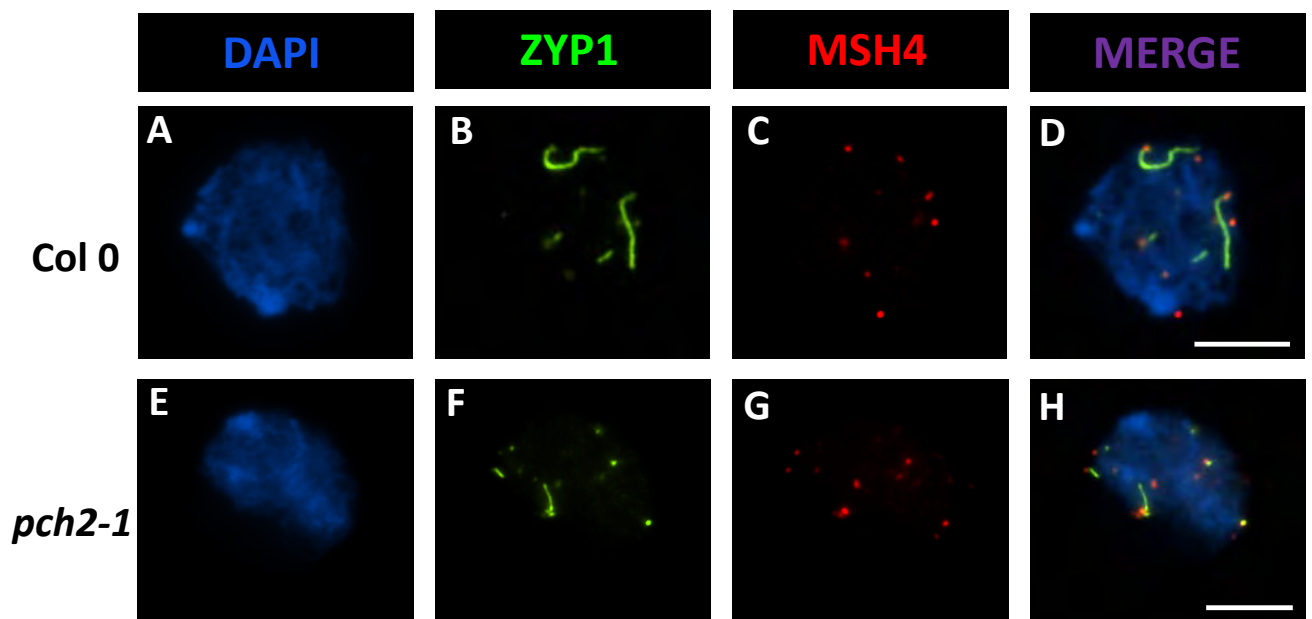


Figure 5.9: ZYP1 colocalised with MSH4 in zygotene Col 0 PMCs and *pch2* meioocytes at an approximately equivalent stage of prophase I, based on the length of stretches of ZYP1. MSH4 foci appear to colocalise with ZYP1 foci and at the termini of the ZYP1 stretches.
Scale bar = 5 μ m

5.2.3 CO patterning is affected by the *Atpch2-1* mutation

The univalent chromosomes seen in *Atpch2-1* metaphase I cells show that the mutant is defective in formation of the obligate CO. To investigate whether this CO control defect included defects in CO patterning/interference, tetrad analysis was used to measure the frequency of COs formed across specific genetic intervals. The FTL (fluorescent tetrad line) system is used to detect genetic COs which form between three transgenic markers, which constitute a pair of linked genetic intervals. These markers are genes for fluorescent proteins, expressed in pollen by the *AtLAT52* promoter (Berchowitz and Copenhaver, 2008). The lines are in a *quartet* (*qrt*) background, which causes the 4 pollen grains produced from an individual meiosis, to remain attached, rather than separate. CO formation within the interval can then be assessed in lines heterozygous for the FTL T-DNAs, by scoring inheritance of colour between pollen grains of each individual tetrad (See Figure 3.15 for further explanation). I decided to analyse the effects of the *Atpch2-1* mutation on the CO frequency at a pair of adjacent intervals on chromosome 2, I2f and I2g, in addition to two intervals previously assessed on chromosome 5. *Atpch2-1* heterozygotes were crossed with homozygous I2fg FTL mutants, and the progeny selfed to acquire *Atpch2-1/-;I2fg/+;qrt/-* lines. After pollen tetrad scoring, the Perkins equation was used to determine the genetic distances (Perkins, 1949). Interval I2f showed a significant increase in genetic distance from 6.14cM in Col 0, to 8.04cM in *Atpch2-1* (Z-test; P= 0.007). I2g also showed a significant increase from 5.05cM in Col 0, to 7.06cM in *Atpch2-1* (P = 0.0003) (Figure 5.10 and Appendix A).

The FTL system can also be used to estimate the level of CO interference acting over the genetic interval. The interference ratio (IR) is calculated from the ratio between the map-distance of a particular interval when there is a CO in the adjacent interval

and when there is not. The IR is 1 when there is a complete absence of interference acting over the interval, meaning the probability of a CO forming in one interval is independent of the presence of a CO in the adjacent interval. IR for all intervals tested in Col o and *Atpch2-1* is summarized in Table 5.1. For I2f the IR was significantly increased in *Atpch2-1* (0.315) compared to Col o (0.116) (Z-test, $P=0.024$). I2g showed a similar change in IR (*Atpch2-1*; 0.319 vs Col o; 0.116, $P=0.022$). Analysis of two other pairs of FTL intervals on chromosome 5, I5a/I5b and I5c/I5d was also carried out as part of the same project, by other members of our lab (C. Lambing and K. Nuntasontorn) (Lambing et al., 2015). I5c and I5d did not show a significant difference in the genetic distance (I5c: Col o 5.47cM, *Atpch2-1* 6.01cM, $P=0.41$. I5d: Col o 6.09cM, *Atpch2-1* 6.80cM, $P=0.31$) or IR (I5c: Col o =0.565, *Atpch2-1* =0.544, Z-test; $P=0.45$. I5d: Col o =0.569, *Atpch2-1* =0.552; $P=0.46$) between Col o and *Atpch2-1* backgrounds. I5a showed a significant decrease in genetic distance in *Atpch2-1* (15.1 cM) compared to Col o (27.7cM, $P<0.0001$), while I5b showed the opposite effect, with an increase in genetic distance in *Atpch2-1* (22.6cM) compared to Col o (17.3cM, $P<0.0001$). Like in I2f and I2g, the IR for I5a and I5b was increased in *Atpch2-1* (I5a =0.976, I5b =0.870) compared to Col o (I5a =0.412, I5b =0.307), which was statistically significant ($P<0.0001$ for both).

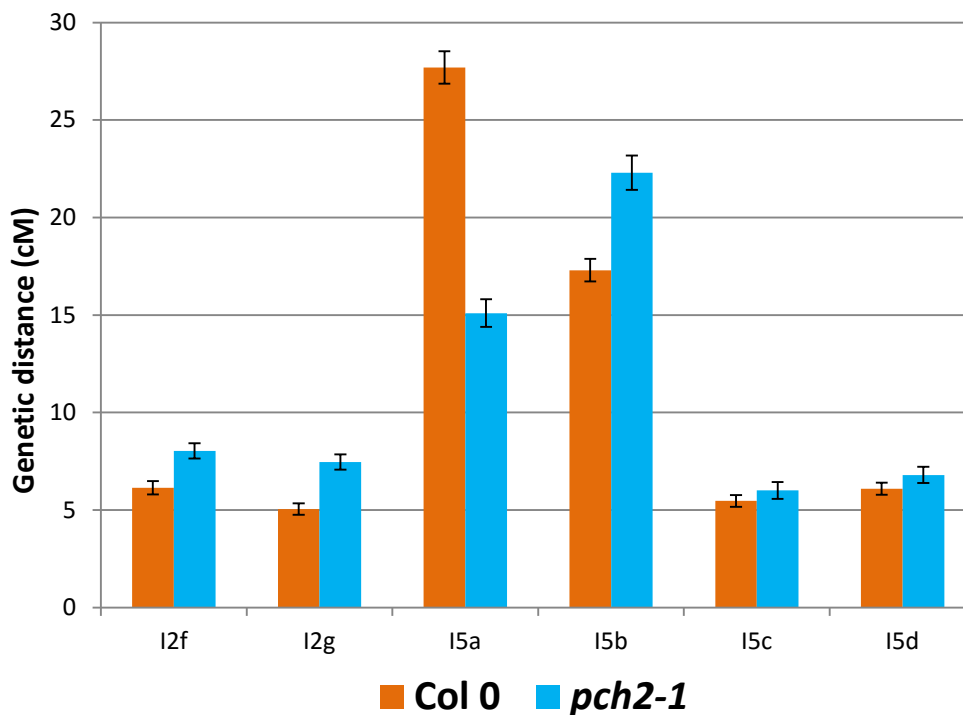


Figure 5.10. FTL analysis in Col 0 and *pch2-1*.

Error bar = Standard error

Note: I5ab and I5cd data was collected and analysed by C. Lambing and K. Nuntasontorn, published in Lambing et al, 2015.

	I2f	I2g	I5a	I5b	I5c	I5d
Col 0	0.116	0.116	0.412	0.307	0.565	0.569
<i>pch2-1</i>	0.315 (P=0.02)	0.319 (P=0.02)	0.976 (P<0.001)	0.870 (P<0.001)	0.544 (P=0.45)	0.552 (P=0.46)

Table 5.1. CO interference ratios (IR) for the 6 genetic intervals calculated from FTL data from Col 0 and *pch2-1*. IR=1 in the absence of interference.

Statistical significance was calculated using a Z-test (P values shown in table).

5.2.4 Chromosomes axis remodelling is defective in *Atpch2-1*

As homologs of PCH2 have been reported to have roles in the organisation of Hop1 homologs on the meiotic axis in yeast, mice and rice, I decided to investigate the organisation of the axis in *Arabidopsis*. Immunolocalisation of ASY1, the axis-associated HORMA domain-containing protein and ZYP1, the synaptonemal complex transverse filament protein, was performed on fixed and fresh *Arabidopsis* bud material from Col o and *Atpch2-1* (Figure 5.11). In Col o PMCs, the ASY1 signal transitions from numerous foci at G2, to a linear, axis-associated signal at leptotene, which is made up of alternating domains of high and low abundance. ZYP1 forms foci at this stage at synapsis initiation sites, which are likely to be associated with future crossover sites, based on studies in yeast (Agarwal and Roeder, 2000; Fung et al., 2004; Tsubouchi et al., 2006). During zygotene, ASY1 localises to the unsynapsed chromosome axes and produces a strong, linear signal which becomes diffuse and less intense in regions which have synapsed (Figure 5.11 I-K). ZYP1 gives a bright, linear signal on these synapsed regions, as a single track in chromosome spread preparations made from fresh material (Lipsol spreading technique; see materials and methods, Figure 5.11), and two parallel signals in preparations made from fixed material ('microwave' technique) (Figure 5.12). Full synapsis is evident from fully linear ZYP1 signals and diffuse ASY1 staining, but this was never observed in *Atpch2-1* PMCs. Stretches of ZYP1 signal of varying lengths were observed in *Atpch2-1*, suggesting that synapsis initiation is asynchronous (Figure 5.11 G and H). These stretches of ZYP1 display overlapping, linear ASY1 signal at the same intensity as in the unsynapsed axes (Figure 5.11 L-N). Like ZYP1, this ASY1 signal in *Atpch2-1* forms two parallel signal tracks in the synapsed regions in fresh material preparations, though the two tracks were only resolved when imaged with super-resolution SIM. Imaging with standard

epi-fluorescence produces a single ASY1 signal in synapsed regions which is thicker and brighter than in the unsynapsed regions (data not shown). When preparations are made from fixed material, the signal appears as two parallel signals in the synapsed regions, which can be resolved with standard epi-fluorescence microscopy, probably due to the greater degree of chromosome spreading afforded by this technique (Figure 5.12). Together, this demonstrates that AtPCH2 is required for the reduction in ASY1 signal that is seen between unsynapsed and synapsed chromosome regions, suggesting that AtPCH2 has a role in remodelling of the meiotic axis.

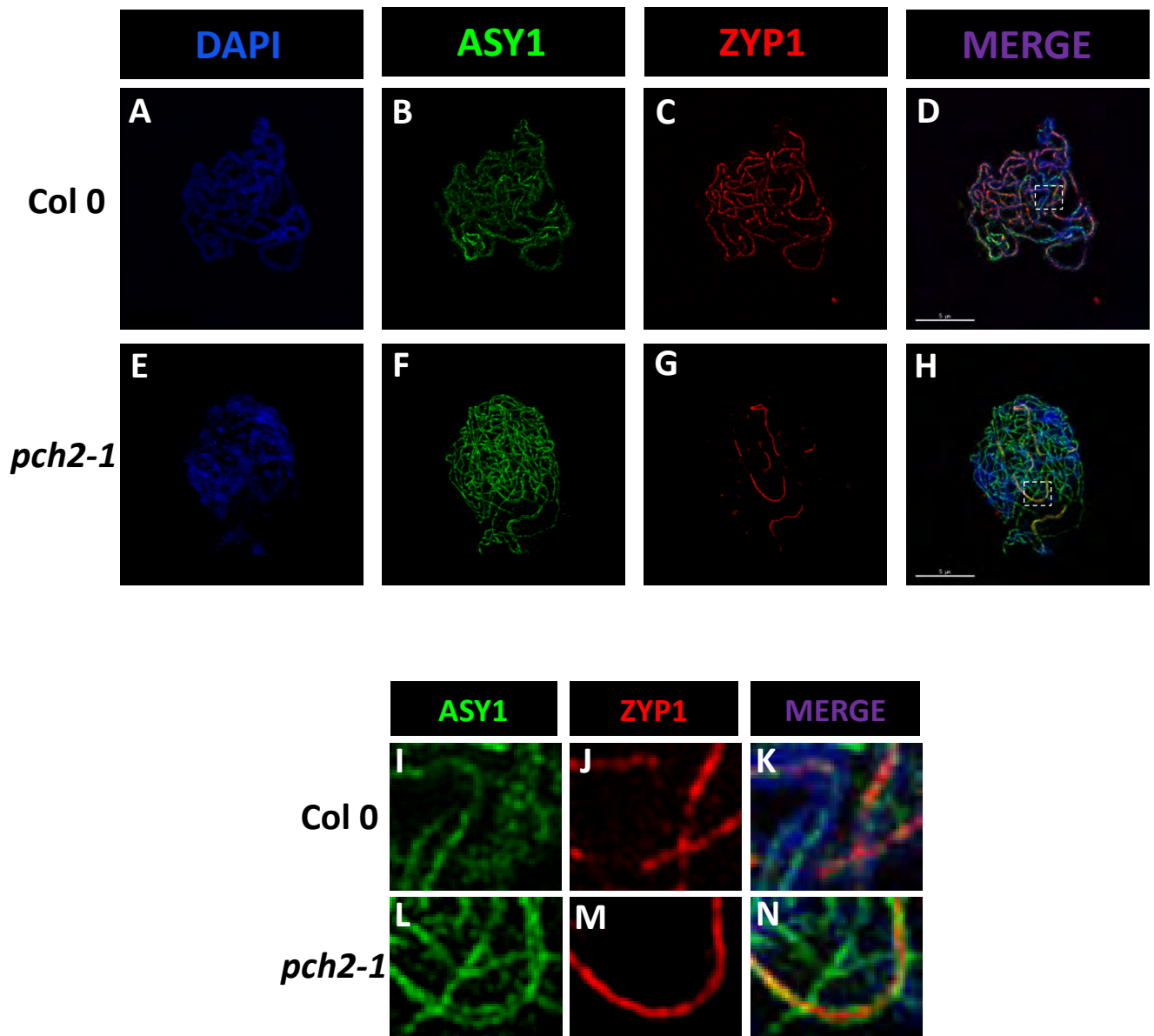


Figure 5.8: Immunolocalisation of ASY1 and ZYP1 in *Col 0* (A-D, I-K) and *pch2-1* (E-H, L-N), using structured illumination microscopy. ASY1 staining is more diffuse in synapsed regions in *Col 0*, compared to unsynapsed regions (I–K). ASY staining in *pch2-1* appears unchanged in synapsed vs unsynapsed regions (L–N). Scale bar = 5 μ m

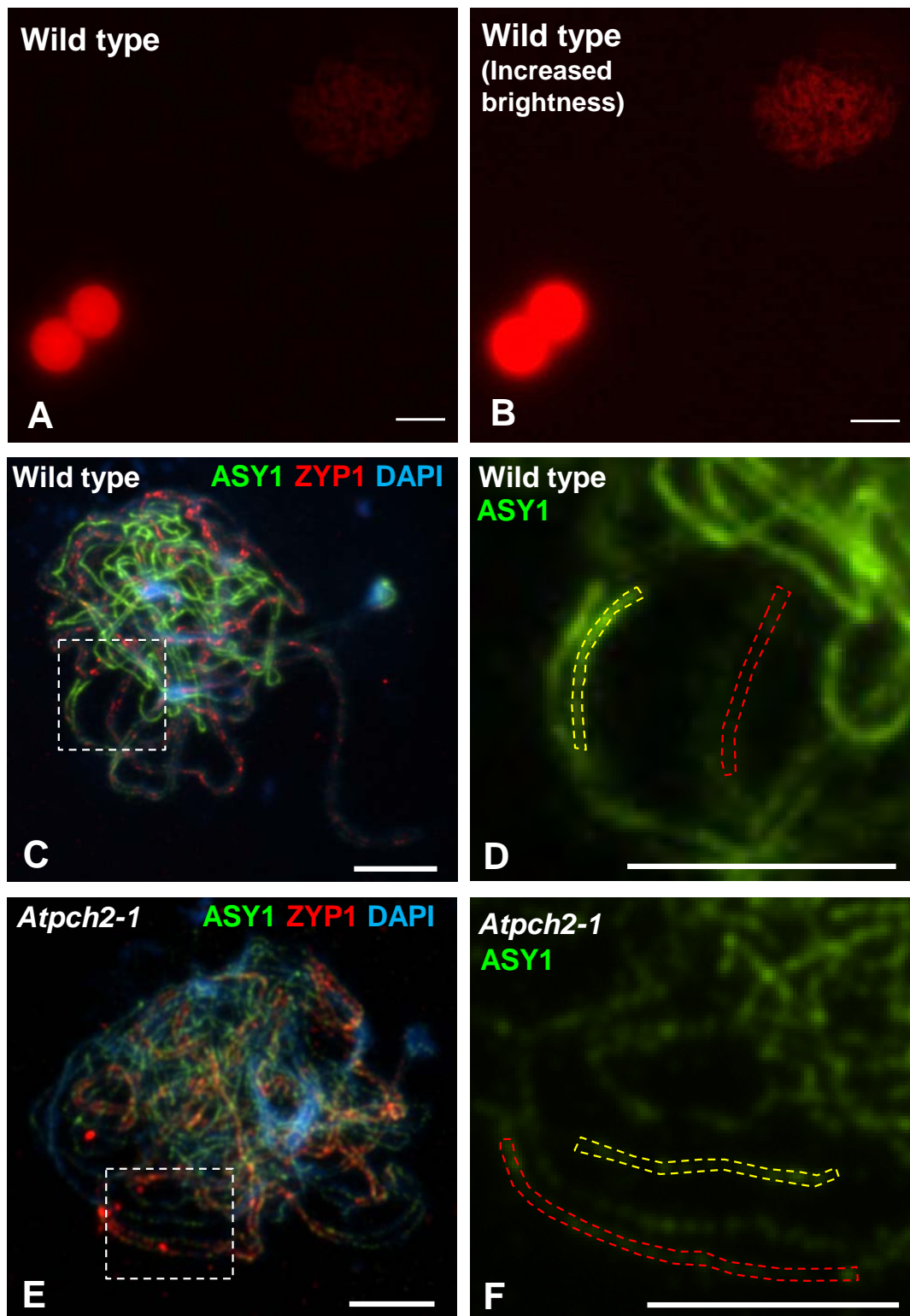


Figure 5.12. ASY1 immunostained PMC with fluorescent microsphere control, made from fresh material (A and B) and fixed material preparations immunostained with anti-ASY1, anti-ZYP1 and DAPI (C-F). A and B are the same image with the brightness increased in B for clarity. Sections of axis were analysed for ASY1 signal intensity (D and F). In wild type meiocytes, ASY1 signal intensity is reduced in synapsed chromosome regions (red dotted outline) compared to unsynapsed regions (yellow dotted outline). Chromosomes in *Atpch2-1* meiocytes show no such reduction. (Published in Lambing et al, 2015).

Scale bar = 5µm

5.2.5 AtPCH2 is required for normal loading of ASY1 onto meiotic chromosomes

I decided to investigate whether there was any change in ASY1 signal intensity between synapsed and unsynapsed regions in *Atpch2-1*, and to quantify the change in signal intensity which is observed in Col o. To do this, I used fluorescent microspheres (InSpeck microspheres, Life Technologies) as a control for signal intensity, which were applied to slides and imaged during the same session as the ASY1/ZYP1 immunostained cells. All imaging was performed using specified exposure times, which were kept constant between slides, and sets of slides were prepared on the same day. Immunolocalisation of ASY1 on preparations of fresh material showed that in early prophase I PMCs, approximately leptotene stage, the intensity of ASY1 signal over whole nuclei was reduced by 41.8% in *Atpch2-1* compared to Col o (2-tailed T-test; $P=0.0002$, Col o $n=14$, *Atpch2-1* $n=13$). Using immunolocalisation on chromosome spread preparations of fixed material, regions of axis or SC were defined as regions of interest and analysed for mean signal intensity (Figure 5.12). In Col o, mean signal intensity for unsynapsed axes was 1079.44 (greyscale units, 23 sections sampled from 17 zygotene nuclei), compared to a mean of 356.28 for the synapsed regions; a reduction of 67.0% (2 tailed, paired T-test $P<0.00001$) (Appendix B). In *Atpch2-1*, as expected, no such depletion was detectable between the unsynapsed and synapsed regions, which were 269.28 and 292.11 respectively ($P=0.25$, 22 sections sampled from 16 cells, adjusted to 99.01% of original intensity based on differences in microsphere fluorescence intensity). Surprisingly, these mean values are lower than the mean intensity for Col o unsynapsed ASY1, meaning that AtPCH2 is not only required for the change between the linear and diffuse ASY1 signals, it is also required for its deposition on the axis at wild-type levels.

5.2.6 Meiotic progression in *Atpch2-1* is delayed

I next wanted to determine whether the meiotic defects in *Atpch2-1* include a delay in meiotic progression compared to wild-type, as is the case in yeast (Börner et al., 2008). 5-ethynyl-2'-deoxyuridine (EdU) pulse labelling was used to carry out a time-course experiment in Col 0 and *Atpch2-1* plants to test this hypothesis. Plant stems were cut and immersed in a solution of EdU for 1 hour, then transferred to water and bud material was fixed at specific time points. The EdU was detected cytologically at different meiotic stages to determine the rate of meiotic progression (Table 5.2 and Figure 5.13). In both Col 0 and *Atpch2-1* plants, leptotene nuclei labelled with EdU were detected 10 hours post S-phase. Col 0 PMCs progressed from zygotene, detected at 20 hours, to pachytene at 25 hours, reaching the dyad stage by 36 hours. In contrast, *Atpch2-1* PMCs remained at leptotene at 20 hours, and did not reach zygotene until 25 hours, remaining at this stage at 36 hours. This suggests a considerable delay, of up to 16 hours.

Time post S phase (h)	Latest stage of meiotic progress observed in sample	
	Col 0	<i>Atpch2-1</i>
10	Leptotene	Leptotene
20	Zygotene	Leptotene
25	Pachytene	Zygotene*
30	Diplotene	Zygotene*
32	Diakinesis	Zygotene*
36	Dyad	Zygotene*

Table 5.2. Time course of prophase I progression in wild-type and *Atpch2-1* PMCs. Cells were pulse-labelled with EdU during meiotic S phase as previously described (Armstrong et al., 2003). Samples were taken at different time points and the extent of meiotic progression of labelled nuclei was assessed cytologically. This revealed a delay in progression through prophase I in *Atpch2-1* cells of 5-8h. (* Note: as synapsis was incomplete in *Atpch2-1*, fully synapsed pachytene cells were not observed).

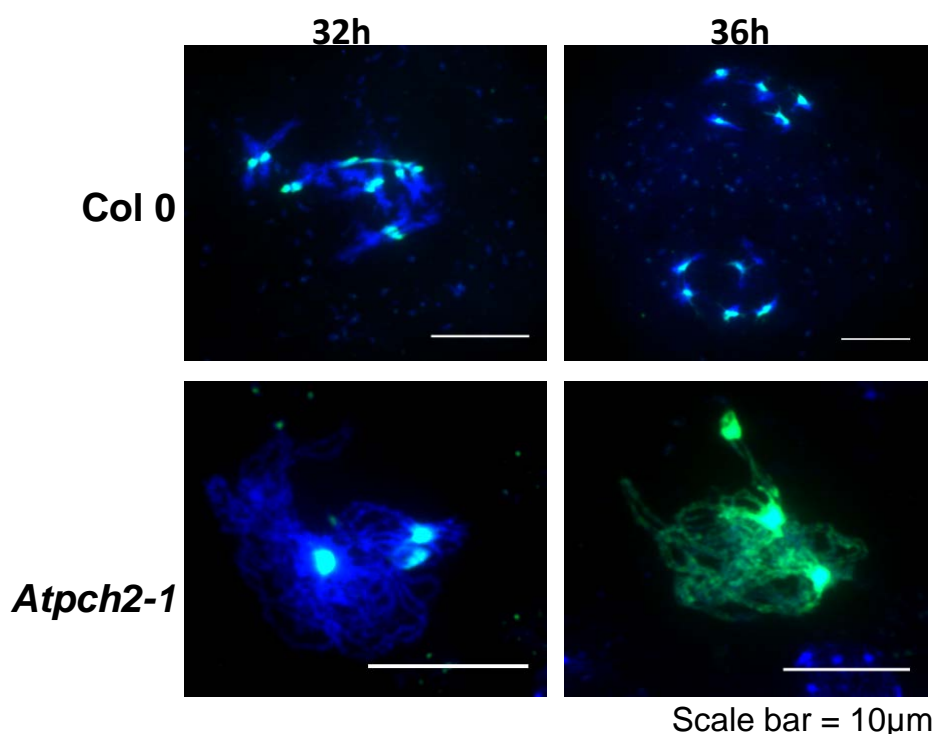


Figure 5.13 PMCs observed at 32 and 36 hours post-S phase at the latest EdU-labelled stage of meiosis. Col 0 PMCs reach diakinesis and dyad stages at 32 and 36 hours respectively, while *pch2-1* PMCs remain in zygotene at these time points. EdU staining = green, DAPI-stained chromatin = blue.

5.3 Discussion

Some of the functions of AtPCH2 appear to be conserved between *Arabidopsis* and other species in which it has been studied, such as its involvement in remodelling of the axis during prophase I, and in CO control. It is likely that the axis-remodelling defects seen in *Atpch2-1* are linked to the defects in synapsis and CO maturation.

5.3.1 AtPCH2 is required for normal ASY1 dynamics during prophase I

The co-immunolocalisation of ASY1 and ZYP1 shows that in Col o, ASY1 is depleted from the axes during synapsis, producing a weaker and more diffuse signal on the chromosomal regions where ZYP1 has loaded. In *Atpch2-1*, the ASY1 signal appears just as bright in the ZYP1 containing, synapsed regions as it does in the unsynapsed regions. This demonstrates that ASY1 is remodelled by AtPCH2 during prophase I. An interaction between the homologous proteins in yeast was demonstrated *in vitro* (Chen et al., 2013).

In addition to this, my subsequent analysis indicates that the brightness of the ASY1 signal in *Atpch2*, is actually only as bright as in the ASY1-depleted, synapsed regions of Col o chromosomes (Appendix B). This analysis was performed in zygotene PMCs, so that measurements could be made of the unsynapsed and synapsed regions, allowing a paired statistical analysis, so it remains unknown whether ASY1 loading is normal or defective in *Atpch2-1* during leptotene. A model where AtPCH2 is required for normal ASY1 deposition would fit with data describing the immunolocalisation analysis of AtPCH2, in *Arabidopsis* and *Brassica*, which forms numerous foci during G2 and co-localises with short stretches of ASY1 (Lambing et al., 2015). The AtPCH2

signal is distinct from the ASY1 signal during G₂, but the signals increasingly overlap during the formation of the fully linear axis in leptotene.

A requirement for AtPCH2 in normal ASY1 loading would be a similarity between the *Arabidopsis Atpch2* phenotype and that of *crc1* in rice, which fails to recruit the ASY1 homologue, PAIR2, onto meiotic chromosomes (Miao et al., 2013). *trip13* mutants in mouse and *Atpch2* mutants in yeast, also show defective loading of their ASY1 homologs, HORMAD1 and Hop1 respectively, onto meiotic chromosomes, but as a loss of domainal organisation rather than a general reduction in loading (Börner et al., 2008; Wojtasz et al., 2009). The phenotypic severity of *Arabidopsis Atpch2-1* appears to lie between rice and yeast in terms of ASY1 loading, in that it is required for ASY1 loading at wild-type levels.

5.3.2 AtPCH2 is dispensable for the early stages of recombination and DSB repair

Rice *crc1* mutants are unable to produce programmed DSBs (Miao et al., 2013), while in yeast, loss of Pch2 leads to a reduced number of DSBs (Farmer et al., 2012). In contrast, *Atpch2-1* mutants do not appear to show any defects in the initial stages of recombination, based on immunostaining with RAD51 and DMC1. The lack of chromosome fragmentation seen in the chromosome spread preparations of *Atpch2-1* PMCs indicates that repair of these DSBs is carried out efficiently, though with a smaller proportion of recombination events resulting in COs. The observed delay in meiotic progression demonstrated by the EdU timecourse is consistent with a defect at some point in the recombination pathway, as delays have been seen in mutants affected at different stages of recombination (*Atmsh4*; Higgins et al., 2004, *Atzyp1*;

Higgins et al., 2005 and *Atmlh3*; Jackson et al., 2006). The reduction in CO formation affects both interference-sensitive and interference-insensitive pathways, based on chiasmata analysis of *Atpch2/Atmsh5* double mutants (Lambing et al., 2015). This would be consistent with the idea that the underlying cause of the recombination defect is a result of defective axis organisation, such as in an *Atasy3* mutant (Ferdous et al., 2012).

5.3.3 CO interference is established in *Atpch2-1* prior to a CO maturation defect

Based on the fluorescent tetrad analysis in *Atpch2-1* and Col 0, genetic distance was significantly increased in the mutant in three out of the six intervals, found on both chromosomes 2 and 5, while one of the six showed a significant decrease. This shows that despite the overall decrease in CO number in *Atpch2-1*, based on chiasma scoring in metaphase I nuclei, the CO frequency still increases in some chromosomal regions. CO interference appears to show a significant reduction in 2 out of the 3 pairs of genetic intervals tested, one on chromosome 2 and the other on chromosome 5, again producing different results for different chromosome regions.

A reduction in MLH1 foci was seen in *Atpch2-1* compared to Col 0 (7.1 vs 9.9 respectively), which is consistent with the chiasmata count data. Foci of HEI10 appeared with the same frequency in *Atpch2-1* and Col 0 in early prophase I (10.2 vs 10.6) but by late prophase I, numbers were reduced in *Atpch2-1* until the counts appeared highly similar to those of MLH1 foci (6.9 vs 9.9). This suggests that the number of CO-designated sites in early prophase I is unchanged in *Atpch2-1*, but that some of these sites do not mature into COs, resulting in an overall reduction. In late

prophase I, remaining MLH1 and HEI10 foci seen in *Atpch2-1* were associated with stretches of ZYP1, very often only displaying a single focus per ZYP1 stretch, implying that CO interference is still active.

In budding yeast, foci of Zip3 (similar to HEI10), show the same spatial separation along the axis in *pch2* mutants as they do in wild-type (Zhang et al., 2014b). This demonstrates that interference is still active in *pch2* mutants, though when the inter-focus distance of Mlh1 foci is used as a metric for interference in these mutants, CO interference is inferred to be reduced (Joshi et al., 2009; Zanders and Alani, 2009). This implies that interference is initially established in early prophase I, but that not all of these sites fully mature into COs in an *Atpch2* background, leaving a reduced number of both Zip3 and Mlh1 foci. If these remaining foci show a decrease in interference, however small, it implies that additional recombination events and CO designations may have taken place, following the establishment of interference at the Zip3 deposition stage. One possible explanation for this relies on the recent finding that DSBs continue to be produced in unsynapsed chromatin (Thacker et al., 2014). This study included the finding that ZMM mutants produce more DSBs than in wild-type, which could also be true of *Atpch2* mutants.

5.3.4 Synapsis initiates uni-directionally in *Arabidopsis*

Co-localisation of ZYP1 with MSH4 and HEI10 (Figures 5.12 and 5.13), show foci of MSH4 and HEI10 at the termini of the ZYP1 stretches, suggesting polymerisation is occurring outwards from recombination complexes in a uni-directional manner, at least at this early stage. This would fit with the model of how synapsis initiates in *Sordaria macrospora*, where synapsis initiates in one direction from synapsis

initiation sites (Zickler et al., 1992; Zhang et al., 2014b). EM microscopy of zygotene nuclei in *Sordaria* showed that late recombination nodules (destined to become COs) are associated with longer stretches of SC, while early nodules (destined to become NCOs) are associated with shorter stretches of SC (Zhang et al., 2014b). This suggests that synapsis initiates first at the CO designated sites. The images showing large HEI10 foci at the termini of SC stretches indicates that this is also the case in *Arabidopsis*. This appears to still be true for *Atpch2-1*, indicating that its function is not essential for this property of synapsis.

An alternative possibility is that these foci, in *Atpch2-1* and Col o, could be telomeric sites, and the foci of recombination proteins seen are actually binding non-specifically to these protein-rich structures. This seems unlikely since these antibodies do not appear to bind to telomeres at pachytene when the telomeres can be easily identified.

Chapter 6

The effects of temperature on meiosis in wild-type Col o and meiotic mutants

6.1 Introduction

Temperature affects various biological processes in plants, including circadian rhythm function (Gould et al., 2006), RNA splicing (Balasubramanian et al., 2006) and DNA replication during S-phase (Higgins et al., 2012). Meiotic processes are also known to be sensitive to temperature, as well as other environmental influences. Global mean surface temperatures are projected to increase by 1.8-4.0°C by 2100, with high northern latitudes experiencing the greatest change, so understanding the relationship between temperature and plant reproduction is important for agriculture and crop breeding (Reviewed in Solomon, S. et al., 2007; Hedhly et al., 2009; Singh et al., 2013). Both low and high temperatures have been shown to cause meiotic defects in a variety of organisms, including plants (De Storme and Geelen, 2014; Bomblies et al., 2015). These defects include asynapsis, failure to form sufficient chiasmata, failure to resolve chromosome interlocks and errors in nuclear division. These errors are also variable depending on experimental design, with prolonged exposure to temperature extremes causing different effects to shorter heat shocks, which might be applied only for the duration of meiosis or a particular stage of meiosis.

In *Arabidopsis*, the distribution of crossovers (COs) has been shown to be sensitive to changing temperatures. A study using the fluorescent tetrad analysis (FTL) system (See Chapter 3 for description), saw a steady increase in CO formation in two genetic intervals between 19°C and 28°C (Francis et al., 2007). In barley, exposure to temperatures of 30°C causes a slight reduction in chiasma frequency, compared to plants grown at 22°C, but also causes a modest but significant shift in chiasma localisation from centromere distal regions to more centromere proximal regions, with some chromosomes showing greater susceptibility than others (Higgins et al., 2012). These changes were thought to be linked to variations in the DNA replication

programme during S-phase, which at typical temperatures (22 °C) would initiate in the distal/telomeric regions of chromosomes and slowly progress towards the centromeres and heterochromatic regions over the course of about 13 hours. At high temperatures (30 °C), DNA replication progressed more quickly in the centromere proximal and heterochromatic regions, showing completion within 9 hours. At 30 °C the shift in CO localisation was concomitant with a small reduction in the overall chiasma frequency. An earlier study, also in barley, supports these changes in the spatiotemporal regulation of recombination, having reported that ASY1 is upregulated earlier in plants exposed to high temperature treatment, resulting premature initiation of prophase I (Oshino et al., 2007). Later it was demonstrated that SC length in barley is increased in meiocytes exposed to high temperatures, and that this effect was specific to male meiosis (Phillips et al., 2015). CO frequency was also shown to increase in PMCs, with increasing temperature between 15 and 25 °C, again in a chromosome-specific manner. Based on immunolocalisation of MLH3, COs were redistributed from centromere distal to proximal regions, but did not reflect the increased CO number which was determined genetically. This suggested that interference-sensitive COs were redistributed but that the increase in overall CO number could be due to an increase in non-interfering COs. The increased SC length and sex-specific differences are consistent with earlier observations that in species where one sex is more recombinogenic than the other (heterochiasmy), longer SCs are observed in the sex with higher CO frequency (Lynn et al., 2002; Tease and Hultén, 2004).

Various studies in *Arabidopsis* have looked at the epigenetic effects of temperature. Naydenov et al., 2015, investigated the expression of several genes involved in DNA methylation in response to exposure to 36 °C for time periods ranging from 6 to 48 hours. The expression of these methyltransferase genes increased, as did expression

of ROS1, a DNA demethylase, and genes involved in the plant-specific RNA-directed DNA methylation (RdDM) pathway. Study of *Arabidopsis* has shown DNA methylation to be an important factor in meiosis, involved in the suppression of CO formation in parts of the genome which are normally transcriptionally repressed, such as centromere proximal regions (Yelina et al., 2012). Supporting this, DNA methylation has been demonstrated to be inversely associated with recombination hotspot localisation, though other factors are also involved (Choi et al., 2013). In mouse, a similar situation was observed in DNA methylation deficient mutants, which adopted a recombination permissive chromatin state in transposons, which would normally be repressed for this activity (Zamudio et al., 2015). This shift in chromatin state was associated with a shift from the repressive H3K9Me2 chromatin modification to the recombination hotspot-associated H3K4Me3 mark (Choi et al., 2013 and discussed in more detail in Chapter 3). Another study showed that the accelerated flowering seen in *Arabidopsis* grown at high temperatures is due to stabilisation of JMJ30, a histone demethylase which binds to *FLOWERING LOCUS C* and removes a repressive histone modification, H3K27Me3 (Gan et al., 2014).

The H2A.Z histone variant shows a sharp decline in promoter-nucleosome occupancy between *Arabidopsis* grown 17°C and 27°C (Kumar and Wigge, 2010). *arp6* mutants, which are defective in H2A.Z deposition, have transcriptomes which phenocopy plants grown at higher temperature. The authors also demonstrated the same relationship between temperature and H2A.Z occupancy in budding yeast. H2A.Z, like H3K4Me3, is also enriched at recombination hotspots (Choi et al., 2013).

Meiosis-specific temperature induced defects have been recorded in several *Arabidopsis* mutants; *Atcdkg1* and *Atrbr-2*. AtCDKG1 (Cyclin-dependent kinase G) is a protein kinase, related to cyclin-dependent kinases found in the Ph1 locus of

hexaploid wheat which ensures CO formation between homologs rather than homeologs (Greer et al., 2012; Zheng et al., 2014). CDKG1 is required for efficient chromosome synapsis and chiasma formation at normal temperatures (14-30 °C) (Zheng et al., 2014). At low temperatures (12 °C), *Atcdkg1* mutants appear to display synapsis indistinguishable from wild-type. At higher temperatures, mutants experience synaptic defects as well as a strong reduction in class I CO formation, based on MLH1 staining. Similar to the effects of high temperature treatment on barley, the defects seen in *Arabidopsis cdkg1* mutants are restricted to male meiosis. The authors hypothesize that the observed difference is due to the *Atcdkg1* mutation causing a downward shift in the temperature range at which meiosis can proceed without error, possibly due to the role of the kinase in a thermodynamically unstable meiotic pathway. The activity of recombinase enzymes for example, has been shown to be sensitive to variations in temperature in mice and lilies (Hotta et al., 1988, 1985).

Arabidopsis contains a single homologue of the tumour suppressor gene, Rb (Retinoblastoma), called *Retinoblastoma-related (RBR)*, and the two are similar in sequence and predicted structure (Kong *et al*, 2000). The loss of AtRBR is gametophyte lethal due to misregulated cell division during gametogenesis (Ebel et al., 2004; Johnston et al., 2008). An *Arabidopsis* RBR T-DNA insertional mutant called *Atrbr-2*, expresses the wild-type protein in vegetative tissues, but in reproductive cells the *AtRBR* transcript undergoes an aberrant splicing event, leading to loss of the C-terminal region of the protein (Chen et al., 2011). This mutation therefore allows the meiotic effects of AtRBR loss-of function to be studied. The study found that AtRBR has a direct role in meiosis, beyond its role in the regulation of genes controlled by the E2F transcription factor, to which it binds. In *Atrbr-2*, plant fertility is severely reduced, due to meiotic defects (Chen et al., 2011). Immunolocalisation of the protein

in wild-type plants revealed that it localises on meiotic chromosomes as discrete foci early in prophase I in a DSB dependent manner, as foci were absent in a *spo11* background (Chen et al., 2011). The *Atrbr-2* mutant showed normal DSB formation but defective SC formation and severely reduced CO formation. Though both RAD51 and DMC1 localise normally in the mutant, MSH4 foci were severely reduced, as were MLH1 foci. A *msh4/rbr-2* double mutant showed that the protein is required for both class I and class II crossover formation. AtRBR therefore seems to have a role somewhere between DMC1 and MSH4 loading. The researchers involved in this study suspected that the meiotic defects seen in *Atrbr2*, may have been temperature dependent, based on phenotypic differences observed during the summer compared to the winter, specifically that the phenotypic severity was reduced in periods of warm weather (James Higgins, personal communication). These temperature-sensitive effects have not yet been characterised in *Atrbr-2*.

Temperature is not the only form of stress to affect meiosis in plants, and it is possible that the effects of temperature are also due to a secondary consequence of stress sensing, rather than a direct, mechanistic effect on the recombination machinery. It has previously been reported that water-deficit stress can cause an increase in meiotic recombination in maize (Verde, 2003). An increase in meiotic, and also somatic recombination was also seen in Tobacco Mosaic Virus infected tobacco plants (Kovalchuk et al., 2003). Increased somatic recombination has also been observed in plants experiencing stress from UV radiation, 50 °C heat shock, high salt levels and heavy metal exposure (reviewed in De Storme and Geelen, 2014). The stress response signalling hormone abscisic acid (ABA), may be the link between these various stresses and recombination. Study of an ABA sensitive mutant (*abo4-1*) showed that somatic recombination was increased. MRE11 was upregulated in the mutant, and increasingly

so in response to ABA, while KU70, involved in non-homologous end joining, was suppressed, as was RAD51 (Yin et al., 2009). Whether or not these ABA-mediated effects on MRE11 and KU70 and RAD51 are the cause of the observed increase in homologous recombination in the mutant, or in the stress response of other plants is not clear. The same study also showed that in the *abo1-4* mutant, H3K27Me3 was deposited more heavily at *FLOWERING LOCUS C* while H3K4Me3 was deposited less, and that at *FLOWERING LOCUS T*, the inverse was true.

Temperature fluctuations have also been demonstrated to affect the spatial organisation of meiotic chromosomes. Chromosome interlocks are entanglements caused by synapsis converging from two directions, trapping another chromosome in between the two unsynapsed axes (Zickler and Kleckner, 1999). Resolution of these interlocks has been shown to require the activity of Mlh1 and TopoII (Rasmussen, 1986; Storlazzi et al., 2010), but the process has been shown to be impaired at high temperatures in various animals and in wheat (reviewed in Bomblies et al., 2015).

I have performed preliminary work to survey meiotic progression at a range of different temperatures in Col o plants and in mutants that are affected in meiosis. In addition to *Atcdkg* and *Atrbr-2*, I have also included *Atsdg2-1* and *Atpch2-1* mutants (described in Chapters 3 and 5 respectively) in my screening for temperature-specific defects.

6.2 Results

Arabidopsis plants were sowed and grown under glasshouse conditions (see materials and methods) for ~5 weeks before being transferred to a growth cabinet (Snijders, Microclima) for 3 days at 14, 20, 28, 30 (Col o only at 30 °C) or 32 °C. *Atsdg2-1* plants

were sowed a week earlier than Col o and other mutants, due to their slower rate of growth. Buds were then fixed in ice-cold 3:1 fixative and analysed cytologically, by making chromosome spread preparations stained with DAPI (see materials and methods). This was performed on Col o plants as well as four mutant lines in parallel (*Atpch2-1*, *Atsdg2-1*, *Atrbr-2*, *Atcdkg1*). Dual immunolocalisation of the axis component ASY1 and the synaptonemal complex central element, ZYP1, was carried out on fixed material of Col o and *Atsdg2-1*. The cytological analysis of each of the lines at each temperature point will be described.

6.2.1 Col o

20°C – The cytological appearance of meiosis in Col o at 20°C will be described first, as it appeared error free and could best be described as the ‘normal’ meiotic progression, based on previous observations and published descriptions. PMCs in *Arabidopsis* are easily identifiable by their increased size, which is approximately 10 times that of the surrounding somatic cells, and their high concentrations of organelles. Following G2, prophase I begins with leptotene (Figure 6.1 A), where chromosomes are arranged as thin threads on a proteinaceous axis. When visualised using immunolocalisation, the axis component, ASY1 appears as a bright, linear signal at this stage but has a domainal organisation of alternating regions of hyper and lower abundance. These axes begin to synapse together with their homologous counterparts throughout zygotene (Figure 6.1 B), and achieve full synapsis at pachytene (Figure 6.1 C) where chromosomes appear as thick threads. During synapsis, the ASY1 signal becomes less bright and more diffuse in the synapsed regions (Figure 6.2 A). These regions display continuous, linear ZYP1 staining, as the protein polymerises between

homologous chromosomes. Following pachytene, during the diplotene stage chromosomes begin to de-synapse (Figure 6.1 D). As diplotene continues, chromosomes condense further until they can be resolved as 5 distinct, bivalent structures at diakinesis, which is the last sub-stage of prophase I (Figure 6.1 E). The five bivalent chromosomes display their highest level of compaction at metaphase I, where homologs are visibly connected by chiasmata (Figure 6.1 F). The characteristic shapes of the metaphase I chromosomes results from their being pulled toward opposite cell poles via spindle attachments and can indicate the number of crossovers formed during prophase I. Accurate chromosome segregation is ensured by each pair of homologs forming at least one (obligate) CO. At anaphase I, homologous chromosomes separate, and pairs of sister chromatids are pulled towards opposite poles by the spindle (Figure 6.1 G). Once separated, the five pairs of sister chromatids decondense and the PMC appears as a dyad, with two nuclei (though no new nuclear envelope has formed around them), and a strong concentration of organelles in between them (Figure 6.1 H). Chromosomes then condense again at prophase II and are aligned again by spindle attachments at metaphase II (Figure 6.1 I). At anaphase II, sister chromatids separate and are drawn apart, this time into 5 distinct nuclei of 5 chromosomes each at the telophase II stage. The chromosomes in the four nuclei decondense again and 4 new nuclear envelopes are formed, and the PMC appears as a tetrad (Figure 6.1 J).

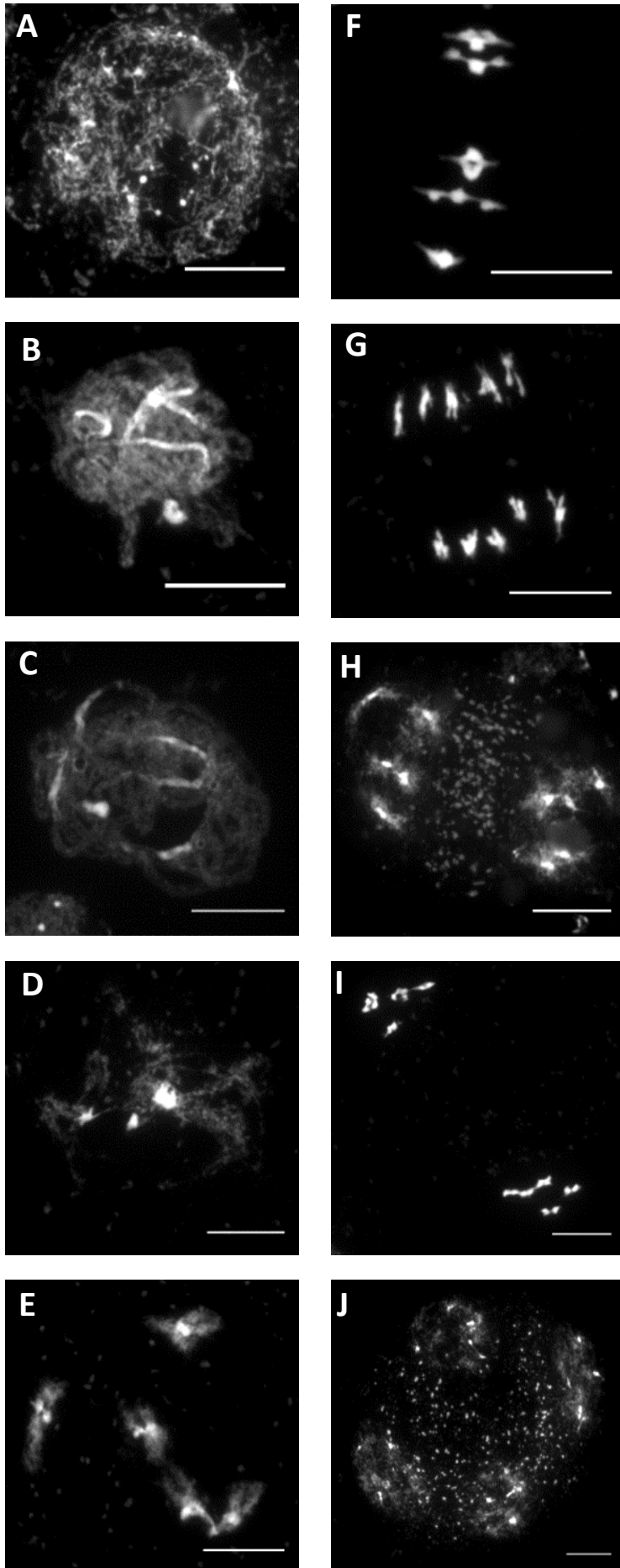


Figure 6.1: DAPI stained Col 0 PMCs grown under glasshouse conditions then grown for 3 days at 20°C before fixation.

Scale bar = 10µm

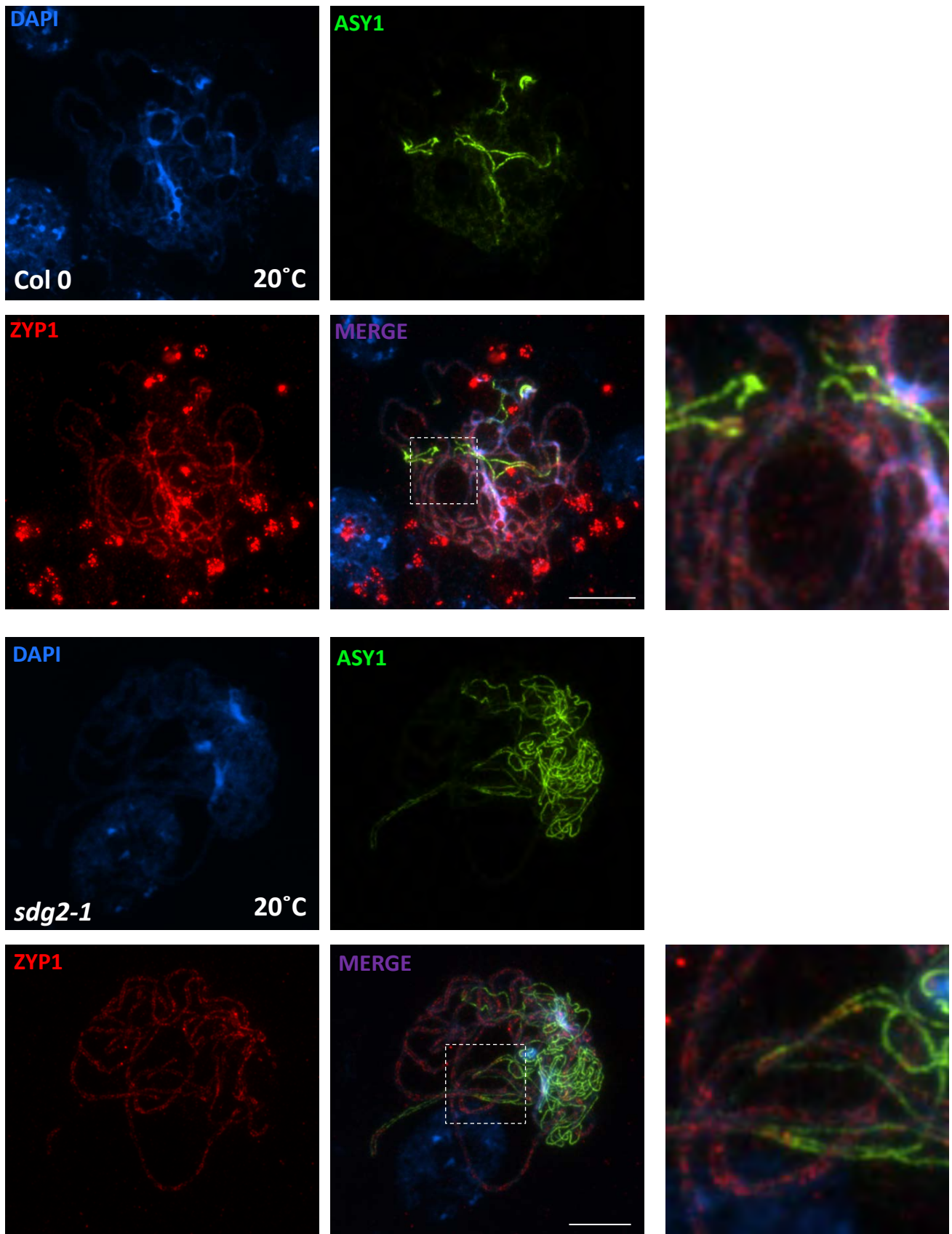


Figure 6.2 A: *Col 0* and *sdg2-1* zygote PMCs following 3 days 20°C treatment.
Scale bar = 10µm

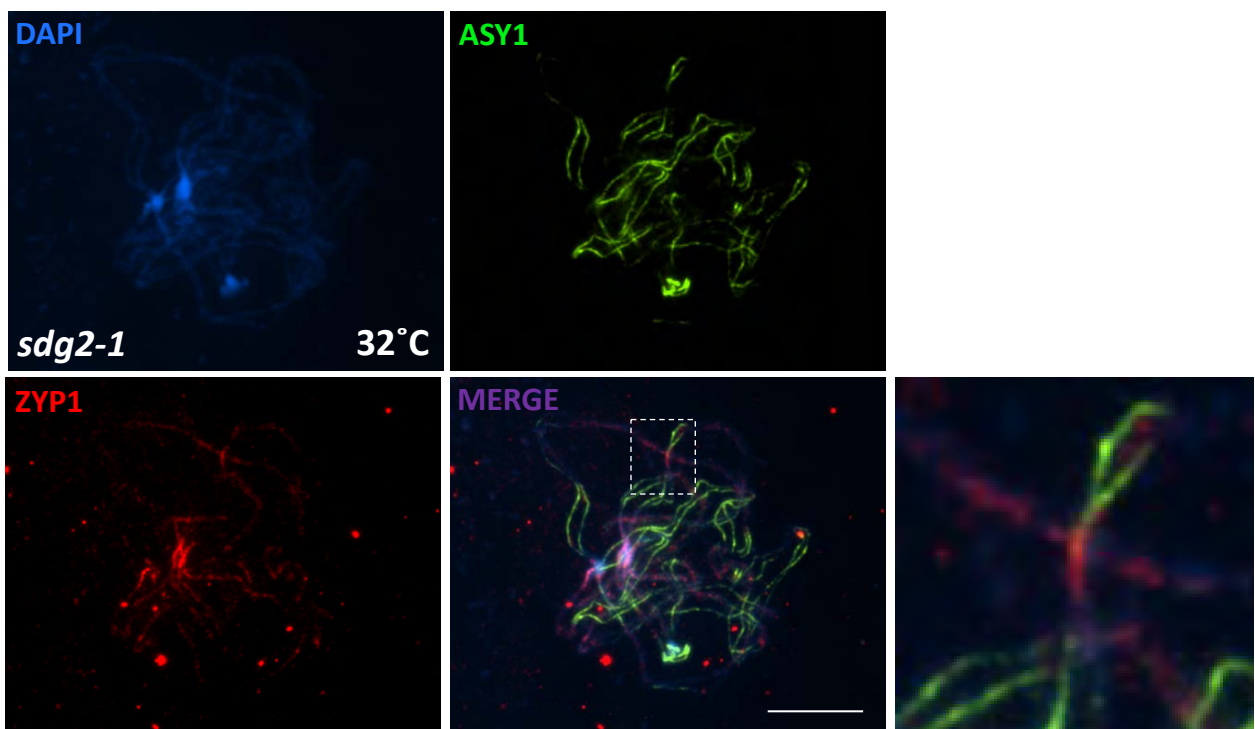
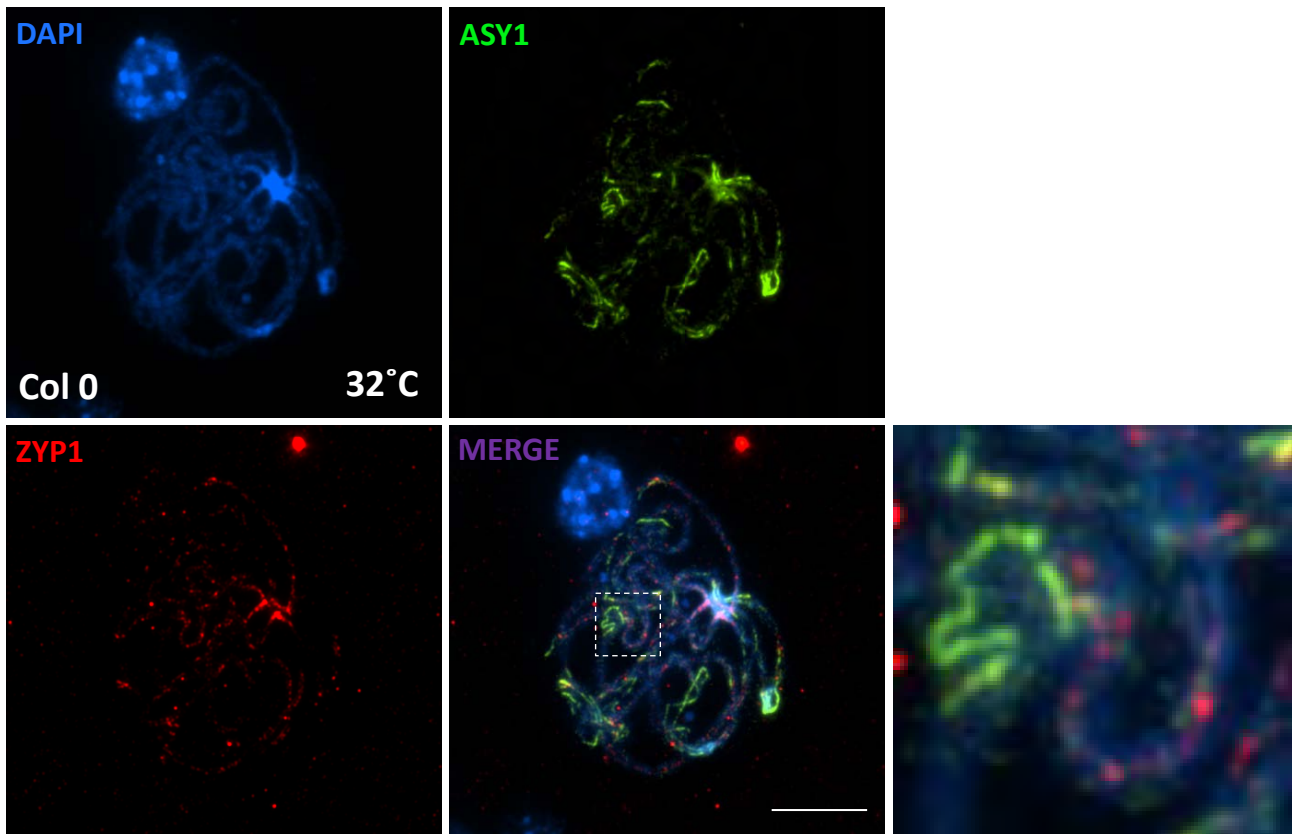


Figure 6.2 B: Col 0 and *sdg2-1* zygote PMCs following 3 days 32°C treatment.
Scale bar = 10µm

All subsequent atlases can be found in Appendix C. The meiotic defects observed in these lines following the temperature treatments, are summarized in Table 6.1.

14°C – A single chromosome fragment was observed at the dyad stage, though only in one cell. All other stages and cells appeared normal.

ASY1 and ZYP1 localisation appeared as it does at 20°C.

28°C – Several chromosome fragments were observed at the dyad stage in a single cell. All other stages and cells appeared normal.

ASY1 and ZYP1 localisation appeared as it does at 20°C.

30°C – No fragmentation was observed at this temperature, but some interlocks, where chromosomes become entangled between two homologs during synapsis, were observed in a late zygotene cell (Figure 6.3 B and H). Two pachytene stage cells displayed chromosomes which appeared slightly wider than normal (Figure 6.3 B), though pachytene cells of normal appearance were also observed. Other meiotic stages appeared as normal.

ASY1 and ZYP1 localisation appeared as it does at 20°C.

32°C – Various meiotic defects were observed at this stage. Leptotene and zygotene stages appeared normal, and some pachytene cells also appeared normal, with others showing wider than normal chromosomes, more severe than that described for 30°C, sometimes with a visible gap between the synapsed chromosomes (Figure 6.3 C). These could be seen as being completely separate, were it not for the fact that they show clear pairing, with chromosomes following each other in parallel along their length. Various defects in chromatin condensation were observed, with fuzzy/cloudy

chromosomes seen in several cells. Out of 5 identifiable metaphase I cells, 2 nuclei presented with 5 bivalent chromosomes, one showed 4 bivalents, one showed only 2 bivalents (6 univalents) and another showed zero (10 univalents), which is consistent with a defect in CO formation (Figure 6.4 F). Various problems are apparent at the tetrad stage, with cells appearing as polyads (more or less than 4 nuclei), which sometimes show different levels of chromosome condensation, fragmentation and missegregation (Figure 6.5 F). The chromosome fragmentation suggests that DSB repair is also defective at this temperature.

Dual immunolocalisation of ASY1 and ZYP1 showed normal ASY1 localisation in many cells, similar to that seen at 20°C, but others displayed large, brightly stained aggregates of ASY1 (Figure 6.6). These were axis associated, and align with the direction of the underlying axis as elongated/pointed oval shapes, rather than round structures sitting on top the axis. The underlying DAPI signal appears to follow the shape of the structures, but does not appear any brighter itself, so identification using only DAPI staining is not possible. Foci of ZYP1 were often associated with the ASY1 aggregates, though many ASY1 aggregates did not co-localise with ZYP1 (Figure 6.6 A-Y). Where the ASY1 and ZYP1 signals did show colocalisation, they did not overlap perfectly, and seemed to form distinct and irregular shapes. One of the most common features was the localisation of ZYP1 into pairs of foci, located at either end of an ASY1 aggregation (Figure 6.6 F, M, P and Y). The aggregates of ASY1 were not observed at any other temperature point. At 32°C, they were frequently observed, on two separate slides made from material from different plants.

The ZYP1 signal on synapsed regions, appeared more punctate than it did at 20°C and other temperatures (Figure 6.2 A and B). The protein still localises to the synapsed

chromosomes, but as foci of variable size and brightness, with variable amounts of spacing between them.

6.2.2 *Atcdkg*

Atcdkg mutants were chosen as a control due to their previously reported temperature-dependent meiotic defects (Zheng et al., 2014). These mutants were described as displaying a wild-type like meiotic phenotypes at 12°C, and as showing reduced fertility at 23°C, caused by defective synapsis and CO formation.

14°C – Early stages of prophase I appeared normal, though no fully synapsed pachytene cells were observed. This could be due to a small number of cells of this stage being identified though. At metaphase I, one cell showed 4 bivalents/2 univalents, with another showing 4 or 5 bivalents (though overlaid chromosomes made it impossible to be accurate). These were the only two metaphase I cells identified. At the dyad stage, one cell showed a chromosome fragment, while another showed a lagging chromosome (localised at neither pole).

20°C – This temperature showed similar defects to those seen at 14°C. Early stages of prophase I appeared normal, but metaphase I chromosomes included univalent chromosomes in all 5 cells observed. Dyads and tetrads showed missegregated chromosomes, and some chromosome fragmentation.

28°C – Early stages of prophase I appeared normal, though no pachytene cells were identified. Tetrads showed similar defects to those at 20°C, with chromosome missegregation and fragmentation.

32°C - Leptotene cells were not identified at this temperature point. Zygotene cells appeared normal and one normal-looking pachytene cell was identified. Other pachytene cells appeared to show similar defects to those of Col 0 at 32°C, with wider spacing seen between lateral elements and sometimes more fuzzy chromosomes (Figure 6.3 G). Univalent chromosomes were seen at metaphase I (Figure 6.4 J). Tetrads with differently sized nuclei at different levels of condensation were also apparent, most likely resulting from missegregated chromosomes (Figure 6.5 J).

6.2.3 *Atpch2-1*

The 'normal' cytological description of meiosis for *Atpch2-1* is described in full in Chapter 5 and Lambing et al., 2015, but to summarise the defects, complete synapsis is never observed and univalent chromosomes are frequently present at metaphase I, leading to errors in chromosome segregation.

14°C – Early stages of prophase I appeared normal though fully synapsed pachytene cells were not observed. 7 metaphase I PMCs were observed, 3 of which displayed 5 bivalents, while the remaining 4 PMCs showed univalent chromosomes in varying numbers. A chromosome fragment was observed in one PMC, at the late anaphase I stage. No cells were observed past the anaphase I stage.

20°C – Similar to that described for 14°C, though no fragmentation was seen. Dyad and tetrad stages (Figure 6.5 B) appeared normal apart from the presence of observable chromosome missegregation at the dyad stage.

28°C – Early stages of prophase I appeared normal, again without any fully synapsed pachytene cells being observed. Metaphase I chromosomes showed the presence of

univalents to varying degrees. Chromosome fragmentation was observed in three separate dyad stage cells. Tetrads appeared normal.

32°C – Leptotene stage cells were not observed but zygotene cells appeared normal. Fully synapsed pachytene chromosomes were not observed, but some approximately ‘pachytene equivalent’ cells, displayed a similar phenotype to that described for Col o at this temperature, with fuzzy, wide-spaced chromosomes. Metaphase I cells displayed univalent chromosomes to varying degrees (Figure 6.4 G). Only two tetrad cells were observed, one of which showed some evidence of fragmentation (Figure 6.5 G). These tetrads did not show the same level of defects displayed by Col o at this temperature, nor were cells observed at earlier stages showing the sorts of chromatin condensation defects which were seen in Col o.

6.2.4 *Atsdg2-1*

14°C – Meiosis appeared normal, with no visible fragmentation or missegregation. All metaphase I cells observed displayed 5 bivalents.

20°C – Leptotene stage was not identified, but all subsequent stages appeared normal. 5 bivalents were formed at metaphase I (Figure 6.4 C) and no fragmentation was detectable at the tetrad stage (Figure 6.5 C)

28°C – All meiotic stages appeared normal. Only 2 metaphase I cells were observed but both displayed 5 bivalent chromosomes.

32°C – Leptotene was not observed but zygotene stage appeared normal. Some pachytene cells appeared normal though many displayed the same wide-spacing between lateral elements and fuzzy chromatin appearance that was seen in Col o at

this temperature. Out of 22 metaphase I cells observed, 15 displayed 5 bivalent chromosomes, 5 cells had 4 bivalents and the remaining 2 cells had 3 bivalents (Figure 6.4 H). Only one cell showed a chromosome fragment, at anaphase II. Telophase II PMCs appeared normal, and did not show defects like the ones seen in Col 0 at this temperature (Figure 6.5 H).

6.2.5 *Atrbr-2*

14°C – Only a small number of PMCs were observed at this temperature point. Prophase I appeared normal. Two metaphase I cells were observed, each showing 10 univalents (though some chromosomes being overlaid makes this uncertain). No later stages were observed.

20°C – Prophase I appeared normal. At metaphase I, between 3 and 5 bivalents were observed in 4 cells seen at this stage (Figure 6.4 D). A chromosome fragment was present in a cell at the prophase II stage. Dyad and tetrad stages appeared normal and chromosome fragmentation was not observed (Figure 6.5 D).

28°C – Prophase I appeared normal. Only two metaphase I cells were observed, one with 3 and one with 4 bivalent chromosomes. Some fragmentation was observed at the dyad and tetrad stages.

32°C – Leptotene, zygotene and pachytene stages were not observed at this temperature. Some normal looking diplotene cells were observed. Univalent chromosomes were observed at diakinesis and metaphase I (Figure 6.4 I). Fragmentation was observed at diakinesis, dyad and telophase II stages. Some tetrads

showed similar defects to those observed in Col o at this temperature, with differently sized nuclei showing different levels of condensation (Figure 6.5 I).

	14°C	20°C	28°C	30°C	32°C
Col 0	Single fragment at dyad stage Normal ASY1/ZYP1 localisation	No defects observed Normal ASY1/ZYP1 localisation	Fragmentation at dyad stage in one cell Normal ASY1/ZYP1 localisation	Interlocks, Widely-spaced pachytene Normal ASY1/ZYP1 localisation	Abnormal chromatin condensation, wide pachytene chromosomes, fragmentation, CO failure, missegregation, abnormal tetrads ASY1 aggregates, abnormal loading of ZYP1
<i>cdkg1</i>	Fragmentation at dyad stage in one cell CO failure	CO failure Fragmentation Missegregation	CO failure Fragmentation Missegregation	N/A	CO failure, wide pachytene chromosomes, missegregation, abnormal tetrads
<i>pch2-1</i>	CO failure Fragmentation at anaphase I in one cell	CO failure Missegregation	CO failure Missegregation Fragmentation at dyad stage	N/A	Wide pachytene-equivalent chromosomes, CO failure, fragmentation in one tetrad
<i>sdg2-1</i>	No defects observed	No defects observed	No defects observed	N/A	Wide pachytene chromosomes, fragmentation in one anaphase II cell, some CO failure
<i>rbr-2</i>	CO failure	CO failure Fragmentation in one prophase II cell	CO failure Fragmentation	N/A	CO failure, fragmentation, abnormal tetrads

Table 6.1: Summary of defects induced by different temperature treatments in different genetic backgrounds. 30°C treatment was only applied to Col 0. ASY1/ZYP1 immunolocalisation was only applied to Col 0 and *sdg2-1*

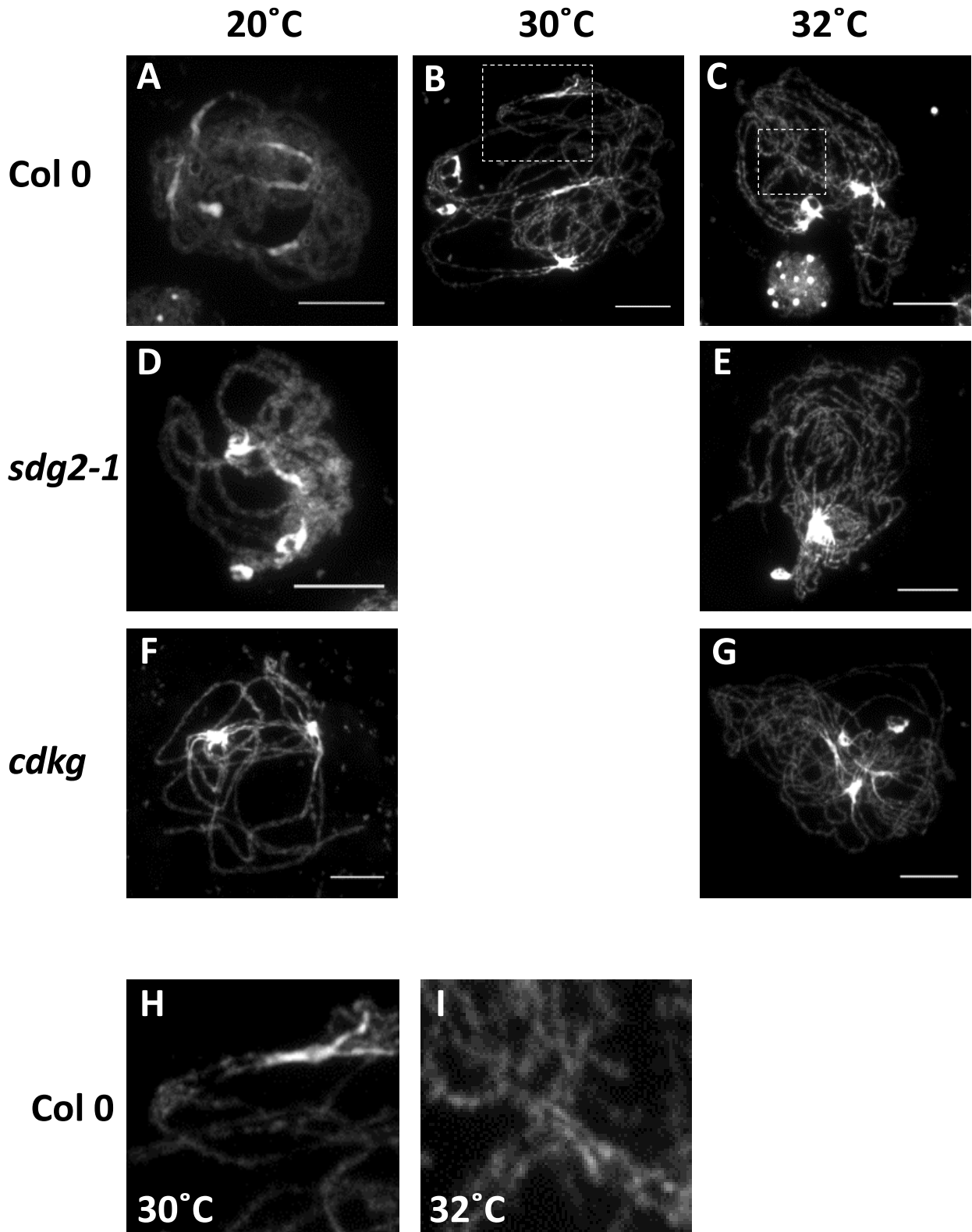


Figure 6.3: Synapsed chromosomes in *Col 0*, *sdg2-1* and *cdkg* at 20°C and 32°C. Spacing between paired chromosomes at 32°C sometimes appears unusually wide, in *Col 0*, *sdg2-1* and *cdkg*. *Col 0* also received 30°C treatment. Scale bar = 10 μm
Enlargements (H-I) show interlocks present in *Col 0* PMCs.

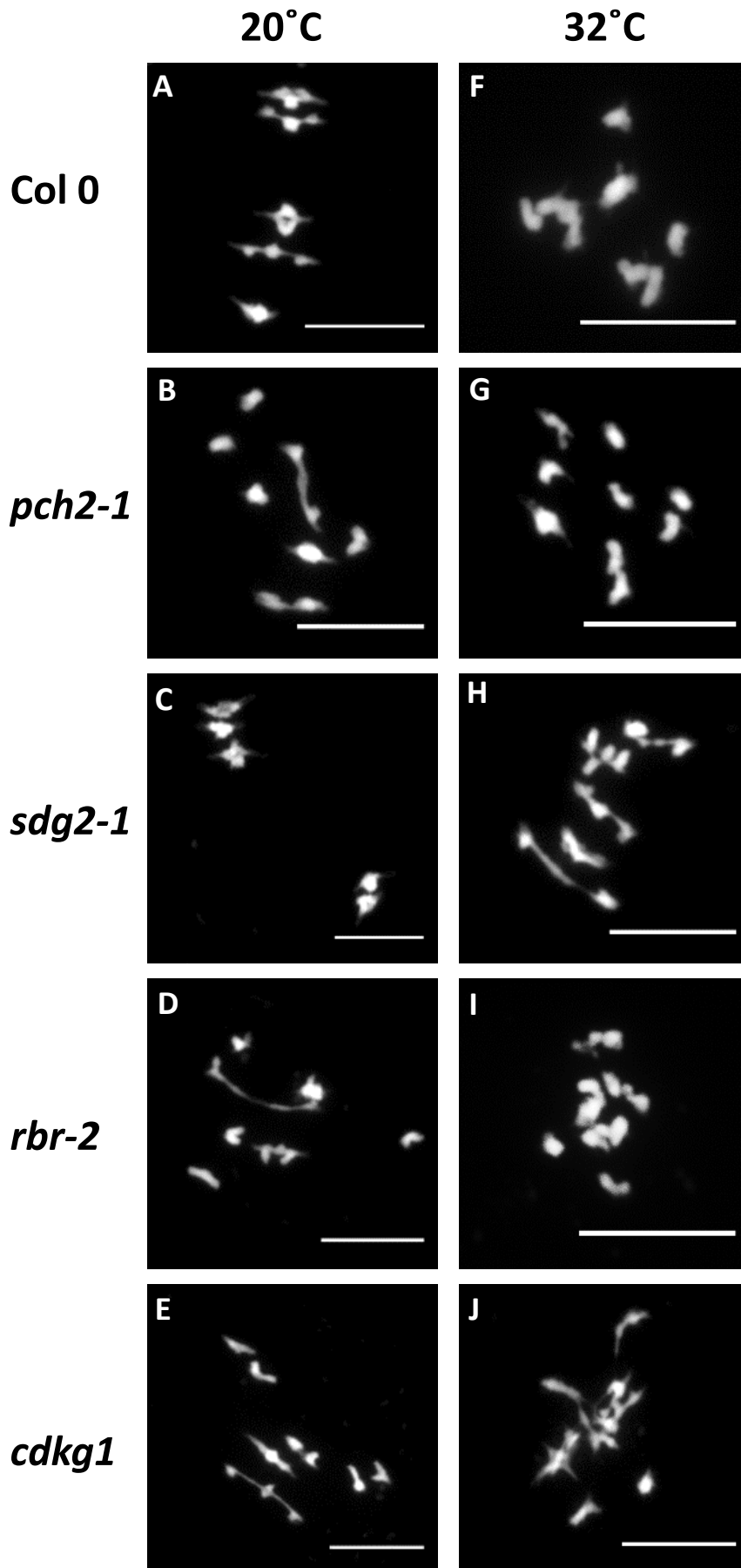


Figure 6.4: Metaphase I PMCs at 20°C and 32°C in Col 0, *pch2-1*, *sdg2-1*, *rbr-2* and *cdkg1*.

Scale bar = 10µm

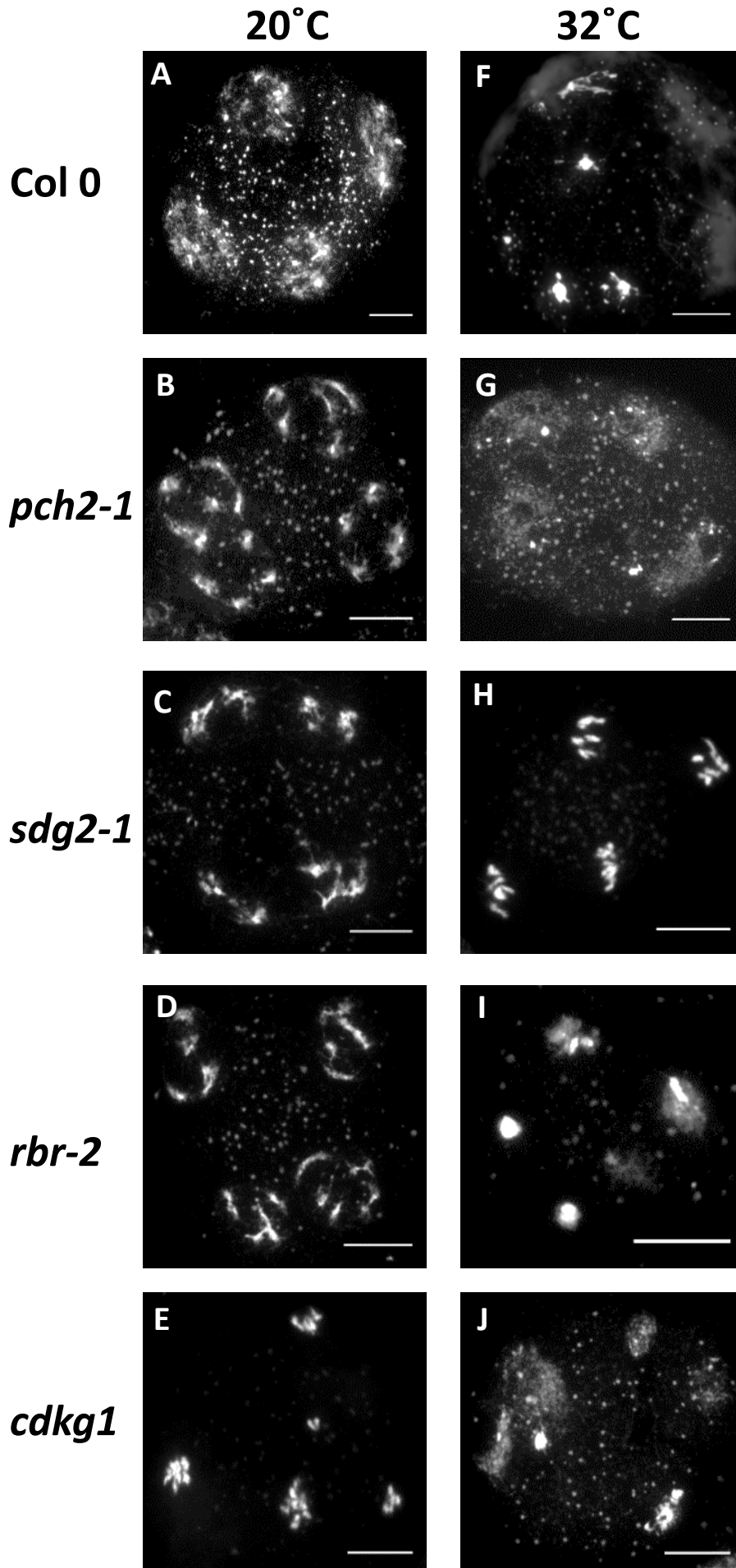


Figure 6.5: Tetrad and telophase II PMCs at 20°C and 32°C in Col 0, *pch2-1*, *sdg2-1*, *rbr-2* and *cdkg*.

Scale bar = 10µm

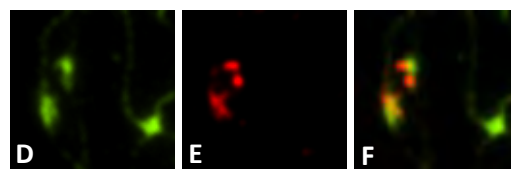
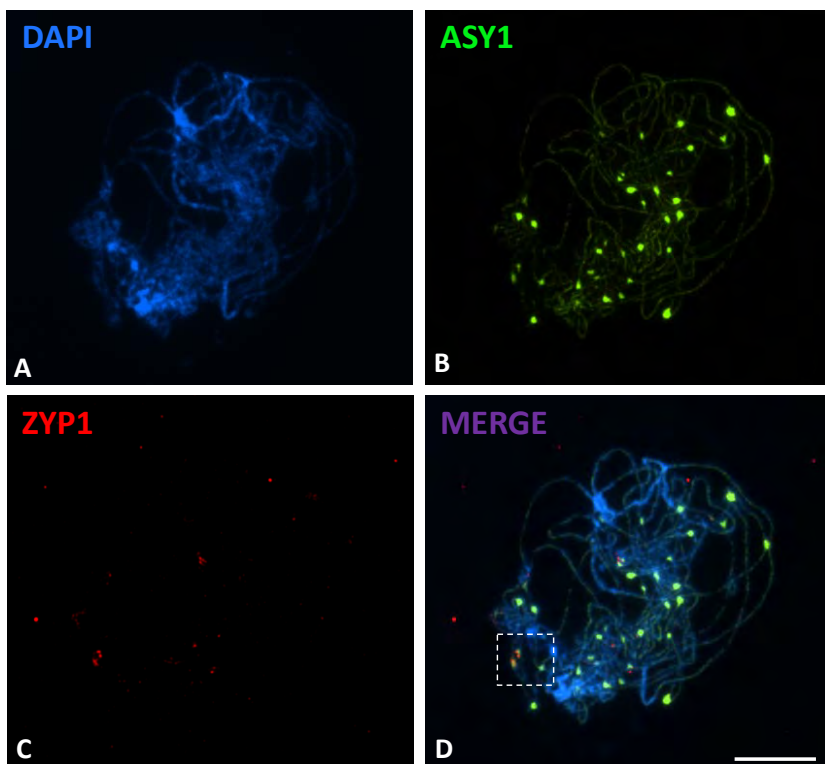
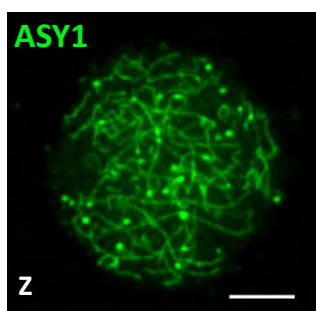
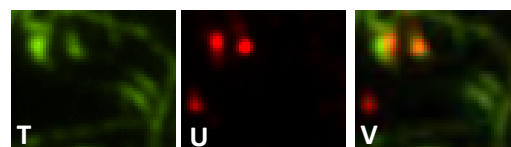
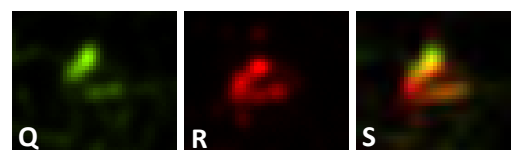
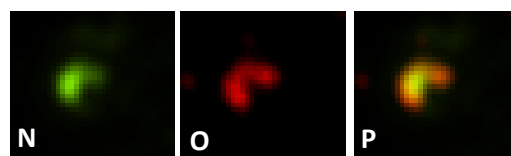
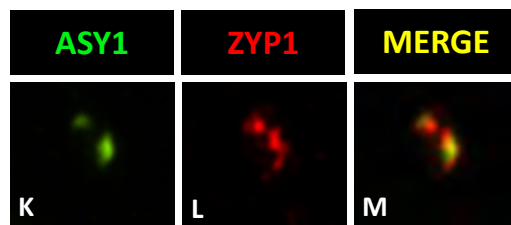
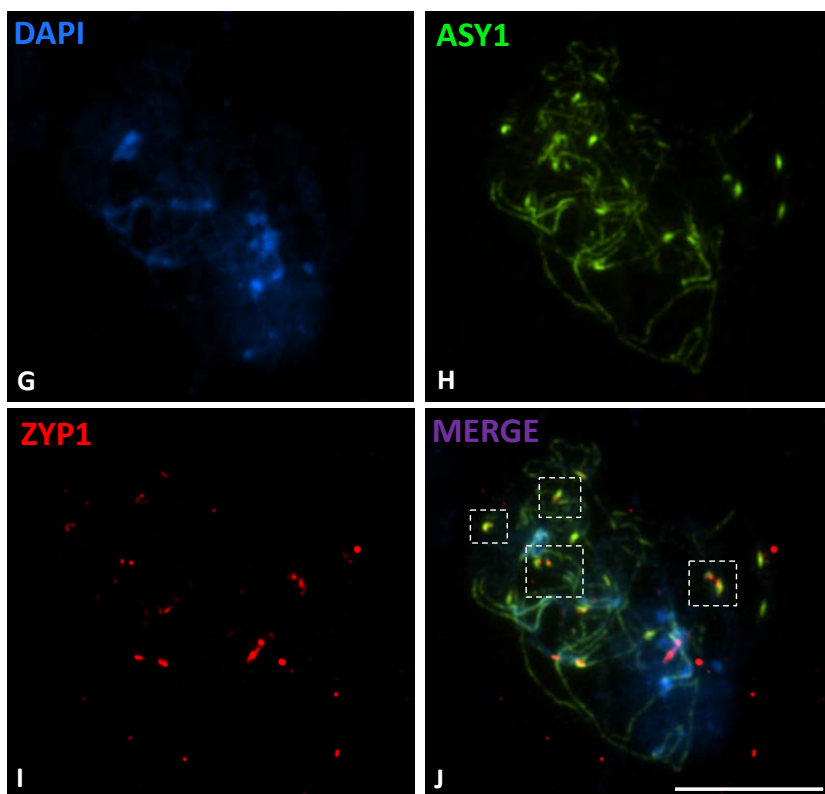
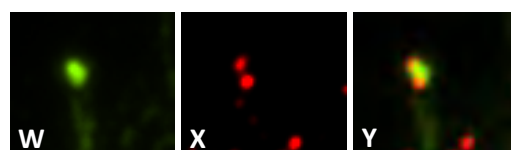


Figure 6.6: Prophase I PMCs in Col 0, immunostained with ASY1 and ZYP1 after 3 days growth at 32°C. Cutaways show some of the co-localisations between irregular structures of ZYP1 and bright concentrations of ASY1.

Scale bar = 10µm



Z - Similar ASY1 aggregations are occasionally seen in *Brassica oleracea*, grown under standard glasshouse conditions (Courtesy of Kim Osman)
Scale bar = 5µm



6.3 Discussion

This analysis has revealed that in Col o severe temperature-induced meiotic defects arise within a narrow temperature range between 30 °C and 32 °C. I also show that two of the mutant lines in my analysis, *Atsdg2-1* and *Atpch2-1* do not appear to show defects as severe as those seen in Col o after 3 days treatment at 32 °C.

6.3.1 Synapsis is defective following growth at 32 °C

My investigations have revealed the occurrence of wide spacing between clearly paired chromosomes (where the axes are parallel along their entire length), which display slightly fuzzy-looking chromatin at 32 °C. This was seen at 32 °C in every line tested apart from *Atrbr2*, where the relevant early/mid prophase I stages were not observed. The effect was also seen in Col o at 30 °C, though it remains unknown if the mutant lines also show this phenotype at this temperature, since only Col o was studied at this temperature. Where the effect was apparent, it was not observed in every cell, and many PMCs were present which displayed wild-type like synapsis.

The presence of the widely-spaced but paired/fuzzy chromosome defect in *Atsdg2-1* and *Atpch2-1*, which did not appear to display as severe defects in the later meiotic stages, suggests that the two defects might be functionally separate. *Atsdg2-1* also showed fewer temperature-induced effects on chiasma frequency, suggesting that the CO formation defect may also be functionally separate from the chromosome organisation defects seen in mid-prophase I. Whether or not this separation is specific to these mutant lines, or particular temperatures, would require further investigation.

ZYP1 loading appears abnormal/defective in Col o after 3 days treatment at 32°C, based on immunostaining of fixed material, compared with its appearance at other temperatures tested (Figure 6.2 A and 6.2 B). In terms of ZYP1 staining, *Atsdg2-1* appeared unaffected by the 32°C treatment. Higgins et al, 2005 showed that *Atzyp1* mutants show around 80% of wild-type chiasmata frequency, suggesting that in the wild-type at least, high-temperature induced defects in ZYP1 loading could account for the reduction in crossover formation, suggesting that the chromosome organisation and CO defects might not be functionally separate after all (Higgins et al., 2005). This would also be consistent with the comparatively reduced effects of temperature on ZYP1 immunostaining and chiasma frequency *Atsdg-1*. The study by Higgins et al also reported the presence of non-homologous recombination in the absence of ZYP1, which was not detected in my analysis.

6.3.2 ASY1 aggregates visible after 32°C treatment

Following 3 days of growth at 32°C, blob-like aggregates of ASY1 were visible on the chromosome axes of some early prophase I PMCs, when visualised using immunolocalisation on fixed material. Similar structures were reported in a study by Loidl, 1989, using electron microscopy to study silver-stained meiotic chromosomes in *Allium ursinum* (wild garlic) which had been subjected to 30 hours of high temperature treatment at 35°C. The author suggested that heat treatment might prolong the leptotene stage, as this stage was not observed in plants grown under standard conditions, but could be found readily following high temperature treatment. Chiasma frequency in *Allium* decreased slightly following 30 hours of high temperature treatment, and decreased further after 60 hours of treatment. The study

also showed the presence of silver-stained structures visible by electron microscopy which resembled the aggregates of ASY1 observed in my studies. Polycomplex type structures on the axis and SC have also been reported by Stack & Anderson, 1986, in *Lycopersicon esculentum* (Tomato).

Work performed in our laboratory by Kim Osman and F. Chris. H. Franklin, has shown that aggregates of ASY1 very similar in appearance to the silver-stained structures described by Loidl and the ASY1 aggregates seen in Col o at 32°C described above, are present in *Brassica oleracea* A12 (Kim Osman, personal communication) (Figure 6.6 Z). The ASY1 blobs seen in *Brassica* are only present infrequently and are not thought to correlate with high glasshouse temperatures. Structures that appear similar are also occasionally seen in *Brassica* at the pachytene stage, when stained with ZYP1. The fact that these were seen in immunolocalisation experiments performed using fresh material, rather than fixed, suggests that these structures are not exclusively detected by using the fixed material ('microwave') immunolocalisation technique, which was used in the high-temperature treated *Arabidopsis*.

There are at least two possibilities as to the nature of these ASY1 aggregates; either that they directly result from high temperature treatment, or that their presence is normally too transient to notice and is prolonged by the high temperature treatment, probably by a prolongation of the leptotene stage. These two possibilities are not entirely exclusive, as a prolonged leptotene as suggested by Loidl, might allow the aggregation of the protein into polycomplexes which would not otherwise form. The idea that they represent normally occurring but transient structures might seem unlikely due to the high number of immunolocalisation studies performed using ASY1 over the course of my own studies and within our laboratory group in recent years, without this phenomenon having been reported before. However, these structures

have been observed in *Brassica*, and their appearance might be independent of glasshouse temperature fluctuations. This supports the hypothesis that the structures are a normal but transient feature of meiosis. A prolonged leptotene stage is still a possibility though, and could be tested using EdU pulse-labelling of plants under different temperature treatments. The frequent colocalisation of the ASY1 aggregates with ZYP1 localisations is interesting (Figure 6.6), as it suggests these ASY1 structures might be involved in synapsis initiation and/or recombination. ZYP1 is not associated with every aggregate of ASY1 and when they are co-localised, they do not overlap entirely. One of the more common patterns observed in their co-localisation is ZYP1 forming a focus at either end of an ASY1 aggregate, in line with the underlying axis (Figure 6.3). While this could support the possibility that they represent synapsis initiation sites, the ASY1 aggregates do not appear to be strongly correlated with points of axis interaction. Similar observations were made by Loidl, 1989, who suggested that the axial thickenings might be prematurely resolved synapsis initiation sites.

Synapsis initiation requires the early stages of recombination, such as DSB formation (Higgins et al., 2005). Co-immunolocalisation of MSH4/ZYP1 and HEI10/ZYP1 (PCH2 chapter, Figure 5.12, 5.13) shows that these recombination proteins are also associated with synapsis initiation sites. It would be interesting in future experiments to investigate if these and other recombination proteins are associated with ASY1 aggregates at high temperature. Future experiments using the fresh material/lipsol spreading immunolocalisation technique might determine if these ASY1 aggregates also co-localise with AtPCH2, which co-localises with ZYP1 foci in early prophase I (Lambing et al., 2015). Immunolocalisation of ASY1 in the *Atpch2-1* mutant, after high temperature treatment, might show whether or not the formation of these aggregates requires the axis remodelling functions of PCH2 as well as its role in loading of ASY1.

The study by Loidl also showed the presence of ladder-type structures, visible by electron microscopy, which connected the axial thickenings. These structures appeared to be putting some tension on the axis, by causing visible deformation at the points of attachment. Recent work performed in our laboratory, also using immunolocalisation on fixed material, has found what appear to be the same ladder-type structures, as well as ASY1 aggregations in *Arabidopsis arenosa* (accession Triberg, tetraploid), after 6 weeks of growth at 33°C (Chris Morgan, personal communication). These structures were revealed by staining with ZYP1 antibody, suggesting that the 'ladders' are aberrant stretches of SC which have polymerised along a single axis, rather than between two. This length of ZYP1 then appears to provide a scaffold for another stretch to form in parallel, with the process then repeating until another stretch of ASY1 is encountered. This appears to be the case, since these ladders are often seen starting/ending at ASY1 stained axes, but occasionally only have ASY1 at one end with the unconnected end trailing off. Often these structures emanated from ASY1 aggregations and sometimes connected pairs of aggregations together, highly similar to those found by Loidl, 1989. These structures were never observed in *Arabidopsis thaliana*, possibly because of the shorter duration or lower temperature of the heat-shock used in my experiment. It is also possible that they are *aerenosa* specific though this seems less likely given their appearance in *Allium*.

6.3.3 *Atsdg2-1* and *Atpch2-1* display increased resistance to temperature induced defects

Col o plants grown at 32°C showed a more severe reduction in chiasma frequency compared to *Atsdg2-1* (Col o; 2 cells with 5 bivalents, 1 with 4 bivalents, 1 with 2

bivalents and 1 with 0 bivalents vs *Atsdg2-1*; 15 with 5 bivalents, 5 with 4 bivalents and 2 with 3 bivalents). The low numbers of Col 0 metaphase I PMCs analysed mean this could be a sampling error, but in combination with a reduction in other meiotic defects in *Atsdg2-1* compared to Col 0, this initial data is suggestive of a genuine difference in the effects of temperature in these lines.

In *Atsdg2-1*, it is conceivable that this resistance stems from the slightly increased number of COs in this mutant (see Chapter 3), which would allow it to lose more of them before suffering loss of an obligate CO for each bivalent. Although this might be true, it does not explain all the observed differences. Mutant lines which produce fewer, or even zero, COs form tetrads/polyads with incorrectly segregated chromosomes, but do not show the kind of phenotype seen in tetrads of Col 0 plants grown at 32°C (Figure 6.5 F). This suggests that the extensive defects seen in Col 0 at the tetrad stage are not solely due to the reduction in CO formation. The observed fragmentation suggests that at 32°C, Col 0 plants are also suffering from defective DSB repair mechanisms. In *Atsdg2-1* PMCs, fragmentation was observed in only a single cell. In *Atpch2-1* following 32°C treatment, some evidence of fragmentation was apparent in one of the two tetrad PMCs observed in this study, but appeared to be less affected than Col 0, despite the reduced CO frequency of *Atpch2-1*. Again, more cells would be required to draw any strong conclusions, but initially it appears that like *Atsdg2-1*, *Atpch2-1* might show greater resistance to temperature-induced meiotic defects compared to Col 0.

One possible alternative explanation for the observed differences in *Atsdg2-1* is that the large number of genes misregulated in this mutant could include genes involved in heat-stress response (Reviewed in von Koskull-Döring et al., 2007). However, a cross-reference of the 21 known HSPs (heat-shock proteins) against the list of genes

misregulated in *Atsdg2-1* from Berr et al., 2010, did not reveal any matches. The effects in *Atpch2-1* might be explained by the role of AtPCH2 in ASY1 deposition on the axis. An immunolocalisation experiment to visualise ASY1 in *Atpch2-1* after 32 °C treatment would reveal whether AtPCH2 is required for the presence of ASY1 aggregates. If these aggregations were the root cause of the other meiotic defects which result from this temperature treatment, then it might explain why reduced severity is seen in *Atpch2-1*.

6.3.4 Temperature induced effects on *Atrbr-2*

These experiments have not provided any conclusive evidence that the phenotypic severity of the *Atrbr-2* mutation is reduced at higher temperatures. However, a low number of PMCs were analysed so the possibility is not entirely ruled out. If a specific temperature range is required for this effect, it could lie between 20 °C and 28 °C, so would have been missed by this experiment. Based on the defects in chromosome condensation and fragmentation at 32 °C, it seems unlikely that the *Atrbr-2* mutation is increasing the resilience of *Arabidopsis* to high temperatures, as may be the case for *Atsdg2-1* and *Atpch2-1* mutants.

Chapter 7

General discussion

7.1 Discussion

The work described in chapters 3, 4 and 5 of this thesis was undertaken to better understand the relationship between homologous recombination and the properties of the underlying chromosomes, whether they be histone modifications or the dynamics of axis-protein organisation. Chapter 6 described investigations into whether the application of temperature stress affected either the meiotic chromosome structure or the progression of homologous recombination. An interesting link between these studies is the observation that mutants for specific chromosome structural defects can be less susceptible to the effects of high temperature treatment.

7.1.1 *Atsdg2-1* and *Atpch2-1* meiosis at high temperature

These studies demonstrated that resistance is conferred by the *Atsdg2-1* and *Atpch2-1* mutations, to the meiotic effects of high temperature treatment, compared to Col o. *Atsdg2-1* appears to be more competent at loading the SC at high temperature and seems to make more chiasmata than Col o, though univalents are still sometimes present. The maintenance of COs at high temperature could be a consequence of more efficient ZYP1 loading, but why ZYP1 should load more efficiently is difficult to explain. It has been reported for *Arabidopsis* that synapsis is not required for establishing interference and that COs form in the *Atzyp1* mutant at ~70% of wild-type levels, but that synapsis is dependent on recombination (Higgins et al., 2005). This would suggest that the unperturbed ZYP1 loading seen in *Atsdg2-1* at high temperature may be more likely to be a result of the relatively high chiasma frequency, rather than being a direct consequence of the temperature treatment. Future immunolocalisation experiments

could investigate whether the severity of the synaptic defect seen in *Atpch2-1* is reduced following high temperature treatment.

The unchanged length of the SC, suggests that in plants grown under standard glasshouse conditions, alterations in the organisation of the SC might not be responsible for the change in CO distribution.

Another change in the chromosome structure of high-temperature treated *Atsdg2-1* is evident in their lack of ASY1 aggregations, though it remains possible that this is a sampling error resulting from a smaller number of cells analysed in the *Atsdg2-1* mutant. Alternatively, the H3K4Me3 modification could have some role in axis organisation. No differences were apparent in the organisation of ASY1 in *Atsdg2-1* grown under glasshouse conditions, based on immunolocalisation using SIM, though it remains possible that like with *Atpch2-1*, any differences would not be noticeable until an intensity analysis is performed. An altered CO pattern was also reported for barley grown at high temperature (Higgins et al, 2012). *Atsdg2-1* is apparently less susceptible to temperature induced recombination defects. Could the altered CO patterning seen in *Atsdg2-1* be related to this? A possible, though difficult to confirm, explanation for the observed change in CO distribution in *Atsdg2-1* is that the axis-bound loops into which the DNA of meiotic chromosomes is organised, has been shifted. In this hypothesis, H3K4Me3 would have a role in determination of which chromosomal regions are located at the loop bases or in the loops themselves, so an *Atsdg2-1* mutant would show a different profile in this regard compared to wild-type. This may seem unlikely given the known association of H3K4Me3 with recombination hotspots found in the meiotic chromatin loop regions (Acquaviva et al., 2013; Sommermeyer et al., 2013), though since these associations are far from simple (Zhu and Keeney, 2015), the possibility will require further study to rule out or confirm. The

hypothesis fits loosely with the findings of a yeast study which demonstrated the strong relationship between transcription and axis-association (Sun et al., 2015). This study showed that the 3' ends of genes, where cohesin proteins are thought to be 'pushed' by the transcription machinery, are enriched for Hop1, Red1 and Rec8, and that this correlation is dependent of the strength of the gene expression. The *Atsdg2-1* mutation causes the misregulation of hundreds of genes (Berr et al., 2010; Guo et al., 2010), so could perhaps be altering axis-loop associations by this mechanism.

7.1.2 Future perspectives

The central finding of this work, that CO frequency is increased in *Atsdg2-1*, is supported by both cytological and genetic data. Recent developments in cytological techniques now allow us to immunolocalise foci-producing recombination proteins on chromosome spread preparations of fixed bud material from *Arabidopsis*. This will potentially allow us to make accurate counts of MLH1 and HEI10 foci on pachytene, diplotene and diakinesis PMCs more easily and also make distance measurements between these foci easier and more accurate. It would also allow these measurements to be performed in a higher number of cells, therefore making the statistical analysis more robust.

Plants heterozygous for the *Atsdg2-1* mutation, which appear phenotypically wild-type like, were analysed cytologically early in this study with metaphase I chromosomes appearing indistinguishable from Col o. It would be interesting to analyse the levels of H3K4Me3 signal in PMCs, as I did for the homozygous mutant, to see if there is an intermediate effect. It will also be interesting to investigate whether the CO distribution effects can be replicated in plants with a meiosis-specific knockdown of

SDG2 expression, such as via RNAi or CRISPR/inactive-Cas9 to block transcription, driven by a meiosis-specific promoter, like *pDMC1*.

Another approach that could be taken in future investigations would be to over-express a H3K4 de-methylase, such as jumonji-15 (*AtJMJ15*), to see if similar effects can be achieved. Over-expression of this gene has previously been demonstrated in a study on salt tolerance, and experienced repression of genes which normally showed strong H3K4Me3 marking (Shen et al., 2014). The same study also showed that *AtJMJ15* is strongly expressed in young anthers. This might help to show whether the phenotype of *Atsdg2-1* is due to reduced H3K4Me3 or not, but could also lead to a different distribution of COs since *AtJMJ15* might de-methylate H4K4 residues to produce a H3K4Me3 profile completely distinct from *Atsdg2-1*.

The roles of other SET domain proteins might be difficult to spot. If the effects of mutating these proteins are similar to those seen in *Atsdg2-1*, but more subtle, they could potentially not be noticeable based on cytological analysis of metaphase I chromosomes, and performing a full FTL analysis on each of them would be lengthy and laborious. High throughput flow cytometry can be performed on FTL lines to detect single CO events in individual pollen grains, and could be useful in identifying affected mutant lines (Yelina et al., 2012).

The main finding of these studies into *AtMRG2* was the unfortunate conclusion that the meiotic defects in the mutant line I had been investigating were actually the result of an as-yet-uncharacterised mutation to *AtPRD3*. The subsequent finding that the two MRG genes, *AtMRG1* and *AtMRG2* function redundantly, means that any future investigations into their meiotic function should use a double homozygous mutant of both genes. It is still possible that meiosis would be affected in a double mutant,

resulting from the associated reduction in histone acetylation, but these effects could be subtle if similar to the alteration in CO distribution seen in *Atsdg2-1*, making them unlikely to have been recognised by the researchers involved in these studies. Any such future studies should also take into account the effects of day length on the phenotype of the double mutant, which would have the additional benefit of the wild-type control providing an insight into the normal influence of day length on meiosis.

With regards to the effects of temperature, I have yet to determine whether or not the temperature-induced meiotic defects I have observed are exclusive to male meiosis, as was previously reported for the *Atcdgk1* mutation in *Arabidopsis* and the increased CO frequency in barley (Zheng et al., 2014; Phillips et al., 2015). This could be tested by fertilizing high-temperature treated plants with pollen from plants grown in standard glasshouse conditions and vice-versa, then assessing the resulting siliques for fertility. Other experiments into the meiotic effects of exposure to high temperature may determine the duration of heat-shock required to induce particular defects during meiosis. The ladder-type ZYP1 structures described in section 6.3.2 were observed in *Arabidopsis arenosa* apparent after 6 weeks of growth at 33°C. It would be interesting to determine if this phenomenon is specific to the different species used, the single degree difference in temperature treatment or, most likely, the increased duration of exposure to high temperature.

Overall, the results of my studies highlight that recombination is affected by the structure of meiotic chromosomes, at their various levels of organisation. They also show that these organisational defects can change the way PMCs react to high temperature.

References

- Abe, K., Osakabe, K., Nakayama, S., Endo, M., Tagiri, A., Todoriki, S., Ichikawa, H. and Toki, S. (2005) Arabidopsis RAD51C gene is important for homologous recombination in meiosis and mitosis. **Plant physiology**, 139 (2): 896–908
- Acquaviva, L., Székvölgyi, L., Dichtl, B., Dichtl, B.S., de La Roche Saint André, C., Nicolas, A. and Géli, V. (2013) The COMPASS subunit Spp1 links histone methylation to initiation of meiotic recombination. **Science**, 339 (6116): 215–8
- Agarwal, S. and Roeder, G.S. (2000) Zip3 provides a link between recombination enzymes and synaptonemal complex proteins. **Cell**, 102 (2): 245–255
- Alberts, B., Johnson, A., Lewis, J., Raff, M., Roberts, K. and Walter, P. (2008) **Molecular Biology of the Cell**. 5th ed. New York: Garland Science
- Allers, T. and Lichten, M. (2001) Differential timing and control of noncrossover and crossover recombination during meiosis. **Cell**, 106 (1): 47–57
- Alvarez-Venegas, R. and Avramova, Z. (2005) Methylation patterns of histone H3 Lys 4, Lys 9 and Lys 27 in transcriptionally active and inactive Arabidopsis genes and in atx1 mutants. **Nucleic acids research**, 33 (16): 5199–207
- Alvarez-Venegas, R., Pien, S., Sadler, M., Witmer, X., Grossniklaus, U. and Avramova, Z. (2003) ATX-1, an Arabidopsis homolog of trithorax, activates flower homeotic genes. **Current Biology**, 13 (8): 627–637
- Armstrong, S. (2013a) “A time course for the analysis of meiotic progression in Arabidopsis thaliana.” In Pawlowski, W.P., Grelon, M. and Armstrong, S. (eds.) **Plant Meiosis: Methods and Protocols**. New York, United States: Springer Science+Business Media. pp. 119–123
- Armstrong, S. (2013b) “Spreading and fluorescence in situ hybridization of male and female meiocyte chromosomes from Arabidopsis thaliana for cytogenetical analysis.” In Pawlowski, W.P., Grelon, M. and Armstrong, S. (eds.) **Plant Meiosis: Methods and Protocols**. New York, United States: Springer Science+Business Media. pp. 3–11
- Armstrong, S.J. (2002) Asy1, a protein required for meiotic chromosome synapsis, localizes to axis-associated chromatin in Arabidopsis and Brassica. **Journal of Cell Science**, 115 (18): 3645–3655
- Armstrong, S.J. and Osman, K. (2013) “Immunolocalisation of Meiotic Proteins in Arabidopsis thaliana: Method 2.” In Pawlowski, W., Grelon, M. and Armstrong, S.J. (eds.) **Plant Meiosis: Methods and Protocols**. New York: Springer Science+Business Media. pp. 103–107
- Ausió, J. (2015) The shades of gray of the chromatin fiber. **BioEssays**, 37 (1): 46–51

- Bachrati, C.Z., Borts, R.H. and Hickson, I.D. (2006) Mobile D-loops are a preferred substrate for the Bloom's syndrome helicase. **Nucleic Acids Research**, 34 (8): 2269–2279
- Bahler, J., Wyler, T., Loidl, J. and Kohli, J. (1993) Unusual Nuclear-Structures in Meiotic Prophase of Fission Yeast - a Cytological Analysis. **Journal of Cell Biology**, 12 (2): 241–256
- Bai, X., Peirson, B.N., Dong, F., Xue, C. and Makaroff, C. (1999) Isolation and characterization of SYN1, a RAD21-like gene essential for meiosis in Arabidopsis. **The Plant cell**, 11 (3): 417–30
- Baker, C.L., Walker, M., Kajita, S., Petkov, P.M. and Paigen, K. (2014) PRDM9 binding organizes hotspot nucleosomes and limits Holliday junction migration. **Genome research**, 24 (5): 724–32
- Balasubramanian, S., Sureshkumar, S., Lempe, J. and Weigel, D. (2006) Potent induction of Arabidopsis thaliana flowering by elevated growth temperature. **PLoS Genetics**, 2 (7): 0980–0989
- Bannister, a J., Zegerman, P., Partridge, J.F., Miska, E. a, Thomas, J.O., Allshire, R.C. and Kouzarides, T. (2001) Selective recognition of methylated lysine 9 on histone H3 by the HP1 chromo domain. **Nature**, 410 (6824): 120–124
- Barakate, A., Higgins, J.D., Vivera, S., Stephens, J., Perry, R.M., Ramsay, L., Colas, I., Oakey, H., Waugh, R., Franklin, F.C.H., Armstrong, S.J. and Halpin, C. (2014) The synaptonemal complex protein ZYP1 is required for imposition of meiotic crossovers in barley. **The Plant cell**, 26 (2): 729–40
- Barski, A., Cuddapah, S., Cui, K., Roh, T.Y., Schones, D.E., Wang, Z., Wei, G., Chepelev, I. and Zhao, K. (2007) High-Resolution Profiling of Histone Methylations in the Human Genome. **Cell**, 129 (4): 823–837
- Basu-Roy, S., Gauthier, F., Giraut, L., Mézard, C., Falque, M. and Martin, O.C. (2013) Hot regions of noninterfering crossovers coexist with a nonuniformly interfering pathway in Arabidopsis thaliana. **Genetics**, 195 (3): 769–79
- Baudat, F., Manova, K., Yuen, J.P., Jasin, M. and Keeney, S. (2000) Chromosome synapsis defects and sexually dimorphic meiotic progression in mice lacking Spo11. **Molecular cell**, 6 (5): 989–998
- Baulcombe, D., Crute, I., Davies, B., Dunwell, J., Gale, M., Jones, J., Pretty, J., Sutherland, W. and Toulmin, C. (2009) Reaping the benefits: Science and the sustainable intensification of global agriculture. **The Royal Society**
- Bender, L.B., Suh, J., Carroll, C.R., Fong, Y., Ian, M., Briggs, S.D., Cao, R., Zhang, Y., Reinke, V. and Strome, S. (2008) MES-4: an autosome-associated histone methyltransferase that participates in silencing the X chromosomes in the C. elegans germ line. **Development**, 133 (19): 3907–3917

- Berchowitz, L. and Copenhaver, G.P. (2008) Fluorescent Arabidopsis tetrads: a visual assay for quickly developing large crossover and crossover interference data sets. **Nature Protocols**, 3 (1): 41–50
- Berchowitz, L.E. and Copenhaver, G.P. (2010) Genetic interference: don't stand so close to me. **Current genomics**, 11 (2): 91–102
- Berr, A., McCallum, E.J., Ménard, R., Meyer, D., Fuchs, J., Dong, A. and Shen, W.-H. (2010) Arabidopsis SET DOMAIN GROUP2 is required for H3K4 trimethylation and is crucial for both sporophyte and gametophyte development. **The Plant cell**, 22 (10): 3232–3248
- Bertram, M.J., Bérubé, N.G., Hang-Swanson, X., Ran, Q., Leung, J.K., Bryce, S., Spurgers, K., Bick, R.J., Baldini, a, Ning, Y., Clark, L.J., Parkinson, E.K., Barrett, J.C., Smith, J.R. and Pereira-Smith, O.M. (1999) Identification of a gene that reverses the immortal phenotype of a subset of cells and is a member of a novel family of transcription factor-like genes. **Molecular and cellular biology**, 19 (2): 1479–1485
- Bertram, M.J. and Pereira-Smith, O.M. (2001) Conservation of the MORF4 related gene family: Identification of a new chromo domain subfamily and novel protein motif. **Gene**, 266 (1-2): 111–121
- Bhalla, N., Wynne, D.J., Jantsch, V. and Dernburg, A.F. (2008) ZHP-3 acts at crossovers to couple meiotic recombination with synaptonemal complex disassembly and bivalent formation in *C. elegans*. **PLoS Genetics**, 4 (10)
- Bhatt, A.M., Lister, C., Page, T., Fransz, P., Findlay, K., Jones, G.H., Dickinson, H.G. and Dean, C. (1999) The DIF1 gene of Arabidopsis is required for meiotic chromosome segregation and belongs to the REC8/RAD21 cohesin gene family. **Plant Journal**, 19 (4): 463–472
- Bian, Q. and Belmont, A.S. (2012) Revisiting higher-order and large-scale chromatin organization. **Current Opinion in Cell Biology**, 24 (3): 359–366
- Bishop, D.K., Park, D., Xu, L. and Kleckner, N. (1992) DMC1: a meiosis-specific yeast homolog of *E. coli* recA required for recombination, synaptonemal complex formation, and cell cycle progression. **Cell**, 69 (3): 439–456
- Bishop, D.K. and Zickler, D. (2004) Early Decision: Meiotic Crossover Interference prior to Stable Strand Exchange and Synapsis Review. **Cell**, 117: 9–15
- Bleuyard, J.Y., Gallego, M.E., Savigny, F. and White, C.I. (2005) Differing requirements for the Arabidopsis Rad51 paralogs in meiosis and DNA repair. **Plant Journal**, 41 (4): 533–545
- Bleuyard, J.-Y., Gallego, M.E. and White, C.I. (2004) Meiotic defects in the Arabidopsis rad50 mutant point to conservation of the MRX complex function in early stages of meiotic recombination. **Chromosoma**, 113 (4): 197–203

- Bleuyard, J.-Y. and White, C.I. (2004) The Arabidopsis homologue of Xrcc3 plays an essential role in meiosis. **The EMBO journal**, 23 (2): 439–49
- Bocker, T., Barusevicius, A., Snowden, T., Rasio, D., Guerrette, S., Robbins, D., Schmidt, C., Burczak, J., Croce, C.M., Copeland, T., Kovatich, A.J. and Fishel, R. (1999) hMSH5: A human MutS homologue that forms a novel heterodimer with hMSH4 and is expressed during spermatogenesis. **Cancer Research**, 59 (4): 816–822
- De Boer, E., Jasin, M. and Keeney, S. (2015) Local and sex-specific biases in crossover vs . noncrossover outcomes at meiotic recombination hot spots in mice. **Genes and Development**, 29: 1721–1733
- Bomblies, K., Higgins, J.D. and Yant, L. (2015) Tansley review Meiosis evolves: adaptation to external and internal environments. **New Phytologist**
- Bonner, W.M., Redon, C.E., Dickey, J.S., Nakamura, A.J., Olga, A., Solier, S. and Pommier, Y. (2008) H2AX and cancer. **Nature Reviews. Cancer**, 8 (12): 957–967
- Borde, V., Robine, N., Lin, W., Bonfils, S., Geli, V. and Nicolas, A. (2009) Histone H3 lysine 4 trimethylation marks meiotic recombination initiation sites. **The EMBO journal**, 28 (2): 99–111
- Börner, G.V., Barot, A. and Kleckner, N. (2008) Yeast Pch2 promotes domainal axis organization, timely recombination progression, and arrest of defective recombinosomes during meiosis. **Proceedings of the National Academy of Sciences of the United States of America**, 105 (9): 3327–32
- Börner, G.V., Kleckner, N. and Hunter, N. (2004) Crossover/noncrossover differentiation, synaptonemal complex formation, and regulatory surveillance at the leptotene/zygotene transition of meiosis. **Cell**, 117 (1): 29–45
- Brehm, A., Tufteland, K.R., Aasland, R. and Becker, P.B. (2004) The many colours of chromodomains. **BioEssays**, 26 (2): 133–140
- Brick, K., Smagulova, F., Khil, P., Camerini-Otero, R.D. and Petukhova, G. V. (2012) Genetic recombination is directed away from functional genomic elements in mice. **Nature**, 485 (7400): 642–645
- Bu, Z., Yu, Y., Li, Z., Liu, Y., Jiang, W., Huang, Y. and Dong, a W. (2014) Regulation of Arabidopsis Flowering by the Histone Mark Readers MRG1/2 via Interaction with CONSTANS to Modulate FT Expression. **PLoS Genetics**, 10 (9): 1–11
- Buard, J., Barthès, P., Grey, C. and de Massy, B. (2009) Distinct histone modifications define initiation and repair of meiotic recombination in the mouse. **The EMBO journal**, 28 (17): 2616–2624
- Bundock, P., van Attikum, H. and Hooykaas, P. (2002) Increased telomere length and hypersensitivity to DNA damaging agents in an Arabidopsis KU70 mutant.

Nucleic acids research, 30 (15): 3395–3400

Burma, S., Chen, B.P., Murphy, M., Kurimasa, a and Chen, D.J. (2001) ATM phosphorylates histone H2AX in response to DNA double-strand breaks. **The Journal of biological chemistry**, 276 (45): 42462–42467

Cai, X., Dong, F., Edelman, R.E. and Makaroff, C. a (2003) The Arabidopsis SYN1 cohesin protein is required for sister chromatid arm cohesion and homologous chromosome pairing. **Journal of cell science**, 116 (Pt 14): 2999–3007

Cannavo, E. and Cejka, P. (2014) Sae2 promotes dsDNA endonuclease activity within Mre11–Rad50–Xrs2 to resect DNA breaks. **Nature**, 514 (7520): 122–125

Cao, R., Wang, L., Wang, H., Xia, L., Erdjument-Bromage, H., Tempst, P., Jones, R.S. and Zhang, Y. (2002) Role of histone H3 lysine 27 methylation in Polycomb-group silencing. **Science**, 298 (5595): 1039–1043

Carballo, J. a., Panizza, S., Serrentino, M.E., Johnson, A.L., Geymonat, M., Borde, V., Klein, F. and Cha, R.S. (2013) Budding Yeast ATM/ATR Control Meiotic Double-Strand Break (DSB) Levels by Down-Regulating Rec114, an Essential Component of the DSB-machinery. **PLoS Genetics**, 9 (6)

Carrozza, M.J., Li, B., Florens, L., Suganuma, T., Swanson, S.K., Lee, K.K., Shia, W.J., Anderson, S., Yates, J., Washburn, M.P. and Workman, J.L. (2005) Histone H3 methylation by Set2 directs deacetylation of coding regions by Rpd3S to suppress spurious intragenic transcription. **Cell**, 123 (4): 581–592

Caryl, A.P., Armstrong, S.J., Jones, G.H. and Franklin, F.C.H. (2000) A homologue of the yeast HOP1 gene is inactivated in the Arabidopsis meiotic mutant *asy1*. **Chromosoma**, 109 (1-2): 62–71

Chan, Y.-L., Brown, M.S., Qin, D., Handa, N. and Bishop, D.K. (2014) The 3rd Exon of the Budding Yeast Meiotic Recombination Gene HOP2 is Required for Calcium-dependent and Recombinase Dmc1-specific Stimulation of Homologous Strand Assimilation. **The Journal of biological chemistry**, 289 (26): 18076–86

Chang, Y., Gong, L., Yuan, W., Li, X., Chen, G., Li, X., Zhang, Q. and Wu, C. (2009) Replication protein A (RPA1a) is required for meiotic and somatic DNA repair but is dispensable for DNA replication and homologous recombination in rice. **Plant physiology**, 151 (4): 2162–2173

Cheema, M. and Ausiό, J. (2015) The Structural Determinants behind the Epigenetic Role of Histone Variants. **Genes**, 6 (3): 685–713

Chelysheva, L., Vezon, D., Chambon, A., Gendrot, G., Pereira, L., Lemhemdi, A., Vrielynck, N., Le Guin, S., Novatchkova, M. and Grelon, M. (2012) The Arabidopsis HEI10 is a new ZMM protein related to Zip3. **PLoS genetics**, 8 (7): e1002799

Chelysheva, L.A., Grandont, L. and Grelon, M. (2013) “Immunolocalization of

meiotic proteins in Brassicaceae: method 1.” In Pawlowski, W.P., Grelon, M. and Armstrong, S. (eds.) **Plant Meiosis: Methods and Protocols**. New York, United States: Springer Science+Business Media. pp. 93–101

Chen, C., Farmer, A.D., Langley, R.J., Mudge, J., Crow, J. a, May, G.D., Huntley, J., Smith, A.G. and Retzel, E.F. (2010) Meiosis-specific gene discovery in plants: RNA-Seq applied to isolated Arabidopsis male meiocytes. **BMC plant biology**, 10 (1): 280

Chen, C., Jomaa, A., Ortega, J. and Alani, E.E. (2013) Pch2 is a hexameric ring ATPase that remodels the chromosome axis protein Hop1. **Proceedings of the National Academy of Sciences**

Chen, C., Zhang, W., Timofejeva, L., Gerardin, Y. and Ma, H. (2005) The Arabidopsis ROCK-N-ROLLERS gene encodes a homolog of the yeast ATP-dependent DNA helicase MER3 and is required for normal meiotic crossover formation. **Plant Journal**, 43 (3): 321–334

Chen, N., Zhou, W.-B., Wang, Y.-X., Dong, A.-W. and Yu, Y. (2014) Polycomb-group histone methyltransferase CLF is required for proper somatic recombination in Arabidopsis. **Journal of Integrative Plant Biology**

Chen, Z., Higgins, J.D., Hui, J.T.L., Li, J., Franklin, F.C.H. and Berger, F. (2011) Retinoblastoma protein is essential for early meiotic events in Arabidopsis. **The EMBO journal**, 30 (4): 744–55

Cheng, Y.-H., Chuang, C.-N., Shen, H.-J., Lin, F.-M. and Wang, T.-F. (2013) Three distinct modes of Mec1/ATR and Tel1/ATM activation illustrate differential checkpoint targeting during budding yeast early meiosis. **Molecular and cellular biology**, 33 (16): 3365–76

Choi, K., Zhao, X., Kelly, K. a, Venn, O., Higgins, J.D., Yelina, N.E., Hardcastle, T.J., Ziolkowski, P. a, Copenhaver, G.P., Franklin, F.C.H., McVean, G. and Henderson, I.R. (2013) Arabidopsis meiotic crossover hot spots overlap with H2A.Z nucleosomes at gene promoters. **Nature genetics**, 45 (11): 1327–36

Chuang, C.-N., Cheng, Y.-H. and Wang, T.-F. (2012) Mek1 stabilizes Hop1-Thr318 phosphorylation to promote interhomolog recombination and checkpoint responses during yeast meiosis. **Nucleic acids research**, 40 (22): 11416–27

Ciosk, R., Zachariae, W., Michaelis, C., Shevchenko, A., Mann, M. and Nasmyth, K. (1998) An ESP1/PDS1 complex regulates loss of sister chromatid cohesion at the metaphase to anaphase transition in yeast. **Cell**, 93 (6): 1067–1076

Clerici, M., Mantiero, D., Guerini, I., Lucchini, G. and Longhese, M.P. (2008) The Yku70-Yku80 complex contributes to regulate double-strand break processing and checkpoint activation during the cell cycle. **EMBO reports**, 9 (8): 810–818

Cloud, V., Chan, Y.-L., Grubb, J., Budke, B. and Bishop, D.K. (2012) Rad51 is an

accessory factor for Dmc1-mediated joint molecule formation during meiosis.

Science, 337 (6099): 1222–5

Cole, F., Kauppi, L., Lange, J., Roig, I., Wang, R., Keeney, S. and Jasin, M. (2012a) Homeostatic Control of Recombination is Implemented Progressively in Mouse Meiosis. **Nature cell biology**, 14 (4): 424–430

Cole, F., Keeney, S. and Jasin, M. (2012b) Preaching about the converted: how meiotic gene conversion influences genomic diversity. **Annals of the New York Academy of Sciences**, 1267: 95–102

Colome-Tatche, M., Cortijo, S., Wardenaar, R., Morgado, L., Lahouze, B., Sarazin, a., Etcheverry, M., Martin, a., Feng, S., Duvernois-Berthet, E., Labadie, K., Wincker, P., Jacobsen, S.E., Jansen, R.C., Colot, V. and Johannes, F. (2012) Features of the Arabidopsis recombination landscape resulting from the combined loss of sequence variation and DNA methylation. **Proceedings of the National Academy of Sciences**, 109 (40): 16240–16245

Connelly, J.C. and Leach, D.R.F. (2002) Tethering on the brink: The evolutionarily conserved Mre11-Rad50 complex. **Trends in Biochemical Sciences**, 27 (8): 410–418

Couteau, F., Belzile, F., Horlow, C., Grandjean, O., Vezon, D. and Doutriaux, M.P. (1999) Random chromosome segregation without meiotic arrest in both male and female meiocytes of a dmc1 mutant of Arabidopsis. **The Plant cell**, 11 (9): 1623–34

Crismani, W., Girard, C., Froger, N., Pradillo, M., Santos, J.L., Chelysheva, L., Copenhaver, G.P., Horlow, C. and Mercier, R. (2012) FANCM Limits Meiotic Crossovers. **Science**, 336 (6088): 1588–1590

Cutter, A.R. and Hayes, J.J. (2015) A brief review of nucleosome structure. **FEBS Letters**, pp. 1–9

Deal, R.B., Topp, C.N., McKinney, E.C. and Meagher, R.B. (2007) Repression of flowering in Arabidopsis requires activation of FLOWERING LOCUS C expression by the histone variant H2A.Z. **The Plant cell**, 19 (1): 74–83

Dernburg, A.F., McDonald, K., Moulder, G., Barstead, R., Dresser, M. and Villeneuve, A.M. (1998) Meiotic recombination in *C. elegans* initiates by a conserved mechanism and is dispensable for homologous chromosome synapsis. **Cell**, 94 (3): 387–398

Deshong, A.J., Ye, A.L., Lamelza, P. and Bhalla, N. (2014) A quality control mechanism coordinates meiotic prophase events to promote crossover assurance. **PLoS genetics**, 10 (4): e1004291

Dombecki, C.R., Chiang, A.C.Y., Kang, H.J., Bilgir, C., Stefanski, N. a., Neva, B.J., Klerkx, E.P.F. and Nabeshima, K. (2011) The Chromodomain Protein MRG-1 Facilitates SC-Independent Homologous Pairing during Meiosis in *Caenorhabditis*

elegans. **Developmental Cell**, 21 (6): 1092–1103

Drouaud, J., Mercier, R., Chelysheva, L., Bérard, A., Falque, M., Martin, O., Zanni, V., Brunel, D. and Mézard, C. (2007) Sex-specific crossover distributions and variations in interference level along *Arabidopsis thaliana* chromosome 4. **PLoS Genetics**, 3 (6): 1096–1107

Ebel, C., Mariconti, L. and Gruissem, W. (2004) **Plant retinoblastoma homologues control nuclear proliferation in the female gametophyte.**, 429 (June): 8–12

Eram, M.S., Bustos, S.P., Lima-Fernandes, E., Siarheyeva, A., Senisterra, G., Hajian, T., Chau, I., Duan, S., Wu, H., Dombrowski, L., Schapira, M., Arrowsmith, C.H. and Vedadi, M. (2014) Trimethylation of Histone H3 Lysine 36 by Human Methyltransferase PRDM9 Protein. **The Journal of biological chemistry**, 289 (17): 12177–88

Erayman, M., Sandhu, D., Sidhu, D., Dilbirligi, M., Baenziger, P.S. and Gill, K.S. (2004) Demarcating the gene-rich regions of the wheat genome. **Nucleic Acids Research**, 32 (12): 3546–3565

Falk, J.E., Chan, A.C., Hoffmann, E. and Hochwagen, A. (2010) A Mec1- and PP4-dependent checkpoint couples centromere pairing to meiotic recombination. **Developmental cell**, 19 (4): 599–611

Farmer, S., Hong, E.J.E., Leung, W.K., Argunhan, B., Terentyev, Y., Humphries, N., Toyozumi, H. and Tsubouchi, H. (2012) Budding yeast Pch2, a widely conserved meiotic protein, is involved in the initiation of meiotic recombination. **PLoS ONE**, 7 (6)

Faucher, D. and Wellinger, R.J. (2010) Methylated H3K4, a transcription-associated histone modification, is involved in the DNA damage response pathway. **PLoS genetics**, 6 (8): e1001082

Fell, V.L. and Schild-Poulter, C. (2015) The Ku heterodimer: Function in DNA repair and beyond. **Mutation Research/Reviews in Mutation Research**, 763: 15–29

Ferdous, M., Higgins, J.D., Osman, K., Lambing, C., Roitinger, E., Mechtler, K., Armstrong, S.J., Perry, R., Pradillo, M., Cuñado, N. and Franklin, F.C.H. (2012) Inter-homolog crossing-over and synapsis in *Arabidopsis* meiosis are dependent on the chromosome axis protein AtASY3. **PLoS genetics**, 8 (2): e1002507

Fishel, R. (2015) Mismatch Repair. **Journal of Biological Chemistry**, 290 (44): jbc.R115.660142

Francis, K.E., Lam, S.Y., Harrison, B.D., Bey, A.L., Berchowitz, L.E. and Copenhaver, G.P. (2007) Pollen tetrad-based visual assay for meiotic recombination in *Arabidopsis*. **Proceedings of the National Academy of Sciences of the United States of America**, 104 (10): 3913–8

- Franklin, a E., McElver, J., Sunjevaric, I., Rothstein, R., Bowen, B. and Cande, W.Z. (1999) Three-dimensional microscopy of the Rad51 recombination protein during meiotic prophase. **The Plant cell**, 11 (5): 809–824
- Franklin, T.B., Russig, H., Weiss, I.C., Grff, J., Linder, N., Michalon, A., Vizi, S. and Mansuy, I.M. (2010) Epigenetic transmission of the impact of early stress across generations. **Biological Psychiatry**, 68 (5): 408–415
- Fukuda, T., Pratto, F., Schimenti, J.C., Turner, J.M. a, Camerini-Otero, R.D. and Höög, C. (2012) Phosphorylation of chromosome core components may serve as axis marks for the status of chromosomal events during mammalian meiosis. **PLoS Genetics**, 8 (2): e1002485
- Fung, J.C., Rockmill, B., Odell, M. and Roeder, G.S. (2004) Imposition of crossover interference through the nonrandom distribution of synapsis initiation complexes. **Cell**, 116 (6): 795–802
- Fusco, C., Reymond, A. and Zervos, A.S. (1998) Molecular Cloning and Characterization of a Novel Retinoblastoma-Binding Protein. **Genomics**, 51: 351–358
- Gan, E.-S., Xu, Y., Wong, J.-Y., Geraldine Goh, J., Sun, B., Wee, W.-Y., Huang, J. and Ito, T. (2014) Jumonji demethylases moderate precocious flowering at elevated temperature via regulation of FLC in Arabidopsis. **Nat Communications**, 5 (5098)
- Gasior, S.L., Wong, A.K., Kora, Y., Shinohara, A. and Bishop, D.K. (1998) Rad52 associates with RPA and functions with Rad55 and Rad57 to assemble meiotic recombination complexes. **Genes and Development**, 12 (14): 2208–2221
- Girard, C., Chelysheva, L., Choinard, S., Froger, N., Macaisne, N., Lemhemdi, A., Mazel, J., Crismani, W. and Mercier, R. (2015) AAA-ATPase FIDGETIN-LIKE 1 and Helicase FANCM Antagonize Meiotic Crossovers by Distinct Mechanisms. **PLoS Genetics**, 11 (7): e1005369
- Girard, C., Crismani, W., Froger, N., Mazel, J., Lemhemdi, A., Horlow, C. and Mercier, R. (2014) FANCM-associated proteins MHF1 and MHF2, but not the other Fanconi anemia factors, limit meiotic crossovers. **Nucleic acids research**, 42 (14): 1–9
- Giraut, L., Falque, M., Drouaud, J., Pereira, L., Martin, O.C. and Mézard, C. (2011) Genome-wide crossover distribution in Arabidopsis thaliana meiosis reveals sex-specific patterns along chromosomes. **PLoS genetics**, 7 (11): e1002354
- Goldfarb, T. and Lichten, M. (2010) Frequent and efficient use of the sister chromatid for DNA double-strand break repair during budding yeast meiosis. **PLoS Biology**, 8 (10): 10–12
- Gould, P.D., Locke, J.C.W., Larue, C., Southern, M.M., Davis, S.J., Hanano, S., Moyle, R., Milich, R., Putterill, J., Millar, A.J. and Hall, A. (2006) The molecular

basis of temperature compensation in the Arabidopsis circadian clock. **The Plant Cell**, 18 (5): 1177–1187

Greer, E., Martin, a. C., Pendle, a., Colas, I., Jones, a. M.E., Moore, G. and Shaw, P. (2012) The Ph1 Locus Suppresses Cdk2-Type Activity during Premeiosis and Meiosis in Wheat. **The Plant Cell**, 24 (1): 152–162

Grelon, M., Vezon, D., Gendrot, G. and Pelletier, G. (2001) AtSPO11-1 is necessary for efficient meiotic recombination in plants. **EMBO Journal**, 20 (3): 589–600

Grey, C., Barthès, P., Chauveau-Le Fric, G., Langa, F., Baudat, F. and de Massy, B. (2011) Mouse PRDM9 DNA-binding specificity determines sites of histone H3 lysine 4 trimethylation for initiation of meiotic recombination. **PLoS biology**, 9 (10): e1001176

Guo, L., Yu, Y., Law, J. a and Zhang, X. (2010) SET DOMAIN GROUP2 is the major histone H3 lysine [corrected] 4 trimethyltransferase in Arabidopsis. **Proceedings of the National Academy of Sciences of the United States of America**, 107 (43): 18557–18562

Gursoy-Yuzugullu, O., Ayrapetov, M.K. and Price, B.D. (2015) Histone chaperone Anp32e removes H2A.Z from DNA double-strand breaks and promotes nucleosome reorganization and DNA repair. **Proceedings of the National Academy of Sciences**, 112 (24): 201504868

Hardy, S., Jacques, P.É., Gévry, N., Forest, A., Fortin, M.E., Laflamme, L., Gaudreau, L. and Robert, F. (2009) The euchromatic and heterochromatic landscapes are shaped by antagonizing effects of transcription on H2A.Z deposition. **PLoS Genetics**, 5 (10): e1000687

Hartung, F., Plchová, H. and Puchta, H. (2000) Molecular characterisation of RecQ homologues in Arabidopsis thaliana. **Nucleic acids research**, 28 (21): 4275–4282

Hartung, F., Wurz-Wildersinn, R., Fuchs, J., Schubert, I., Suer, S. and Puchta, H. (2007) The catalytically active tyrosine residues of both SPO11-1 and SPO11-2 are required for meiotic double-strand break induction in Arabidopsis. **The Plant cell**, 19 (10): 3090–3099

Hauf, S., Waizenegger, I.C. and Peters, J.M. (2001) Cohesin cleavage by separase required for anaphase and cytokinesis in human cells. **Science**, 293 (5533): 1320–1323

Hayakawa, T., Zhang, F., Hayakawa, N., Ohtani, Y., Shinmyozu, K., Nakayama, J. and Andreassen, P.R. (2010) MRG15 binds directly to PALB2 and stimulates homology-directed repair of chromosomal breaks. **Journal of cell science**, 123 (Pt 7): 1124–1130

Hayashi, K., Yoshida, K. and Matsui, Y. (2005) A histone H3 methyltransferase controls epigenetic events required for meiotic prophase. **Nature**, 438 (7066): 374–

8

- Hedhly, A., Hormaza, J.I. and Herrero, M. (2009) Global warming and sexual plant reproduction. **Trends in Plant Science**, 14 (1): 30–36
- Henderson, K. a and Keeney, S. (2004) Tying synaptonemal complex initiation to the formation and programmed repair of DNA double-strand breaks. **Proceedings of the National Academy of Sciences of the United States of America**, 101 (13): 4519–4524
- Higgins, J.D., Armstrong, S.J., Franklin, F.C.H. and Jones, G.H. (2004) The Arabidopsis MutS homolog AtMSH4 functions at an early step in recombination: evidence for two classes of recombination in Arabidopsis. **Genes & Development**, 18 (20): 2557–70
- Higgins, J.D., Buckling, E.F., Franklin, F.C.H. and Jones, G.H. (2008a) Expression and functional analysis of AtMUS81 in Arabidopsis meiosis reveals a role in the second pathway of crossing-over. **The Plant Journal**, 54 (1): 152–62
- Higgins, J.D., Osman, K., Jones, G.H. and Franklin, F.C.H. (2014) Factors Underlying Restricted Crossover Localization in Barley Meiosis. **Annual review of genetics**, (July): 29–47
- Higgins, J.D., Perry, R.M., Barakate, A., Ramsay, L., Waugh, R., Halpin, C., Armstrong, S.J. and Franklin, F.C.H. (2012) Spatiotemporal asymmetry of the meiotic program underlies the predominantly distal distribution of meiotic crossovers in barley. **The Plant cell**, 24 (10): 4096–109
- Higgins, J.D., Sanchez-Moran, E., Armstrong, S.J., Jones, G.H. and Franklin, F.C.H. (2005) The Arabidopsis synaptonemal complex protein ZYP1 is required for chromosome synapsis and normal fidelity of crossing over. **Genes & development**, 19 (20): 2488–500
- Higgins, J.D., Vignard, J., Mercier, R., Pugh, A.G. and Jones, G.H. (2008b) AtMSH5 partners AtMSH4 in the class I meiotic crossover pathway in Arabidopsis thaliana , but is not required for synapsis. **The Plant Journal**, 55: 28–39
- Ho, H.C. and Burgess, S.M. (2011) Pch2 acts through Xrs2 and Tel1/ATM to modulate interhomolog bias and checkpoint function during meiosis. **PLoS Genetics**, 7 (11)
- Holliday, R. (1964) A mechanism for gene conversion in fungi. **Genetical research**, 89 (5-6): 285–307
- Hollingsworth, N.M. and Brill, S.J. (2004) The Mus81 solution to resolution: generating meiotic crossovers without Holliday junctions. **Genes & development**, 18 (2): 117–25
- Hollingsworth, N.M., Ponte, L. and Halsey, C. (1995) MSH5, a novel MutS homolog,

- facilitates meiotic reciprocal recombination between homologs in *Saccharomyces cerevisiae* but not mismatch repair. **Genes and Development**, 9 (14): 1728–1739
- Hotta, Y., Fujisawa, M., Tabata, S., Stern, H. and Yoshida, S. (1988) The effect of temperature on recombination activity in testes of rodents. **Experimental cell research**, 178 (1): 163–168
- Hotta, Y., Tabata, S., Bouchard, R., Piñon, R. and Stern, H. (1985) General recombination mechanisms in extracts of meiotic cells. **Chromosoma**, 93 (2): 140–151
- Hunter, N. and Kleckner, N. (2001) The single-end invasion: an asymmetric intermediate at the double-strand break to double-holliday junction transition of meiotic recombination. **Cell**, 106 (1): 59–70
- Da Ines, O., Degroote, F., Amiard, S., Goubely, C., Gallego, M.E. and White, C.I. (2013a) Effects of XRCC2 and RAD51B mutations on somatic and meiotic recombination in *Arabidopsis thaliana*. **Plant Journal**, 74 (6): 959–970
- Da Ines, O., Degroote, F., Goubely, C., Amiard, S., Gallego, M.E. and White, C.I. (2013b) Meiotic recombination in *Arabidopsis* is catalysed by DMC1, with RAD51 playing a supporting role. **PLoS genetics**, 9 (9): e1003787
- Ismail, M., Shinohara, M. and Shinohara, A. (2014) Dot1-Dependent Histone H3K79 Methylation Promotes the Formation of Meiotic Double-Strand Breaks in the Absence of Histone H3K4 Methylation in Budding Yeast Dawson, D.S. (ed.). **PLoS ONE**, 9 (5): e96648
- Jackson, N., Sanchez-Moran, E., Buckling, E., Armstrong, S.J., Jones, G.H. and Franklin, F.C.H. (2006) Reduced meiotic crossovers and delayed prophase I progression in AtMLH3-deficient *Arabidopsis*. **The EMBO journal**, 25 (6): 1315–23
- Jacobs, S. a and Khorasanizadeh, S. (2002) Structure of HP1 chromodomain bound to a lysine 9-methylated histone H3 tail. **Science**, 295 (5562): 2080–2083
- Johnston, A.J., Matveeva, E., Kirioukhova, O., Grossniklaus, U. and Grusissem, W. (2008) A Dynamic Reciprocal RBR-PRC2 Regulatory Circuit Controls *Arabidopsis* Gametophyte Development. **Current Biology**, 18 (21): 1680–1686
- Jones, D.O., Cowell, I.G. and Singh, P.B. (2000) Mammalian chromodomain proteins: Their role in genome organisation and expression. **BioEssays**, 22 (2): 124–137
- Jones, G.H. and Franklin, F.C.H. (2006) Meiotic crossing-over: obligation and interference. **Cell**, 126 (2): 246–8
- Jones, K.T. (2008) Meiosis in oocytes: Predisposition to aneuploidy and its increased incidence with age. **Human Reproduction Update**, 14 (2): 143–158

- Joshi, A. a. and Struhl, K. (2005) Eaf3 chromodomain interaction with methylated H3-K36 links histone deacetylation to pol II elongation. **Molecular Cell**, 20 (6): 971–978
- Joshi, N., Barot, A., Jamison, C. and Börner, G.V. (2009) Pch2 links chromosome axis remodeling at future crossover sites and crossover distribution during yeast meiosis. **PLoS genetics**, 5 (7): e1000557
- Joyce, E.F. and McKim, K.S. (2009) Drosophila PCH2 is required for a pachytene checkpoint that monitors double-strand-break-independent events leading to meiotic crossover formation. **Genetics**, 181 (1): 39–51
- Joyce, E.F. and McKim, K.S. (2010) Chromosome axis defects induce a checkpoint-mediated delay and interchromosomal effect on crossing over during drosophila meiosis. **PLoS Genetics**, 6 (8): e1001059
- Jun, S.-H., Kim, T.G. and Ban, C. (2006) DNA mismatch repair system. Classical and fresh roles. **The FEBS journal**, 273 (8): 1609–19
- Kasinsky, H.E., Lewis, J.D., Dacks, J.B. and Ausió, J. (2001) Origin of H1 linker histones. **The FASEB journal**, 15 (1): 34–42
- Keeney, S. (2008) Spo11 and the Formation of DNA Double-Strand Breaks in Meiosis. **Genome Dynamics and Stability**, (1;2): 81–123
- Keeney, S., Giroux, C.N. and Kleckner, N. (1997) Meiosis-specific DNA double-strand breaks are catalyzed by Spo11, a member of a widely conserved protein family. **Cell**, 88 (3): 375–84
- Keogh, M.C., Kurdistani, S.K., Morris, S. a., et al. (2005) Cotranscriptional set2 methylation of histone H3 lysine 36 recruits a repressive Rpd3 complex. **Cell**, 123 (4): 593–605
- Kikuchi, K., Narita, T., Pham, V.T., Iijima, J., Hirota, K., Keka, I.S., Mohiuddin, Okawa, K., Hori, T., Fukagawa, T., Essers, J., Kanaar, R., Whitby, M.C., Sugawara, K., Taniguchi, Y., Kitagawa, K. and Takeda, S. (2013) Structure-specific endonucleases xpf and mus81 play overlapping but essential roles in DNA repair by homologous recombination. **Cancer research**, 73 (14): 4362–71
- Kim, K.P., Weiner, B.M., Zhang, L., Jordan, A., Dekker, J. and Kleckner, N. (2010) Sister cohesion and structural axis components mediate homolog bias of meiotic recombination. **Cell**, 143 (6): 924–37
- King, J.S. and Mortimer, R.K. (1990) A polymerization model of chiasma interference and corresponding computer simulation. **Genetics**, 126 (4): 1127–1138
- Kitajima, T.S., Kawashima, S. a and Watanabe, Y. (2004) The conserved kinetochore protein shugoshin protects centromeric cohesion during meiosis. **Nature**, 427 (6974): 510–517

- Kleckner, N. (2006) Chiasma formation: chromatin/axis interplay and the role(s) of the synaptonemal complex. **Chromosoma**, 115 (3): 175–94
- Kleckner, N., Zickler, D., Jones, G.H., Dekker, J., Padmore, R., Henle, J. and Hutchinson, J. (2004) A mechanical basis for chromosome function. **Proceedings of the National Academy of Sciences of the United States of America**, 101 (34): 12592–7
- Klein, F., Mahr, P., Galova, M., Buonomo, S.B.C., Michaelis, C., Nairz, K. and Nasmyth, K. (1999) A central role for cohesins in sister chromatid cohesion, formation of axial elements, and recombination during yeast meiosis. **Cell**, 98 (1): 91–103
- Knezetic, J.A. and Luse, D.S. (1986) The presence of nucleosomes on a DNA template prevents initiation by RNA polymerase II in vitro. **Cell**, 45 (1): 95–104
- Knoll, A., Higgins, J.D., Seeliger, K., Reha, S.J., Dangel, N.J., Bauknecht, M., Schröpfer, S., Franklin, F.C.H. and Puchta, H. (2012) The Fanconi anemia ortholog FANCM ensures ordered homologous recombination in both somatic and meiotic cells in Arabidopsis. **The Plant cell**, 24 (4): 1448–64
- Kohli, J. and Bähler, J. (1994) Homologous recombination in fission yeast: Absence of crossover interference and synaptonemal complex. **Experientia**, 50 (3): 295–306
- Kolasinska-zwierz, P., Down, T., Latorre, I., Liu, T., Liu, X.S. and Ahringer, J. (2009) Differential chromatin marking of introns and expressed exons by H3K36me3. **Nature Genetics**, 41 (3): 376–381
- von Koskull-Döring, P., Scharf, K.-D. and Nover, L. (2007) The diversity of plant heat stress transcription factors. **Trends in plant science**, 12 (10): 452–457
- Kouzarides, T. (2007) Chromatin modifications and their function. **Cell**, 128 (4): 693–705
- Kovalchuk, I., Kovalchuk, O., Kalck, V., Boyko, V., Filkowski, J., Heinlein, M. and Hohn, B. (2003) Pathogen-induced systemic plant signal triggers DNA rearrangements. **Nature**, 423 (6941): 760–762
- Kumar, S.V. and Wigge, P. a. (2010) H2A.Z-Containing Nucleosomes Mediate the Thermosensory Response in Arabidopsis. **Cell**, 140 (1): 136–147
- Kurzbauer, M.-T., Uanschou, C., Chen, D. and Schlögelhofer, P. (2012) The recombinases DMC1 and RAD51 are functionally and spatially separated during meiosis in Arabidopsis. **The Plant cell**, 24 (5): 2058–70
- Lachner, M., O’Carroll, D., Rea, S., Mechtler, K. and Jenuwein, T. (2001) Methylation of histone H3 lysine 9 creates a binding site for HP1 proteins. **Nature**, 410 (6824): 116–120
- Lambing, C. (2014) Investigating the interplay between chromosome axes and

homologous recombination in Arabidopsis meiosis. **PhD Thesis, Univeristy of Birmingham**

Laming, C., Osman, K., Nuntasontorn, K., West, A., Higgins, J.D., Copenhaver, G.P., Yang, J., Armstrong, S.J., Mechtler, K., Roitinger, E. and Franklin, F.C.H. (2015) Arabidopsis PCH2 Mediates Meiotic Chromosome Remodeling and Maturation of Crossovers. **PLOS Genetics**, 11 (7): e1005372

Landry, J., Sutton, A., Hesman, T., Min, J., Xu, R., Johnston, M. and Sternglanz, R. (2003) Set2-Catalyzed Methylation of Histone H3 Represses Basal Expression of GAL4 in Saccharomyces cerevisiae Set2-Catalyzed Methylation of Histone H3 Represses Basal Expression of GAL4 in Saccharomyces cerevisiae. **Molecular and Cellular Biology**, 23 (17): 5972–5978

Lang, J., Smetana, O., Sanchez-Calderon, L., Lincker, F., Genestier, J., Schmit, A.-C., Houlné, G. and Chabouté, M.-E. (2012) Plant γ H2AX foci are required for proper DNA DSB repair responses and colocalize with E2F factors. **The New phytologist**, 194 (2): 353–63

Lao, J.P., Cloud, V., Huang, C.-C., Grubb, J., Thacker, D., Lee, C.-Y., Dresser, M.E., Hunter, N. and Bishop, D.K. (2013) Meiotic crossover control by concerted action of Rad51-Dmc1 in homolog template bias and robust homeostatic regulation. **PLoS genetics**, 9 (12): e1003978

Lauberth, S.M., Nakayama, T., Wu, X., Ferris, A., Tang, Z., Hughes, S.H. and Roeder, R.G. (2013) NIH Public Access. **Cell**, 152 (5): 1021–1036

Lee, D.Y., Hayes, J.J., Pruss, D. and Wolffe, A.P. (1993) A Positive Role for Histone Acetylation in Transcription Factor Access to Nucleosomal DNA. **Cell**, 72: 73–84

Lee, J.Y. and Orr-Weaver, T.L. (2001) The Molecular Basis of Sister-Chromatid Cohesion. **Annual Review of Cellular and Developmental Biology**, 17: 757–777

Lee, J.Y., Terakawa, T., Qi, Z., Steinfeld, J., Redding, S., Kwon, Y., Gaines, W.A., Zhao, W., Sung, P. and Greene, E.C. (2015) Base triplet stepping by the Rad51/RecA family of recombinases. **Science**, 349 (6251): 977–981

Leung, J.K., Berube, N., Venable, S., Ahmed, S., Timchenko, N. and Pereira-Smith, O.M. (2001) MRG15 Activates the B-myb Promoter through Formation of a Nuclear Complex with the Retinoblastoma Protein and the Novel Protein PAM14. **Journal of Biological Chemistry**, 276 (42): 39171–39178

Li, G. and Widom, J. (2004) Nucleosomes facilitate their own invasion. **Nature structural & molecular biology**, 11 (8): 763–9

Li, W., Chen, C., Markmann-Mulisch, U., Timofejeva, L., Schmelzer, E., Ma, H. and Reiss, B. (2004) The Arabidopsis AtRAD51 gene is dispensable for vegetative development but required for meiosis. **Proceedings of the National Academy of**

Sciences of the United States of America, 101 (29): 10596–601

Li, W., Yang, X., Lin, Z., Timofejeva, L., Xiao, R., Makaroff, C. a and Ma, H. (2005) The AtRAD51C gene is required for normal meiotic chromosome synapsis and double-stranded break repair in Arabidopsis. **Plant physiology**, 138 (2): 965–976

Li, X. and Schimenti, J.C. (2007) Mouse pachytene checkpoint 2 (Trip13) is required for completing meiotic recombination but not synapsis. **PLoS Genetics**, 3 (8): 1365–1376

Libuda, D.E., Uzawa, S., Meyer, B.J. and Villeneuve, A.M. (2013) Meiotic chromosome structures constrain and respond to designation of crossover sites. **Nature**, 502 (7473): 703–6

Lin, F.-M., Lai, Y.-J., Shen, H.-J., Cheng, Y.-H. and Wang, T.-F. (2010) Yeast axial-element protein, Red1, binds SUMO chains to promote meiotic interhomologue recombination and chromosome synapsis. **The EMBO journal**, 29 (3): 586–96

Liu, C., Lu, F., Cui, X. and Cao, X. (2010) Histone methylation in higher plants. **Annual review of plant biology**, 61: 395–420

Liu, C.L., Kaplan, T., Kim, M., Buratowski, S., Schreiber, S.L., Friedman, N. and Rando, O.J. (2005) Single-Nucleosome Mapping of Histone Modifications in *S. cerevisiae*. **PLoS Biology**, 3 (10): e328

Lo, Y.-H., Chuang, C.-N. and Wang, T.-F. (2014) Pch2 prevents Mec1/Tel1-mediated Hop1 phosphorylation occurring independently of Red1 in budding yeast meiosis. **PLoS one**, 9 (1): e85687

Loidl, J. (1989) Effects of elevated temperature on meiotic chromosome synapsis in *Allium ursinum*. **Chromosoma**, 97 (6): 449–458

Lorch, Y., LaPointe, J.W. and Kornberg, R.D. (1987) Nucleosomes inhibit the initiation of transcription but allow chain elongation with the displacement of histones. **Cell**, 49 (2): 203–10

Lorenz, A., Osman, F., Sun, W., Nandi, S., Steinacher, R. and Whitby, M.C. (2012) The Fission Yest FANCM Ortholog Directs Non-Crossover Recombination During Meiosis. **Science**, 336: 1585–1588

Luger, K. and Hansen, J.C. (2005) Nucleosome and chromatin fiber dynamics. **Current Opinion in Structural Biology**, 15 (2): 188–196

Luger, K., Sargent, D.F., Richmond, T.J., Ma, A.W. and Richmond, R.K. (1997) Crystal structure of the nucleosome core particle at 2 . 8 Å resolution. **Nature**, 7: 251–260

Lynn, A., Koehler, K.E., Judis, L., Chan, E.R., Cherry, J.P., Schwartz, S., Seftel, A., Hunt, P. a and Hassold, T.J. (2002) Covariation of synaptonemal complex length and mammalian meiotic exchange rates. **Science**, 296 (5576): 2222–2225

Ma, H. (2006) A molecular portrait of Arabidopsis meiosis. **The Arabidopsis book / American Society of Plant Biologists**, 4: e0095

Macaisne, N., Novatchkova, M., Peirera, L., Vezon, D., Jolivet, S., Froger, N., Chelysheva, L., Grelon, M. and Mercier, R. (2008) SHOC1, an XPF endonuclease-related protein, is essential for the formation of class I meiotic crossovers. **Current Biology**, 18 (18): 1432–7

Macaisne, N., Vignard, J. and Mercier, R. (2011) SHOC1 and PTD form an XPF-ERCC1-like complex that is required for formation of class I crossovers. **Journal of cell science**, 124 (Pt 16): 2687–91

MacQueen, A.J. and Roeder, G.S. (2009) Fpr3 and Zip3 Ensure that Initiation of Meiotic Recombination Precedes Chromosome Synapsis in Budding Yeast. **Current Biology**, 19 (18): 1519–1526

Mahadevaiah, S.K., Turner, J.M., Baudat, F., Rogakou, E.P., de Boer, P., Blanco-Rodríguez, J., Jasin, M., Keeney, S., Bonner, W.M. and Burgoyne, P.S. (2001) Recombinational DNA double-strand breaks in mice precede synapsis. **Nature genetics**, 27 (3): 271–276

Malik, S.B., Ramesh, M. a., Hulstrand, A.M. and Logsdon, J.M. (2007) Protist homologs of the meiotic Spo11 gene and topoisomerase VI reveal an evolutionary history of gene duplication and lineage-specific loss. **Molecular Biology and Evolution**, 24 (12): 2827–2841

Malkova, A., Swanson, J., German, M., McCusker, J.H., Housworth, E. a., Stahl, F.W. and Haber, J.E. (2004) Gene conversion and crossing over along the 405-kb left arm of *Saccharomyces cerevisiae* chromosome VII. **Genetics**, 168 (1): 49–63

Mancera, E., Bourgon, R., Brozzi, A., Huber, W. and Steinmetz, L.M. (2008) High-resolution mapping of meiotic crossovers and non-crossovers in yeast. **Nature**, 454 (7203): 479–485

Manfrini, N., Guerini, I., Citterio, A., Lucchini, G. and Longhese, M.P. (2010) Processing of Meiotic DNA Double Strand Breaks Requires Cyclin-dependent Kinase and Multiple Nucleases. **The Journal of Biological Chemistry**, 285 (15): 11628–11637

Mari, P.-O., Florea, B.I., Persengiev, S.P., Verkaik, N.S., Brüggewirth, H.T., Modesti, M., Giglia-Mari, G., Bezstarosti, K., Demmers, J. a a, Luiders, T.M., Houtsmuller, A.B. and van Gent, D.C. (2006) Dynamic assembly of end-joining complexes requires interaction between Ku70/80 and XRCC4. **Proceedings of the National Academy of Sciences of the United States of America**, 103 (49): 18597–18602

Martini, E., Diaz, R.L., Hunter, N. and Keeney, S. (2006) Crossover homeostasis in yeast meiosis. **Cell**, 126 (2): 285–95

- Marzluff, W.F., Wagner, E.J. and Duronio, R.J. (2009) Metabolism and regulation of canonical histone mRNAs: life without a poly(A) tail. **Nature reviews Genetics**, 9 (11): 843–854
- Mayer, K.F.X., Martis, M., Hedley, P.E., et al. (2011) Unlocking the barley genome by chromosomal and comparative genomics. **The Plant cell**, 23 (4): 1249–1263
- Mazina, O.M., Mazin, A. V, Nakagawa, T., Kolodner, R.D. and Kowalczykowski, S.C. (2004) Saccharomyces cerevisiae Mer3 Helicase Stimulates 3 – 5 Heteroduplex Extension by Rad51: Implications for Crossover Control in Meiotic Recombination of Medicine. **Cell**, 117: 47–56
- Mckee, H.Z. and Kleckner, N. (1997) A General Method for Identifying Recessive Diploid-Specific Mutations in Saccharomyces cerevisiae, its Application to the Isolation of Mutants Blocked at Intermediate Stages of Meiotic Prophase and Characterization of a New Gene SAE2. **Genetics**, 146: 796–816
- McKim, K.S., Green-Marroquin, B.L., Sekelsky, J.J., Chin, G., Steinberg, C., Khodosh, R. and Hawley, R.S. (1998) Meiotic synapsis in the absence of recombination. **Science**, 279 (5352): 876–878
- McMahill, M.S., Sham, C.W. and Bishop, D.K. (2007) Synthesis-dependent strand annealing in meiosis. **PLoS Biology**, 5 (11): 2589–2601
- Melamed-Bessudo, C. and Levy, A. a (2012) Deficiency in DNA methylation increases meiotic crossover rates in euchromatic but not in heterochromatic regions in Arabidopsis. **Proceedings of the National Academy of Sciences of the United States of America**, 109 (16): E981–8
- Mercier, R., Jolivet, S., Vezon, D., Huppe, E., Chelysheva, L., Giovanni, M., Nogué, F., Doutriaux, M.-P., Horlow, C., Grelon, M. and Mézard, C. (2005) Two meiotic crossover classes cohabit in Arabidopsis: one is dependent on MER3, whereas the other one is not. **Current biology**, 15 (8): 692–701
- Mets, D.G. and Meyer, B.J. (2009) Condensins regulate meiotic DNA break distribution, thus crossover frequency, by controlling chromosome structure. **Cell**, 139 (1): 73–86
- Miao, C., Tang, D., Zhang, H., Wang, M., Li, Y., Tang, S., Yu, H., Gu, M. and Cheng, Z. (2013) CENTRAL REGION COMPONENT1, a Novel Synaptonemal Complex Component, Is Essential for Meiotic Recombination Initiation in Rice. **The Plant Cell**, 25 (8): 2998–3009
- Mieczkowski, P., Dominska, M., Buck, M.J., Gerton, J.L., Lieb, J.D. and Petes, T.D. (2006) Global Analysis of the Relationship between the Binding of the Bas1p Transcription Factor and Meiosis-Specific Double-Strand DNA Breaks in. **Society**, 26 (3): 1014–1027
- Mieczkowski, P., Dominska, M., Buck, M.J., Lieb, J.D. and Petes, T.D. (2007) Loss of

a histone deacetylase dramatically alters the genomic distribution of Spo11p-catalyzed DNA breaks in *Saccharomyces cerevisiae*. **Proceedings of the National Academy of Sciences of the United States of America**, 104 (10): 3955–3960

Mimitou, E.P. and Symington, L.S. (2008) Sae2, Exo1 and Sgs1 collaborate in DNA double-strand break processing. **Nature**, 455 (7214): 770–774

Mirouze, M., Lieberman-Lazarovich, M., Aversano, R., Bucher, E., Nicolet, J., Reinders, J. and Paszkowski, J. (2012) Loss of DNA methylation affects the recombination landscape in *Arabidopsis*. **Proceedings of the National Academy of Sciences**, 109 (15): 5880–5885

Moens, P.B., Marcon, E., Shore, J.S., Kochakpour, N. and Spyropoulos, B. (2007) Initiation and resolution of interhomolog connections: crossover and non-crossover sites along mouse synaptonemal complexes. **Journal of cell science**, 120 (Pt 6): 1017–27

Molinier, J., Ries, G., Zipfel, C. and Hohn, B. (2006) Transgeneration memory of stress in plants. **Nature**, 442 (7106): 1046–1049

Molnar, M., Bahler, J., Sipiczki, M. and Kohli, J. (1995) The *rec8* gene of *Schizosaccharomyces pombe* is involved in linear element formation, chromosome pairing and sister-chromatid cohesion during meiosis. **Genetics**, 141 (1): 61–73

Muñoz-Galván, S., Jimeno, S., Rothstein, R. and Aguilera, A. (2013) Histone H3K56 Acetylation, Rad52, and Non-DNA Repair Factors Control Double-Strand Break Repair Choice with the Sister Chromatid. **PLoS Genetics**, 9 (1): e1003237

De Muyt, A., Jessop, L., Kolar, E., Sourirajan, A., Chen, J., Dayani, Y. and Lichten, M. (2012) BLM Helicase Ortholog Sgs1 Is a Central Regulator of Meiotic Recombination Intermediate Metabolism. **Molecular Cell**, 46 (1): 43–53

De Muyt, A., Pereira, L., Vezon, D., Chelysheva, L., Gendrot, G., Chambon, A., Lainé-Choinard, S., Pelletier, G., Mercier, R., Nogué, F. and Grelon, M. (2009) A high throughput genetic screen identifies new early meiotic recombination functions in *Arabidopsis thaliana*. **PLoS Genetics**, 5 (9): e1000654

De Muyt, A., Zhang, L., Pilot, T., Kleckner, N., Espagne, E. and Zickler, D. (2014) E3 ligase Hei10: a multifaceted structure-based signaling molecule with roles within and beyond meiosis. **Genes & development**, 28 (10): 1111–23

Nakagawa, T. and Kolodner, R.D. (2002) *Saccharomyces cerevisiae* Mer3 Is a DNA Helicase Involved in Meiotic Crossing Over *Saccharomyces cerevisiae* Mer3 Is a DNA Helicase Involved in Meiotic Crossing Over. **Molecular and Cellular Biology**, 22 (10): 3281–3291

Nakagawa, T. and Ogawa, H. (1999) The *Saccharomyces cerevisiae* MER3 gene, encoding a novel helicase-like protein, is required for crossover control in meiosis. **EMBO Journal**, 18 (20): 5714–5733

- Naranjo, T. (2012) Finding the correct partner: the meiotic courtship. **Scientifica**, 2012: 509073
- Naydenov, M., Baev, V., Apostolova, E., Gospodinova, N., Sablok, G., Gozmanova, M. and Yahubyan, G. (2015) High-temperature effect on genes engaged in DNA methylation and affected by DNA methylation in Arabidopsis. **Plant Physiology and Biochemistry**, 87: 102–108
- Neale, M.J., Pan, J. and Keeney, S. (2005) Endonucleolytic processing of covalent protein-linked DNA double-strand breaks. **Nature**, 436 (7053): 1053–1057
- Ng, D.W., Wang, T., Chandrasekharan, M.B., Aramayo, R. and Hall, T.C. (2007) Plant SET domain-containing proteins: structure, function and regulation. **Biochim Biophys Acta**, 1769 (5-6): 316–329
- Nick McElhinny, S. a, Snowden, C.M., McCarville, J. and Ramsden, D. a (2000) Ku recruits the XRCC4-ligase IV complex to DNA ends. **Molecular and cellular biology**, 20 (9): 2996–3003
- Niu, H., Wan, L., Baumgartner, B., Schaefer, D., Loidl, J. and Hollingsworth, N.M. (2005) Partner Choice during Meiosis Is Regulated by Hop1-promoted Dimerization of Mek1. **Molecular Biology of the Cell**, 16 (December): 5804–5818
- Niu, H., Wan, L., Busygina, V., Kwon, Y., Allen, J. a., Li, X., Kunz, R.C., Kubota, K., Wang, B., Sung, P., Shokat, K.M., Gygi, S.P. and Hollingsworth, N.M. (2009) Regulation of Meiotic Recombination via Mek1-Mediated Rad54 Phosphorylation. **Molecular Cell**, 36 (3): 393–404
- Nonomura, K.-I., Nakano, M., Fukuda, T., Eiguchi, M., Miyao, A., Hirochika, H. and Kurata, N. (2004) The novel gene HOMOLOGOUS PAIRING ABERRATION IN RICE MEIOSIS1 of rice encodes a putative coiled-coil protein required for homologous chromosome pairing in meiosis. **The Plant cell**, 16 (4): 1008–1020
- Novak, J.E., Ross-Macdonald, P.B. and Shirleen Roeder, G. (2001) The budding yeast Msh4 protein functions in chromosome synapsis and the regulation of crossover distribution. **Genetics**, 158 (3): 1013–1025
- Nuntasontorn, K. (2013) Functional analysis of the Arabidopsis thaliana meiotic proteins AtPCH2 and AtCHR24. **PhD Thesis, Univeristy of Birmingham**
- Olins, A.L. and Olins, D.E. (1974) Spheroid chromatin units (v bodies). **Science**, 183 (4122): 330–2
- Oliver-Bonet, M., Campillo, M., Turek, P.J., Ko, E. and Martin, R.H. (2007) Analysis of replication protein A (RPA) in human spermatogenesis. **Molecular Human Reproduction**, 13 (12): 837–844
- Orr-Weaver, T.L. (1999) The ties that bind: Localization of the sister-chromatid cohesin complex on yeast chromosomes. **Cell**, 99 (1): 1–4

- Oshino, T., Abiko, M., Saito, R., Ichiishi, E., Endo, M., Kawagishi-Kobayashi, M. and Higashitani, A. (2007) Premature progression of anther early developmental programs accompanied by comprehensive alterations in transcription during high-temperature injury in barley plants. **Molecular Genetics and Genomics**, 278 (1): 31–42
- Osman, F., Dixon, J., Doe, C.L. and Whitby, M.C. (2003) Generating crossovers by resolution of nicked Holliday junctions: A role for Mus81-Eme1 in meiosis. **Molecular Cell**, 12 (3): 761–774
- Osman, K., Higgins, J.D., Sanchez-moran, E., Susan, J. and Franklin, F.C.H. (2011) Tansley review: Pathways to meiotic recombination in *Arabidopsis thaliana*. **New Phytologist**, 190: 523–544
- Osman, K., Roitinger, E., Yang, J., Armstrong, S., Mechtler, K. and Franklin, F.C. (2013) “Analysis of Meiotic Protein Complexes from *Arabidopsis* and *Brassica* Using Affinity-Based Proteomics.” In Pawlowski, W.P., Grelon, M. and Armstrong, S. (eds.) **Plant Meiosis: Methods and Protocols**. Methods in Molecular Biology. New York: Springer Science+Business Media. pp. 215–226
- Osman, K., Sanchez-Moran, E., Mann, S.C., Jones, G.H. and Franklin, F.C.H. (2009) Replication protein A (AtRPA1a) is required for class I crossover formation but is dispensable for meiotic DNA break repair. **The EMBO journal**, 28 (4): 394–404
- Pan, J., Sasaki, M., Kniewel, R., Murakami, H., Blitzblau, H.G., Tischfield, S.E., Zhu, X., Neale, M.J., Jasin, M., Socci, N.D., Hochwagen, A. and Keeney, S. (2011) A hierarchical combination of factors shapes the genome-wide topography of yeast meiotic recombination initiation. **Cell**, 144 (5): 719–731
- Panizza, S., Mendoza, M. a., Berlinger, M., Huang, L., Nicolas, A., Shirahige, K. and Klein, F. (2011) Spo11-accessory proteins link double-strand break sites to the chromosome axis in early meiotic recombination. **Cell**, 146 (3): 372–383
- Pardo, P.S., Leung, J.K., Lucchesi, J.C. and Pereira-Smith, O.M. (2002) MRG15, a novel chromodomain protein, is present in two distinct multiprotein complexes involved in transcriptional activation. **Journal of Biological Chemistry**, 277 (52): 50860–50866
- Parisi, S., McKay, M.J., Molnar, M., Thompson, M. a, van der Spek, P.J., van Drunen-Schoenmaker, E., Kanaar, R., Lehmann, E., Hoeijmakers, J.H. and Kohli, J. (1999) Rec8p, a meiotic recombination and sister chromatid cohesion phosphoprotein of the Rad21p family conserved from fission yeast to humans. **Molecular and cellular biology**, 19 (5): 3515–3528
- Pena, A.N. and Pereira-Smith, O.M. (2007) The role of the MORF/MRG family of genes in cell growth, differentiation, DNA repair, and thereby aging. **Annals of the New York Academy of Sciences**, 1100: 299–305

- Pena, A.N., Tominaga, K. and Pereira-Smith, O.M. (2011) NIH Public Access. **Experimental cell research**, 317 (11): 1534–1540
- Perkins, D.D. (1949) Biochemical mutants in the smut fungus *Ustilago maydis*. **Genetics**, 34 (5): 607–626
- Perrella, G., Consiglio, M.F., Aiese-Cigliano, R., Cremona, G., Sanchez-Moran, E., Barra, L., Errico, A., Bressan, R. a, Franklin, F.C.H. and Conicella, C. (2010) Histone hyperacetylation affects meiotic recombination and chromosome segregation in *Arabidopsis*. **The Plant Journal**, 62 (5): 796–806
- Petukhova, G. (2000) Promotion of Rad51-dependent D-loop formation by yeast recombination factor Rdh54/Tid1. **Genes & Development**, 14 (17): 2206–2215
- Phillips, D., Jenkins, G., Macaulay, M., Nibau, C., Wnetrzak, J., Fallding, D., Colas, I., Oakey, H., Waugh, R., Ramsay, L. and Ramsay, L. (2015) The effect of temperature on the male and female recombination landscape of barley. **New Phytologist**
- Pien, S., Fleury, D., Mylne, J.S., Crevillen, P., Inzé, D., Avramova, Z., Dean, C. and Grossniklaus, U. (2008) ARABIDOPSIS TRITHORAX1 dynamically regulates FLOWERING LOCUS C activation via histone 3 lysine 4 trimethylation. **The Plant Cell**, 20 (3): 580–8
- Pradillo, M., López, E., Linacero, R., Romero, C., Cuñado, N., Sánchez-Morán, E. and Santos, J.L. (2012) Together yes, but not coupled: new insights into the roles of RAD51 and DMC1 in plant meiotic recombination. **The Plant Journal**, 69 (6): 921–33
- Prieto, I., Suja, J. a, Pezzi, N., Kremer, L., Martínez-A, C., Rufas, J.S. and Barbero, J.L. (2001) Mammalian STAG3 is a cohesin specific to sister chromatid arms in meiosis I. **Nature cell biology**, 3 (8): 761–766
- Prinz, S., Amon, A. and Klein, F. (1997) Isolation of COM1, a new gene required to complete meiotic double- strand break-induced recombination in *Saccharomyces cerevisiae*. **Genetics**, 146 (3): 781–795
- Puizina, J., Siroky, J., Mokros, P., Schweizer, D. and Riha, K. (2004) Mre11 Deficiency in Arabidopsis Is Associated with Chromosomal Instability in Somatic Cells and Spo11-Dependent Genome Fragmentation during Meiosis. **The Plant Cell**, 16 (August): 1968–1978
- Qi, Z., Redding, S., Lee, J.Y., Gibb, B., Kwon, Y., Niu, H., Gaines, W.A., Sung, P. and Greene, E.C. (2015) DNA Sequence Alignment by Microhomology Sampling during Homologous Recombination. **Cell**, 160 (5): 856–869
- Qiao, H., Rao, H.B.D.P., Yang, Y., Fong, J.H., Cloutier, J.M., Cohen, P.E., Schimenti, J., Ward, J. and Hunter, N. (2015) Antagonistic roles of ubiquitin ligase HEI10 and SUMO ligase RNF212 regulate meiotic recombination. **Nature genetics**, 46 (2): 194–199

Ranjha, L., Anand, R. and Cejka, P. (2014) The *Saccharomyces cerevisiae* Mlh1-Mlh3 heterodimer is an endonuclease that preferentially binds to Holliday junctions. **The Journal of Biological Chemistry**, 289 (9): 5674–86

Rasmussen, S. (1986) Chromosome Interlocks During Synapsis- a Transient Disorder. **Tokai Journal of Experimental Clinical Medicine**, 6: 437–451

Rea, S., Eisenhaber, F., Carroll, Â.O., Strahl, B.D., Sun, Z., Schmid, M., Opravil, S., Mechtler, K., Ponting, C.P., Allis, C.D. and Jenuwein, T. (2000) Regulation of chromatin structure by site-specific histone H3 methyltransferases. **Nature**, 406: 593–599

Revenkova, E., Eijpe, M., Heyting, C., Gross, B. and Jessberger, R. (2001) Novel meiosis-specific isoform of mammalian SMC1. **Molecular and cellular biology**, 21 (20): 6984–6998

Reynolds, A., Qiao, H., Yang, Y., Chen, J.K., Jackson, N., Biswas, K., Holloway, J.K., Baudat, F., de Massy, B., Wang, J., Höög, C., Cohen, P.E. and Hunter, N. (2013) RNF212 is a dosage-sensitive regulator of crossing-over during mammalian meiosis. **Nature genetics**, 45 (3): 269–78

Roberts, N.Y. (2009) Investigating the control of homologous chromosome pairing and crossover formation in meiosis of *Arabidopsis thaliana*. **PhD Thesis, Univeristy of Birmingham**

Rogakou, E.P., Pilch, D.R., Orr, A.H., Ivanova, V.S. and Bonner, W.M. (1998) Double-stranded Brekas Induce Histone H2AX phosphorylation on Serine 139. **The Journal of Biological Chemistry**, 273 (10): 5858–5868

Rohs, R., West, S.M., Sosinsky, A., Liu, P., Mann, R.S. and Honig, B. (2009) The role of DNA shape in protein-DNA recognition. **Nature**, 461 (7268): 1248–1253

Roig, I., Dowdle, J. a., Toth, A., de Rooij, D.G., Jasin, M. and Keeney, S. (2010) Mouse TRIP13/PCH2 is required for recombination and normal higher-order chromosome structure during meiosis. **PLoS Genetics**, 6 (8)

Rosu, S., Libuda, D.E. and Villeneuve, A.M. (2011) Robust Crossover Assurance and Regulated Interhomolog Access Maintain Meiotic Crossover Number. **Science**, 334 (December): 1286–1290

de Ruijter, A.J.M., van Gennip, A.H., Caron, H.N., Kemp, S. and van Kuilenburg, A.B.P. (2003) Histone deacetylases (HDACs): characterization of the classical HDAC family. **The Biochemical journal**, 370 (Pt 3): 737–49

Sanchez-Moran, E., Santos, J.-L., Jones, G.H. and Franklin, F.C.H. (2007) ASY1 mediates AtDMC1-dependent interhomolog recombination during meiosis in *Arabidopsis*. **Genes & Development**, 21 (17): 2220–33

Sauvageau, S., Stasiak, A.Z., Banville, I., Ploquin, M., Stasiak, A. and Masson, J.-Y.

- (2005) Fission yeast rad51 and dmc1, two efficient DNA recombinases forming helical nucleoprotein filaments. **Molecular and cellular biology**, 25 (11): 4377–4387
- Schotta, G., Ebert, A., Krauss, V., Fischer, A., Hoffmann, J., Rea, S., Jenuwein, T., Dorn, R. and Reuter, G. (2002) Central role of Drosophila SU(VAR)3-9 in histone H3-K9 methylation and heterochromatic gene silencing. **EMBO Journal**, 21 (5): 1121–1131
- Schuettengruber, B., Chourrout, D., Vervoort, M., Leblanc, B. and Cavalli, G. (2007) Genome Regulation by Polycomb and Trithorax Proteins. **Cell**, 128 (4): 735–745
- Schwacha, A. and Kleckner, N. (1997) Interhomolog bias during meiotic recombination: Meiotic functions promote a highly differentiated interhomolog-only pathway. **Cell**, 90 (6): 1123–1135
- Seeliger, K., Dukowic-Schulze, S., Wurz-Wildersinn, R., Pacher, M. and Puchta, H. (2012) BRCA2 is a mediator of RAD51- and DMC1-facilitated homologous recombination in Arabidopsis thaliana. **The New phytologist**, 193 (2): 364–75
- Shen, Y., Conde E Silva, N., Audonnet, L., Servet, C., Wei, W. and Zhou, D.-X. (2014) Over-expression of histone H3K4 demethylase gene JMJ15 enhances salt tolerance in Arabidopsis. **Frontiers in plant science**, 5 (June): 290
- Shinohara, A., Ogawa, H. and Ogawa, T. (1992) Rad51 protein involved in repair and recombination in *S. cerevisiae* is a RecA-like protein. **Cell**, 69 (3): 457–470
- Shinohara, M., Oh, S.D., Hunter, N. and Shinohara, A. (2008) Crossover assurance and crossover interference are distinctly regulated by the ZMM proteins during yeast meiosis. **Nature genetics**, 40 (3): 299–309
- Siaud, N., Dray, E., Gy, I., Gérard, E., Takvorian, N. and Doutriaux, M.-P. (2004) Brca2 is involved in meiosis in Arabidopsis thaliana as suggested by its interaction with Dmc1. **The EMBO journal**, 23 (6): 1392–401
- Singh, R.P., Prasad, P.V.V. and Reddy, K.R. (2013) Impacts of Changing Climate and Climate Variability on Seed Production and Seed Industry. **Advances in Agronomy**, 118: 49–110
- Smagulova, F., Gregoret, I. V, Brick, K., Khil, P., Camerini-Otero, R.D. and Petukhova, G. V (2011) Genome-wide analysis reveals novel molecular features of mouse recombination hotspots. **Nature**, 472 (7343): 375–8
- Smith, A. V. and Roeder, G.S. (1997) The yeast Red1 protein localizes to the cores of meiotic chromosomes. **Journal of Cell Biology**, 136 (5): 957–967
- Smith, K.C. and Wang, T.-C. V (1989) recA-dependent DNA repair processes. **Bioessays**, 10 (1): 12–16
- Smith, K.C., Wang, T.-C. V and Sharma, R.C. (1987) recA-Dependent DNA repair in

UV-Irradiated Escherichia Coli. **Journal of Photochemistry and Photobiology**, 1: 1–11

Snowden, T., Acharya, S., Butz, C., Berardini, M. and Fishel, R. (2004) hMSH4-hMSH5 recognizes Holliday Junctions and forms a meiosis-specific sliding clamp that embraces homologous chromosomes. **Molecular cell**, 15 (3): 437–51

Sollier, J., Lin, W., Soustelle, C., Suhre, K., Nicolas, A., Géli, V. and de La Roche Saint-André, C. (2004) Set1 is required for meiotic S-phase onset, double-strand break formation and middle gene expression. **The EMBO journal**, 23 (9): 1957–67

Solomon, S., D., Qin, M., Manning, Z., Chen, M., Marquis, K.B., Averyt, M.T. and Miller HL (2007) **Climate Change 2007: The Physical science basis. Contribution of Working Group 1 to the Fourth Assessment Report of the Intergovernmental Panel on Climate Change**. New York

Sommermeier, V., Beneut, C., Chaplais, E., Serrentino, M.E. and Borde, V. (2013) Spp1, a Member of the Set1 Complex, Promotes Meiotic DSB Formation in Promoters by Tethering Histone H3K4 Methylation Sites to Chromosome Axes. **Molecular Cell**, 49 (1): 43–54

Stacey, N.J., Kuromori, T., Azumi, Y., Roberts, G., Breuer, C., Wada, T., Maxwell, A., Roberts, K. and Sugimoto-Shirasu, K. (2006) Arabidopsis SPO11-2 functions with SPO11-1 in meiotic recombination. **The Plant Journal**, 48 (2): 206–16

Stack, S.M. and Anderson, L.K. (1986) Two-dimensional spreads of synaptonemal complexes from solanaceous plants II. synopsis in *Lycopersicon esculentum* (tomato). **American Journal of Botany**, 73 (2): 264–281

Stahl, F.W., Foss, H.M., Young, L.S., Borts, R.H., Abdullah, M.F.F. and Copenhaver, G.P. (2004) Does crossover interference count in *Saccharomyces cerevisiae*? **Genetics**, 168 (1): 35–48

Stiff, T., O'Driscoll, M., Rief, N., Iwabuchi, K., Löbrich, M. and Jeggo, P. a. (2004) ATM and DNA-PK Function Redundantly to Phosphorylate H2AX after Exposure to Ionizing Radiation. **Cancer Research**, 64 (7): 2390–2396

Storlazzi, a, Xu, L., Schwacha, a and Kleckner, N. (1996) Synaptonemal complex (SC) component Zip1 plays a role in meiotic recombination independent of SC polymerization along the chromosomes. **Proceedings of the National Academy of Sciences of the United States of America**, 93 (17): 9043–9048

Storlazzi, A., Gargano, S., Ruprich-Robert, G., Falque, M., David, M., Kleckner, N. and Zickler, D. (2010) Recombination Proteins Mediate Meiotic Spatial Chromosome Organization and Pairing. **Cell**, 141 (1): 94–106

De Storme, N. and Geelen, D. (2014) The impact of environmental stress on male reproductive development in plants: biological processes and molecular mechanisms. **Plant, cell & environment**, 37 (1): 1–18

- Sun, X., Huang, L., Markowitz, T.E., Blitzblau, H.G., Chen, D., Klein, F. and Hochwagen, A. (2015) Transcription dynamically patterns the meiotic chromosome-axis interface. **eLife**, 4: 1–23
- Sun, Y., Ambrose, J.H., Haughey, B.S., Webster, T.D., Pierrie, S.N., Muñoz, D.F., Wellman, E.C., Cherian, S., Lewis, S.M., Berchowitz, L.E. and Copenhaver, G.P. (2012) Deep Genome-Wide Measurement of Meiotic Gene Conversion Using Tetrad Analysis in *Arabidopsis thaliana*. **PLoS Genetics**, 8 (10): e1002968
- Sy, S.M.H., Huen, M.S.Y. and Chen, J. (2009) MRG15 Is a Novel PALB2-interacting Factor Involved in Homologous Recombination. **The Journal of Biological Chemistry**, 284 (32): 21127–21131
- Sym, M., Engebrecht, J. a and Roeder, G.S. (1993) ZIP1 is a synaptonemal complex protein required for meiotic chromosome synapsis. **Cell**, 72 (3): 365–378
- Takasaki, T., Liu, Z., Habara, Y., Nishiwaki, K., Nakayama, J.-I., Inoue, K., Sakamoto, H. and Strome, S. (2007) MRG-1, an autosome-associated protein, silences X-linked genes and protects germline immortality in *Caenorhabditis elegans*. **Development**, 134 (4): 757–767
- Talbert, P.B., Ahmad, K., Almouzni, G., et al. (2012) A unified phylogeny-based nomenclature for histone variants. **Epigenetics & chromatin**, 5: 7
- Talbert, P.B. and Henikoff, S. (2010) Histone variants--ancient wrap artists of the epigenome. **Nature reviews Molecular cell biology**, 11 (4): 264–275
- Talbert, P.B. and Henikoff, S. (2014) Environmental responses mediated by histone variants. **Trends in Cell Biology**, 24 (11): 642–650
- Tamada, Y., Yun, J.-Y., Woo, S.C. and Amasino, R.M. (2009) ARABIDOPSIS TRITHORAX-RELATED7 is required for methylation of lysine 4 of histone H3 and for transcriptional activation of FLOWERING LOCUS C. **The Plant cell**, 21 (10): 3257–69
- Tang, J., Cho, N.W., Cui, G., Manion, E.M. and Shanbhag, N.M. (2013) Acetylation Limits 53BP1 Association with Damaged Chromatin to Promote Homologous Recombination. **Nature structural & molecular biology**, 20 (3): 317–325
- Tease, C. and Hultén, M.A. (2004) Inter-sex variation in synaptonemal complex lengths largely determine the different recombination rates in male and female germ cells. **Cytogenetic and Genome Research**, 107 (3-4): 208–215
- Terentyev, Y., Johnson, R., Neale, M.J., Khisroon, M., Bishop-Bailey, A. and Goldman, A.S.H. (2010) Evidence that MEK1 positively promotes interhomologue double-strand break repair. **Nucleic acids research**, 38 (13): 4349–60
- Tessarz, P. and Kouzarides, T. (2014) Histone core modifications regulating nucleosome structure and dynamics. **Nature Reviews Molecular Cell Biology**,

15 (11): 703–708

Thacker, D., Mohibullah, N., Zhu, X. and Keeney, S. (2014) Homologue engagement controls meiotic DNA break number and distribution. **Nature**, 510 (7504): 241–6

Tischfield, S.E. and Keeney, S. (2012) Scale Matters. **Cell Cycle**, 11 (8): 1496–1503

Tsabar, M., Eapen, V. V., Mason, J.M., Memisoglu, G., Waterman, D.P., Long, M.J., Bishop, D.K. and Haber, J.E. (2015a) Caffeine impairs resection during DNA break repair by reducing the levels of nucleases Sae2 and Dna2. **Nucleic Acids Research**, 43 (14): 6889–6901

Tsabar, M., Mason, J.M., Chan, Y.-L., Bishop, D.K. and Haber, J.E. (2015b) Caffeine inhibits gene conversion by displacing Rad51 from ssDNA. **Nucleic Acids Research**, 43 (14): 6902–6918

Tschiersch, B., Hofmann, a, Krauss, V., Dorn, R., Korge, G. and Reuter, G. (1994) The protein encoded by the *Drosophila* position-effect variegation suppressor gene *Su(var)3-9* combines domains of antagonistic regulators of homeotic gene complexes. **The EMBO journal**, 13 (16): 3822–3831

Tsubouchi, T., Zhao, H. and Roeder, G.S. (2006) The Meiosis-Specific Zip4 Protein Regulates Crossover Distribution by Promoting Synaptonemal Complex Formation Together with Zip2. **Developmental Cell**, 10 (6): 809–819

Uanschou, C., Siwiec, T., Pedrosa-Harand, A., Kerzendorfer, C., Sanchez-Moran, E., Novatchkova, M., Akimcheva, S., Woglar, A., Klein, F. and Schlögelhofer, P. (2007) A novel plant gene essential for meiosis is related to the human CtIP and the yeast COM1/SAE2 gene. **The EMBO journal**, 26 (24): 5061–5070

Uhlmann, F., Lottspeich, F. and Nasmyth, K. (1999) Sister-chromatid separation at anaphase onset is promoted by cleavage of the cohesin subunit Scc1. **Nature**, 400 (6739): 37–42

Vakoc, C.R., Mandat, S. a., Olenchock, B. a. and Blobel, G. a. (2005) Histone H3 lysine 9 methylation and HP1 are associated with transcription elongation through mammalian chromatin. **Molecular Cell**, 19 (3): 381–391

Verde, L.A. (2003) The effect of stress on meiotic recombination in maize (*Zea mays* L). **PhD Thesis, Iowa State University**

Vermeulen, M., Mulder, K.W., Denissov, S., Pijnappel, W.W.M.P., van Schaik, F.M. a, Varier, R. a., Baltissen, M.P. a, Stunnenberg, H.G., Mann, M. and Timmers, H.T.M. (2007) Selective Anchoring of TFIID to Nucleosomes by Trimethylation of Histone H3 Lysine 4. **Cell**, 131 (1): 58–69

Wang, M., Wang, K., Tang, D., Wei, C., Li, M., Shen, Y., Chi, Z., Gu, M. and Cheng, Z. (2010) The central element protein ZEP1 of the synaptonemal complex regulates the number of crossovers during meiosis in rice. **The Plant cell**, 22 (2): 417–430

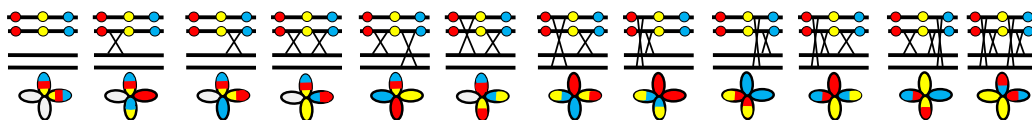
- Ward, I.M. and Chen, J. (2001) Histone H2AX Is Phosphorylated in an ATR-dependent Manner in Response to Replicational Stress. **Journal of Biological Chemistry**, 276 (51): 47759–47762
- Watanabe, Y. and Nurse, P. (1999) Cohesin Rec8 is required for reductional chromosome segregation at meiosis. **Nature**, 400 (6743): 461–464
- Wojtasz, L., Daniel, K., Roig, I., Bolcun-Filas, E., Xu, H., Boonsanay, V., Eckmann, C.R., Cooke, H.J., Jasin, M., Keeney, S., McKay, M.J. and Toth, A. (2009) Mouse **HORMAD1** and **HORMAD2**, two conserved meiotic chromosomal proteins, are depleted from synapsed chromosome axes with the help of **TRIP13** AAA-ATPase. **PLoS genetics**, 5 (10): e1000702
- Woodcock, C.L. and Ghosh, R.P. (2010) Chromatin higher-order structure and dynamics. **Cold Spring Harbor perspectives in biology**, 2 (5): a000596
- Wozniak, G.G. and Strahl, B.D. (2014) Hitting the “mark”: Interpreting lysine methylation in the context of active transcription. **Biochimica et biophysica acta**, pp. 2–10
- Xu, J., Sun, X., Jing, Y., Wang, M., Liu, K., Jian, Y., Yang, M., Cheng, Z. and Yang, C. (2012a) **MRG-1** is required for genomic integrity in *Caenorhabditis elegans* germ cells. **Cell Research**, 22 (5): 886–902
- Xu, Y., Ayrapetov, M.K., Xu, C., Gursoy-Yuzugullu, O., Hu, Y. and Price, B.D. (2012b) Histone H2A.Z Controls a Critical Chromatin Remodeling Step Required for DNA Double-Strand Break Repair. **Molecular Cell**, 48 (5): 723–733
- Xu, Y., Gan, E.-S., Zhou, J., Wee, W.-Y., Zhang, X. and Ito, T. (2014) Arabidopsis **MRG** Domain Proteins Bridge Two Histone Modifications to Elevate Expression of Flowering Genes. **Nucleic Acids Research**, 42 (17): 10960–10974
- Yamada, S., Ohta, K. and Yamada, T. (2013) Acetylated Histone H3K9 is associated with meiotic recombination hotspots, and plays a role in recombination redundantly with other factors including the H3K4 methylase **Set1** in fission yeast. **Nucleic Acids Research**, 41 (6): 3504–3517
- Yang, S., Yuan, Y., Wang, L., Li, J., Wang, W., Liu, H., Chen, J. -q., Hurst, L.D. and Tian, D. (2012) Great majority of recombination events in Arabidopsis are gene conversion events. **Proceedings of the National Academy of Sciences**, 109 (51): 20992–20997
- Yao, X., Feng, H., Yu, Y., Dong, A. and Shen, W.H. (2013) **SDG2**-Mediated H3K4 Methylation Is Required for Proper Arabidopsis Root Growth and Development. **PLoS ONE**, 8 (2): e56537
- Yelina, N., Diaz, P., Lambing, C. and Henderson, I.R. (2015) Epigenetic control of meiotic recombination in plants. **Science China Life Sciences**, 58 (3): 223–231

- Yelina, N.E., Choi, K., Chelysheva, L., Macaulay, M., de Snoo, B., Wijnker, E., Miller, N., Drouaud, J., Grelon, M., Copenhaver, G.P., Mezard, C., Kelly, K. a. and Henderson, I.R. (2012) Epigenetic Remodeling of Meiotic Crossover Frequency in *Arabidopsis thaliana* DNA Methyltransferase Mutants. **PLoS Genetics**, 8 (8): e1002844
- Yin, H., Zhang, X., Liu, J., Wang, Y., He, J., Yang, T., Hong, X., Yang, Q. and Gong, Z. (2009) Epigenetic regulation, somatic homologous recombination, and abscisic acid signaling are influenced by DNA polymerase epsilon mutation in *Arabidopsis*. **The Plant Cell**, 21 (2): 386–402
- Youds, J.L., Mets, D.G., McIlwraith, M.J., Martin, J.S., Ward, J.D., O'Neil, N.J., Rose, A.M., West, S.C., Meyer, B.J. and Boulton, S.J. (2010) RTEL-1 Enforces Meiotic Crossover Interference and Homeostasis. **Science**, 237: 1254–1258
- Yu, Y., Bu, Z., Shen, W.H. and Dong, A. (2009) An update on histone lysine methylation in plants. **Progress in Natural Science**, 19 (4): 407–413
- Yun, J.Y., Tamada, Y., Kang, Y.E. and Amasino, R.M. (2012) *Arabidopsis* trithorax-related3/set domain group2 is required for the winter-annual habit of *arabidopsis thaliana*. **Plant and Cell Physiology**, 53 (5): 834–846
- Zakharyevich, K., Tang, S., Ma, Y. and Hunter, N. (2012) Delineation of joint molecule resolution pathways in meiosis identifies a crossover-specific resolvase. **Cell**, 149 (2): 334–347
- Zamariola, L., Tiang, C.L., De Storme, N., Pawlowski, W. and Geelen, D. (2014) Chromosome segregation in plant meiosis. **Frontiers in plant science**, 5 (June): 279
- Zamudio, N., Barau, J., Teissandier, A., Walter, M., Borsos, M., Servant, N. and Bourc, D. (2015) DNA methylation restrains transposons from adopting a chromatin signature permissive for meiotic recombination. **Genes and Development**, pp. 1256–1270
- Zanders, S. and Alani, E. (2009) The pch2 mutation in baker's yeast alters meiotic crossover levels and confers a defect in crossover interference. **PLoS Genetics**, 5 (7): e1000571
- Zanders, S., Brown, M.S., Chen, C. and Alani, E. (2011) Pch2 modulates chromatid partner choice during meiotic double-strand break repair in *Saccharomyces cerevisiae*. **Genetics**, 188 (3): 511–521
- Zhang, L., Liang, Z., Hutchinson, J. and Kleckner, N. (2014a) Crossover Patterning by the Beam-Film Model: Analysis and Implications. **PLoS Genetics**, 10 (1)
- Zhang, L., Wang, S., Yin, S., Hong, S., Kim, K.P. and Kleckner, N. (2014b) Topoisomerase II mediates meiotic crossover interference. **Nature**, 511 (7511): 551–556

- Zhang, P., Zhao, J., Wang, B., Du, J., Lu, Y., Chen, J. and Ding, J. (2006) The MRG domain of human MRG15 uses a shallow hydrophobic pocket to interact with the N-terminal region of PAM14. **Protein science**, 15 (10): 2423–2434
- Zhang, X., Bernatavichute, Y. V, Cokus, S., Pellegrini, M. and Jacobsen, S.E. (2009) Genome-wide analysis of mono-, di- and trimethylation of histone H3 lysine 4 in *Arabidopsis thaliana*. **Genome biology**, 10 (6): R62
- Zheng, T., Nibau, C., Phillips, D.W., Jenkins, G., Armstrong, S.J. and Doonan, J.H. (2014) CDKG1 protein kinase is essential for synapsis and male meiosis at high ambient temperature in *Arabidopsis thaliana*. **Proceedings of the National Academy of Sciences of the United States of America**, 111 (6): 2182–7
- Zhu, X. and Keeney, S. (2015) High-resolution global analysis of the influences of Bas1 and Ino4 transcription factors on meiotic DNA break distributions in. **Genetics**, 1 (212): 1–30
- Zhu, Z., Chung, W.H., Shim, E.Y., Lee, S.E. and Ira, G. (2008) Sgs1 Helicase and Two Nucleases Dna2 and Exo1 Resect DNA Double-Strand Break Ends. **Cell**, 134 (6): 981–994
- Zickler, D. and Kleckner, N. (1999) Meiotic chromosomes: integrating structure and function. **Annual review of genetics**, 33: 603–754
- Zickler, D., Moreau, P.J.F., Huynh, a. D. and Slezec, a. M. (1992) Correlation between pairing initiation sites, recombination nodules and meiotic recombination in *Sordaria macrospora*. **Genetics**, 132 (1): 135–148
- Zilberman, D., Coleman-Derr, D., Ballinger, T. and Henikoff, S. (2008) Histone H2A.Z and DNA methylation are mutually antagonistic chromatin marks. **Nature**, 456 (7218): 125–129

Appendix

Appendix A – FTL analysis raw data



I2fg	Total	A	B	C	D	E	F	G	H	I	J	K	L
Col	2526	1970	251	300	1	0	2	1	1	0	0	0	0
<i>sdg2</i>	1464	1170	102	188	1	1	1	1	0	0	0	0	0

I5ab	Total	A	B	C	D	E	F	G	H	I	J	K	L
Col	2607	737	1070	614	36	41	38	35	21	9	4	2	0
<i>sdg2</i>	2262	445	962	532	68	80	64	60	30	13	7	1	0

I5cd	Total	A	B	C	D	E	F	G	H	I	J	K	L
Col	3146	2343	399	371	3	7	12	7	3	1	0	0	0
<i>sdg2</i>	1719	1027	336	329	10	5	5	5	2	0	0	0	0

I2fg	Total	A	B	C	D	E	F	G	H	I	J	K	L
Col	2526	1970	251	300	1	0	2	1	0	1	0	0	0
<i>pch2</i>	2849	2029	378	411	7	5	7	4	4	4	0	0	0

I5ab	Total	A	B	C	D	E	F	G	H	I	J	K	L
Col	2324	590	945	590	41	50	30	42	21	5	8	1	1
<i>pch2</i>	2321	1094	371	595	48	52	59	44	13	33	7	5	0

I5cd	Total	A	B	C	D	E	F	G	H	I	J	K	L
Col	3060	2386	343	305	7	5	6	6	1	1	0	0	0
<i>pch2</i>	2080	1586	252	219	5	6	4	4	2	2	0	0	0

Appendix B – ASY1 intensity analysis in Col o and *Atpch2-1* PMCs

Col 0 unsynapsed (blue) vs synapsed (orange) ASY1 intensity

Source	RoiID	ROIArea	MeasuredArea	Perimeter	MeanIntensity	MinIntensity	MaxIntensity
slide 2 3_crop roi.nd2	1	0.24	698.22	3.07	582.51	392	911
slide 2 3_crop roi.nd2	3	0.35	698.22	3.61	280.69	213	352
slide 2 3_crop roi.nd2	4	0.45	698.22	3.61	247.97	201	328
10_crop roi.nd2	3	0.46	5452.92	4.47	418.54	272	573
7_crop roi.nd2	1	0.32	1358.79	4.48	1070.84	573	1716
slide 2 3_crop roi.nd2	2	0.38	698.22	4.5	593.65	296	801
10_crop roi.nd2	7	0.52	5452.92	4.55	224.67	158	372
10_crop roi.nd2	9	0.4	5452.92	4.81	1208.53	759	1689
8_crop roi.nd2	5	0.56	744.37	4.92	426.06	371	503
10_crop roi.nd2	1	0.4	5452.92	4.96	830.54	360	1256
7_crop roi.nd2	3	0.57	1358.79	5	426.68	316	616
10_crop roi.nd2	8	0.51	5452.92	5.03	233.07	165	368
8_crop roi.nd2	6	0.77	744.37	6.35	516.59	390	662
7_crop roi.nd2	4	0.71	1358.79	5.25	396.39	278	564
10_crop roi.nd2	2	0.47	5452.92	5.79	902.1	413	1607
7_crop roi.nd2	2	0.38	1358.79	5.89	1199.68	766	1683
10_crop roi.nd2	4	0.48	5452.92	5.9	318.09	212	477
10_crop roi.nd2	6	0.59	5452.92	6.13	619.59	318	1068
8_crop roi.nd2	2	0.48	744.37	6.48	1572.28	1104	2144
8_crop roi.nd2	1	0.84	744.37	7.75	761.16	463	1215
10_crop roi.nd2	11	1.14	5452.92	8.55	217.96	141	350
10_crop roi.nd2	5	0.98	5452.92	9.3	553.36	277	912
10_crop roi.nd2	12	2.19	5452.92	10.52	209.19	132	326
10_crop roi.nd2	10	0.96	5452.92	11.67	856.65	362	1414
slide 3 8_crop roi.nd2	1	1	1516.08	12.01	648.56	329	1080
slide 3 8_crop roi.nd2	2	1.72	1516.08	12.22	155.84	114	225
slide 4 13a_crop	2	0.37	781.5	3.9	543.85	398	681
slide 4 14_crop	2	0.31	1756.41	3.94	437.82	336	584
slide 4 19_crop	2	0.39	1580.05	4.26	588.33	478	734
slide 4 12_crop	1	0.37	898.56	4.69	1993.49	1355	2909
slide 4 17_crop	2	0.54	2388.22	4.76	403.93	315	561
slide 4 18_crop	2	0.36	1082.33	4.92	346.31	244	417
slide 4 13a_crop	1	0.4	781.5	4.93	1016.34	559	1371
slide 4 13b_crop	2	0.61	696.8	5.23	374.31	256	522
slide 4 19_crop	1	0.49	1580.05	5.57	1414.14	826	2206
slide 4 12_crop	2	0.82	898.56	5.62	492.83	385	677
slide 4 16_crop	2	0.66	1589.8	5.7	305.95	202	436
slide 4 15_crop	2	0.54	1872.5	5.78	371.73	262	507
slide 4 13b_crop	1	0.5	696.8	5.81	1490.56	786	2485
slide 4 14_crop	1	0.49	1756.41	5.83	1176.63	792	1541
slide 4 11_crop	2	0.69	643.41	5.92	257.56	213	324
slide 4 18_crop	1	0.54	1082.33	6.72	2045.42	1493	2765
slide 4 17_crop	1	0.79	2388.22	8.18	1079.87	585	1598
slide 4 16_crop	1	0.58	1589.8	8.22	1581.99	933	2296
slide 4 11_crop	1	0.77	643.41	8.82	543.05	366	889
slide 4 15_crop	1	0.93	1872.5	10.4	1086.09	480	2053

Atpch2-1 synapsed (blue) vs unsynapsed (orange) ASY1 intensity

Source	RoIID	ROIArea	MeasuredArea	Perimeter	MeanIntensity	MinIntensity	MaxIntensity
9_crop roi.nd2	4	0.2	1007.95	2.25	388.45	274	507
8_crop roi.nd2	4	0.18	563.29	3	433.39	359	500
11_crop roi.nd2	4	0.32	1532.5	3.45	235.45	172	305
23_crop roi.nd2	2	0.28	854.18	3.89	435.34	309	715
11_crop roi.nd2	3	0.35	1532.5	3.9	318.64	233	417
8_crop roi.nd2	2	0.31	563.29	4.63	378	282	564
14_crop roi.nd2	4	0.33	1029.75	4.65	321.47	173	537
29_crop roi.nd2	2	0.45	801.68	4.78	373.95	250	486
27_crop roi.nd2	1	0.48	606	5.4	296.36	242	397
27_crop roi.nd2	2	0.52	606	5.54	282.6	226	358
8_crop roi.nd2	3	0.46	563.29	5.56	284.93	199	401
8_crop roi.nd2	1	0.41	563.29	5.79	337.73	207	533
15_crop roi.nd2	1	0.57	1529.35	5.8	245.76	144	416
15_crop roi.nd2	3	0.47	1529.35	5.8	286.54	157	476
16_crop roi.nd2	3	0.59	2790.27	5.83	239.01	165	330
11_crop roi.nd2	1	0.52	1532.5	6.01	287.19	164	424
30_crop roi.nd2	2	0.68	1530.2	6.02	291.97	193	504
11_crop roi.nd2	2	0.52	1532.5	6.06	286.94	179	456
14_crop roi.nd2	2	0.47	1029.75	6.47	283.24	152	589
14_crop roi.nd2	1	0.48	1029.75	6.64	274.42	194	374
16_crop roi.nd2	2	0.65	2790.27	6.67	190.85	127	272
15_crop roi.nd2	4	0.51	1529.35	6.67	290.19	163	476
14_crop roi.nd2	3	0.48	1029.75	6.98	239.51	152	467
9_crop roi.nd2	3	0.61	1007.95	6.98	351.67	190	541
16_crop roi.nd2	4	0.62	2790.27	7.09	217.84	156	315
30_crop roi.nd2	1	0.78	1530.2	7.1	262.79	169	400
16_crop roi.nd2	1	0.75	2790.27	7.23	155.05	114	246
28_crop roi.nd2	1	0.53	783.99	7.35	349.97	211	498
9_crop roi.nd2	2	0.59	1007.95	7.35	224.99	130	411
22_crop roi.nd2	1	0.71	1637.37	7.93	296.39	169	501
29_crop roi.nd2	1	0.74	801.68	8.21	277.13	160	552
23_crop roi.nd2	1	0.62	854.18	8.22	320.07	213	521
28_crop roi.nd2	2	0.79	783.99	8.33	266.96	171	521
20_crop roi.nd2	2	0.81	1340.85	8.53	348.71	227	517
9_crop roi.nd2	1	0.72	1007.95	9.34	292.31	154	506
32_crop roi.nd2	1	1.09	2065.5	10.09	163.66	112	254
15_crop roi.nd2	2	0.85	1529.35	10.61	333.64	200	538
25_crop roi.nd2	1	1.08	1688.98	11.18	198.68	123	391
18_crop roi.nd2	2	1.08	2357.81	11.21	198.92	128	413
22_crop roi.nd2	2	0.9	1637.37	11.36	268	130	443
25_crop roi.nd2	2	1.18	1688.98	12.09	198.45	132	320
32_crop roi.nd2	2	1.66	2065.5	12.57	154.43	114	236
20_crop roi.nd2	1	1.11	1340.85	15.82	272.55	189	418
18_crop roi.nd2	1	2.4	2357.81	25.85	196.34	107	496

Control InSpeck microsphere intensity

Col 0 slides

Source	RoilD	ROIArea	MeasuredArea	Perimeter	MeanIntensity	MinIntensity	MaxIntensity
3.nd2	1	20.34	252.61	15.96	707.89	527	1344
12.nd2	1	20.31	380.63	15.96	848.42	650	1225
12.nd2	2	20.14	380.63	15.96	841.69	623	1139
6.nd2	1	21.74	1904.27	16.45	690.78	519	1425
11.nd2	1	23.05	5452.92	17.14	611.37	463	1098
6.nd2	2	22.99	1904.27	17.14	695.2	514	1245
5.nd2	1	23.35	429.52	17.14	686.33	521	1074
5.nd2	2	23.35	429.52	17.14	677.52	512	1092
11.nd2	2	24.2	5452.92	17.55	615.09	484	1012
4.nd2	1	27.51	650.14	18.46	641.37	445	1135
4.nd2	2	27.51	650.14	18.46	654.87	448	1249

Atpch2-1 slides

Source	RoilD	ROIArea	MeasuredArea	Perimeter	MeanIntensity	MinIntensity	MaxIntensity
4.nd2	2	23.93	5452.92	17.28	563.81	417	911
6.nd2	1	24.18	5452.92	17.48	718.29	552	1341
6.nd2	2	24.18	5452.92	17.48	727.19	558	1450
6.nd2	1	24.18	5452.92	17.48	718.29	552	1341
6.nd2	2	24.18	5452.92	17.48	727.19	558	1450
6.nd2	3	24.18	5452.92	17.48	773.55	588	1338
6.nd2	4	24.18	5452.92	17.48	697.85	536	1193
6.nd2	5	24.18	5452.92	17.48	771.89	573	1421
6.nd2	6	24.18	5452.92	17.48	710.84	539	1454
1.nd2	1	26.01	278.87	18.12	585.2	400	1115
2.nd2	1	29.72	241.03	19.3	600.47	411	1149

Col 0 ASY1 intensity summary

Unsynapsed mean	1079.44
Synapsed mean	356.28

	Mean ASY1 intensity- bead corrected					
	Unsynapsed axial elements	Synapsed lateral elements	Samples (total)	Number of cells	Bead mean intensity	Number of beads
Col	1079.44	356.28	23	17	697.32	11

Col 0 synapsed vs unsynapsed ASY1 intensity, two-tailed paired T-test $P < 0.00001$

Atpch2-1 ASY1 intensity summary

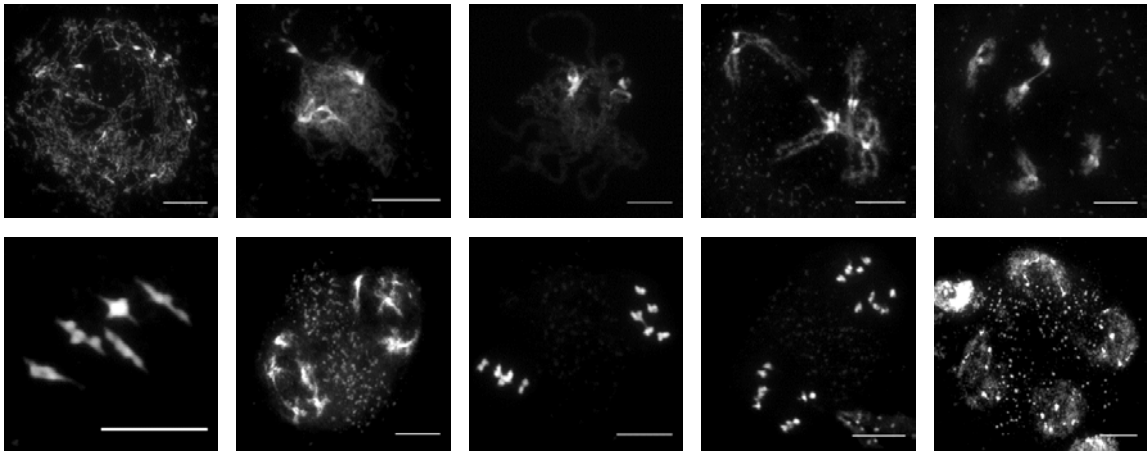
Unsynapsed mean	269.28
Synapsed mean	292.11

	Mean ASY1 intensity - bead corrected					
	Unsynapsed axial elements	Synapsed lateral elements	Samples (total)	Number of cells	Bead mean intensity	Number of beads
pch2-1	269.28	292.11	22	16	690.42	11

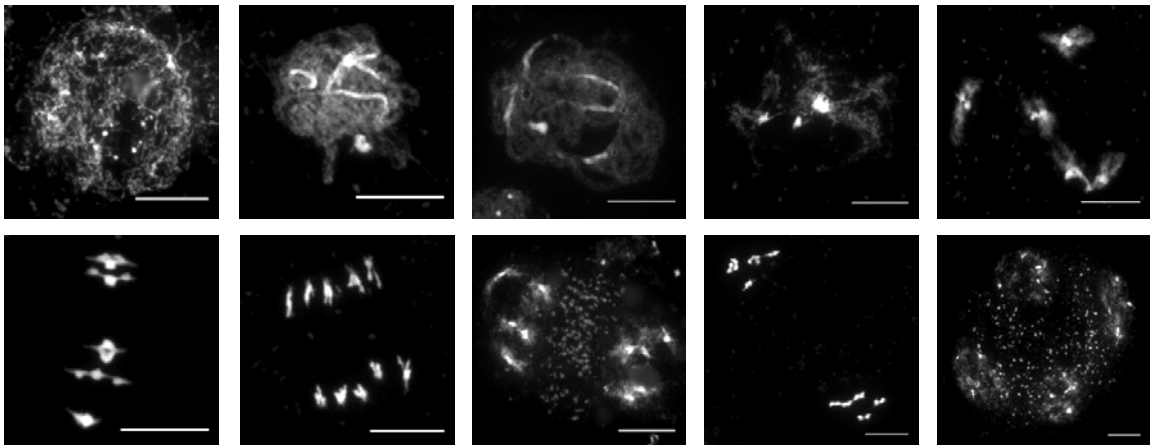
Atpch2-1 synapsed vs unsynapsed ASY1 intensity, two-tailed paired T-test $P = 0.251$

Appendix C – Cytological atlases of meiosis following temperature treatments

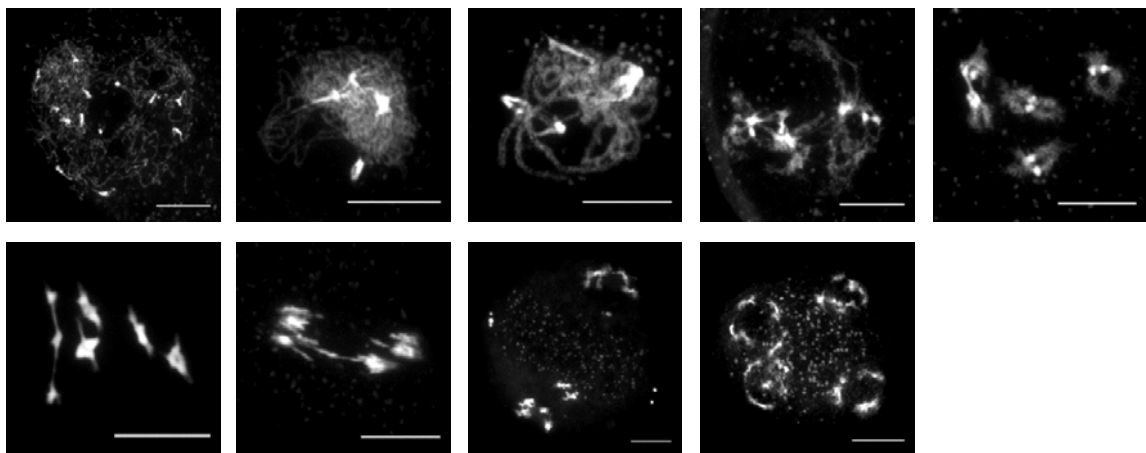
Col 14°C



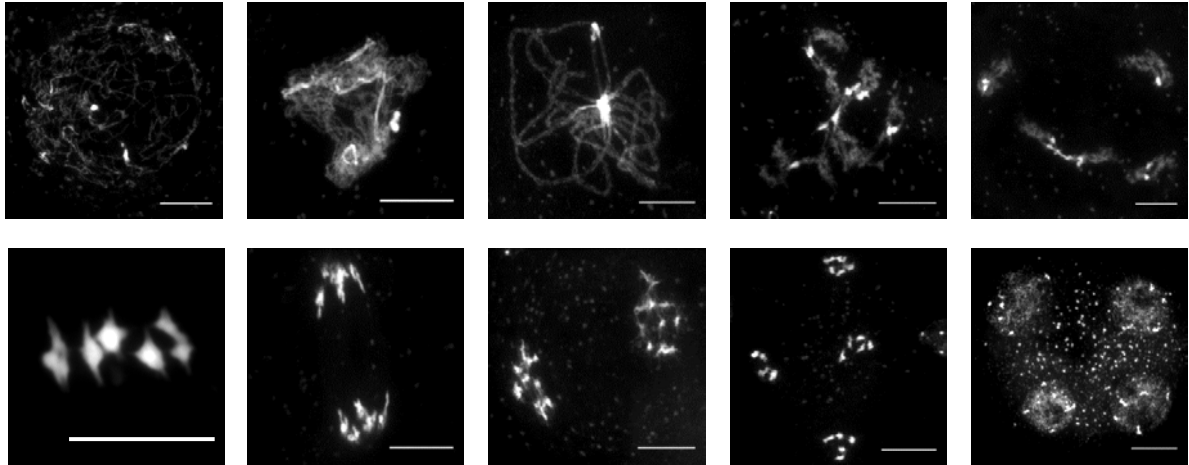
Col 20°C



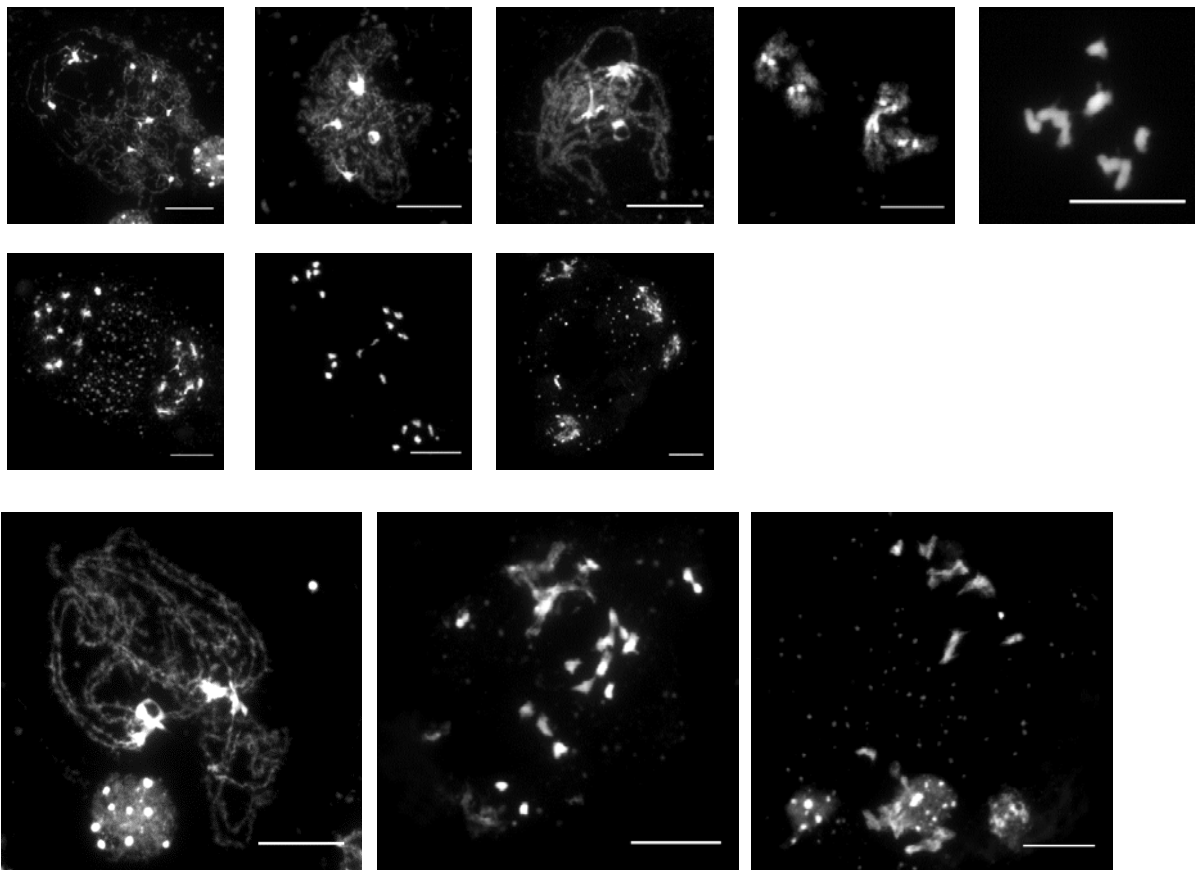
Col 28°C



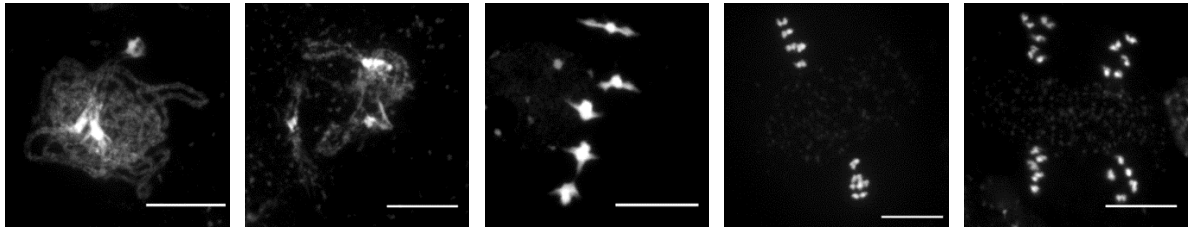
Col 30°C



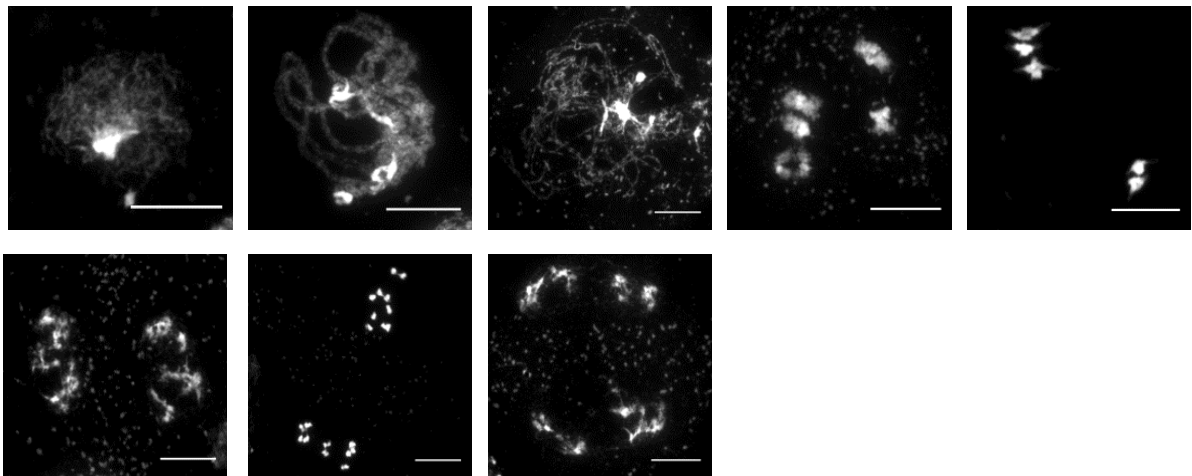
Col 32°C



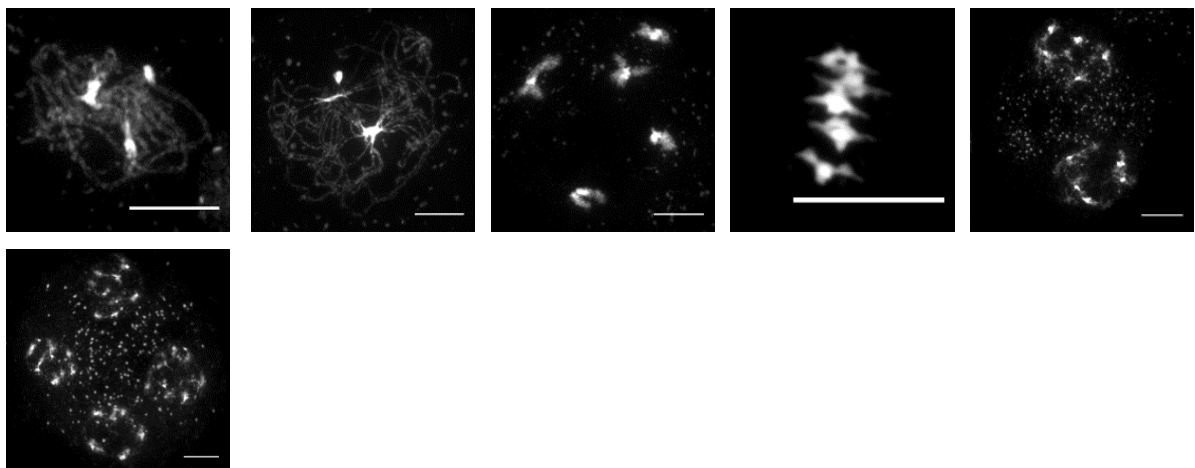
sdg2 14°C



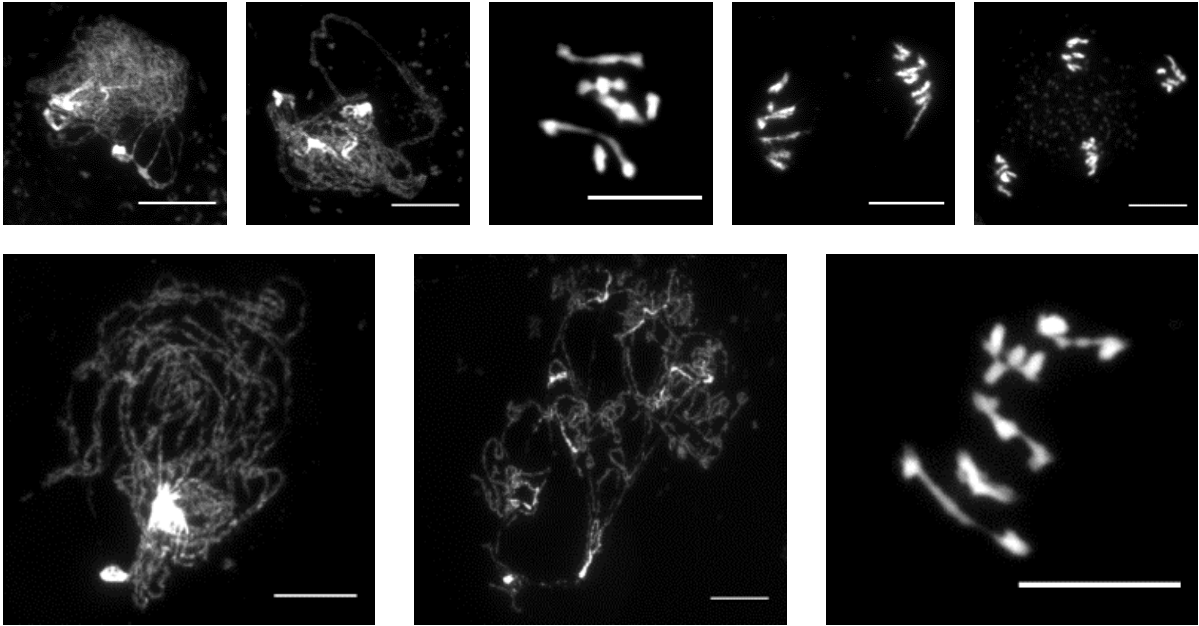
sdg2 20°C



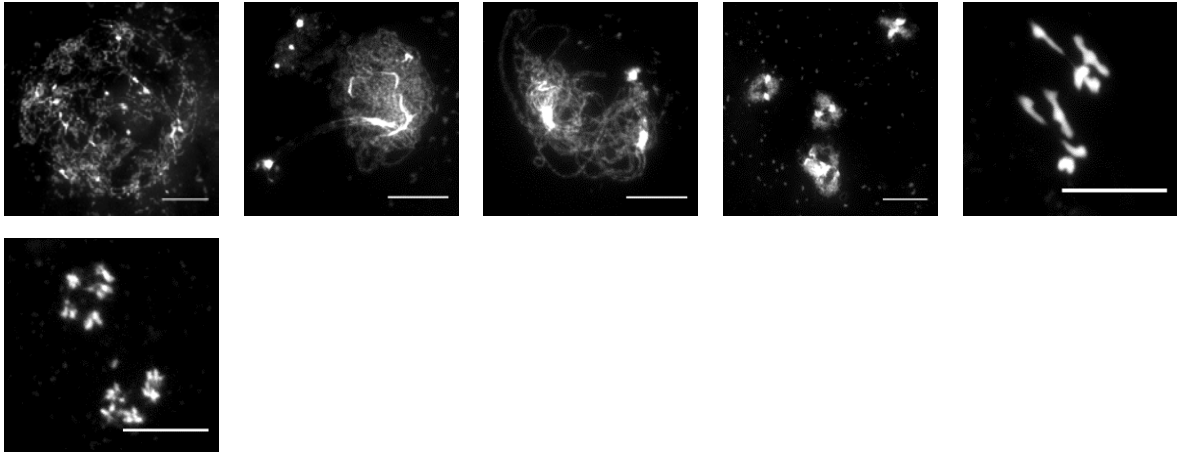
sdg2 28°C



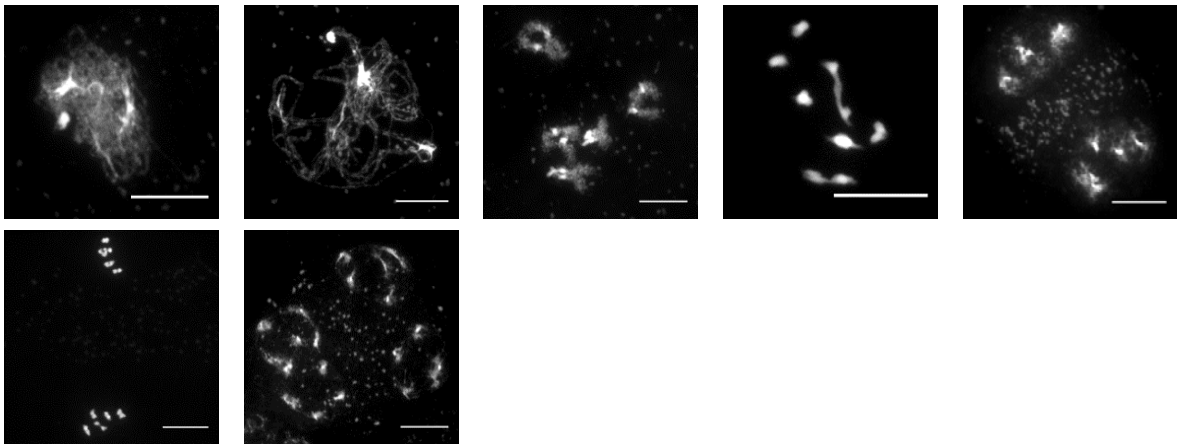
sdg2 32°C



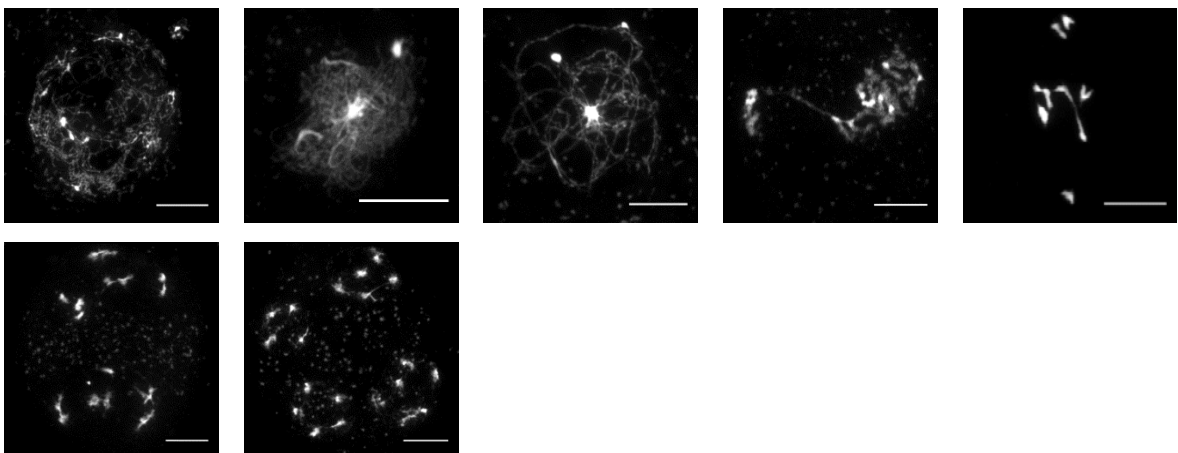
pch2 14°C



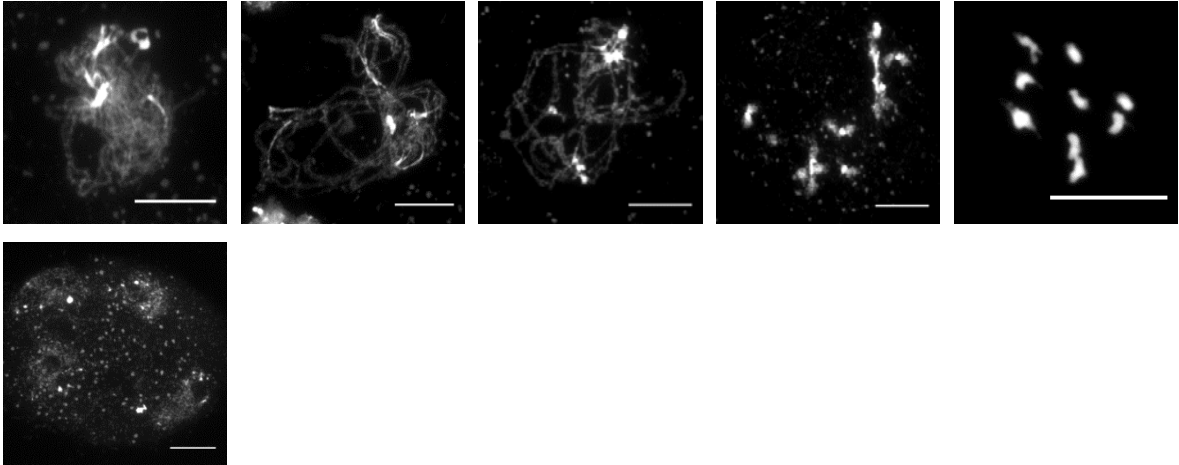
pch2 20°C



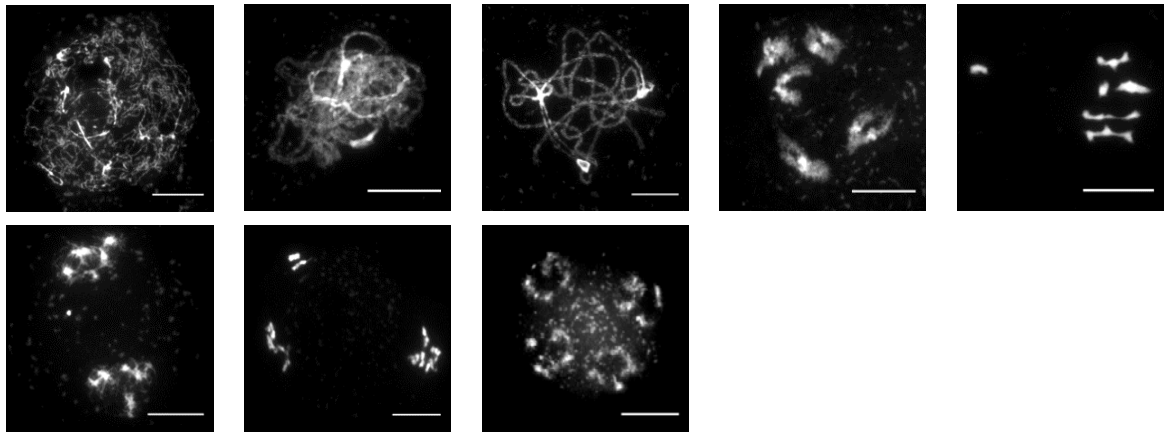
pch2 28°C



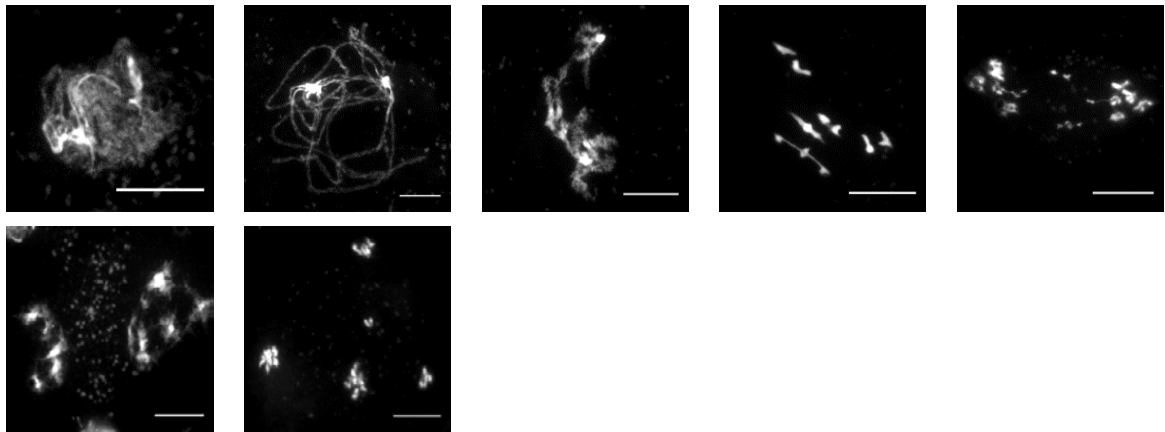
pch2 32°C



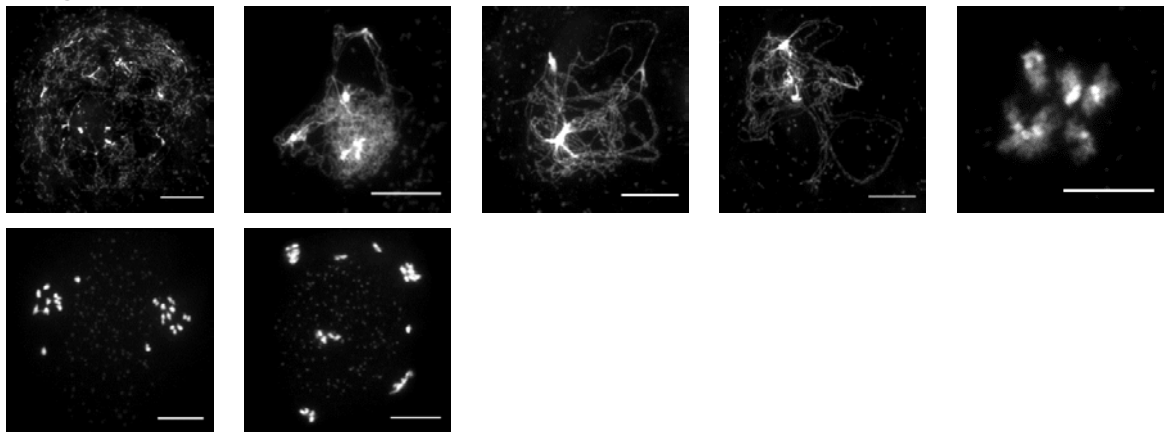
cdkg 14°C



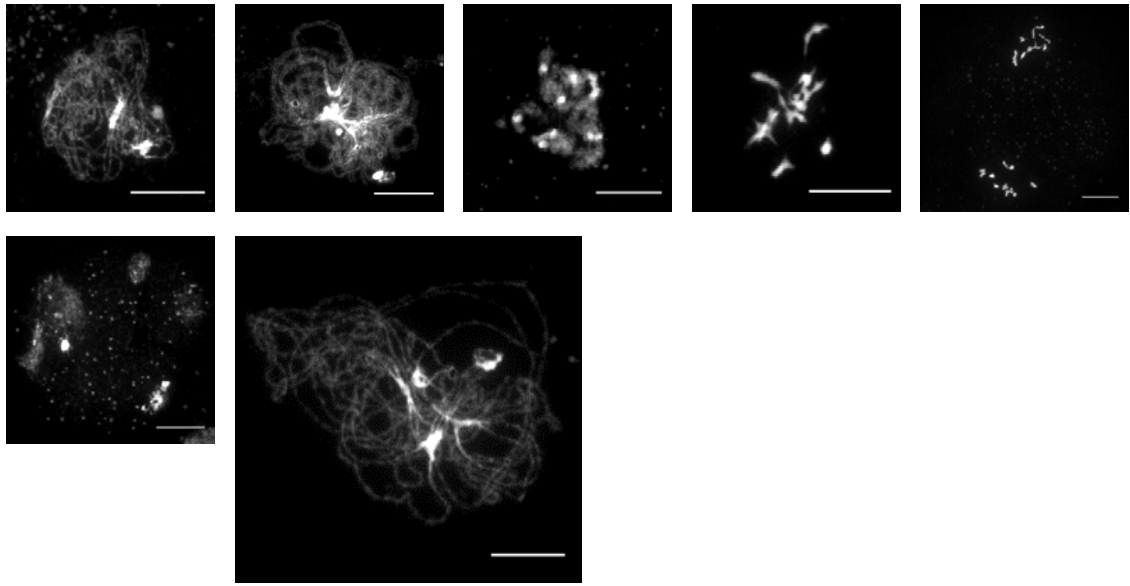
cdkg 20°C



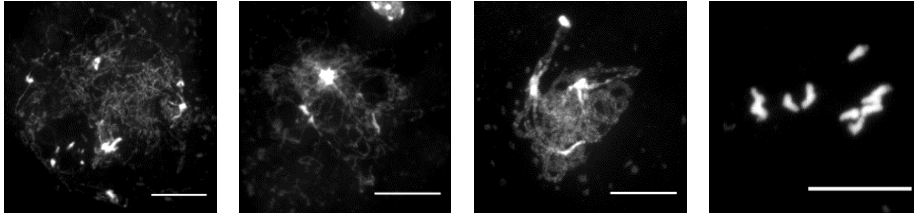
cdkg 28°C



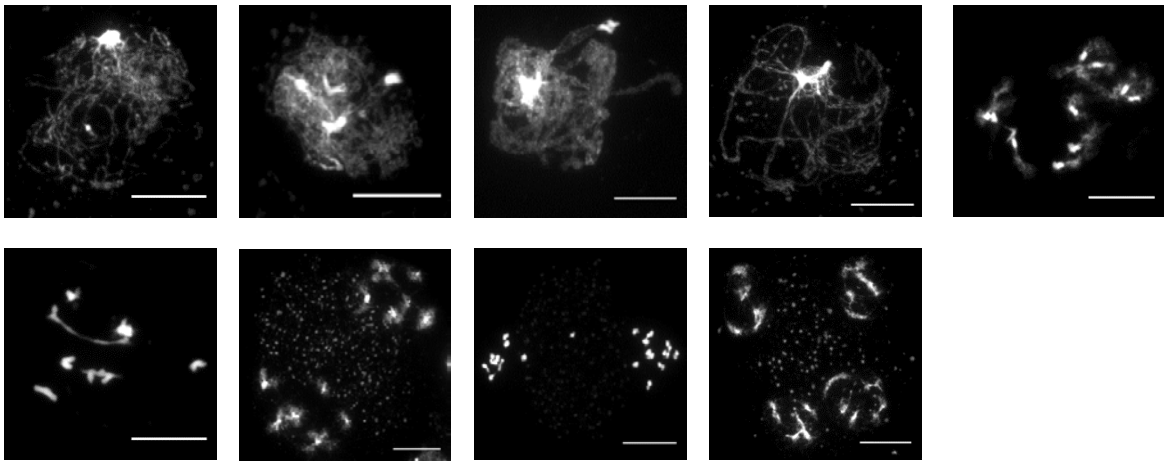
cdkg 32°C



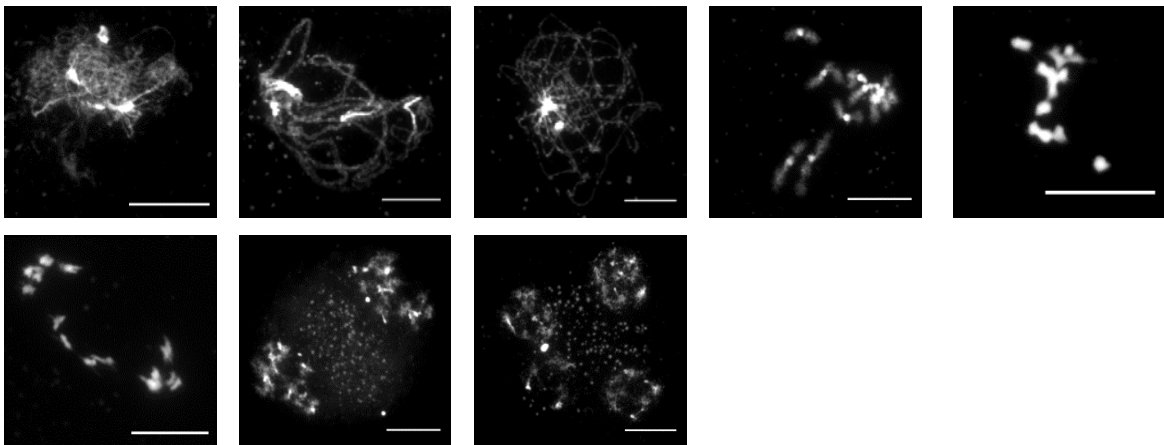
rbr2 14°C



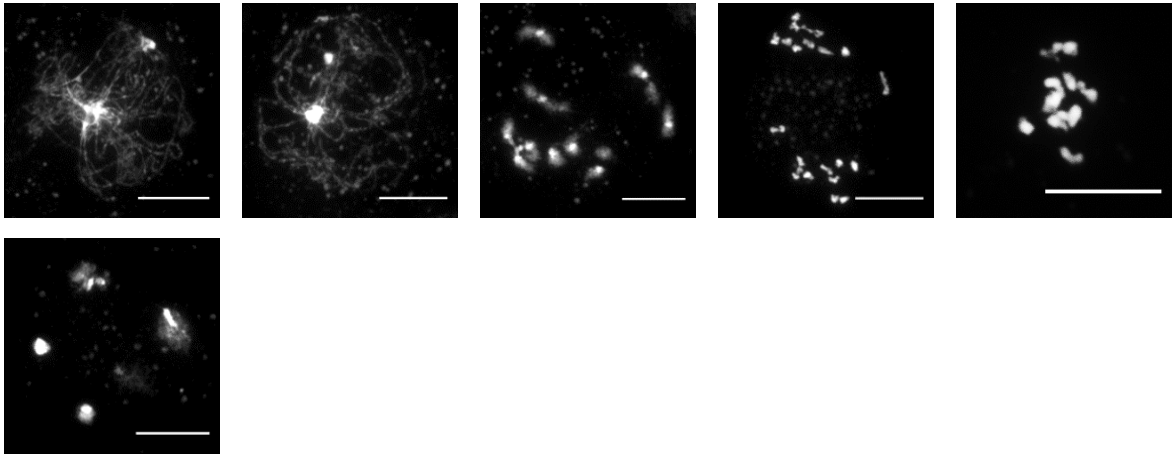
rbr2 20°C



rbr2 28°C



rbr2 32°C



Appendix D - Primer list

Primer name	Sequence 5' → 3'	T _m (°C)
SALK_035089 GT_a	TCACAACAAATATATTCATGCGAC	55.9
SALK_035089 GT_b	AAATGATTTCTTTTGGCAGGG	54.0
LBb1.3	ATTTTGCCGATTTTCGGAAC	52.4
SAIL_317_F11 LP	CTTCTTCAAGATGCCATCCAC	57.9
SAIL_317_F11 RP	AAATGATTTCTTTTGGCAGGG	54.0
SAIL LB2	GCTTCCTATTATATCTTCCCAAATTACC	60.7
RAD51-3 LP	CTTCAGGATGGTGTCTCAGAGC	62.1
RAD51-3 RP	TTGAAGGTGTTGCTTATACTCCG	58.9
SDG2-1 GEN (FW)	GGAGAACGGTGAAATCTCTCC	59.8
SDG2-1 T-DNA (RV)	TCCGTACCAGTCTGACAATCC	59.8
WISC LB	AACGTCCGCAATGTGTTATTAAGTTGTC	62.2
PRD3 GEN FW	GTGAGCAAAGGTATGGAGTTATGG	61.0
PRD3 GEN RV	CTTCTTGTGGTGATCTTCTCTCC	61.0
PRD3 FW2 RTPCR	CTTCACTTCAGCAGCTGAGAAAGG	62.7
PRD3 RV2 RTPCR	CTGAGGCGTCATTTGGATTTCTCG	62.7
GAPD FW	CTTGAAGGGTGGTGCCAAGAAGG	64.2
GAPD RV	CCTGTTGTCGCAACGAAGTCAG	64.2
MRG2 trnc1Fw	GATGATTTTCATCGGAGACACACG	60.6
MRG2 trnc1Rv	CCAAGCCATAGCACTCTTAATCC	60.6
MRG2 postT-DNA fw	GCCCTAATGTTGCTAGAGGAAG	60.3
MRG2 postT-DNA rv	CTTCCTCTAGCAACATTAGGGC	58.4

Appendix E - FTL interval locations

Interval	T-DNA 1 position	T-DNA 2 position	Size (Mb)
I2f	18,286,716 dsRed2	18,957,093 YFP	0.67
I2g	18,957,093 YFP	19,373,634 CFP	0.41
I5a	18,164,269 dsRed2	23,080,567 YFP	4.91
I5b	23,080,567 YFP	25,731,311 CFP	2.65
I5c	2,372,623 CFP	3,760,675 YFP	1.39
I5d	3,760,675 YFP	5,497,513 dsRed2	1.74

List of publications and presentations

Presentations

March 2013: **British Meiosis Meeting** – Cambridge, UK. **Poster presentation** - The meiotic role of MRG2 during homologous recombination in *Arabidopsis thaliana*

April 2013 – **Biosciences Graduate School Research Symposium** – Birmingham, UK. **Poster presentation** - The meiotic role of MRG2 during homologous recombination in *Arabidopsis thaliana*.

March 2014: **British Meiosis Meeting** – Edinburgh, UK. **Poster presentation** – The influence of histone H3 methylation during homologous recombination in *Arabidopsis thaliana*.

July 2014: **Plant Genome Stability and Change Conference** – Pacific Grove, California, USA. **Talk** – The meiotic role of the histone methyltransferase SDG2 in *Arabidopsis*.

March 2015: **SET for Britain poster competition** – House of Commons, London, UK. **Poster presentation** – Reorganising genetic recombination in crops.

April 2015 – **Biosciences Graduate School Research Symposium** – Birmingham, UK. **Talk**- The effects of meiotic chromosome structure on homologous recombination.

Publications

Maheshwari S, Tan EH, **West A**, Franklin FC, Comai L and Chan SW. (2015). Naturally occurring differences in CENH3 affect chromosome segregation in zygotic mitosis of hybrids. **PLoS Genetics**

This publication was produced in collaboration with researchers at UC Davis. I met the lead author of the study at the Plant Genome Stability and Change conference in 2014, who wanted cytological techniques, such as the ones I presented in my talk on SDG2, applied to their study of CENH3 mutants.

Lambing C, Osman K, Nuntasontorn K, **West A**, Higgins JD, Copenhaver GP, Yang J, Armstrong SJ, Mechtler K, Roitinger E and Franklin FCH. (2015) *Arabidopsis* PCH2 mediates meiotic chromosome remodeling and maturation of crossovers. **PLoS Genetics**

West A, Cassey P and Thomas C. (2015) Microbiology of Nests and Eggs. In: Deeming CD and Reynolds JS. *Nests, Eggs and Incubation: New ideas about avian reproduction*. Oxford, OUP. Chapter 7.

I was approached to write this book chapter based on my previous research in this area, performed during an undergraduate summer project.

RESEARCH ARTICLE

Arabidopsis PCH2 Mediates Meiotic Chromosome Remodeling and Maturation of Crossovers

Christophe Lambing¹[✉], Kim Osman¹[✉], Komsun Nuntasontorn¹[✉], Allan West¹, James D. Higgins¹[✉], Gregory P. Copenhaver², Jianhua Yang¹[✉], Susan J. Armstrong¹, Karl Mechtler³, Elisabeth Roitinger³, F. Chris H. Franklin¹*

1 School of Biosciences, University of Birmingham, Edgbaston, Birmingham, United Kingdom, **2** Department of Biology and Carolina Center for Genome Scientists, University of North Carolina, Chapel Hill, Chapel Hill, North Carolina, United States of America, **3** IMP-IMBA, Vienna, Austria

 These authors contributed equally to this work.

[✉] **✉** Current address: Department of Plant Sciences, University of Cambridge, Cambridge, United Kingdom

[✉] **✉** Current address: Faculty of Science and Technology, Rajamangala University of Technology Srivijaya, Nakhon Si Thammarat Province, Thailand

[✉] **✉** Current address: School of Biological Sciences, University of Leicester, Leicester, United Kingdom

[✉] **✉** Current address: Faculty of Engineering and Computing, Coventry University, Coventry, United Kingdom

* F.C.H.Franklin@bham.ac.uk



CrossMark
click for updates

 OPEN ACCESS

Citation: Lambing C, Osman K, Nuntasontorn K, West A, Higgins JD, Copenhaver GP, et al. (2015) Arabidopsis PCH2 Mediates Meiotic Chromosome Remodeling and Maturation of Crossovers. *PLoS Genet* 11(7): e1005372. doi:10.1371/journal.pgen.1005372

Editor: Holger Puchta, Karlsruhe Institute of Technology, GERMANY

Received: October 28, 2014

Accepted: June 19, 2015

Published: July 16, 2015

Copyright: © 2015 Lambing et al. This is an open access article distributed under the terms of the [Creative Commons Attribution License](https://creativecommons.org/licenses/by/4.0/), which permits unrestricted use, distribution, and reproduction in any medium, provided the original author and source are credited.

Data Availability Statement: All relevant data are within the paper and its Supporting Information files.

Funding: The research leading to these results has received funding from the European Community's Seventh Framework Program FP7/2007-2013 under grant agreement number KBBE-2009-222883 (FCHF, SJA) and from Biotechnology and Biological Sciences Research Council, United Kingdom grants BB/M004902/1 and BB/K007505/1 (FCHF). GPC is funded by a National Science Foundation Grant (MCB-1121563). Use of the OMX microscope was supported by the MRC Next Generation Optical

Abstract

Meiotic chromosomes are organized into linear looped chromatin arrays by a protein axis localized along the loop-bases. Programmed remodelling of the axis occurs during prophase I of meiosis. Structured illumination microscopy (SIM) has revealed dynamic changes in the chromosome axis in *Arabidopsis thaliana* and *Brassica oleracea*. We show that the axis associated protein ASY1 is depleted during zygotene concomitant with synaptonemal complex (SC) formation. Study of an *Atpch2* mutant demonstrates this requires the conserved AAA+ ATPase, PCH2, which localizes to the sites of axis remodelling. Loss of PCH2 leads to a failure to deplete ASY1 from the axes and compromises SC polymerisation. Immunolocalization of recombination proteins in *Atpch2* indicates that recombination initiation and CO designation during early prophase I occur normally. Evidence suggests that CO interference is initially functional in the mutant but there is a defect in CO maturation following designation. This leads to a reduction in COs and a failure to form COs between some homologous chromosome pairs leading to univalent chromosomes at metaphase I. Genetic analysis reveals that CO distribution is also affected in some chromosome regions. Together these data indicate that the axis remodelling defect in *Atpch2* disrupts normal patterned formation of COs.

Author Summary

In the reproductive cells of many eukaryotes, a process called meiosis generates haploid gametes. During meiosis, homologous parental chromosomes (homologs) recombine

Microscopy Award (Ref: MR/K015869/1). The funders had no role in study design, data collection and analysis, decision to publish, or preparation of the manuscript.

Competing Interests: The authors have declared that no competing interests exist.

forming crossovers (CO) that provide genetic variation. CO formation generates physical links called chiasmata, which are essential for accurate homolog segregation. CO control designates a sub-set of recombination precursors that will mature to form at least one chiasma between each homolog pair. Recombination is accompanied by extensive chromosome reorganization. Formation of a proteinaceous axis organizes the pairs of sister chromatids of each homolog into conjoined linear looped chromatin arrays. Pairs of homologs then align and synapse becoming closely associated along their length by a protein structure, the synaptonemal complex (SC). The SC is disassembled at the end of prophase I and recombination is completed. We have investigated the link between recombination and chromosome remodelling by analysing the role of a protein, PCH2, which we show is required for remodelling of the chromosome axis during SC formation. In wild type, immunolocalization reveals depletion of the axis-associated signal of the axis component, ASY1, along synapsed regions of the chromosomes. In the absence of PCH2, the ASY1 signal is not depleted from the chromosome axis and the SC does not form normally. Although this defect in chromosome remodelling has no obvious effect on CO designation, CO maturation is perturbed such that the formation of at least one CO per homolog pair no longer occurs.

Introduction

During meiosis genetic crossovers (COs), the products of homologous recombination, in conjunction with sister chromatid cohesion establish physical links, referred to cytologically as chiasmata, between homologous chromosome pairs (homologs) to ensure accurate chromosome segregation at the first nuclear division that follows prophase I. In the absence of crossing over the homologs segregate randomly. This leads to the formation of aneuploid gametes following the second meiotic division [1]. Recombination is initiated by the programmed formation of DNA double-strand breaks (DSBs), catalysed by the topoisomerase type II related protein Spo11 [2,3]. In *Saccharomyces cerevisiae* (budding yeast) around 40% of DSBs are repaired as non-CO (NCO) products with the remainder progressing to form COs [4]. In *Arabidopsis thaliana* and other multicellular organisms the proportion of COs is substantially less, typically 5–10% [5]. Importantly, the CO/NCO balance is highly controlled. This control is manifested in several ways. First, each pair of homologs acquires at least one CO. Second, CO interference ensures that multiple COs are well spaced along the chromosomes. Finally, CO homeostasis maintains CO numbers in the face of perturbations that may affect the number of earlier recombinational interactions [6–10]. It is hypothesized that a CO patterning phenomenon, that can be simulated by the beam-film model, underlies these three features of CO control [11,12].

In budding yeast, DSBs form in early leptotene coincident with the elaboration of a proteinaceous chromosome axis that organizes each pair of sister chromatids into linear looped chromatin arrays conjoined by a shared axis. DSBs occur in the context of the chromosome axis [13–15]. At the transition from leptotene to zygotene, formation of the synaptonemal complex (SC), a tripartite structure comprising the chromosome axes linked by overlapping transverse filaments (TFs), is initiated at multiple synapsis initiation sites [1,16,17]. Synapsis continues throughout zygotene bringing the axes into close apposition and is completed at the onset of pachytene when the SC is fully formed. This programmed morphogenesis of the chromosome axes and SC is critical for the coordination of recombination, playing important roles in the

meiosis-specific bias that favours inter-homolog recombination and the maturation of CO designated recombination intermediates [18–26].

In budding yeast mutation of the *PCH2* gene, which encodes a member of the conserved AAA+ ATPase protein family, disrupts remodelling of the chromosome axis during prophase I of meiosis [27,28]. In wild type cells the chromosome axis protein, Hop1, and the SC transverse filament protein, Zip1, appear to load uniformly at a basal level along the chromosomes. Superimposed on this, each forms a series of non-overlapping, alternating hyper-abundant domains. In a *pch2* mutant this domainal loading is disrupted to give a uniform overlapping signal for each protein along the chromosomes [27,28]. Pch2 may modulate inter-homolog bias by remodelling the chromosome structure in the vicinity of DSBs and have a role in a recombination checkpoint [29,30]. Loss of the protein also affects CO formation. In one study, a *pch2Δ* mutant had increased COs on larger chromosomes, while CO frequency on the small chromosome III was unaffected [31]. Genetic data suggested the mutant also exhibited a defect in CO interference. A link with CO interference was also established in a parallel study, although in this instance no effect on overall CO number was observed [28]. However, further analysis based on the distribution of foci of the E3 ligase Zip3, which arise at CO designated intermediates and so provide an early marker for CO interference, reported that interference is not affected in a *pch2* deletion mutant [32].

Orthologs of *PCH2* have been identified in a variety of organisms. In mouse, analysis of a weak hypomorphic allele of *TRIP13* (*PCH2*) indicated that the protein was required for the efficient repair of DSBs that enter the NCO pathway but not CO designated intermediates, which were processed normally. Despite the presence of unrepaired DSBs synapsis was normal in these mice [33]. Subsequently, a study of a more severe *Trip13* mutant reported a defect in CO formation and synapsis [34]. Similar to Pch2 in budding yeast, TRIP13 is required for the depletion of the Hop1 orthologs HORMAD1 and HORMAD2 along synapsed regions of the chromosome axes [35]. In *Drosophila*, PCH2 acts in a checkpoint to monitor defects in recombination and chromosome structure [36]. In *Caenorhabditis elegans* it is reported to maintain the fidelity of recombination and synapsis during prophase I by acting to constrain these processes [37]. A *PCH2* ortholog, referred to as *CRC1* (*CENTRAL REGION COMPONENT1*) has also been identified in rice (*Oryza sativa*) [38]. The *CRC1* protein is 43.8% identical to TRIP13 and 23.1% identical to Pch2 from budding yeast. The *crc1* mutant is completely asynaptic and forms univalents at metaphase I due to a failure to make DSBs [39].

Here we describe the identification and analysis of the *PCH2* orthologs from *Brassica oleracea* and its close relative *Arabidopsis thaliana*. Using super-resolution structured illumination microscopy (SIM) we reveal dynamic changes in localization of *PCH2* in relation to chromosome axis and SC morphogenesis during meiotic prophase I. Analysis of *Arabidopsis* mutants lacking *PCH2* reveals a meiotic role that is markedly different to that reported for the rice *CRC1* protein. Loss of *PCH2* results in a failure to deplete ASY1 from the chromosome axes during zygotene coupled with a synaptic defect. Although recombination initiation and CO designation appears to occur normally during early prophase I, the defects in remodelling of the chromosome axes which influence SC formation are associated with a disruption of the patterned formation of COs along the homologous chromosomes.

Results

PCH2 and ASY1 co-immunoprecipitate in a meiotic protein complex

Protein complexes were immunoprecipitated from *Brassica oleracea* var. albolabra A12DH pollen mother cells (PMCs) in meiotic prophase I using an anti-ASY1 antibody as previously described [40]. Co-precipitating proteins were analysed by mass-spectrometry and identified

using the *Brassica rapa* sequence [41]. Up to 10 unique peptides corresponding to 25% sequence coverage (124/490 amino acids) of the Bra013827 predicted gene product were detected in three independent experiments and were absent from control samples (S1A Fig). The protein was identified as a P-loop containing nucleoside triphosphate hydrolase superfamily member. BLAST searches revealed that the protein is 87% identical to the Arabidopsis At4g24710 predicted gene product. ClustalW2 analysis (<http://www.ebi.ac.uk>) showed that Bra013827 and At4g24710 are members of a sub-family of the AAA+ ATPase super-family that contains the budding yeast *PCH2* and mouse *TRIP13* genes (S1B Fig).

Atpch2 mutants exhibit a reduced fertility phenotype

To determine whether At4g24710 encodes a functional ortholog of Pch2/TRIP13 we obtained three T-DNA insertion lines: SAIL_1187_C06, SALK_031449 and SALK_130138, hereafter referred to as *Atpch2-1*, *Atpch2-2* and *Atpch2-3* respectively. For all lines, the T-DNA insertion site was confirmed by DNA sequencing and the absence of a full-length *AtPCH2* transcript confirmed by RT-PCR (S2 and S3 Figs). The vegetative phenotype of each line was indistinguishable from wild type Arabidopsis, Col-0, but their fertility was reduced (S4A and S4B Fig). Quantification of the fertility defect in *Atpch2-1* revealed a slight, yet significant reduction in mean silique length from 1.66 ± 0.05 cm in wild type to 1.41 ± 0.06 cm ($n = 50$; $P < 0.05$) in *Atpch2-1* ($n = 50$). This was accompanied by numerous gaps between the seeds within the siliques such that overall the mean seed-set was significantly reduced from 67.8 per silique in wild type to 34.6 in *Atpch2-1* ($n = 50$; $P < 0.01$). Analysis of *Atpch2-2* and *Atpch2-3* revealed very similar fertility defects (S4C Fig).

Loss of AtPCH2 results in a reduction of chiasmata

The *Atpch2* reduced fertility phenotype suggested a meiotic defect. Cytogenetic analysis of DAPI stained chromosome spreads from *Atpch2-1* PMCs at leptotene revealed the threadlike chromosomes with no obvious differences to the wild type controls (Fig 1A and 1B). In wild type PMCs, the homologs achieved full synapsis at pachytene with the threadlike signals visibly paired along their lengths, giving a thicker appearance than at leptotene (Fig 1C). However, in *Atpch2-1* pachytene stage cells were not observed, instead the majority of the chromosomes remained as single threadlike signals with some limited regions where paired axes were visible (Fig 1D). During diplotene both *Atpch2-1* and wild type chromosomes desynapsed and began to condense, such that by diakinesis chiasmata linking the homologs were visible. At metaphase I, following further condensation, distinct bivalents were observed. Five bivalents were invariably present in wild type, but some *Atpch2-1* nuclei contained a mixture of bivalent and univalent chromosomes (Fig 1E and 1F). To quantify this we counted chiasmata in *Atpch2-1* in metaphase I chromosome spreads using fluorescent *in situ* hybridization (FISH) with 45S and 5S rDNA probes to identify individual chromosomes [42] (Fig 1G and 1H). This revealed a significant reduction in the mean chiasma frequency in *Atpch2-1* compared to wild type (6.9; $n = 50$ versus 9.6; $n = 50$; $P < 0.001$). No univalents were observed in the wild type sample, whereas they were present at a frequency of 10.0% in *Atpch2-1* with all chromosomes affected. Similar results were obtained for *Atpch2-2* (6.9; $n = 37$; $P < 0.001$; univalent frequency 14.6%) and *Atpch2-3* (6.2; $n = 26$; $P < 0.001$; univalent frequency 7.7%). As a consequence of this, in contrast to wild type, mis-segregation of the chromosomes was observed at the first meiotic division in *Atpch2-1* (Fig 1I and 1J) leading to unbalanced tetrads (Fig 1K and 1L). No precocious sister chromatid separation was observed suggesting that there was no cohesion defect. Analyses of *Atpch2-2* and *Atpch2-3* revealed that the meiotic defect in the three mutants is essentially identical (S5A–S5H Fig). To confirm that the observed phenotype was due to a loss

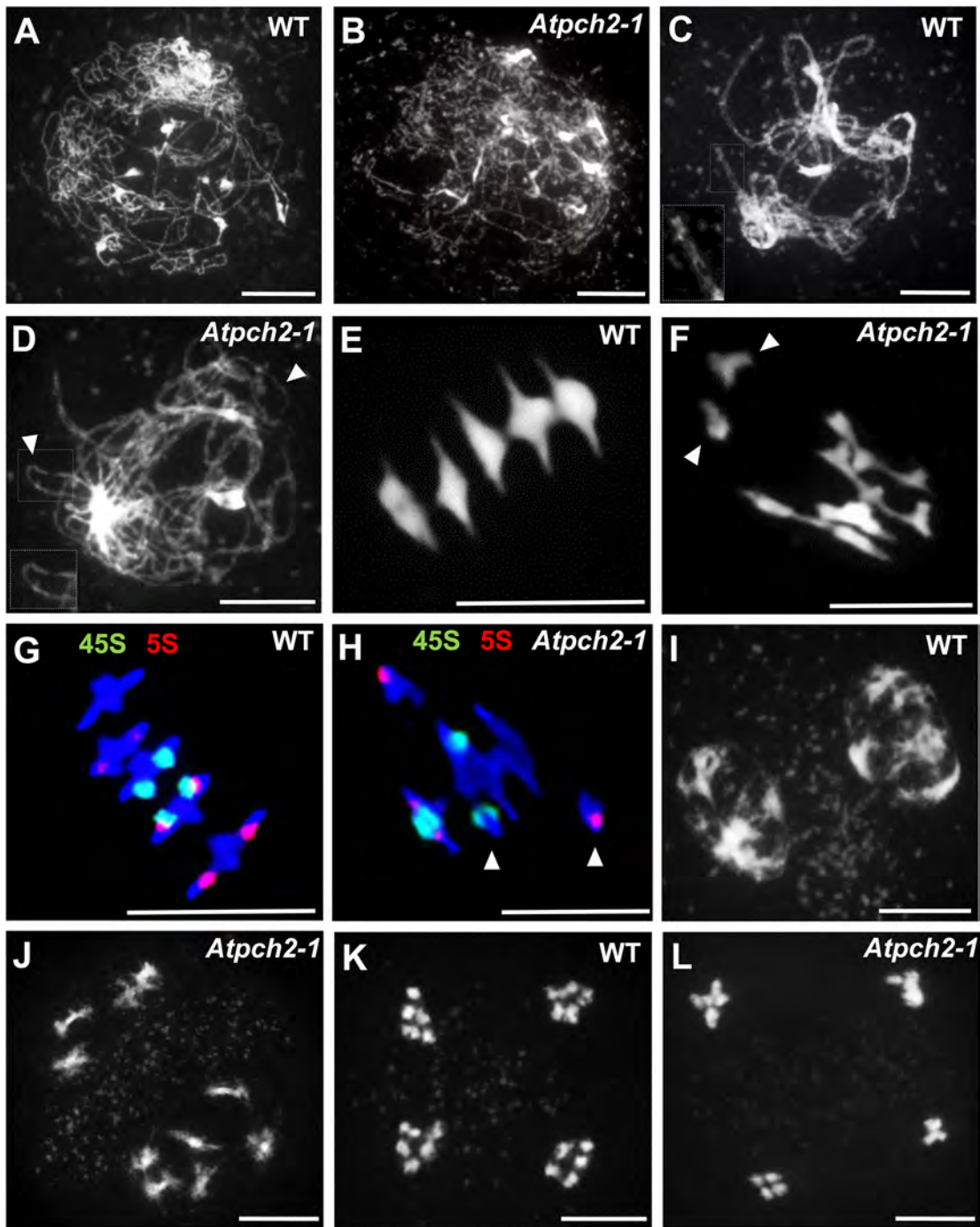


Fig 1. Meiotic stages from wild type *Arabidopsis* and *Atpch2-1* pollen mother cells. Chromosome spread preparations from wild type (A,C,E,G,I,K) and *Atpch2-1* (B,D,F,H,J,L) PMCs. (A,B) leptotene; (C,D) pachytene (note in *Atpch2-1* cell is at late prophase I normal pachytene stage was not observed). Arrowheads mark unsynapsed regions. (E,F) metaphase I. Arrowheads mark univalent chromosomes; (G,H) metaphase I stage labelled with 5S (red) and 45S (green) rDNA probes to identify the individual chromosomes. Arrowheads mark univalent chromosomes; (I,J) dyad; (K-L) tetrad. DNA is stained with DAPI. Bar = 10 μ m.

doi:10.1371/journal.pgen.1005372.g001

of AtPCH2 function, an allelism test was conducted by crossing *Atpch2-1* with *Atpch2-2*. Phenotypic and cytological analysis of the *Atpch2-1/Atpch2-2* progeny revealed the same defects

as in the parental lines confirming that these arose due to the loss of AtPCH2 function (S5I–S5M Fig).

We next investigated if the reduction in chiasmata in *Atpch2-1* reflected a defect in CO formation. Approximately 85% of COs in Arabidopsis exhibit CO interference [43]. Formation of these, so-called Class I COs, require a group of proteins known as ZMMs (Zip1, Zip2, Zip3/Hei10, Zip4, Mer3, Msh4 and Msh5) [5,18]. The remainder (Class II) are insensitive to CO interference and dependent on the structure-specific endonuclease AtMUS81 [44]. To determine if the loss of AtPCH2 affected one or both classes of COs we generated an *Atmsh5-1/Atpch2-1* double mutant. In *Atmsh5-1*, the number of chiasmata per PMC ranged between 0 and 4 with a mean chiasma frequency of 1.2 ($n = 50$) (S6B Fig). In comparison, the mean chiasma frequency in the *Atmsh5-1/Atpch2-1* double mutant was significantly reduced to 0.3 ($n = 50$; $P < 0.001$), with the number of chiasmata per nucleus ranging between 0 and 2 (S6C Fig).

Thus, overall the cytological analysis suggests that the reduction in chiasmata in *Atpch2-1* arises from a recombination defect that impacts on both interference sensitive and insensitive CO formation, rather than through an effect on sister chromatid cohesion.

Chromosome axis remodelling is disrupted in *Atpch2-1*

The failure to observe pachytene stage PMCs in *Atpch2-1* suggested a defect in formation of the SC. To investigate further, we examined chromosome axis reorganization during early to mid-prophase I using immunocytochemistry combined with fluorescence light microscopy and SIM. At leptotene in wild type Arabidopsis, the HORMA domain protein ASY1 is detected in chromosome spreads of PMCs as a linear axis-associated signal. This appears to be comprised of a series of alternating regions of higher and lower signal intensity, suggestive of a domainal organization of ASY1 abundance along the chromosome axis [19,45] (Fig 2A and 2C). Analysis of *Atpch2-1* PMCs at leptotene did not reveal any obvious differences, with localization of ASY1 appearing normal (Fig 2B and 2D). Similarly, the cohesin complex protein SYN1 [46,47] (S7A and S7B Fig) and the chromosome axis protein ASY3 [19] (S7C and S7D Fig) appeared unaffected in *Atpch2-1*, with both forming a linear axis-associated signal from leptotene through to mid-prophase I. That SYN1 localization was normal supported the cytological observation that there was no evidence of a sister chromatid cohesion defect. Consistent with these observations, comparison of the mean total axis length per PMC at leptotene was not significantly different to wild type (*Atpch2-1*: 229 μm versus wt: 220 μm , $n = 10$, $P = 0.53$).

Previous immunolocalization studies show that the Arabidopsis SC TF protein ZYP1 begins to polymerize between the aligned homologous chromosomes from multiple sites of synapsis initiation at the onset of zygotene. Polymerization continues throughout zygotene until completion of SC formation at pachytene [20]. Dual-localization of ZYP1 and ASY1 in wild type Arabidopsis revealed that SC formation is accompanied by a reduction in the intensity of ASY1 signal which appeared less continuous and appeared to be associated with the chromatin loops rather than the axis along synapsed regions (Fig 2E–2J; compare synapsed segment with unsynapsed region in 2G and 2J; S8A–S8C Fig). Quantification of the relative intensity of the ASY1 signal (S9 Fig) indicated a significant reduction of 67.0% ($n = 23$; $P = <0.001$) on the synapsed region compared to the unsynapsed axes (S9C and S9D Fig; S1 Table). Analysis of *Atpch2-1* PMCs at mid/late-prophase I suggested that unlike wild type, the ASY1 signal intensity along the synapsed compared to unsynapsed regions remained unchanged ($n = 22$; $P = 0.25$) (S9E and S9F Fig; S1 Table). However, the differentiation of the ASY1 signal into putative domains of high and low intensity appeared enhanced in the mutant, possibly a consequence of the

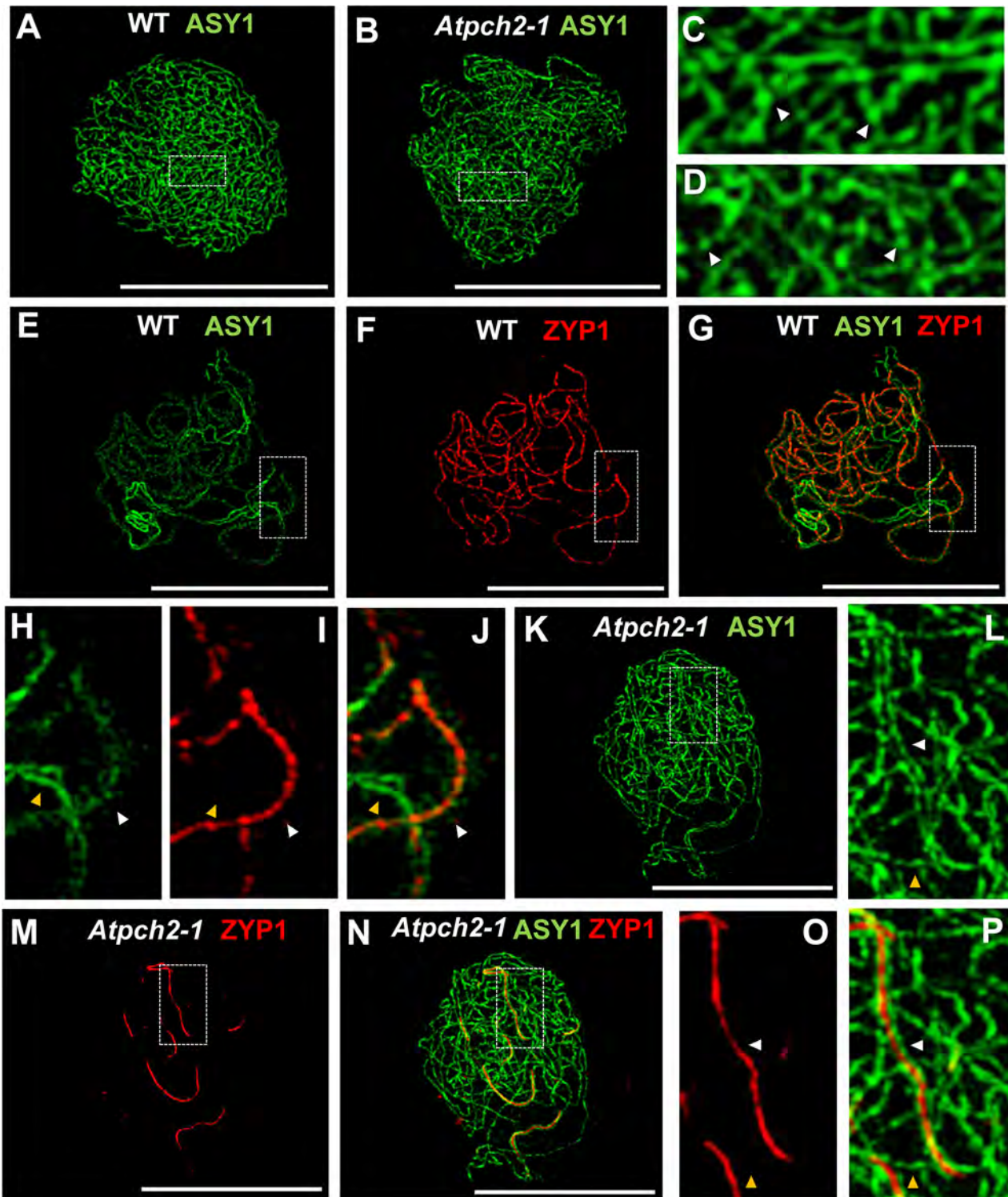


Fig 2. Immunolocalization of ASY1 and ZYP1 in wild type and *Atpch2-1* during prophase I. (A-D) Immunolocalization of ASY1 (green) on chromosome spread preparations from wild type (A,C) and *Atpch2-1* (B,D) nuclei at leptotene. Panels C and D show magnified sections of axes from A and B respectively. White arrowheads mark the regions of ASY1 with higher signal intensity. (E-J) Immunolocalization of ASY1 (green) (E,G,H,J) and ZYP1 (red) (F,G,I,J) and merge images (G,J) on chromosome spreads from wild type at zygotene. Figs H, I and J show magnified sections of axes from E, F and G respectively. (K-P) Immunolocalization of ASY1 (green) (K,L,N,P) and ZYP1 (red) (M-P) and merge images (N,P) on chromosome spread preparations from *Atpch2-1* at mid/late-prophase I. Figs L, O and P show magnified sections of axes from K, M and N respectively. White arrowheads represent synapsed regions while yellow arrowheads represent unsynapsed regions. DNA is stained with DAPI (blue). Bar = 10 μ m.

doi:10.1371/journal.pgen.1005372.g002

delayed synapsis and increased axis compaction relative to leptotene (S9F Fig). SC polymerization was compromised in the mutant (Fig 2M–2P). Stretches of ZYP1 were detected but varied in number and length from cell to cell. On average the SC length at late prophase I in *Atpch2-1* was 32% that of wild type (57 μ M, n = 16 versus 179 μ M, n = 8), although this ranged from 13% to 57%.

PCH2 distribution during prophase I

To gain further insight into the relationship between PCH2 and the components of the chromosome axes, we conducted immunolocalization studies using an anti-PCH2 antibody on chromosome spreads of wild type PMCs from *Arabidopsis* and *B. oleracea* (Figs 3 and 4). Analysis of *Arabidopsis* using SIM revealed numerous chromatin-associated PCH2 foci (mean 165; n = 10) in G2 coinciding with the appearance of foci and short stretches of ASY1 (Fig 3A). Most PCH2 foci remained distinct from the ASY1 signal (Fig 3A, inset 3C). As the chromosome axis formed in leptotene, the ASY1 signal became more linear. At this stage the proteins appeared associated, with 51.2% (n = 12) of the PCH2 foci overlapping the ASY1 signal to some extent (Fig 3B, inset 3D), possibly a consequence of the chromosome reorganization that occurs at leptotene. As the SC formed during zygotene PCH2 distribution changed. ASY1 associated foci were no longer apparent. Instead PCH2 now tracked the depleted ASY1 signal along the synapsed region, forming a linear array of foci that tended to coalesce (Fig 3E and 3I). Dual-immunolocalization of PCH2 and ZYP1 confirmed that the PCH2 signal localized to the regions where SC nucleates and was present as foci along the SC during zygotene through pachytene (Fig 3J–3P and S10A–S10C Fig). Analysis in *Atasy1* and *Atasy3* mutants where SC formation is severely compromised, such that only short stretches or accumulations of ZYP1 are formed [19,23], also revealed colocalization of the PCH2 and ZYP1 signals (S10D–S10I Fig). No PCH2 signal was detected in any of the three *Atpch2* mutant lines (S11 Fig).

Immunolocalization in *B. oleracea* PMCs revealed that similar to *Arabidopsis*, numerous PCH2 foci were detected in late G2/early leptotene (S12A and S12B Fig). At late leptotene/early zygotene PCH2 formed fewer, large foci (mean number per nucleus = 14.2; range = 10–20; n = 18) (Fig 4A–4C). Dual localization of ZYP1 and PCH2 at this stage indicated that these foci correspond to sites of SC nucleation at the leptotene/zygotene transition (Fig 4D–4F) and SIM analysis revealed that the ZYP1 signal at the nucleation site often appeared to form a ‘arrowhead-like’ shape to which PCH2 co-localized (Fig 4G). From the SIM images the arrowhead-like foci were estimated to have a mean length of 602 nm (range = 560–640 nm; n = 40) and a mean maximum width of 419 nm (range 400–480 nm; n = 40) and seemed quite consistent in number (mean 15 per nucleus; range = 12–19; n = 5). In a larger sample, analysed using fluorescence microscopy, a mean of 12.2 foci per nucleus was observed (n = 50). Although the range (5–22) was greater than in the SIM sample, most nuclei (76.0%) contained 10 or more foci. The slight variation in the number of PCH2 foci observed in these experiments probably reflected the dynamics of the process and the increased resolution afforded by SIM relative to fluorescence microscopy. In addition to the large foci, slightly more numerous smaller ZYP1 foci were also observed at early zygotene (mean number per nucleus = 17.0; n = 50). These also co-localized with PCH2 (Fig 4D–4F). As the SC began to extend, SIM revealed extensive overlap between ZYP1 and PCH2 signals each appearing to be comprised of multiple smaller foci (Fig 4H). At zygotene, the ASY1 signal appeared to be reduced along synapsed regions of the chromosomes (S12C Fig) (64.3% reduction relative to unsynapsed axes; n = 14), which were decorated with numerous small PCH2 foci. At pachytene, PCH2 foci were still detected along the entire length of the ZYP1-stained SC as well as in the surrounding chromatin (S12D Fig).

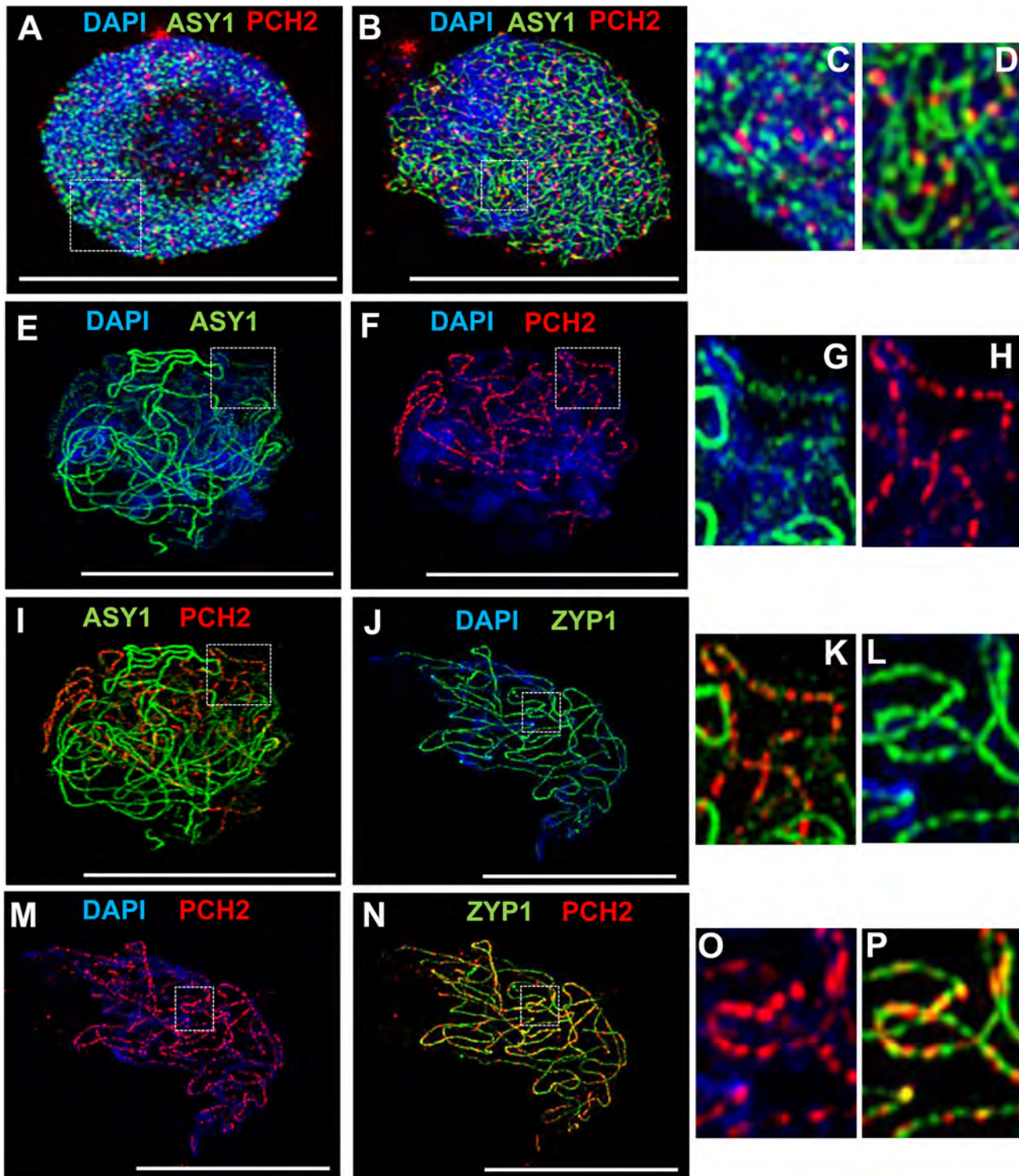


Fig 3. Immunolocalization of PCH2 in wild type Arabidopsis. (A-D) Dual localization of ASY1 (green) and PCH2 (red) on chromosome spread preparations from wild type PMCs at G2 (A) and leptotene (B). Panels (C) and (D) show magnified sections of (A) and (B) respectively. (E-I, K) Immunolocalization of ASY1 (green) and PCH2 (red) and merge (I, K) in wild type at mid-prophase I. Panels G, H and K show magnified sections of axes from images E, F and I respectively. (J, L-P) Immunolocalization of ZYP1 (green) and PCH2 (red) and merge (N, P) in a wild type nucleus at mid-prophase I. Panels L, O and P represent magnified sections of axes from J, M and N respectively. DNA is stained with DAPI. Bar = 10 μm.

doi:10.1371/journal.pgen.1005372.g003

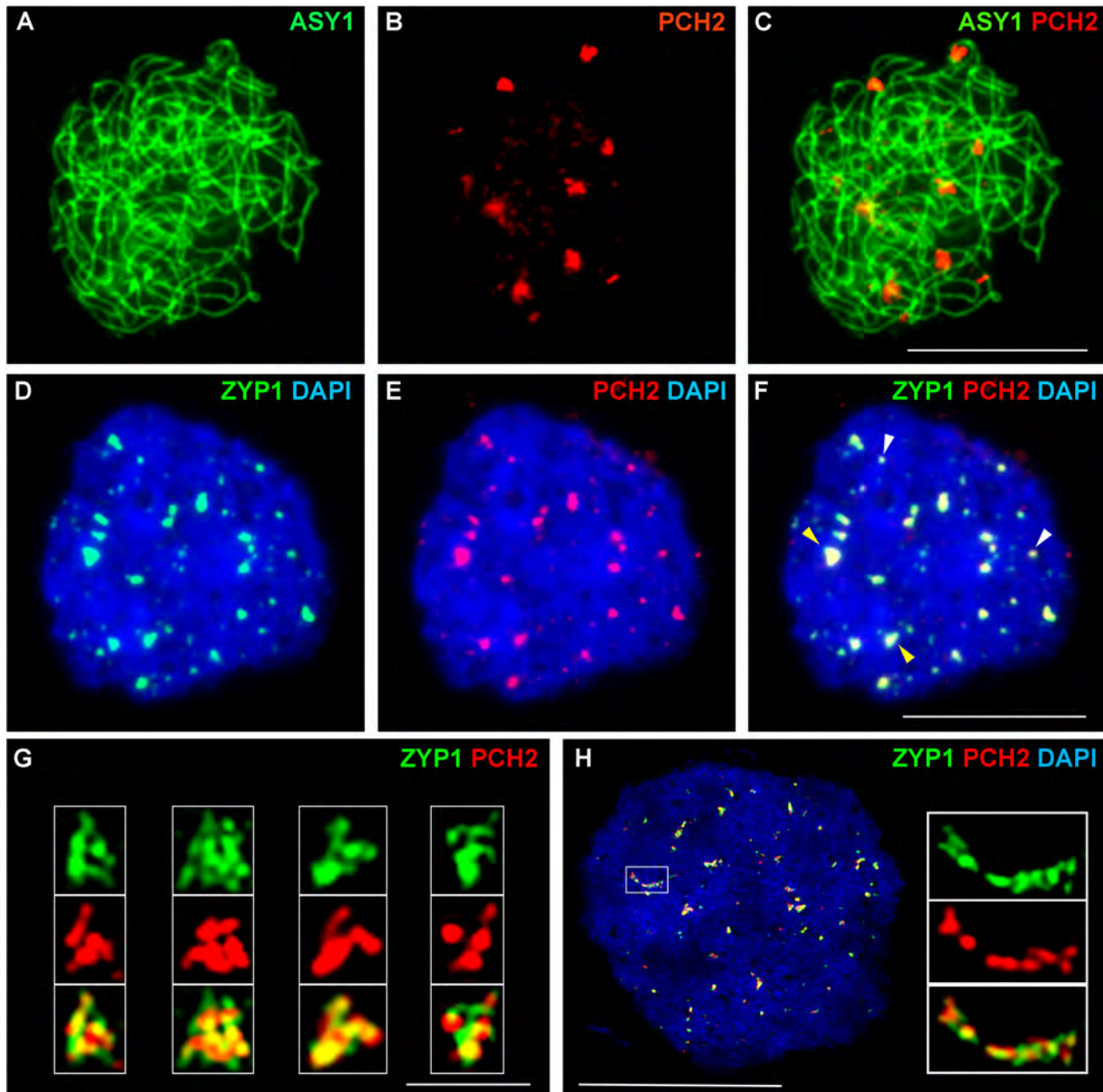


Fig 4. Immunolocalization of PCH2 in *B. oleracea* at the leptotene/zygotene transition. (A-C) Dual localization of ASY1 (green) and PCH2 (red) on chromosome spread preparations from *B. oleracea* PMCs at the leptotene/zygotene transition. (D-F) Dual localization of ZYP1 (green) and PCH2 (red) at SC nucleation sites. Yellow arrows indicate examples of large ‘arrowhead’ shaped foci and white arrows indicate the smaller SC nucleation sites. (G) SIM images of arrowhead SC nucleation sites stained with ZYP1 (green) and PCH2 (red). (H) SIM image of dual localization of ZYP1 (green) and PCH2 (red) on a nascent stretch of SC. DNA is stained with DAPI (blue). Bar = 1 μ m in (G) and 10 μ m in all other images.

doi:10.1371/journal.pgen.1005372.g004

Prophase I progression is delayed in *Atpch2-1*

In budding yeast deletion of *PCH2* results in an accumulation of nuclei in pachytene and a delay in progression through meiosis I [27]. We therefore investigated if the protein has a role in prophase I progression in Arabidopsis. 5-ethynyl-2'-deoxyuridine (EdU) was used to pulse-label *Atpch2-1* PMCs during meiotic S-phase [48]. Progression through meiosis was then monitored (S13A Fig). In wild type and *Atpch2-1*, EdU labelled leptotene nuclei were detected 10h

post S-phase. By 25h all labelled wild type PMCs were at zygotene or pachytene and at zygotene in *Atpch2-1*. At 32h the wild type PMCs had exited pachytene and were at diplotene/diakinesis and by 36h were at the dyad stage, whereas *Atpch2-1* PMCs were still at zygotene suggesting a delay of 5-8h (S13A and S13B Fig).

Fluorescent tetrad analysis supports a CO defect in *Atpch2-1*

The cytological analysis (see earlier) suggested a defect in CO formation in *Atpch2* mutants. To further examine the recombination phenotype of *Atpch2-1* we used the fluorescent-tagged-line (FTL) system [49,50] which relies on the segregation of three genetically linked transgenic markers, each encoding a distinct pollen-specific fluorescent protein expressed post-meiotically. The FTLs are in a *qrt1-2* mutant background which prevents the separation of the gametes and facilitates the visualisation of the meiotic recombination events that have occurred between the transgenic markers in the tetrad pollen [51,52]. Three pairs of adjacent genetic intervals, one on each arm of chromosome 5 and another on chromosome 2 were examined (S14 Fig). This revealed that the genetic map distance determined using the Perkins mapping equation [53] in the adjacent intervals I5c and I5d was not significantly affected by the *Atpch2-1* mutation (I5c wild type 6.1 cM v *Atpch2-1* 6.8 cM; $P = 0.17$; I5d wild type 5.5 cM v *Atpch2-1* 6.0 cM; $P = 0.28$) (Fig 5A). However, interval I5a showed a significant decrease in recombination frequency in the presence of *Atpch2-1* (15.1 cM) compared to wild type (27.7 cM; $P < 0.001$), whereas the map distance in interval I5b exhibited a significant increase from 17.3 cM in wild type to 22.3 cM in the mutant ($P < 0.001$) (Fig 5A). A significant increase in map distance was observed in intervals I2f and I2g in the presence of the *Atpch2-1* mutation (I2f wild type 6.1 cM / *Atpch2-1* 8.0 cM $P < 0.001$; I2g wild type 5.1 cM / *Atpch2-1* 7.1 cM $P < 0.001$) (Fig 5A).

We used the FTL data to obtain a genetic estimate for CO interference in adjacent intervals by calculating the Interference Ratio (IR). This method, developed by Malkova et al. [54], uses the ratio of the genetic map distance in an interval with and without the presence of a CO in an adjacent interval to provide an estimate of the strength of CO interference. When COs in adjacent intervals are entirely independent of each other the IR is 1, indicating no interference. Values less than 1 indicate increasing levels of (positive) interference with a value of 0 indicating complete interference. IR ratios greater than 1 are indicative of negative interference. The CO interference ratio was 0.412 for I5ab in wild type. In *Atpch2-1*, the genetic map distance of I5a was similar with and without the presence of a CO in the interval I5b (14.8 cM with a CO in interval I5b vs 15.2 cM without a CO in interval I5b). The CO interference ratio is 0.976 and is statistically higher than wild type (Z-score = 5.40; $P < 0.001$) (Fig 5B). This suggests that CO interference is reduced in the interval I5ab in *Atpch2-1*. In contrast, the CO interference ratio of I5cd is similar in wild type (0.568) and in *Atpch2-1* (0.552; Z-score = 0.01; $P = 0.92$) (Fig 5B). The interference ratio for interval I2fg is also increased in the *Atpch2-1* mutant. In wild type the ratio is 0.113 whereas in *Atpch2-1* it is 0.315 ($P = 0.021$).

We also used the FTL data to estimate the coefficient of coincidence (CoC) for the three pairs of intervals. The CoC is calculated by dividing the observed frequency of double COs in two adjacent intervals by the expected frequency assuming no interference [55]. When interference is absent the CoC is 1 and where it is complete the CoC is 0. The overall result was similar to that obtained for the IR (S2 Table). For I5a/b interference appeared reduced (CoC wild type = 0.46 v CoC *Atpch2-1* = 0.99), for I5c/d it was unchanged (CoC wild type = 0.60 v CoC *Atpch2-1* = 0.60) and for I2fg there was an apparent decrease (CoC wild type = 0.13 v CoC *Atpch2-1* = 0.37).

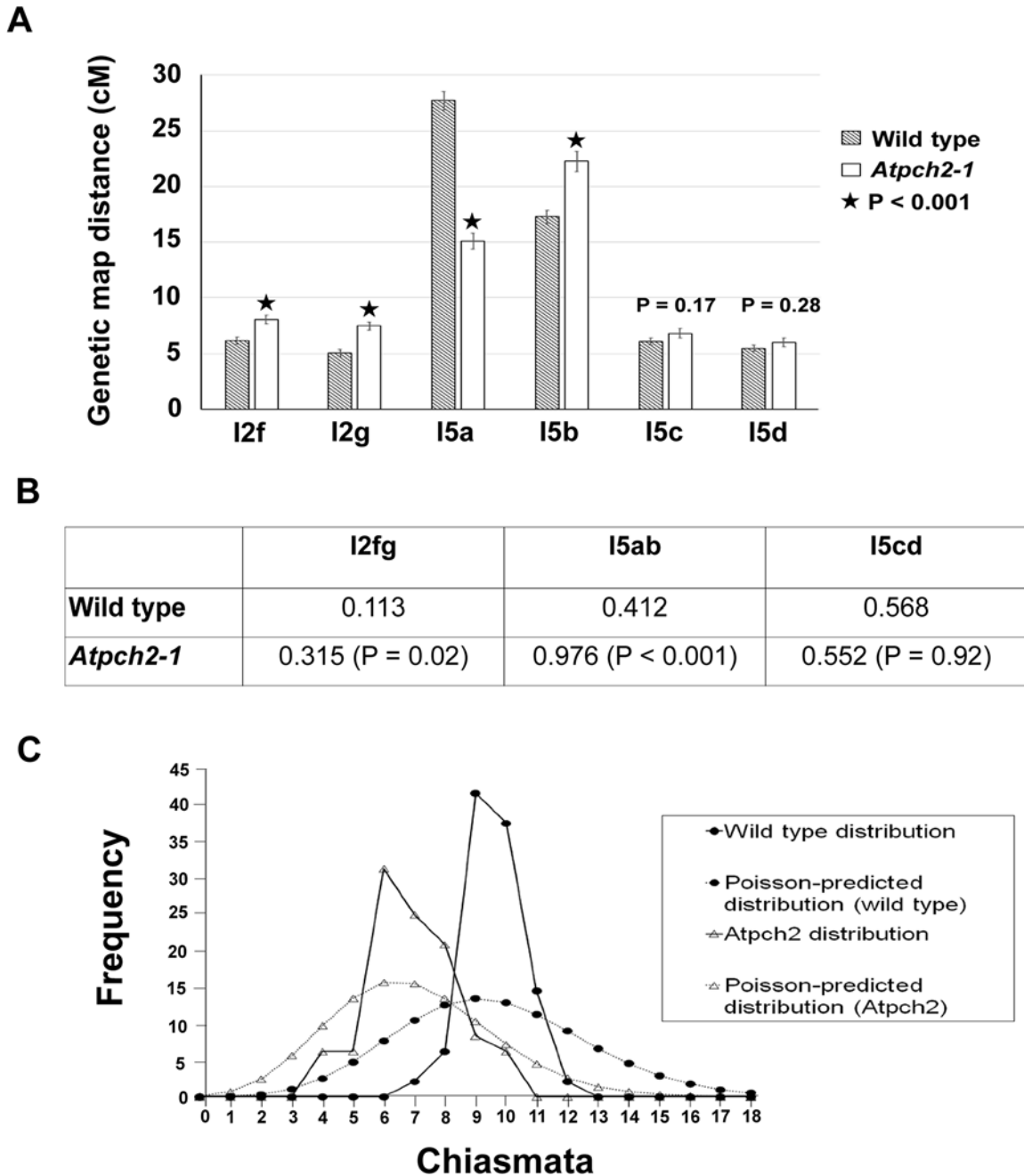


Fig 5. Recombination frequency and chiasma distribution in *Atpch2-1*. (A) Genetic map distance of four distinct intervals on chromosome 5 and two intervals on chromosome 2 in wild type *Arabidopsis* and *Atpch2-1* mutant. Black stars represent a statistical difference in the genetic map distance between wild type and mutant. P value is indicated on the graph when the genetic map distance of an interval is not statistically different between wild type and mutant. Error bars represent the standard error of the mean. (B) Three pairs of adjacent intervals I2fg, I5ab and I5cd were used to estimate genetic CO interference for wild type and *Atpch2-1* mutant. CO interference ratio for each pair of intervals is indicated in the table and P value is shown in parentheses. (C) Observed (solid line) and Poisson-predicted (dotted line) distributions of chiasma numbers per cell for wild type (black circle) and *Atpch2-1* mutant (white triangle).

doi:10.1371/journal.pgen.1005372.g005

Numerical distribution of chiasmata in *Atpch2-1*

In the absence of CO control the numerical distribution of chiasmata between cells is predicted to fit a Poisson distribution [56]. This expectation is borne out in ZMM mutants such as

Atmsh4 and *Atmer3*, whereas in wild type the distribution is non-Poissonian. [43,57,58]. We analysed the chiasma distribution in the sample of *Atpch2-1* cells described above. The number of chiasmata per nucleus ranged between 4 and 10 in *Atpch2-1* and between 7 and 12 in wild type. Further inspection revealed that the proportion of *Atpch2-1* PMCs with a chiasma frequency close to the mean of 6.9 was over-represented in the sample analysed, with 74% having between 6 and 8 chiasmata per cell (vs 42.8% if the numerical distribution of chiasmata was random) (Fig 5C). Over-distribution of chiasma around the mean is also a feature of wild type [43]. The chiasma distribution in *Atpch2-1* differed significantly from a Poisson distribution ($X_{(11)}^2 = 45.2$; $P < 0.001$). This was also confirmed in *Atpch2-2* ($X_{(11)}^2 = 37.2$; $P < 0.001$) and *Atpch2-3* ($X_{(11)}^2 = 40.00$; $P < 0.001$).

Later stages of recombination are aberrant in *Atpch2-1*

We investigated the basis for the reduction in chiasmata in *Atpch2-1* using immunolocalization of recombination pathway proteins on prophase I chromosome spreads from *Atpch2-1* PMCs. Immunolocalization of the strand-exchange proteins RAD51 and DMC1 which are recruited to DSBs at leptotene was used to monitor early recombination and immunolocalization of the ZMM protein AtMSH4 was used to detect later recombination progress [43,59,60]. There were no significant differences between wild type (Fig 6A, 6C and 6E) and *Atpch2-1* (Fig 6B, 6D and 6F) PMCs. At mid-leptotene the mean number of RAD51 foci in *Atpch2-1* was 144 versus 146 in wild type ($n = 12$; $P = 0.37$) (Fig 6A and 6B). For DMC1 the corresponding values were 167 versus 173 ($n = 12$, $P = 0.56$) (Fig 6C and 6D). In PMCs at the leptotene/zygotene transition the mean number of MSH4 foci was 150 in *Atpch2-1* versus 152 in wild type ($n = 12$; $P = 0.63$) (Fig 6E and 6F).

HEI10 (Human enhancer of invasion-10) is a member of the Zip3/Hei10 family of proteins which are thought to possess SUMO/ubiquitin E3 ligase activity [61]. Studies reveal that Zip3/Hei10 marks the sites of future type I COs [61,62]. In *Sordaria macrospora* Hei10 foci that mark COs are ~300 nm in size and emerge from a much larger population of small axis-associated foci during early/mid-prophase I [63]. Dual localisation of ASY1 and HEI10 on chromosome spreads of Arabidopsis wild type and *Atpch2-1* PMCs at late leptotene showed that in both cases HEI10 formed a very similar large number of foci (166 versus 165 respectively, $n = 10$; $P = 0.81$) along the chromosome axes (Fig 6G–6L). As prophase I progressed the foci decreased in number and disappeared by pachytene. Most foci were small (~175 nm) but in addition, a number of larger (>250 nm) HEI10 foci were observed in both sets of PMCs. In wild type at the leptotene/zygotene transition we observed 7 to 15 large HEI10 foci (mean 10.6, $n = 33$). This remained constant through late pachytene (mean 9.9 range 9–12, $n = 14$) (Fig 7A, 7C and 7I). During early prophase I the number and distribution of large HEI10 foci in *Atpch2-1* PMCs was not significantly different to wild type (mean 10.6 versus 10.2; $P = 0.20$; $n = 21$). However, at mid/late prophase the mean number of large HEI10 foci was significantly reduced to 6.9 ($n = 27$) compared to wild type nuclei ($P < 0.001$) (Fig 7B, 7D and 7I). HEI10 foci were mostly found as singletons on the stretches of SC in *Atpch2-1* (83.4% $n = 185$) (Fig 7B and 7D), with two or three HEI10 foci observed in 14.6% and 2.0% of cases respectively.

Dual localization of HEI10 and ZYP1 in *B. oleracea* PMCs at the leptotene/zygotene transition revealed that most of the large ZYP1 foci at SC nucleation sites that had been shown to co-localize with PCH2 at this stage (see earlier), also co-localized with HEI10 (86.0% foci; $n = 30$ nuclei) (S15 Fig).

To confirm that the reduction in large HEI10 foci in *Atpch2-1* reflects a reduced number of mature CO intermediates we analysed the distribution of the late recombination protein MLH1 which marks the sites of Type I COs/chiasmata [64]. Dual immunolocalization of

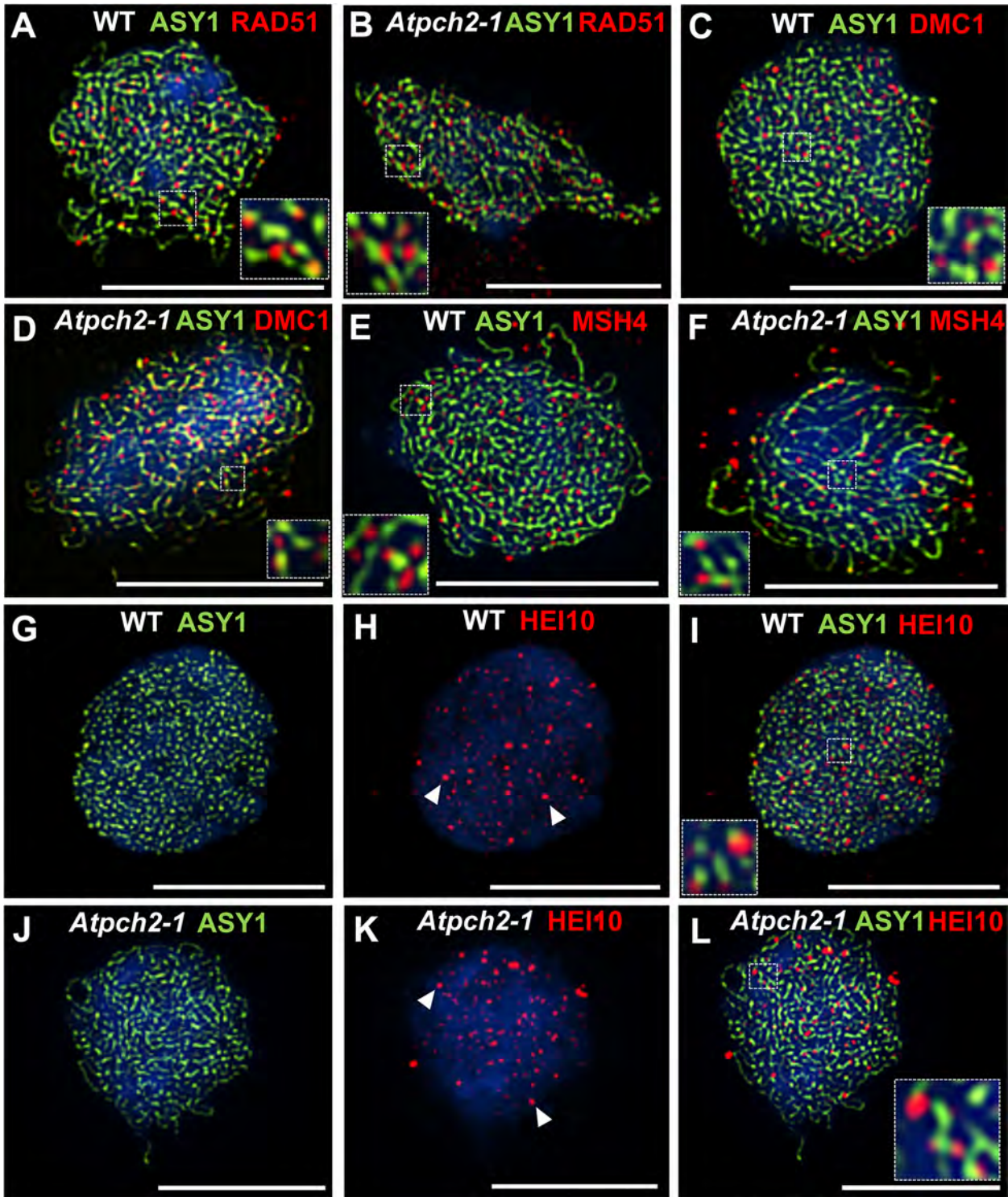


Fig 6. Dual localization of ASY1 and recombination pathway proteins in wild type and *Atpch2-1* meiotic nuclei at early prophase I. Dual localization of ASY1 (green) and RAD51 (red) on wild type (A) and *Atpch2-1* (B) PMCs at mid-leptotene; ASY1 (green) and DMC1 (red) on wild type (C) and *Atpch2-1* (D) PMCs at mid-leptotene; ASY1 (green) and MSH4 (red) on wild type (E) and *Atpch2-1* (F) PMCs at leptotene/zygotene transition; ASY1 (green) and HEI10 (red) on wild type (G-I) and *Atpch2-1* (J-L) PMCs at late-leptotene. DNA is stained with DAPI (blue). Bar = 10 μ m.

doi:10.1371/journal.pgen.1005372.g006

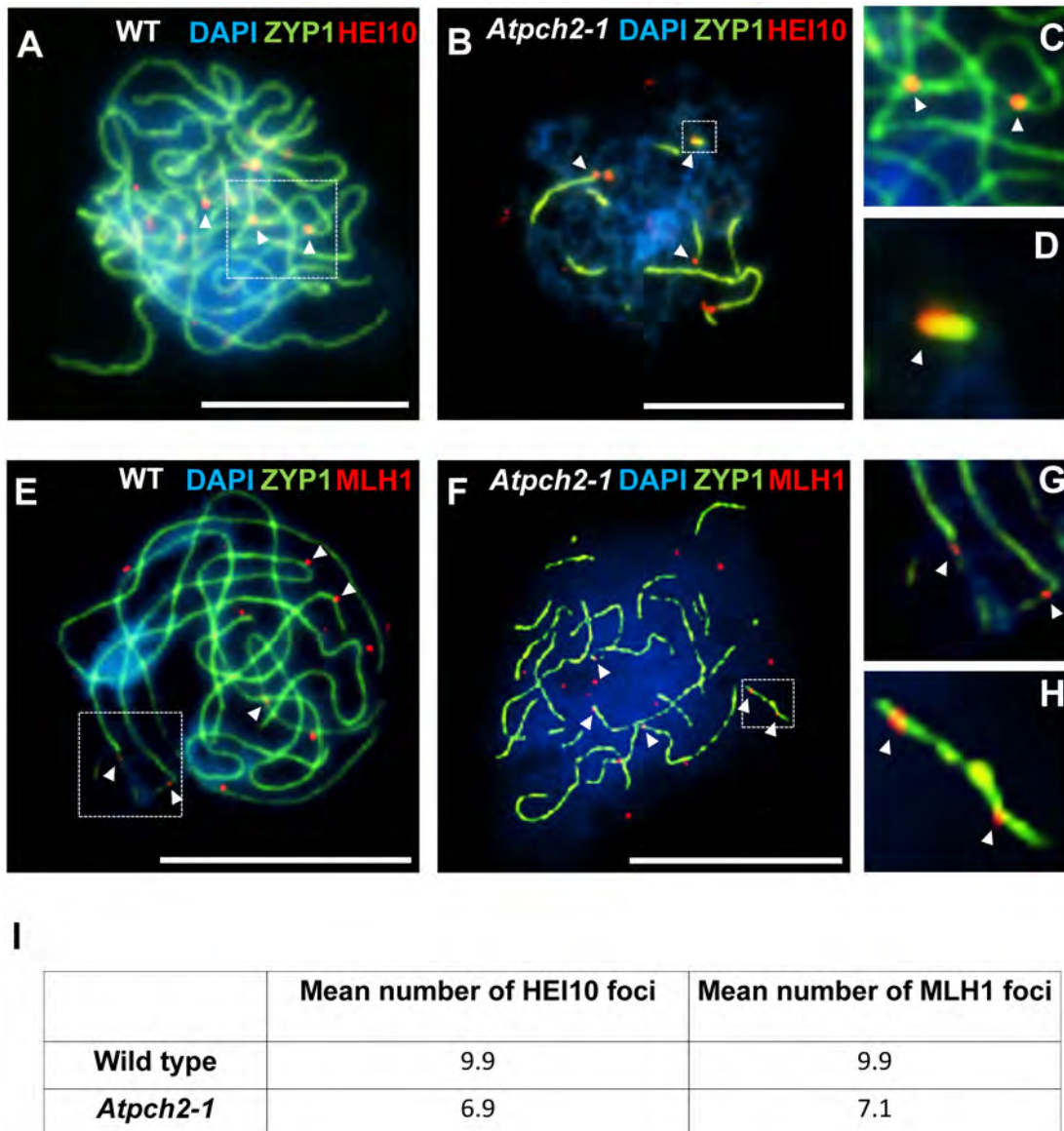


Fig 7. Dual localization of ZYP1 and recombination pathway proteins in wild type Arabidopsis and *Atpch2-1* meiotic nuclei at mid/late prophase. (A-D) Dual localization of ZYP1 (green) and HEI10 (red) on wild type (A,C) and *Atpch2-1* (B,D) PMCs. Panels C and D show magnified sections of SC from A and B respectively. (E-H) Dual localization of ZYP1 (green) and MLH1 (red) on wild-type (E,G) and *Atpch2-1* (F,H) PMCs. Panels G and H show magnified sections of SC from E and F respectively. DNA is stained with DAPI (blue). Bar = 10 μ m. (I) Table showing the mean number of HEI10 and MLH1 foci in wild type and *Atpch2-1*.

doi:10.1371/journal.pgen.1005372.g007

MLH1 and ZYP1 (N-terminus Ab, see [Materials and Methods](#)) on chromosome spreads of wild type PMCs, showed the number of MLH1 foci per nucleus varied between 9 and 11 with a mean count of 9.9 (n = 12) at pachytene ([Fig 7E, 7G and 7I](#)). In *Atpch2-1* the mean number of MLH1 foci per nucleus was 7.1 (n = 12), a significant reduction compared to wild type ($P < 0.002$) ([Fig 7F, 7H and 7I](#)). We noted that in both cases the MLH1 foci were often adjacent to the ZYP1 signal rather than directly over the SC central region. Similar to the distribution of HEI10 foci, MLH1 foci were mostly observed as singletons on stretches of SC in *Atpch2-1* PMCs (61.2% n = 85) with two or three foci occurring in 28.2% and 10.6% cases respectively ([Fig 7F and 7H](#)).

Discussion

Chromosome axis remodeling at the leptotene/zygotene transition is defective in the absence of PCH2

Formation of the chromosome axis in early prophase I appears unaffected by loss of PCH2 based on immunolocalization of the axis proteins and axis length measurements. This differs from rice where the PCH2 ortholog, CRC1, is required for recruitment of the ASY1 ortholog PAIR2 onto the chromosome axes at leptotene [38]. This difference between the two plant species is perhaps surprising but it is not the first example where the phenotype of a rice meiotic mutant is different to that in other plants. For instance, loss of *ZYP1* in Arabidopsis and barley results in a reduction of CO formation whereas mutation of the corresponding rice gene, *ZEP1*, leads to increased COs [20,65,66].

At mid-prophase I in Arabidopsis and *B. oleracea*, PCH2 forms foci along the SC which correlate with regions of ASY1 signal depletion on the axes. The overall distribution of PCH2, together with the fact that ASY1 signal intensity is not reduced along the synapsed axes in *Atpch2* mutants, suggests that PCH2 participates in the depletion of ASY1 from the axis at the leptotene/zygotene transition. This could be a direct effect since biochemical studies in budding yeast show that Pch2 can bind to Hop1 *in vitro* and binding is strongly enhanced if its ATP hydrolysis activity is blocked [67]. In addition, Pch2 was shown to displace Hop1 from double-stranded DNA. Direct interaction *in vivo* has not been established as it is argued that this would be transient in the presence of ATP [67]. Based on the number of peptides recovered, PCH2 is found as an abundant component of a complex that is co-precipitated with ASY1 from Brassica PMCs. Although this could reflect a direct interaction, PCH2 may be co-precipitated as part of a larger chromosome axis-protein complex. Thus, an alternative possibility is that the reduction in the ASY1 signal is an indirect consequence of PCH2-dependent reorganization of the chromosome axis at the onset of zygotene.

PCH2 is important for synapsis but does not appear to be an integral SC component

In rice, loss of the PCH2 ortholog, CRC1 leads to a failure to form SC. This is unsurprising given that DSBs are not formed in a *crc1* mutant [38]. Nevertheless, studies indicate that CRC1 localizes to the central region of the SC at pachytene and interacts with the SC transverse filament protein ZEP1 in a yeast two-hybrid assay, suggesting it is a component of the SC [38]. Analysis of the *Atpch2* mutants indicates that PCH2 plays a critical role in formation of the SC, since loss of the protein results in a substantial defect in polymerization of the SC transverse filament protein ZYP1. An average reduction in SC length of 68% was observed but this was quite variable ranging from 43% to 87%. Similar to rice, co-localization between PCH2 and ZYP1 is also observed from the beginning of zygotene through pachytene. In *Atasy1* and *Atasy3* mutants, where SC polymerization is compromised, PCH2 is associated with the residual ZYP1 signal. Association of ZYP1 and PCH2 is also supported by SIM analysis of the *B. oleracea* SC as it begins to extend, although this suggests that they are not forming a homogeneous complex. This could reflect that any interaction between the proteins is transient. Since ASY1 appears to be the target for PCH2, it is conceivable that ZYP1 or another component of the SC central region acts to couple/guide the PCH2/ASY1 interaction. A precedent for this is seen in the bacterial P1 plasmid partitioning system in which the ParA ATPase is functionally coupled by the ParB protein to move its plasmid DNA cargo via a diffusion-ratchet mechanism [68]. Furthermore the interaction between the *C. elegans* PCH2 ortholog, PCH-2, and the

HORMAD spindle checkpoint protein Mad2, has been shown to involve an adaptor protein, p31 [69].

The SC nucleations seen in *B. oleracea* were consistent in size and their arrowhead-like shape is likely a consequence of the convergence of the homolog axes at the synaptic site. It is noteworthy that in most nuclei examined the number of large foci is broadly similar to the chiasma frequency (13–15) in *B. oleracea* [70,71]. Moreover most of the arrowhead-like ZYP1 foci (86.0%) co-localized with HEI10, a further indication that they occur at designated CO sites. Nuclei with fewer large foci may have been at a slightly earlier stage and reflect the dynamic nature of the initial appearance of foci. The smaller, slightly more numerous ZYP1 foci that were also present at early zygotene are likely to be additional synapsis initiation sites. The apparent existence of two classes of SC nucleation structures is reminiscent of observations in *S. macrospora* [72]. These have revealed distinct types of designations, one defining SC nucleation sites that correspond to CO designated recombination events and another that defines a similar number of sites where SC nucleation alone occurs. Importantly, the distribution of both classes exhibit interference and fits the prediction of the ‘beam-film’ model [11,12]. This posits that mechanical stress arises within a chromatin-axis meshwork as a result of global chromatin expansion during leptotene. Subsequent bi-directional relief of this stress results in a set of CO designations (and SC nucleations) that are spatially separated along the chromosomes. Further studies will be required to establish if the observed SC nucleations in *B. oleracea* also reflect a corresponding underlying interference-dependent distribution.

In other species loss of PCH2 orthologs leads to a variety of different effects on synapsis. In mouse, mutation of the Pch2 ortholog TRIP13 also results in a synaptic defect, albeit less severe than in Arabidopsis, with the unsynapsed regions accounting for just under 30% of the total axis length [34]. Loss of Pch2 in budding yeast does not appear to affect SC formation [27]. However, budding yeast forms high levels of COs and each designated CO site is thought to nucleate SC formation [73]. Hence, loss of Pch2 may not impact on SC installation to the degree observed in Arabidopsis where the relative CO rates are far lower. PCH2 also impacts on SC formation in *C. elegans* but in this case SC formation occurs more quickly than in wild type [37]. Interestingly, this defect was suppressed at lower temperatures. Thus loss of Pch2 has differing effects on the extent of SC polymerization in different species but in each case is associated with a recombination defect. Together, these observations suggest that PCH2 is not an integral structural component of the SC and more likely, regulates the coordination of synapsis with the controlled formation of COs.

Early recombination pathway events appear normal and DSBs are repaired in *Atpch2-1*

The controlled formation of COs via homologous recombination is an essential feature of meiosis. Studies of PCH2 in several species have linked loss of the protein to a variety of recombination defects. In the most severe case, loss of the rice PCH2 ortholog, CRC1, is reported to result in a failure to form DSBs [38]. In budding yeast, a minor role for Pch2 in DSB formation has been reported [74]. It is also involved in processing of early occurring, low abundance DSBs and loss of the protein leads to a coordinate delay in the repair of DSBs to form both CO and NCO products [27,28].

In mouse, studies suggest that a severe reduction in TRIP13 expression does not compromise DSB formation but loading of RAD51 onto the resected DSBs is reduced [34]. In Arabidopsis, immunolocalization of RAD51 and DMC1 in *Atpch2-1* PMCs indicated that early stages in recombination occur normally. As there is no evidence of chromosome fragmentation, it seems DSBs are also repaired, albeit with a reduction in CO formation, but progression

through prophase I is delayed by 5–8h. This is reminiscent of that seen in some meiotic mutants and is indicative of an underlying defect in the recombination pathway [20,43,64]. Since a significant reduction in CO frequency was observed in an *Atpch2/Atmsh5* double mutant relative to an *Atmsh5* mutant it appears that loss of PCH2 impacts on the formation of both Class I and Class II COs.

CO interference is likely established in *Atpch2-1* but maturation of designated COs appears defective

Studies in different species have reported a CO interference defect associated with mutation of *Pch2/TRIP13*. Genetic analysis in budding yeast using intervals across a range of chromosomes of different sizes has revealed an increased frequency of closely spaced double-CO events in the absence of Pch2 [28,31]. In a *Trip13* hypomorphic mutant mouse, despite an overall reduction in MLH1 foci at pachytene, a small, yet significant, reduction in the mean inter-focus distance between pairs of foci was observed. This implies that although the COs remain subject to interference, there has been some weakening in its effect, although a subtle change in the positioning of the DSB complexes cannot be excluded [34]. Despite these observations recent evidence from budding yeast has found that inter-focus distance of Zip3 foci that mark future COs is not affected by loss of Pch2, indicating CO interference is normal [32]. Why the discrepancy? Zip3 foci are the earliest known marker of CO designation, appearing in late leptotene. However, maturation of designated intermediates to form COs is dependent on additional later events during the remainder of prophase I [5]. Other analyses of *pch2* mutants have used genetic markers or MLH1 foci, which mark mature CO sites. Hence it is conceivable that while loss of Pch2/Trip13 affects the final CO patterning, CO designation occurs and hence interference is initially established. Analysis of *Atpch2-1* is consistent with this possibility. The localization of HEI10 foci in wild type and *Atpch2-1* at early prophase I was identical. Numerous small axis-associated foci were observed together with around 10 large (~250 nm) foci. At present, it is not technically possible to measure inter-focus distance at early prophase I in Arabidopsis, nevertheless inspection of the nuclei reveals these large HEI10 foci are usually spatially well separated. These are still observed at mid/late prophase I when a similar number of MLH1 foci, which mark interference sensitive CO sites, are also observed. By analogy with budding yeast and *S. macrospora* where the appearance of Zip3/Hei10 foci are indicative of CO designation in early prophase I, it seems likely this is also the case in Arabidopsis as the number of HEI10 foci at the leptotene/zygotene transition appeared normal in the absence of PCH2. However, the maturation of the CO designated intermediates is compromised by the defect in remodelling of the chromosomes axes in *Atpch2-1*, leading to a deficit in COs. Overall, our data imply that in Arabidopsis, as in budding yeast and *S. macrospora*, CO designation and interference arise, and are complete, during zygotene.

We noted that in both wild type and *Atpch2-1* some MLH1 foci appeared adjacent to the ZYP1 signal rather than directly over it. This has not been previously recorded in Arabidopsis. It may be a consequence of the spreading procedure but it is worth noting that in this study, the anti-ZYP1 antibody was raised to the N-terminus of the protein which is predicted to mark the central region of the SC. This could suggest the MLH1 containing complexes are not in direct contact with the SC central region. However the basis and significance of this remains unclear.

Other features of the CO distribution in the mutants indicate that CO interference is established. A predicted outcome of CO interference is that the numerical distribution of interference-sensitive COs between nuclei does not fit a Poisson distribution, whereas the converse applies for non-interfering COs [56]. The distribution of COs in *Atpch2-1* does not fit a

Poisson distribution, suggesting that COs remain subject to spatial patterning and do not arise by the random maturation of a proportion of the recombination initiations into COs. Also, there was a strong tendency for any HEI10 or MLH1 foci that were found associated with stretches of SC in *Atpch2-1* to occur as single foci.

Although the data indicate that CO designation occurs normally, it seems that precursor maturation to form CO products is perturbed in *Atpch2*. This is manifested in several ways. Most obviously, the mean chiasma frequency in *Atpch2* mutants is ~ 7 , a reduction of around 30% relative to wild type. This is accompanied by the presence of univalents at metaphase I at a frequency of $\sim 10\%$. A global reduction in CO formation has also been reported in TRIP13/Pch2-deficient mice and PCH2-deficient *C. elegans* [34,37]. In budding yeast, an increase in COs has been reported for some genetic intervals whereas in others wild type levels were recorded [31]. Also, the distribution of MLH1 foci in the mouse *Trip13* mutants suggests there are chromosomal regions which show an increase in CO frequency [34]. This could suggest variation between different species but it is worth noting that despite the global reduction in COs in the absence of PCH2 an increase in recombination frequency was observed in 3 out of 6 intervals (I2f, I2g and I5b) in the Arabidopsis FTL lines used in this study. However, this comes with the caveat that this approach scores only viable tetrads which could influence the analysis. Estimation of genetic CO interference using the FTL lines suggested its effect may be diminished in at least some chromosomal regions, since a reduction in strength was detected over regions of chromosome 2 and chromosome 5. This apparent contradiction with the cytological evidence can perhaps be reconciled by data from a study of CO patterning in *S. macrospora* applying the beam-film model to experimental data. This showed that under some circumstances a normal interference signal is established and remains, yet CO interference as measured using CoC as a metric appears to be reduced [7,72].

An altered pattern of COs combined with a synaptic defect and a reduction in genetic interference has been reported in a kinesin mutant, *Atpss1*, and *Ataxr1*, a mutant in the E1 enzyme Arabidopsis neddylation complex [55,75]. Both mutants are strongly defective in synapsis with univalents observed at metaphase I. In each case HEI10 and MLH1 foci are observed in late prophase I in approximately wild type numbers but, in contrast to *Atpch2-1*, often clustered along the limited stretches of SC that have formed. An effect on the distribution of MLH1 foci has also been reported in *as1*, an asynaptic mutant of tomato [76]. The genetic basis of the *as1* mutation is unknown but it is associated with changes in compaction of the chromosome axes. Relative to wild type, the average SC length in *as1* was reduced by 81% with MLH1 inter-focus distance decreased by 71%. However the median number of MLH1 foci was unchanged, although the range was more variable. It is hypothesized that the tendency of these plant mutants to maintain CO numbers may reflect a homeostatic mechanism [76]. This is not so obvious in *Atpch2-1* but it was notable that the mean reduction in CO frequency ($\sim 30\%$) was not-coordinate with that in SC length ($\sim 68\%$).

This study demonstrates that in the absence of PCH2, remodelling of the chromosome axis at zygotene and the normal patterned maturation of CO designated intermediates in Arabidopsis are aberrant. This further emphasises the functional inter-relationship between the chromosome axis and the controlled formation of COs.

Materials and Methods

Plant material and nucleic acid extraction

A. thaliana ecotype Columbia (0) was used for wild type analysis. T-DNA insertion lines *Atpch2-1*: SAIL_1187_C06, *Atpch2-2*: SALK_031449 and *Atpch2-3*: SALK_130138 were

obtained from NASC for mutant analysis. Plants were grown, material harvested and nucleic acid extractions were performed as previously described by Higgins et al. [43].

Proteomic analysis of Brassica PMCs

AtPCH2 peptides were identified by mass spectrometry in protein extracts from *Brassica oleracea* var. *alboglabra* A12DHD PMCs following co-immunoprecipitation with affinity purified anti-ASY1 antibody as previously described [40].

T-DNA insertion site mapping

The T-DNA insertion site of the mutant lines was confirmed as previously described [43]. Details of the primers used are presented in [S3 Table](#).

RNA extraction and RT-PCR

RNA extraction and RT-PCR was carried out as previously described [43]. Details of the primers are given in [S3 Table](#).

Nucleic acid sequencing

Nucleotide sequencing was carried out by the Genomics and Proteomics Unit, School of Biosciences, University of Birmingham, UK.

Antibody production

An anti-PCH2 antibody was raised in rabbit against a 15-residue peptide from the C-terminus of Arabidopsis PCH2 (Abmart Inc., Shanghai, China). Due to the high level of sequence identity between the PCH2 proteins in Arabidopsis and Brassica the antibody was also effective for immunolocalization in Brassica.

Cytological procedures

Cytological studies were carried out as previously described [43]. The following antibodies were used: anti-AtPCH2 (rat 1/200 dilution), anti-AtASY3 (rabbit, 1/200 dilution) [19], anti-AtASY1 (rabbit/rat, 1/1000 dilution) [45], anti-AtMSH4 (rabbit, 1/500 dilution) [43], anti-AtZYP1 (N-terminus Ab aa residues 1–415; C-terminus Ab aa residues 422–845; rabbit/rat, 1/500 dilution), anti-AtRAD51 (rabbit 1/500 dilution), anti-AtSYN1 (rabbit 1/500 dilution), anti-AtDMC1 (rabbit 1/500 dilution) [20,23], anti-AtMLH1 (rabbit/rat, 1/200 dilution) [64], anti-AtHEI10 (rabbit 1/500 dilution) and anti- γ H2AX (ser 139, catalog no. 07–164 Upstate Biotechnology; rabbit, 1/100 dilution). Microscopy was carried out using a Nikon 90i Fluorescence Microscope (Tokyo, Japan). Image capture, image analysis and processing were conducted using NIS-Elements-F software (Nikon, Tokyo, Japan) as previously described [19]. Image deconvolution was carried out using the function “Mexican hat”. This allows better discrimination of the signals. This function performs filtration on the intensity component (or on every selected component—when working with multichannel images) of an image using convolution with 5x5 kernel. Mexican Hat kernel is defined as a combination of Laplacian kernel and Gaussian kernel it marks edges and also reduces noise. SIM was carried out using the OMX facility at the University of Dundee (<http://microscopy.lifesci.dundee.ac.uk/omx/>).

In Arabidopsis, ASY1 intensity analysis was conducted on chromosome spread preparations stained with anti-ASY1 antibody (rat, 1 in 5000 dilution) and anti-ZYP1 (rabbit, 1 in 500 dilution). 5 μ l of 6 μ m, 0.3% relative intensity InSpeck Red microspheres (Life Technologies), were added to slides before coverslips. PMCs and microspheres were imaged using specific exposure

times. Randomly selected, non-overlapping sections of axis, ~2–4 μ m in length, were defined as regions of interest and were analysed for mean signal intensity using Nikon NIS-elements software. Intensities were normalised based on mean intensity of the microspheres. Intensity raw data is shown in grey-scale values. For *B. oleracea*, ASY1 intensity was determined in on PMC chromosome spreads at zygotene comparing non-overlapping segments of unsynapsed and synapsed sections of axis ~2–4 μ m in length.

Chiasma counts were carried out as previously described [42]. Chromosome spread preparations from PMCs at metaphase I were examined by light microscopy after fluorescence *in situ* hybridization (FISH) using 45S and 5S rDNA probes. The use of FISH enabled the identification of individual chromosomes. The overall shape of individual bivalents allowed the number and position of individual chiasmata to be determined and this was also informed by the position of the FISH signals.

The time course of progress through prophase I in wild type and *Atpch2-1* was determined as previously described [48] except that 5-ethynyl-2'-deoxyuridine (EdU) was used to label the PMCs which were analyzed at 5 h intervals from 0–30 h and at 2 h intervals thereafter up to 36 h.

Fluorescent tetrad analysis was carried out as described Berchowitz and Copenhaver [49] using genetic intervals I2f and I2g on chromosome 2 (FTL coordinates for the I2fg interval: FTL#800 18286716 bp DsRed2; FTL#3411 18957093 bp YFP; FTL#3263 19373634 bp AmCyan) and I5a, I5b, I5c, and I5d on chromosome 5 as described [49]. Pollen was scored through eCFP, eYFP and DsRed2 filters using an Olympus BX-61 epifluorescence microscope. The Stahl Lab Online Tools (<http://molbio.uoregon.edu/~fstahl/>) was used for statistical analyses of the data.

Statistical procedures

The statistical procedures were carried out as described previously [43]. Chi-squared (X^2) tests were used to determine agreement between the observed chiasma counts and those expected from a Poisson distribution. Numbers of foci in wild type and mutant PMCs were compared using the Wilcoxon signed-rank test. Mean intensities between synapsed and unsynapsed sections of axis/SC were analysed using a 2 tail paired T-test.

Supporting Information

S1 Fig. PCH2 peptide coverage and orthologs. (A) Sequence coverage of the predicted protein product of Bra013827 (yellow highlight). (B) Cladogram derived from ClustalW2 analysis of AAA+ATPase proteins from *A. thaliana*. At4g24710 belongs to a sub-family which also includes Bra013827 and PCH2 homologues from budding yeast (ScPCH2), mouse (MmTRIP13) and rice (OsCRC1). During the course of this work the sequence of two *B. oleracea* PCH2 orthologues became available (Liu et al. 2014; Parkin et al. 2014) and are included in the analysis.

(TIF)

S2 Fig. Structure and expression of PCH2. (A) Schematic illustration of Arabidopsis PCH2 protein. *AtPCH2* is predicted to encode a protein of 475 amino acids with a putative AAA-ATPase domain located between amino acids 213 and 358. (B) Map of *AtPCH2* locus showing the exon/intron organization. Exons are represented with black boxes. 3' UTR region is represented with a blue box. Triangles represent the location of T-DNA insertion sites for all three *Atpch2* mutants. Red arrows mark the position of the primers used for detecting the full-length *AtPCH2* transcript by RT-PCR. (C) Gene expression analysis of *AtPCH2* using semi-

quantitative RT-PCR from wild type and *Atpch2-1*, *Atpch2-2* and *Atpch2-3* bud tissues. The amount of RNA used for each sample was equalized using the housekeeping gene *AtGAPD*. *AtPCH2* was expressed in wild type buds while no full length transcript was detected in *Atpch2* mutants.

(TIF)

S3 Fig. Nucleotide sequencing of the T-DNA insertion sites in *Atpch2* mutants.

(TIF)

S4 Fig. Phenotype of *Atpch2* mutants. (A) Vegetative growth is normal but fertility is reduced in *Atpch2* mutants. Bar = 5 cm. (B) Silique length is slightly reduced and numerous gaps are observed between the seeds in *Atpch2* mutants. Bar = 1 cm. (C) Graph showing the mean seed-set per silique from 50 siliques of wild type Arabidopsis and *Atpch2* mutants. Error bars represent the standard deviation. Black stars represent a mean statistical difference between wild type and mutant.

(TIF)

S5 Fig. Reduced fertility and meiotic defects in *Atpch2-2* and *Atpch2-3* mutants. (A-D) Meiotic stages in *Atpch2-2* mutant. (A) late prophase I; (B) metaphase I; (C) tetrad; (D) metaphase I nucleus labelled with 5S (red) and 45S (green) rDNA probes. (E-H) Meiotic stages in *Atpch2-3* mutant. (E) late prophase I; (F) metaphase I; (G) tetrad; (H) metaphase I nucleus labelled with 5S (red) and 45S (green) rDNA probes. Bar = 10 μ m. (I-M) Allelism test showing that *Atpch2-1/Atpch2-2* has similar meiotic defects as *Atpch2-1* mutant. Chromosome spread preparations of *Atpch2-1/Atpch2-2* PMCs at late prophase I (I); metaphase I (J) and dyad (K). Graph showing the mean silique length (L) and mean seed-set per silique (M) from 50 siliques of wild type, *Atpch2-1/Atpch2-2* and *Atpch2-1* mutants. Error bars represent the standard deviation. Black stars represent a mean statistical difference between wild type and mutant.

(TIF)

S6 Fig. Metaphase I chromosome spreads in *Atmsh5-1* and *Atmsh5-1/Atpch2-1* PMCs.

(A-C) Chromosome spread preparation of wild type (A), *Atmsh5-1* (B) and *Atmsh5-1/Atpch2-1* (C) PMCs at metaphase I stage. Chromatin was stained with DAPI (blue) and the chromosomes were labelled with 5S (red) and 45S (green) rDNA FISH probes to facilitate the identification of individual chromosomes. The five bivalents were identified and numbered (white), shown for the wild type nucleus. Bar = 10 μ m.

(TIF)

S7 Fig. Immunolocalization of axis proteins in wild type and *Atpch2-1*. (A,B) Immunolocalization of SYN1 (green) on chromosome spread preparations of wild type (A) and *Atpch2-1* mutant (B) PMCs. (C,D) Immunolocalization of ASY3 (green) on chromosome spread preparations of wild type (C) and *Atpch2-1* mutant (D) PMCs. DNA is stained with DAPI (blue).

Bar = 10 μ m.

(TIF)

S8 Fig. ASY1 has an off-axis, chromatin associated localization along synapsed chromosomes in wild type PMCs. (A) Dual localization of ASY1 (green) and ZYP1 (red) on a chromosome spread of an Arabidopsis PMC at zygotene. (B) Localization of ASY1 (green) on chromosome spread of the same meiotic nucleus as A. DNA is stained with DAPI (blue). Scale bar = 10 μ m. (C) shows magnified sections of axes from A and B. Arrowheads indicate the off-axis, chromatin associated signal of ASY1. Scale bar = 1 μ m.

(TIF)

S9 Fig. Quantification of axis associated ASY1 in synapsed and unsynapsed regions. (A) Example immunostained wild type PMC with a fluorescent microsphere control used for calibration (see [Materials and Methods](#) for details); (B) Brighter version of (A) to highlight the PMC; (C-F) Sections of axis (stained as indicated) were analysed for quantification of ASY1 signal intensity. In wild type PMCs (C,D), ASY1 signal intensity is reduced in synapsed chromosome regions (red dotted outline) compared to unsynapsed regions (yellow dotted outline). Chromosomes in *Atpch2-1* PMCs (E,F) show no such reduction. Scale bar = 5µm.
(TIF)

S10 Fig. Co-localization of PCH2 and ZYP1 in wild type and chromosome axis mutants. (A-C) Immunolocalization of ZYP1 (green) and PCH2 (red) in wild type at early zygotene. (D-F) Immunolocalization of ZYP1 (green) and PCH2 (red) in an *Atasy1* nucleus at mid-prophase I. (G-I) Immunolocalization of ZYP1 (green) and PCH2 (red) in an *Atasy3* nucleus at mid-prophase I. DNA is stained with DAPI (blue). Bar = 10 µm.
(TIF)

S11 Fig. PCH2 is not detected in *Atpch2* mutants. (A-C) Immunolocalization of PCH2 (red) on chromosome spreads from *Atpch2-1* (A), *Atpch2-2* (B) and *Atpch2-3* (C) nuclei at mid/late prophase I. DNA is stained with DAPI (blue). Bar = 10 µm.
(TIF)

S12 Fig. Immunolocalization of PCH2 in wild type *B. oleracea* PMCs. (A) Co-localization of ASY1 (green) and PCH2 (red) at late G2 and (B) early leptotene using SIM. (C) Co-localization of ASY1 (green) and PCH2 (red) at late zygotene using SIM. On synapsed regions (boxed region and corresponding inset which has been brightened for clarity of PCH2 foci and residual ASY1 signal) the ASY1 signal strength is reduced relative to remaining unsynapsed axes (arrowed). (D) Co-localization of ZYP1 (green) and PCH2 (red) at pachytene using SIM. DNA is stained with DAPI (blue). Bar = 10 µm.
(TIF)

S13 Fig. Prophase I progression is delayed in *Atpch2-1*. (A) Comparison of progression through prophase I in wild type and *Atpch2-1* PMCs reveals a delay of 5-8h in the mutant. (B) Examples of samples taken at different time points showing the extent of meiotic progression. (Note: as synapsis was incomplete in *Atpch2-1*, fully synapsed pachytene nuclei were not observed).
(TIF)

S14 Fig. FTL analysis. (A) Map indicating the position on the chromosomes of the genetic markers used to measure the recombination frequency. (B) Table showing the location and size of the six FTL genetic intervals used in this study. (C) Tetrad pollen expressing the fluorescent proteins were classified into 12 groups based on the distribution of the fluorescent proteins in the tetrad. A schematic representation of the expected patterns of the fluorescent proteins in the tetrad pollen after recombination events is shown for each group.
(TIF)

S15 Fig. Co-immunolocalization of ZYP1 and HEI10 in wild type *B. oleracea* PMCs at the leptotene/zygotene transition. A-D Dual localization of ZYP1 (green) and HEI10 (red) on chromosome spread preparations of *B. oleracea* PMCs at the leptotene/zygotene transition. White arrows in C and D indicate examples of ZYP1 and HEI10 colocalization at SC nucleation sites. DNA is stained with DAPI (blue). Bar = 10 µm.
(TIF)

S1 Table. ASY1 intensity measurements on synapsed and unsynapsed regions in wild type and *Atpch2-1* PMCs.

(PDF)

S2 Table. Tables showing the recombination frequency (f) of the adjacent sets of genetic intervals I5a/b, I5c/d and I2f/g and their coefficient of coincidence (CoC) in wild type and *Atpch2-1*.

(TIF)

S3 Table. Primer sequences used during this study. Primer pairs 1–2, 3–4, 5–6 were used to map the T-DNA insertions site of *Atpch2-1*, *Atpch2-2* and *Atpch2-3* respectively. Primers 4,6–8 were used for the analysis of *AtPCH2* expression. Primers 1,3,5, 9–14 were used for genotyping.

(TIF)

Acknowledgments

Horticultural and technical support was provided by Karen Staples and Steve Price, University of Birmingham. We would like to thank Dr Markus Posch at the University of Dundee for his expert technical assistance with OMX imaging. We thank the reviewers and appreciate their helpful and constructive comments.

Author Contributions

Conceived and designed the experiments: FCHF CL KO JDH. Performed the experiments: CL KO KM AW KN ER. Analyzed the data: CL KO JDH KN KM JY AW SJA FCHF. Contributed reagents/materials/analysis tools: GPC. Wrote the paper: FCHF CL KO GPC JDH.

References

1. Zickler D, Kleckner N (1998) The leptotene-zygotene transition of meiosis. *Annual Review of Genetics* 32: 619–697. PMID: [9928494](#)
2. Keeney S, Giroux CN, Kleckner N (1997) Meiosis-specific DNA double-strand breaks are catalyzed by Spo11, a member of a widely conserved protein family. *Cell* 88: 375–384. PMID: [9039264](#)
3. Bergerat A, deMassy B, Gadelle D, Varoutas PC, Nicolas A, et al. (1997) An atypical topoisomerase II from archaea with implications for meiotic recombination. *Nature* 386: 414–417. PMID: [9121560](#)
4. Mancera E, Bourgon R, Brozzi A, Huber W, Steinmetz LM (2008) High-resolution mapping of meiotic crossovers and non-crossovers in yeast. *Nature* 454: 479–U471. doi: [10.1038/nature07135](#) PMID: [18615017](#)
5. Osman K, Higgins JD, Sanchez-Moran E, Armstrong SJ, Franklin FCH (2011) Pathways to meiotic recombination in *Arabidopsis thaliana*. *New Phytologist* 190: 523–544. doi: [10.1111/j.1469-8137.2011.03665.x](#) PMID: [21366595](#)
6. Jones GH, Franklin FC (2006) Meiotic crossing-over: obligation and interference. *Cell* 126: 246–248. PMID: [16873056](#)
7. Wang S, Zickler D, Kleckner N, Zhang L (2015) Meiotic crossover patterns: Obligatory crossover, interference and homeostasis in a single process. *Cell cycle (Georgetown, Tex)* 14: 305–314.
8. Copenhagen GP, Housworth EA, Stahl FW (2002) Crossover interference in *Arabidopsis*. *Genetics* 160: 1631–1639. PMID: [11973316](#)
9. Shinohara M, Oh SD, Hunter N, Shinohara A (2008) Crossover assurance and crossover interference are distinctly regulated by the ZMM proteins during yeast meiosis. *Nature Genetics* 40: 299–309. doi: [10.1038/ng.83](#) PMID: [18297071](#)
10. Sturtevant AH (1915) The behavior of chromosomes as studied through linkage. *Z Induct Abstammungs-Vererbungs*, 13: 234–287.
11. Kleckner N, Zickler D, Jones GH, Dekker J, Padmore R, et al. (2004) A mechanical basis for chromosome function. *Proceedings of the National Academy of Sciences of the United States of America* 101: 12592–12597. PMID: [15299144](#)

12. Zhang L, Liang Z, Hutchinson J, Kleckner N (2014) Crossover Patterning by the Beam-Film Model: Analysis and Implications. *Plos Genetics* 10.
13. Kleckner N (2006) Chiasma formation: chromatin/axis interplay and the role(s) of the synaptonemal complex. *Chromosoma* 115: 175–194. PMID: [16555016](#)
14. Blat Y, Protacio RU, Hunter N, Kleckner N (2002) Physical and Functional Interactions among Basic Chromosome Organizational Features Govern Early Steps of Meiotic Chiasma Formation. *Cell* 111: 791–802. PMID: [12526806](#)
15. Panizza S, Mendoza MA, Berlinger M, Huang L, Nicolas A, et al. (2011) Spo11-Accessory Proteins Link Double-Strand Break Sites to the Chromosome Axis in Early Meiotic Recombination. *Cell* 146: 372–383. doi: [10.1016/j.cell.2011.07.003](#) PMID: [21816273](#)
16. Page SL, Hawley RS (2004) The genetics and molecular biology of the synaptonemal complex. *Annual Review of Cell and Developmental Biology* 20: 525–558. PMID: [15473851](#)
17. Fung JC, Rockmill B, Odell M, Roeder GS (2004) Imposition of crossover interference through the non-random distribution of synapsis initiation complexes. *Cell* 116: 795–802. PMID: [15035982](#)
18. Boerner GV, Kleckner N, Hunter N (2004) Crossover/noncrossover differentiation, synaptonemal complex formation, and regulatory surveillance at the leptotene/zygotene transition of meiosis. *Cell* 117: 29–45. PMID: [15066280](#)
19. Ferdous M, Higgins JD, Osman K, Lambing C, Roitinger E, et al. (2012) Inter-Homolog Crossing-Over and Synapsis in Arabidopsis Meiosis Are Dependent on the Chromosome Axis Protein AtASY3. *Plos Genetics* 8.
20. Higgins JD, Sanchez-Moran E, Armstrong SJ, Jones GH, Franklin FCH (2005) The Arabidopsis synaptonemal complex protein ZYP1 is required for chromosome synapsis and normal fidelity of crossing over. *Genes Dev* 19: 2488–2500. PMID: [16230536](#)
21. Kim KP, Weiner BM, Zhang LR, Jordan A, Dekker J, et al. (2010) Sister Cohesion and Structural Axis Components Mediate Homolog Bias of Meiotic Recombination. *Cell* 143: 924–937. doi: [10.1016/j.cell.2010.11.015](#) PMID: [21145459](#)
22. Mao-Draayer Y, Galbraith AM, Pittman DL, Cool M, Malone RE (1996) Analysis of meiotic recombination pathways in the yeast *Saccharomyces cerevisiae*. *Genetics* 144: 71–86. PMID: [8878674](#)
23. Sanchez-Moran E, Santos JL, Jones GH, Franklin FCH (2007) ASY1 mediates AtDMC1-dependent interhomolog recombination during meiosis in Arabidopsis. *Genes & Development* 21: 2220–2233.
24. Schwacha A, Kleckner N (1997) Interhomolog bias during meiotic recombination: Meiotic functions promote a highly differentiated interhomolog-only pathway. *Cell* 90: 1123–1135. PMID: [9323140](#)
25. Xu LH, Weiner BM, Kleckner N (1997) Meiotic cells monitor the status of the interhomolog recombination complex. *Genes & Development* 11: 106–118.
26. Storlazzi A, Tesse S, Ruprich-Robert G, Gargano S, Poeggeler S, et al. (2008) Coupling meiotic chromosome axis integrity to recombination. *Genes & Development* 22: 796–809.
27. Boerner GV, Barot A, Kleckner N (2008) Yeast Pch2 promotes domainal axis organization, timely recombination progression, and arrest of defective recombinosomes during meiosis. *Proceedings of the National Academy of Sciences of the United States of America* 105: 3327–3332. doi: [10.1073/pnas.0711864105](#) PMID: [18305165](#)
28. Joshi N, Barot A, Jamison C, Boerner GV (2009) Pch2 Links Chromosome Axis Remodeling at Future Crossover Sites and Crossover Distribution during Yeast Meiosis. *Plos Genetics* 5.
29. Zanders S, Brown MS, Chen C, Alani E (2011) Pch2 Modulates Chromatid Partner Choice During Meiotic Double-Strand Break Repair in *Saccharomyces cerevisiae*. *Genetics* 188: 511–521. doi: [10.1534/genetics.111.129031](#) PMID: [21515575](#)
30. Ho H-C, Burgess SM (2011) Pch2 Acts through Xrs2 and Tel1/ATM to Modulate Interhomolog Bias and Checkpoint Function during Meiosis. *Plos Genetics* 7.
31. Zanders S, Alani E (2009) The pch2 Delta Mutation in Baker's Yeast Alters Meiotic Crossover Levels and Confers a Defect in Crossover Interference. *Plos Genetics* 5.
32. Zhang L, Wang S, Yin S, Hong S, Kim KP, et al. (2014) Topoisomerase II mediates meiotic crossover interference. *Nature* 511: 551–556. doi: [10.1038/nature13442](#) PMID: [25043020](#)
33. Li X, Schimenti JC (2007) Mouse pachytene checkpoint 2 (Trip13) is required for completing meiotic recombination but not Synapsis. *Plos Genetics* 3: 1365–1376.
34. Roig I, Dowdle JA, Toth A, de Rooij DG, Jasin M, et al. (2010) Mouse TRIP13/PCH2 Is Required for Recombination and Normal Higher-Order Chromosome Structure during Meiosis. *Plos Genetics* 6.
35. Wojtasz L, Daniel K, Roig I, Bolcun-Filas E, Xu HL, et al. (2009) Mouse HORMAD1 and HORMAD2, Two Conserved Meiotic Chromosomal Proteins, Are Depleted from Synapsed Chromosome Axes with the Help of TRIP13 AAA-ATPase. *Plos Genetics* 5.

36. Joyce EF, McKim KS (2009) *Drosophila* PCH2 Is Required for a Pachytene Checkpoint That Monitors Double-Strand-Break-Independent Events Leading to Meiotic Crossover Formation. *Genetics* 181: 39–51. doi: [10.1534/genetics.108.093112](https://doi.org/10.1534/genetics.108.093112) PMID: [18957704](https://pubmed.ncbi.nlm.nih.gov/18957704/)
37. Deshong AJ, Ye AL, Lamelza P, Bhalla N (2014) A Quality Control Mechanism Coordinates Meiotic Prophase Events to Promote Crossover Assurance. *Plos Genetics* 10.
38. Miao C, Tang D, Zhang H, Wang M, Li Y, et al. (2013) CENTRAL REGION COMPONENT1, a Novel Synaptonemal Complex Component, Is Essential for Meiotic Recombination Initiation in Rice. *Plant Cell* 25: 2998–3009. doi: [10.1105/tpc.113.113175](https://doi.org/10.1105/tpc.113.113175) PMID: [23943860](https://pubmed.ncbi.nlm.nih.gov/23943860/)
39. Nonomura KI, Nakano M, Murata K, Miyoshi K, Eiguchi M, et al. (2004) An insertional mutation in the rice PAIR2 gene, the ortholog of Arabidopsis ASY1, results in a defect in homologous chromosome pairing during meiosis. *Molecular Genetics and Genomics* 271: 121–129. PMID: [14758540](https://pubmed.ncbi.nlm.nih.gov/14758540/)
40. Osman K, Roitinger E, Yang J, Armstrong S, Mechtler K, et al. (2013) Analysis of meiotic protein complexes from Arabidopsis and Brassica using affinity-based proteomics. *Methods in molecular biology* (Clifton, NJ) 990: 215–226.
41. Wang X, Wang H, Wang J, Sun R, Wu J, et al. (2011) The genome of the mesopolyploid crop species Brassica rapa. *Nature Genetics* 43: 1035–U1157. doi: [10.1038/ng.919](https://doi.org/10.1038/ng.919) PMID: [21873998](https://pubmed.ncbi.nlm.nih.gov/21873998/)
42. Sanchez-Moran E, Armstrong SJ, Santos JL, Franklin FCH, Jones GH (2002) Variation in chiasma frequency among eight accessions of Arabidopsis thaliana. *Genetics* 162: 1415–1422. PMID: [12454084](https://pubmed.ncbi.nlm.nih.gov/12454084/)
43. Higgins JD, Armstrong SJ, Franklin FCH, Jones GH (2004) The Arabidopsis MutS homolog AtMSH4 functions at an early step in recombination: evidence for two classes of recombination in Arabidopsis. *Genes & Development* 18: 2557–2570.
44. Higgins JD, Buckling EF, Franklin FCH, Jones GH (2008) Expression and functional analysis of AtMUS81 in Arabidopsis meiosis reveals a role in the second pathway of crossing-over. *Plant Journal* 54: 152–162. doi: [10.1111/j.1365-313X.2008.03403.x](https://doi.org/10.1111/j.1365-313X.2008.03403.x) PMID: [18182028](https://pubmed.ncbi.nlm.nih.gov/18182028/)
45. Armstrong SJ, Caryl AP, Jones GH, Franklin FC (2002) Asy1, a protein required for meiotic chromosome synapsis, localizes to axis-associated chromatin in Arabidopsis and Brassica. *J Cell Sci* 115: 3645–3655. PMID: [12186950](https://pubmed.ncbi.nlm.nih.gov/12186950/)
46. Bai XF, Peirson BN, Dong FG, Xue C, Makaroff CA (1999) Isolation and characterization of SYN1, a RAD21-like gene essential for meiosis in Arabidopsis. *Plant Cell* 11: 417–430. PMID: [10072401](https://pubmed.ncbi.nlm.nih.gov/10072401/)
47. Cai X, Dong FG, Edelmann RE, Makaroff CA (2003) The Arabidopsis SYN1 cohesin protein is required for sister chromatid arm cohesion and homologous chromosome pairing. *Journal of Cell Science* 116: 2999–3007. PMID: [12783989](https://pubmed.ncbi.nlm.nih.gov/12783989/)
48. Armstrong SJ, Franklin FCH, Jones GH (2003) A meiotic time-course for Arabidopsis thaliana. *Sexual Plant Reproduction* 16: 141–149.
49. Berchowitz LE, Copenhaver GP (2008) Fluorescent Arabidopsis tetrads: a visual assay for quickly developing large crossover and crossover interference data sets. *Nature Protocols* 3: 41–50. doi: [10.1038/nprot.2007.491](https://doi.org/10.1038/nprot.2007.491) PMID: [18193020](https://pubmed.ncbi.nlm.nih.gov/18193020/)
50. Francis KE, Lam SY, Harrison BD, Bey AL, Berchowitz LE, et al. (2007) Pollen tetrad-based visual assay for meiotic recombination in Arabidopsis. *Proceedings of the National Academy of Sciences of the United States of America* 104: 3913–3918. PMID: [17360452](https://pubmed.ncbi.nlm.nih.gov/17360452/)
51. Francis KE, Lam SY, Copenhaver GP (2006) Separation of Arabidopsis pollen tetrads is regulated by QUARTET1, a pectin methylesterase gene. *Plant Physiology* 142: 1004–1013. PMID: [16980565](https://pubmed.ncbi.nlm.nih.gov/16980565/)
52. Preuss D, Rhee SY, Davis RW (1994) Tetrad analysis is possible in Arabidopsis with mutation in the QUARTET (QRT) genes. *Science* 264: 1458–1460. PMID: [8197459](https://pubmed.ncbi.nlm.nih.gov/8197459/)
53. Perkins DD (1949) Biochemical mutants in the smut fungus Ustilago maydis *Genetics* 34: 607–626. PMID: [17247336](https://pubmed.ncbi.nlm.nih.gov/17247336/)
54. Malkova A, Swanson J, German M, McCusker JH, Housworth EA, et al. (2004) Gene conversion and crossing over along the 405-kb left arm of Saccharomyces cerevisiae chromosome VII. *Genetics* 168: 49–63. PMID: [15454526](https://pubmed.ncbi.nlm.nih.gov/15454526/)
55. Jahns MT, Vezon D, Chambon A, Pereira L, Falque M, et al. (2014) Crossover Localisation Is Regulated by the Neddylation Posttranslational Regulatory Pathway. *Plos Biology* 12.
56. Jones G (1987) Chiasmata. *Meiosis*: 213–244.
57. Chen CB, Zhang W, Timofejeva L, Gerardin Y, Ma H (2005) The Arabidopsis ROCK-N-ROLLERS gene encodes a homolog of the yeast ATP-dependent DNA helicase MER3 and is required for normal meiotic crossover formation. *Plant Journal* 43: 321–334. PMID: [16045469](https://pubmed.ncbi.nlm.nih.gov/16045469/)
58. Mercier R, Jolivet S, Vezon D, Huppe E, Chelysheva L, et al. (2005) Two meiotic crossover classes cohabit in Arabidopsis: One is dependent on MER3, whereas the other one is not. *Current Biology* 15: 692–701. PMID: [15854901](https://pubmed.ncbi.nlm.nih.gov/15854901/)

59. Klimyuk VI, Jones JDG (1997) AtDMC1, the Arabidopsis homologue of the yeast DMC1 gene: Characterization, transposon-induced allelic variation and meiosis-associated expression. *Plant Journal* 11: 1–14. PMID: [9025299](#)
60. Li WX, Chen CB, Markmann-Mulisch U, Timofejeva L, Schmelzer E, et al. (2004) The Arabidopsis AtRAD51 gene is dispensable for vegetative development but required for meiosis. *Proceedings of the National Academy of Sciences of the United States of America* 101: 10596–10601. PMID: [15249667](#)
61. Chelysheva L, Vezon D, Chambon A, Gendrot G, Pereira L, et al. (2012) The Arabidopsis HEI10 Is a New ZMM Protein Related to Zip3. *Plos Genetics* 8.
62. Wang K, Wang M, Tang D, Shen Y, Miao C, et al. (2012) The Role of Rice HEI10 in the Formation of Meiotic Crossovers. *Plos Genetics* 8.
63. De Muyt A, Zhang L, Piolot T, Kleckner N, Espagne E, et al. (2014) E3 ligase Hei10: a multifaceted structure-based signaling molecule with roles within and beyond meiosis. *Genes & Development* 28: 1111–1123.
64. Jackson N, Sanchez-Moran E, Buckling E, Armstrong SJ, Jones GH, et al. (2006) Reduced meiotic crossovers and delayed prophase I progression in AtMLH3-deficient Arabidopsis. *Embo Journal* 25: 1315–1323. PMID: [16467846](#)
65. Barakate A, Higgins JD, Viverra S, Stephens J, Perry RM, et al. (2014) The synaptonemal complex protein ZYP1 is required for imposition of meiotic crossovers in barley. *The Plant Cell*.
66. Wang M, Wang KJ, Tang D, Wei CX, Li M, et al. (2010) The Central Element Protein ZEP1 of the Synaptonemal Complex Regulates the Number of Crossovers during Meiosis in Rice. *Plant Cell* 22: 417–430. doi: [10.1105/tpc.109.070789](#) PMID: [20154151](#)
67. Chen C, Jomaa A, Ortega J, Alani EE (2014) Pch2 is a hexameric ring ATPase that remodels the chromosome axis protein Hop1. *Proceedings of the National Academy of Sciences of the United States of America* 111: E44–E53. doi: [10.1073/pnas.1310755111](#) PMID: [24367111](#)
68. Hwang LC, Vecchiarelli AG, Han Y- W, Mizuuchi M, Harada Y, et al. (2013) ParA-mediated plasmid partition driven by protein pattern self-organization. *Embo Journal* 32: 1238–1249. doi: [10.1038/emboj.2013.34](#) PMID: [23443047](#)
69. Ye Q, Rosenberg, S.C., Moeller, A., Speir, J.A., Su, T.Y., Corbett, K.D. (2015) TRIP13 is a protein-remodelling AAA+ATPase that catalyses MAD2 conformation switching. *eLife* doi: [10.7554/eLife.07367](#)
70. Nilsson NO, Sall T, Bengtsson BO (1993) Chiasma and recombination data in plants-are they compatible? *Trends in Genetics* 9: 344–348. PMID: [8068067](#)
71. Wills AB (1966) Meiotic behaviour in Brassiceae. *Caryologia* 19: 103–&.
72. Zhang L, Espagne E, de Muyt A, Zickler D, Kleckner NE (2014) Interference-mediated synaptonemal complex formation with embedded crossover designation. *Proceedings of the National Academy of Sciences of the United States of America* 111: E5059–E5068. doi: [10.1073/pnas.1416411111](#) PMID: [25380597](#)
73. Henderson KA, Keeney S (2004) Tying synaptonemal complex initiation to the formation and programmed repair of DNA double-strand breaks. *Proceedings of the National Academy of Sciences of the United States of America* 101: 4519–4524. PMID: [15070750](#)
74. Farmer S, Hong E-JE, Leung W-K, Argunhan B, Terentyev Y, et al. (2012) Budding Yeast Pch2, a Widely Conserved Meiotic Protein, Is Involved in the Initiation of Meiotic Recombination. *Plos One* 7.
75. Duroc Y, Lemhemdi A, Larcheveque C, Hurel A, Cuacos M, et al. (2014) The Kinesin AtPSS1 Promotes Synapsis and is Required for Proper Crossover Distribution in Meiosis. *Plos Genetics* 10.
76. Qiao H, Offenberg HH, Anderson LK (2012) Altered distribution of MLH1 foci is associated with changes in cohesins and chromosome axis compaction in an asynaptic mutant of tomato. *Chromosoma* 121: 291–305. doi: [10.1007/s00412-012-0363-z](#) PMID: [22350750](#)

RESEARCH ARTICLE

Naturally Occurring Differences in CENH3 Affect Chromosome Segregation in Zygotic Mitosis of Hybrids

Shamoni Maheshwari¹, Ek Han Tan¹, Allan West², F. Chris H. Franklin², Luca Comai^{1*}, Simon W. L. Chan^{3,4†}

1 Department of Plant Biology and Genome Center, University of California, Davis, Davis, California, United States of America, **2** School of Biosciences, University of Birmingham, Edgbaston, Birmingham, United Kingdom, **3** Department of Plant Biology, University of California, Davis, Davis, California, United States of America, **4** Howard-Hughes Medical Institute and the Gordon and Betty Moore Foundation, University of California, Davis, Davis, California, United States of America

† Deceased.

* lcomai@ucdavis.edu



OPEN ACCESS

Citation: Maheshwari S, Tan EH, West A, Franklin FCH, Comai L, Chan SWL (2015) Naturally Occurring Differences in CENH3 Affect Chromosome Segregation in Zygotic Mitosis of Hybrids. *PLoS Genet* 11(1): e1004970. doi:10.1371/journal.pgen.1004970

Editor: Kirsten Bomblies, Harvard University, UNITED STATES

Received: September 13, 2014

Accepted: December 20, 2014

Published: January 26, 2015

Copyright: © 2015 Maheshwari et al. This is an open access article distributed under the terms of the [Creative Commons Attribution License](https://creativecommons.org/licenses/by/4.0/), which permits unrestricted use, distribution, and reproduction in any medium, provided the original author and source are credited.

Data Availability Statement: Most relevant data are within the paper and its Supporting Information files. Sequence files are available via NCBI under the following numbers: Bioproject ID: PRJNA261254; SRA ID: SRP048570; Genbank: KP202363.

Funding: This work was funded by the Howard Hughes Medical Institute and the Gordon and Betty Moore Foundation through grant GBMF3068 (to LC) and the Gordon and Betty Moore Foundation through Grant GBMF 2550.03 to the Life Sciences Research Foundation (to SM) and Biotechnology and Biological Sciences Research Council, UK (to AW and FCHF).

Abstract

The point of attachment of spindle microtubules to metaphase chromosomes is known as the centromere. Plant and animal centromeres are epigenetically specified by a centromere-specific variant of Histone H3, CENH3 (a.k.a. CENP-A). Unlike canonical histones that are invariant, CENH3 proteins are accumulating substitutions at an accelerated rate. This diversification of CENH3 is a conundrum since its role as the key determinant of centromere identity remains a constant across species. Here, we ask whether naturally occurring divergence in CENH3 has functional consequences. We performed functional complementation assays on *cenh3-1*, a null mutation in *Arabidopsis thaliana*, using untagged CENH3s from increasingly distant relatives. Contrary to previous results using GFP-tagged CENH3, we find that the essential functions of CENH3 are conserved across a broad evolutionary landscape. CENH3 from a species as distant as the monocot *Zea mays* can functionally replace *A. thaliana* CENH3. Plants expressing variant CENH3s that are fertile when selfed show dramatic segregation errors when crossed to a wild-type individual. The progeny of this cross include hybrid diploids, aneuploids with novel genetic rearrangements and haploids that inherit only the genome of the wild-type parent. Importantly, it is always chromosomes from the plant expressing the divergent CENH3 that missegregate. Using chimeras, we show that it is divergence in the fast-evolving N-terminal tail of CENH3 that is causing segregation errors and genome elimination. Furthermore, we analyzed N-terminal tail sequences from plant CENH3s and discovered a modular pattern of sequence conservation. From this we hypothesize that while the essential functions of CENH3 are largely conserved, the N-terminal tail is evolving to adapt to lineage-specific centromeric constraints. Our results demonstrate that this lineage-specific evolution of CENH3 causes inviability and sterility of progeny in crosses, at the same time producing karyotypic variation. Thus, CENH3 evolution can contribute to postzygotic reproductive barriers.

This work used the Vincent J. Coates Genomics Sequencing Laboratory at UC Berkeley, supported by NIH S10 Instrumentation Grants S10RR029668 and S10RR027303. The funders had no role in study design, data collection and analysis, decision to publish, or preparation of the manuscript.

Competing Interests: The authors have declared that no competing interests exist.

Author Summary

As populations evolve into new species they acquire mutations that are compatible with their own genetic background, but often lead to defects when crossed to others. Here, we show that naturally evolved differences in the centromere-specific histone H3 (CENH3) can contribute to this process. Unlike canonical histones, CENH3 differentiates rapidly even between closely related species. To better understand the functional role of natural CENH3 variation, we complemented a null allele of *Arabidopsis* with progressively more distant orthologs. Contrary to previous findings, we discovered that all tested variants, even the highly diverged maize CENH3, could restore normal growth and reproduction in selfing individuals. However, when crossed to the wild type, hybrid progeny suffered from extensive mis-segregation. Genotypes include simple aneuploids, novel genetic rearrangements, and in extreme cases haploids where all the chromosomes from one parent are lost. This indicates that while wide variation in CENH3 is compatible with its essential function, epigenetically different centromeres do not function well when brought together in a hybrid embryo. A better understanding of haploid generation would have profound effects on plant breeding and our results suggest that the natural variation of CENH3 could offer a cache of testable variation.

Introduction

Centromeres are the site where spindle microtubules attach to chromosomes during cell division. This attachment is mediated via a multi-protein complex called the kinetochore, a structure essential for the stable inheritance of genetic information. Contrary to expectation, the centromere is not a genetic locus in the traditional sense of being defined by its DNA sequence [1,2]. The DNA sequence underlying the centromere is not evolutionarily conserved and in most species, is composed of megabases of rapidly evolving tandem repeats [3]. However, these repeats are not essential to centromere formation since neocentromeres or the gain of new centromeric activity has been observed over unique DNA sequences as well [4–6]. The common denominator to all centromeres, old and new, is the presence of a centromere specific histone variant of H3 called CENH3 (or CENP-A) [7]. This and other evidence [8–10] indicate that in both plants and animals, the location of centromeres is specified epigenetically by the presence of CENH3.

Despite this ancient and conserved role of CENH3 in maintaining genetic integrity, the CENH3 protein sequence is not evolving under purifying selection. In contrast to the nearly invariant histone H3, CENH3 homologs are highly divergent. For example, CENH3 from *Arabidopsis thaliana* and *Arabidopsis arenosa*, sister species that shared a common ancestor approximately 5 MYA, differ at 23 of 178 amino acid positions while canonical Histone H3 has accumulated only 4 substitutions out of 136 amino acid positions since the divergence of plants and animals. In the *Brassicaceae* and in *Drosophila*, the diversification of CENH3 at both the Histone Fold Domain (HFD) and the N-terminal tail appears to be driven by adaptive evolution under natural selection [11,12]. This accelerated evolution is especially pronounced at the N-terminal tail of CENH3, which is hyper-variable both in its length and sequence. Why a structure essential for stable inheritance of genetic material is composed of genetically unstable units is a fundamental unsolved question in the field of chromosome biology.

The “centromere drive” hypothesis proposed by Henikoff and Malik puts forward genetic conflict as the source of this striking diversification [13]. This model supposes that DNA sequence can influence centromere function. Female meiosis in animals and plants is

asymmetric, in that only one product survives to become the egg cell. If a sequence variant evolves that can preferentially segregate into the surviving egg cell, it will rapidly sweep through the population [14,15]. However, such driving chromosomes would be associated with fitness costs including fixation of linked deleterious mutations, sterility due to non-disjunction and in the case of sex chromosomes, skewed sex ratios. This in turn is expected to set off the evolution of centromere-associated proteins to suppress the selfish transmission of this centromere. Cycles of centromere drive and suppression could result in the rapid diversification of centromeres and associated factors. One outcome of divergence in centromere components, DNA and/or proteins, could be the evolution of incompatibilities in the segregation machinery, leading to the reproductive isolation of populations.

While there is strong evidence attributing expansion of centromeric repeats to meiotic drive [16], whether CENH3 or other centromeric proteins are co-evolving with DNA sequences to suppress instances of drive remains speculative. The functional consequences of CENH3 divergence are difficult to address because CENH3 is an essential gene and most model systems cannot tolerate the segregation errors caused by mutations or modification to its function. In *D. melanogaster* and mammalian cells, RNAi has been used to down-regulate CENH3 levels [17,18]. However, the interpretation of any loss-of-function phenotypes is confounded by the persistence of CENH3 through multiple rounds of cell division. In contrast, a *cenh3* null mutant in *A. thaliana* allows us to completely replace the endogenous protein with transgenic variants. In addition, *A. thaliana* has high-copy centromeric repeats similar in organization to most plants and animals [19], making it an attractive system for testing general principles of centromere function.

Also unique to *A. thaliana* is the CENH3-mediated genome elimination system [20], which we have leveraged as a sensitive genetic assay for centromere function in this study. This genetic assay is based on the discovery that when a *cenh3* null mutant expressing a GFP-tagged chimeric CENH3 (GFP-tailswap) is crossed to a wild type, missegregation of chromosomes from the GFP-tailswap parent is observed [20]. Since *A. thaliana* has a high tolerance to aneuploidy, the F1 progeny capture a wide range of segregation errors. In the most extreme cases, all the chromosomes from the GFP-tailswap parent are lost (genome elimination) yielding haploid offspring that inherit chromosomes only from the wild-type parent. Importantly, segregation errors are only observed in crosses to wild type and not during normal vegetative growth or when GFP-tailswap plants are selfed. This implies that chromosome missegregation in the F1 zygote is the result of competition between wild-type centromeres and defective centromeres built on the artificial chimeric CENH3. Thus, the frequency of segregation errors and genome elimination can be used as a sensitive assay for centromere function. We were interested in asking what would happen if instead of using an artificial chimeric construct we simply replaced the endogenous CENH3 with natural variants from related species.

Previous studies using GFP-tagged versions of CENH3 orthologs had found a very narrow evolutionary window of functional complementation [21]. This leads to the conclusion that plant CENH3s are evolving under unique and highly dissimilar lineage-specific functional constraints [21]. Here, using untagged natural variants of CENH3 we observed the following: 1) Despite extensive sequence divergence, the essential functions of CENH3 are conserved across a much broader evolutionary time-scale than previously thought; 2) Naturally evolved divergence in CENH3 can contribute to genetic instability by causing chromosome missegregation, generating not only aneuploids and haploids, but also novel genetic rearrangements; 3) It is the divergence in the fast evolving N-terminal tail domain that is responsible for segregation defects and 4) The N-terminal tail appears to be evolving in a modular fashion. With these results, we argue that the core functions of CENH3 have remained unchanged over long evolutionary periods while the N-terminal tail of CENH3 is evolving as a species-specific optimized platform for centromere

organization. Finally, our study presents the first direct evidence for the role of CENH3 divergence in speciation.

Results

Mustard family *CENH3*s complement *Arabidopsis cenH3-1* null mutation

A. thaliana is a member of the mustard family (*Brassicaceae*), known for its agriculturally important Brassica crops. Analysis of CENH3 homologs from several species within the mustard family revealed that it is adaptively evolving, both at the Histone Fold Domain (HFD) and the N-terminal tail (NTT) [11]. Ravi *et al.* (2010) [21] had assayed CENH3s from species within the *Brassicaceae* and beyond for functional complementation of *cenH3-1*, a CENH3 null mutation in *A. thaliana*. They found that GFP-tagged CENH3 from *Brassica rapa* and *Zea mays* localized at *A. thaliana* centromeres, but only GFP-tagged CENH3 from the closely related species *A. arenosa* rescued embryo lethality of the *cenH3-1*. A caveat to these experiments was the presence of the GFP-tag. GFP-tagged *A. thaliana* CENH3 largely complemented the functions of the *A. thaliana cenH3-1* mutation, but when crossed to wild type segregation errors were observed at a low frequency. This hinted that the GFP-tag is not entirely neutral. Thus, to assay only the effects of naturally evolved variation on CENH3 function, we decided to test complementation of the *cenH3* null mutant using native untagged proteins.

We chose CENH3 from *B. rapa* and *Lepidium oleraceum*, two species nested within the *Brassicaceae* family. *L. oleraceum* is more closely related to *A. thaliana* than *B. rapa*, but more distantly than *A. arenosa* [22]. To test for complementation, we transformed *cenH3-1/CENH3* heterozygotes with constructs expressing genomic sequence encoding *L. oleraceum* CENH3 (LoCENH3) and *B. rapa* CENH3 (BrCENH3) under the endogenous *A. thaliana* CENH3 promoter. We recovered transformants that were homozygous for the *cenH3-1* mutation for both variants in the T1 generation. This result is revealing in two ways: firstly it shows that the GFP-tag interferes with CENH3 function and secondly, it indicates that the previously defined boundary of functional complementation is incorrect.

We further characterized the extent of mitotic and meiotic complementation in the T2 generation. *A. thaliana* plants homozygous for *cenH3* null mutation expressing transgenic *L. oleraceum* CENH3 or *B. rapa* CENH3 were phenotypically indistinguishable from wild type (Fig. 1A). We therefore conclude that *B. rapa* and *L. oleraceum* CENH3 can fully complement *A. thaliana* CENH3 mitotic functions required for vegetative growth. Transgenic lines for both CENH3 variants in a *cenH3-1* homozygous background were also self-fertile.

To assay meiotic complementation, we wanted to identify plants that were homozygous for both the *cenH3* null mutation and variant CENH3 transgene. Following segregation ratios of the transgene is not informative in a *cenH3-1* homozygous mutant background, since individuals without transgenic CENH3 cannot survive. Therefore, we decided to use frequency of seed death in selfed siliques of T2 plants to infer the zygosity of the CENH3 transgene. Individuals that are *cenH3 -/-* and heterozygous for the transgene are expected to produce 25% seed death upon selfing. Assuming that the transgene is inserted at a single locus, individuals homozygous for the transgene are expected to produce 0 to less than 25% seed death if fully or partially complementing the meiotic functions of the endogenous *A. thaliana* CENH3.

Using this criterion to infer the zygosity of the transgene, we measured fertility of *A. thaliana* plants in which the endogenous CENH3 is replaced by *L. oleraceum* CENH3 or *B. rapa* CENH3. We measured seed set and frequency of abnormal seeds in selfed siliques from three independent transformation events for each construct (Fig. 1C). The complemented lines were comparable to wild type for both measures of fertility. Furthermore, viability-stained

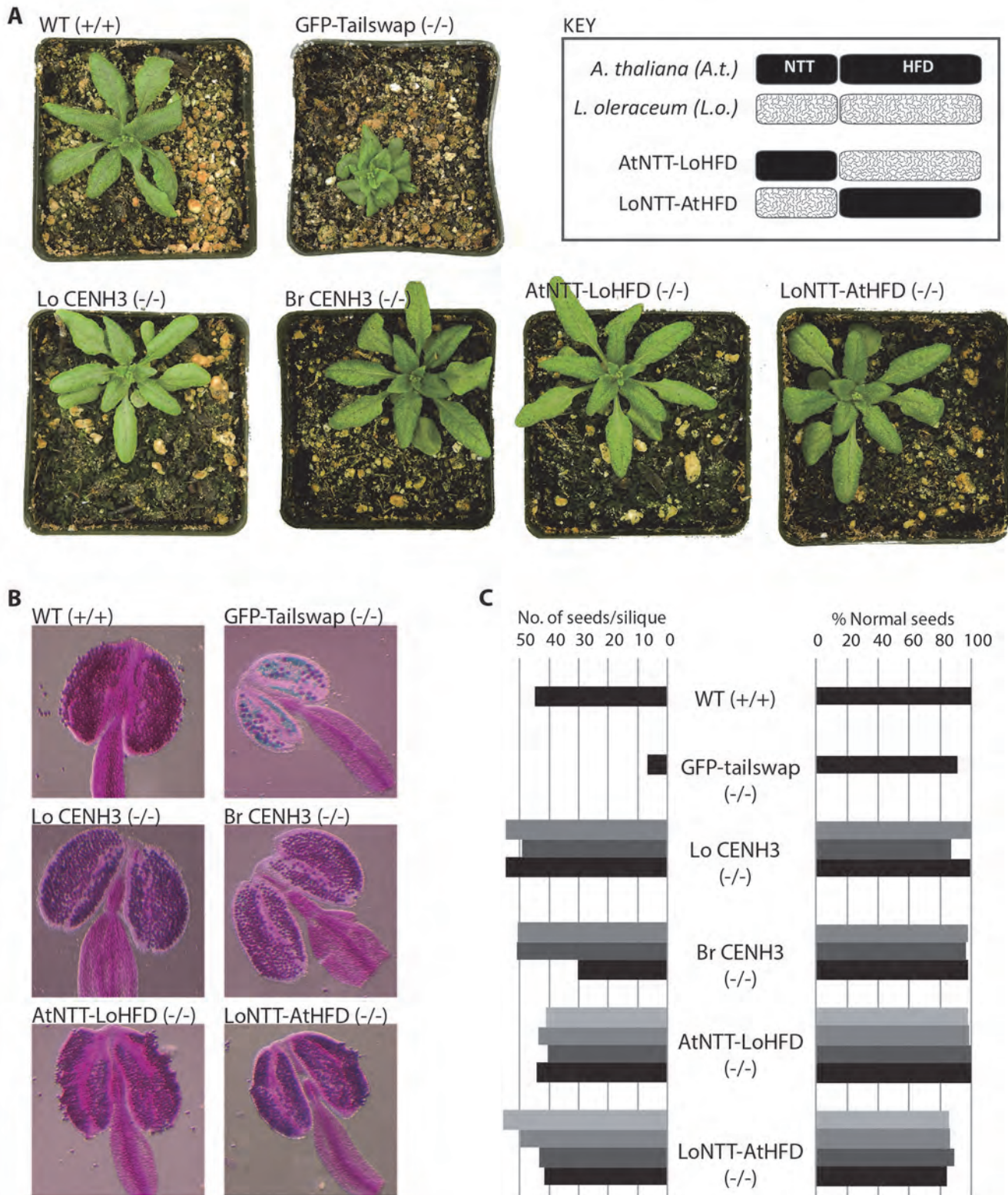


Figure 1. Vegetative and reproductive phenotypes of CENH3 complemented lines. (A) Plants at rosette stage from different complemented lines compared to wild-type Columbia (WT) and GFP-tailswap, a high frequency haploid inducer [20]. The genotype of the endogenous *CENH3* locus is indicated in parentheses. LoCENH3 is *L. oleraceum* CENH3 and BrCENH3 is *B. rapa* CENH3. AtNTT-LoHFD and LoNTT-AtHFD are chimeric CENH3s described in

the key. (B) Anthers stained for viability with Alexander stain. Viable pollen granules stain purple. (C) Measures of fertility based on number of seeds per silique and seed appearance. Bars in different shades of grey represent counts from different T1 lines. For each measurement, seeds from 5 siliques were pooled and counted.

doi:10.1371/journal.pgen.1004970.g001

anthers from the same complemented lines showed live pollen numbers and appearance indistinguishable from wild type (Fig. 1B).

For *L. oleraceum* CENH3 complemented lines we further analysed meiosis cytologically with DAPI stained chromosome spreads from pollen mother cells (PMCs) in two T1 families, 2 and 19. Prophase I of meiosis in both lines was indistinguishable from wild type (S1A Fig.). Chromosome segregation in PMCs at both meiotic divisions was checked for segregation errors. In the T1 = 19 family, metaphase I (n = 26), anaphase I (n = 7), metaphase II (n = 40), anaphase II (n = 5) and telophase II (n = 21) PMCs were scored, none of which displayed segregation errors (Fig. 2). Careful inspection of all post-prophase I PMCs sampled revealed some

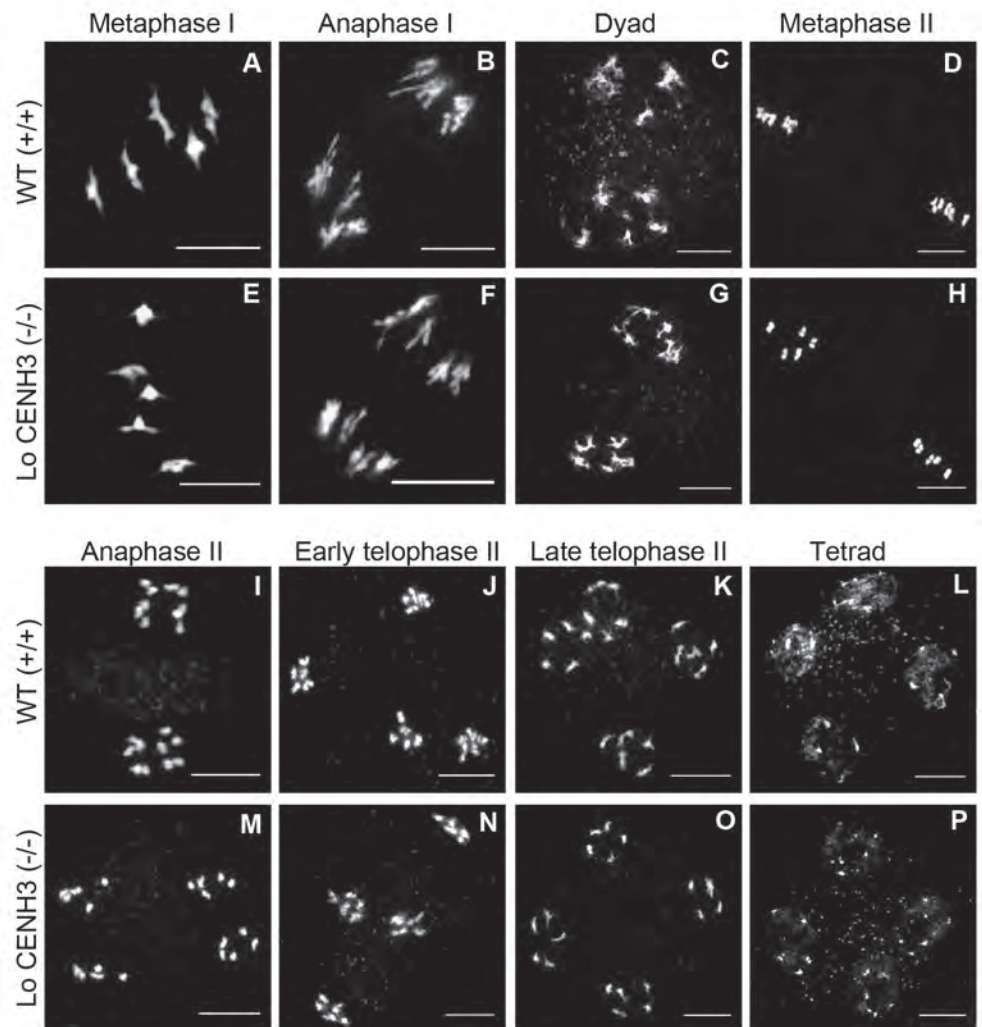


Figure 2. *L. oleraceum* CENH3 complements meiosis in *A. thaliana*. Male meiotic chromosome spreads stained with DAPI for WT Col-0 (A-D, I-L) and *L. oleraceum* CENH3 *cenh3-1/cenh3-1* (T1 family = 19) (E-H, M-P). Scale bar = 10µm.

doi:10.1371/journal.pgen.1004970.g002

Table 1. Natural variation in CENH3, specifically in the N-terminal tail, causes genome elimination.

Transgene	T1 family name	% normal seed	Total No. of Plants Analysed	Haploids (%)	Diploids (%)	Aneuploids (%)
GFP-tailswap	11	20 (n = 1187)	606	240 (40)	167 (28)	199 (32)
<i>L. oleraceum</i> CENH3	2	58 (n = 464)	552	18 (3)	480 (87)	54 (10)
	19	53 (n = 167)	133	15 (11)	93 (70)	25 (19)
	21	86 (n = 294)	529	10 (2)	490 (93)	29 (5)
<i>B. rapa</i> CENH3	1	70 (n = 180)	283	5 (2)	243 (86)	35 (12)
	3	65 (n = 200)	246	2 (1)	219 (89)	25 (10)
	9	84 (n = 304)	464	4 (1)	445 (96)	15 (3)
AtNTT-LoHFD	4	83 (n = 138)	38	0 (0)	35 (92)	3 (8)
	8	97 (n = 393)	249	0 (0)	230 (92)	19 (8)
	9	92 (n = 364)	117	0 (0)	113 (97)	4 (3)
	24	97 (n = 385)	150	0 (0)	150 (100)	0 (0)
LoNTT-AtHFD	1	10 (n = 403)	119	2 (2)	94 (79)	23 (19)
	3	0 (n = 236)	0	N. A.	N. A.	N. A.
	6	1 (n = 152)	5	0 (0)	4 (80)	1 (20)
	19	2 (n = 334)	0	N. A.	N. A.	N. A.

doi:10.1371/journal.pgen.1004970.t001

limited chromosome fragmentation in one anaphase II cell (S1B Fig.). Although, the origin of this cannot be ascertained at present, its low frequency is unlikely to compromise fertility. Thus, we conclude that CENH3 orthologs can complement the essential mitotic and meiotic functions of *A. thaliana* CENH3 under standard growing conditions.

Naturally evolved divergence in CENH3 can cause genome elimination

Next, we wanted to test how *A. thaliana* centromeres built on CENH3 variants functioned in comparison to those built on the native *A. thaliana* CENH3. To do so, we crossed them as females with pollen from wild-type (CENH3 +/+) Landsberg *erecta* (*Ler*) homozygous for the *gl1-1* glabrous mutation, which confers a trichomeless phenotype. We chose *Ler* as the CENH3 wild-type parent because the complemented lines were generated in the Col-0 accession. This allows us to use polymorphisms between Col-0 and *Ler* to determine the parent of origin for all the chromosomes in the F1. In a standard cross we expect only F1 diploid hybrids with trichomes. However, if replacing the endogenous CENH3 with natural variants creates weak centromeres, then we can expect mitotic missegregation in the F1 zygote.

The first indication of abnormal segregation in these crosses was the observation that 14–47% seeds aborted during development (Table 1). In contrast to the uniformly tan-colored plump seeds generated when the complemented lines are selfed, dark nearly black shriveled seeds were seen in crosses to wild type. Upon germination of F1 seeds from *L. oleraceum* CENH3 and *B. rapa* CENH3 crosses, we recovered diploid, aneuploid and haploid progeny. All haploids were sterile and paternal on the basis of having a trichomeless appearance, an expression of the recessive *gl1-1* mutation. We confirmed the haploid genome content of 11 phenotypically selected haploids by flow cytometry (S2 Fig.).

Crosses were between *cenh3-1/cenh3-1* + CENH3 transgene females and pollen from wild type Landsberg CENH3 +/+ strain homozygous for the *gl1-1* glabrous mutation. Sterile offspring expressing the recessive *gl1-1* trichomeless phenotype were scored as paternal haploid. Offspring with developmental defects were scored as aneuploid. Fertile wild-type offspring were scored as diploid.

For each CENH3 construct we tested two individuals from each of the three independent transformation events (T1 families) in crosses to wild-type *Ler gl1-1*. Substantial variation in the frequency of haploids was observed between the different T1 families (Table 1). While the source of this variability is unclear, it is consistent with the variable haploid induction rates observed when GFP-tailswap is crossed to wild type. In cases where *cenh3-1* is complemented with *L. oleraceum* CENH3, the frequency of genome elimination ranged from 2 to 11%. For *B. rapa* CENH3 complemented *cenh3-1*, the range was 1 to 2%. Although, *L. oleraceum* is more closely related to *A. thaliana* than *B. rapa*, substituting endogenous *A. thaliana* CENH3 with the *L. oleraceum* ortholog in an *A. thaliana* plant appeared to have a greater destabilizing effect on *A. thaliana* centromere as inferred from the larger frequency of genome elimination on average ($6 \pm 2.4\%$ vs. $1 \pm 0.2\%$).

We have not observed any instances of aneuploidy and haploidy in the selfed progeny of the complemented lines (S3 Fig.). In addition meiosis in *L. oleraceum* T1 families 2 and 19, which generated the highest frequency of haploids and aneuploids, is wild type in appearance (Fig. 2). From the absence of meiotic defects during selfing, we infer that the segregation errors and genome elimination observed in the crosses to wild type (CENH3 +/+) are not the byproduct of meiotic dysfunction in the inducer parent, but rather the consequences of postzygotic interactions in the hybrid embryo. From this we conclude that natural variation in CENH3 can cause centromere-mediated genome elimination and contribute to genetic instability through changes in ploidy.

Crosses between plants expressing CENH3 variants and the wild type generate novel genetic rearrangements

One of the hallmarks of centromere-mediated genome elimination is the generation of aneuploid progeny at a relatively high frequency (~30% for GFP-tailswap) [20]. Aneuploids have imbalanced karyotypes that perturb gene dosage, with large and variable phenotypic consequences. *A. thaliana* aneuploids exhibit morphological phenotypes in a wide variety of traits including abnormal leaf morphology, irregular branching patterns and infertility [23]. Using these criteria, we estimated that in crosses of *Ler gl1-1* (as the wild-type pollen parent) to *L. oleraceum* CENH3 and *B. rapa* CENH3 complemented lines, the incidence of aneuploidy is 11.3% and 8.3% respectively (Table 1). We selected 48 phenotypically aneuploid progeny from each cross for whole genome sequencing to determine the relative dosage of each chromosome using a bioinformatics approach. Chromosomes and subchromosomal regions that vary from the expected number of 2 can be readily identified by increased or decreased read count relative to the rest of the genome [23]. We identified chromosomal imbalances in 73 of the 96 individuals selected for sequencing (S4 Fig., S5 Fig. and S1 Table). In this dataset we found three classes of aneuploid chromosome types and an example of each is shown in Fig. 3 (B–D). As a comparison diploid Col/*Ler* individual with 2 copies of each of the five *A. thaliana* chromosome is shown in Fig. 3A. The first class contains numerical aneuploids where whole chromosomes are duplicated, as exemplified by an individual trisomic for Chr3 (Fig. 3B). The second class contains aneuploids with truncated chromosomes, such as, for example, an extra copy of Chr5 with a truncated left arm (Fig. 3C). Lastly, the third class displays dosage variation consistent with chromosomes that shattered and have gained or lost DNA segments multiple times across the entire length of the chromosome. An example for a shattered Chr2 is shown in Fig. 3D. Based on our low pass sequencing analysis we cannot infer the chromosomal organization of these dosage variants presented here.

Using SNPs between the parental lines, we were able to infer the origins of the copy variant regions (SNP plots in Fig. 3A–D). In all three classes of dosage variants, the DNA contributing

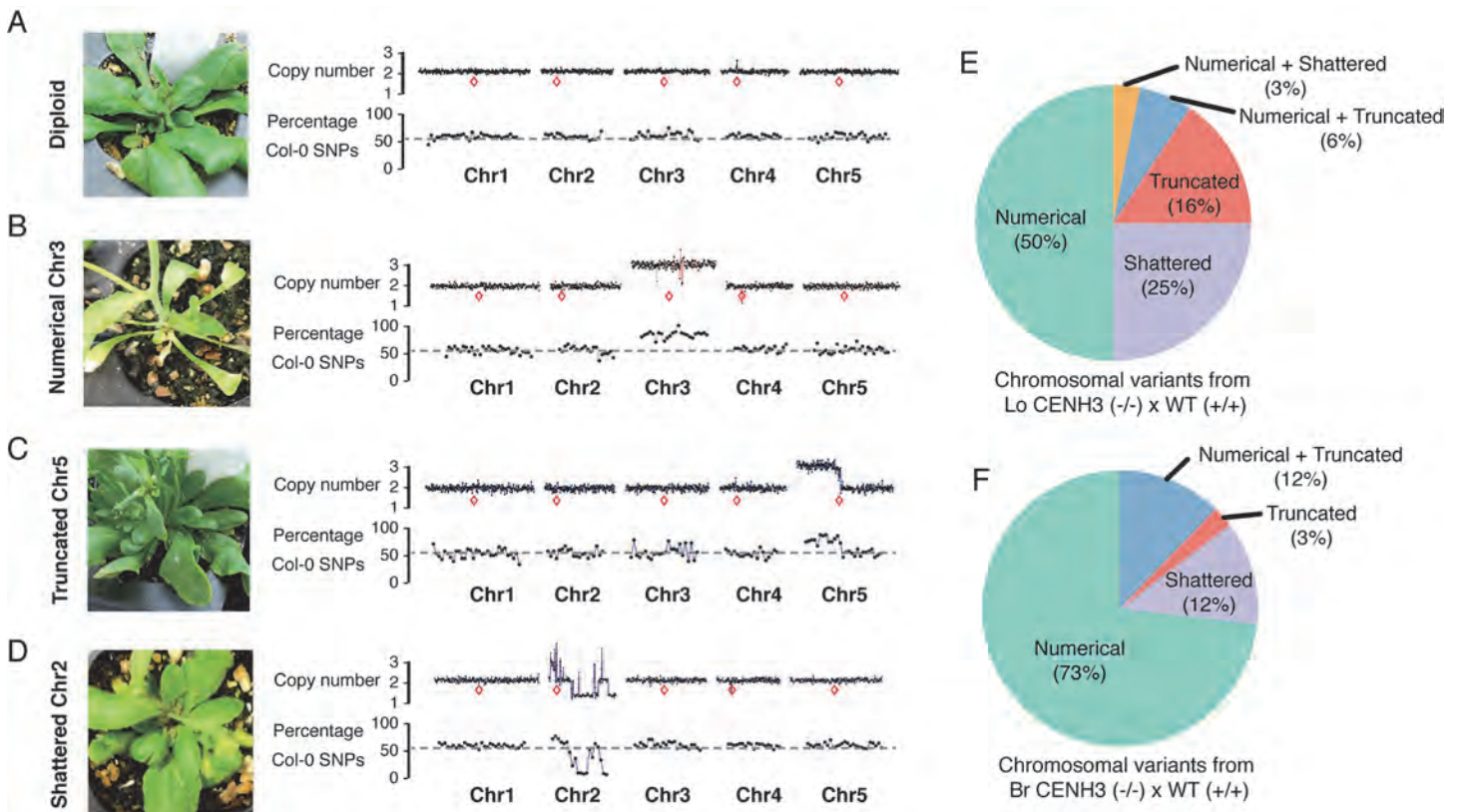


Figure 3. Characterization of aneuploid genotypes using whole-genome sequencing. Shown here are pictures of an individual plant alongside its 100kb bin dosage plot and 1 Mb bin SNP analysis across all five chromosomes. The red boxes indicate their relative centromere positions. (A) A diploid Col-0/Ler hybrid individual from a genome elimination cross mediated by *LoCENH3*. (B–D) The three major aneuploid types represented by examples of each: an individual with a numerical aneuploid chromosome (B), a truncated aneuploid chromosome (C) and a shattered aneuploid chromosome (D). (E–F) Percentage of each type of chromosomal variants of the aneuploids derived from a *LoCENH3* (E) and *BrCENH3* (F) genome elimination cross.

doi:10.1371/journal.pgen.1004970.g003

to the increased copy number originated from the transgenic Col-0 parent, in which the endogenous CENH3 had been replaced by an evolutionary variant. We even observed the loss of heterozygosity in the shattered Chr2 (Fig. 3D), as a result of the complete loss of the Col-0 chromosomal regions. The largest fractions of aneuploids from these crosses were products of whole chromosome missegregation events (Fig. 3E and F). However, there were also a considerable number of aneuploids with sub-chromosomal changes in copy number. This variation in dosage implies the creation of novel genetic karyotypes.

In summary, centromeres built on CENH3 variants appear to missegregate in crosses to wild type. One consequence of which is aneuploidy and segmental dosage variants and with that the introduction of a broad range of phenotypic diversity [24].

Essential functions of CENH3 are conserved between monocots and dicots

Since our results negated the previously identified limits of CENH3 functional complementation, we decided to sample a larger evolutionary space. Flowering plants are divided into two major groups: monocots and dicots that diverged from each other 146–161 MYA. Rosids are the largest clade within the dicots, comprising of around 70,000 species including the model plant *A. thaliana* [25]. To better understand the extent of variation in CENH3 across the plant

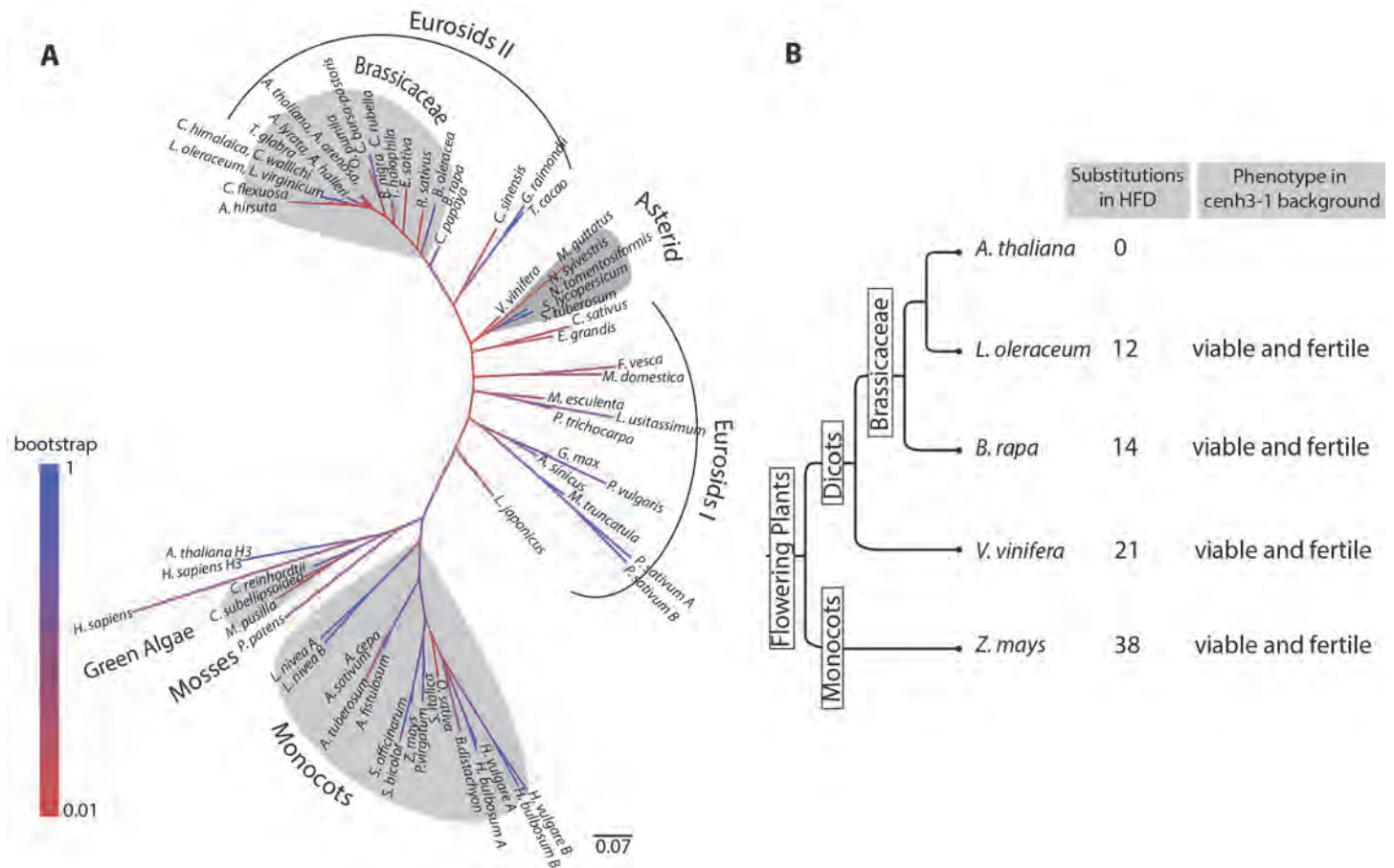


Figure 4. Analysis of evolutionary divergence in plant CENH3 Histone Fold Domains. (A) Phylogenetic tree inferred by using the Maximum Likelihood method based on the JTT matrix-based model [52]. The tree with the highest log likelihood (-3935.2849) is shown. The tree is drawn to scale, with branch lengths measured in the number of substitutions per site. (B) Summary of complementation tests of *A. thaliana cenH3-1* mutation with CENH3 from increasingly distant plant species.

doi:10.1371/journal.pgen.1004970.g004

kingdom, we collated 67 CENH3 sequences from public databases that included homologs from green algae, mosses, monocots and dicots (S2 Table). Using protein sequence from the HFD we generated a multiple sequence alignment and constructed a phylogeny of CENH3 in the plant kingdom (Fig. 4A). This CENH3-HFD based gene tree was largely congruent with the accepted evolutionary relationships between these species (Fig. 4A). The most striking feature of the tree is the size of its branches and the variation in their lengths, illustrating the rapid and variable rates of CENH3 evolution. We chose to test CENH3 from two additional species at increasing degrees of evolutionary distance from *A. thaliana*: grapevine (*Vitis vinifera*), one of the earliest diverging rosid species considered a basal rosid, and corn (*Zea mays*), a monocot.

To test the functional complementation of these distant species, we made constructs expressing *V. vinifera* CENH3 and *Z. mays* CENH3 cDNA under control of the endogenous *A. thaliana* CENH3 promoter. These transgenes were transformed into *cenH3-1*/CENH3 heterozygotes. We recovered both *V. vinifera* CENH3 and *Z. mays* CENH3 transformants in a *cenH3-1* homozygous background in the T1 generation (Fig. 4B and S6 Fig.). *V. vinifera* and *Z. mays* CENH3 have 21 and 38 amino acid substitutions respectively, relative to the 97 amino acid positions in the HFD of *A. thaliana* CENH3 (S7 Fig.). Hence, it was surprising that both

V. vinifera CENH3 and *Z. mays* CENH3 were able to complement the embryo lethality of the *cenh3-1* resulting in plants undistinguishable from the wild type. To the extent that the complemented lines were self-fertile, we can say that both variants also fulfilled the essential meiotic functions of *A. thaliana* CENH3 (Fig. 4B and S6 Fig.).

Divergence in the N-terminal tail of CENH3 causes missegregation

The *L. oleraceum* CENH3 gene has 12 amino acid substitutions in its HFD relative to *A. thaliana* and 31 in its N-terminal tail. We generated chimeric proteins in which the N-terminal tail of *L. oleraceum* CENH3 was fused to the HFD of *A. thaliana* CENH3, and vice versa (Fig. 1A). We assayed complementation of *cenh3-1* and found that both chimeras complemented the embryo lethality of the *cenh3-1* mutation in the T1 generation. The chimeric CENH3s were also similar to wild type with respect to pollen viability as determined by viability staining and in number and appearance of developing seeds within siliques (Fig. 1B and 1C).

We then tested the functionality of centromeres built on these chimeric CENH3 transgenes by making crosses to wild type. It was immediately apparent by visual inspection of the resulting F1 seeds that the two chimeras had entirely different effects. The F1 seeds from the chimera with *A. thaliana* N-terminal tail fused to *L. oleraceum* HFD (AtNTT-LoHFD) crossed to wild type appeared largely normal while most of the F1 seeds from the *L. oleraceum* N-terminal tail fused to *A. thaliana* HFD (LoNTT-AtHFD) were abnormal in appearance (Table 1). We failed to obtain F1 seed germination from crosses of LoNTT-AtHFD to the wild type except from a single T1 family. In this respect, the function of the chimera, LoNTT-AtHFD, is reduced compared to the full-length *L. oleraceum* CENH3. We only recovered 124 F1 progeny from the LoNTT-AtHFD cross, of which 2 were haploids and 23 were phenotypically aneuploid. In contrast, we recovered a large number of F1 progeny from the crosses with AtNTT-LoHFD. However, out of a total of 554 F1's none were haploids. This indicates that restoring the N-terminal tail to the endogenous sequence is sufficient to restore activity to a level similar to wild-type.

Evidence for modular evolution of the N-terminal tail within the plant kingdom

Since our genetic assays highlight a critical role of the N-terminal tail sequence in segregation and genome elimination, we were interested in identifying patterns in its sequence evolution. N-terminal tails of CENH3 proteins are hyper-variable both in their amino acid sequence and length, ranging from 23 amino acids (*Pisum sativum*) to 194 amino acids (*Brachypodium distachyon*). Thus, reconstructing the evolutionary history of N-terminal tails from alignments of distant CENH3 lineages is not possible. Instead, we decided to use an alignment free approach and used the motif search program MEME to identify short conserved blocks of sequence homology in the otherwise unstructured N-terminal tail. A similar approach investigating N-terminal tail evolution in *Drosophila* species identified three conserved blocks of homology shared by all CENH3 alleles in that clade [26]. Our analysis of N-terminal tails includes variation from a significantly broader evolutionary timescale, with CENH3 sequences ranging from green algae to flowering plants. We identified seven stretches of conserved protein sequences, which we have termed Blocks 1–7 (Fig. 5A, S3 Table). The over-representation of *Brassicaceae*-clade specific motifs (4 of 7 Blocks) is a reflection of our sampling bias, in which 22 of the 67 N-terminal tail sequences were from species within the *Brassicaceae*.

Several interesting patterns were immediately apparent: First, Block 1 and Block 2 were identified in nearly all plant CENH3s and in canonical Histone H3 (Fig. 5A). It appears that while the intervening sequence is highly variable in both length and content, the N- and C-terminus of N-terminal tails are evolving under strict constraint. These Blocks were not

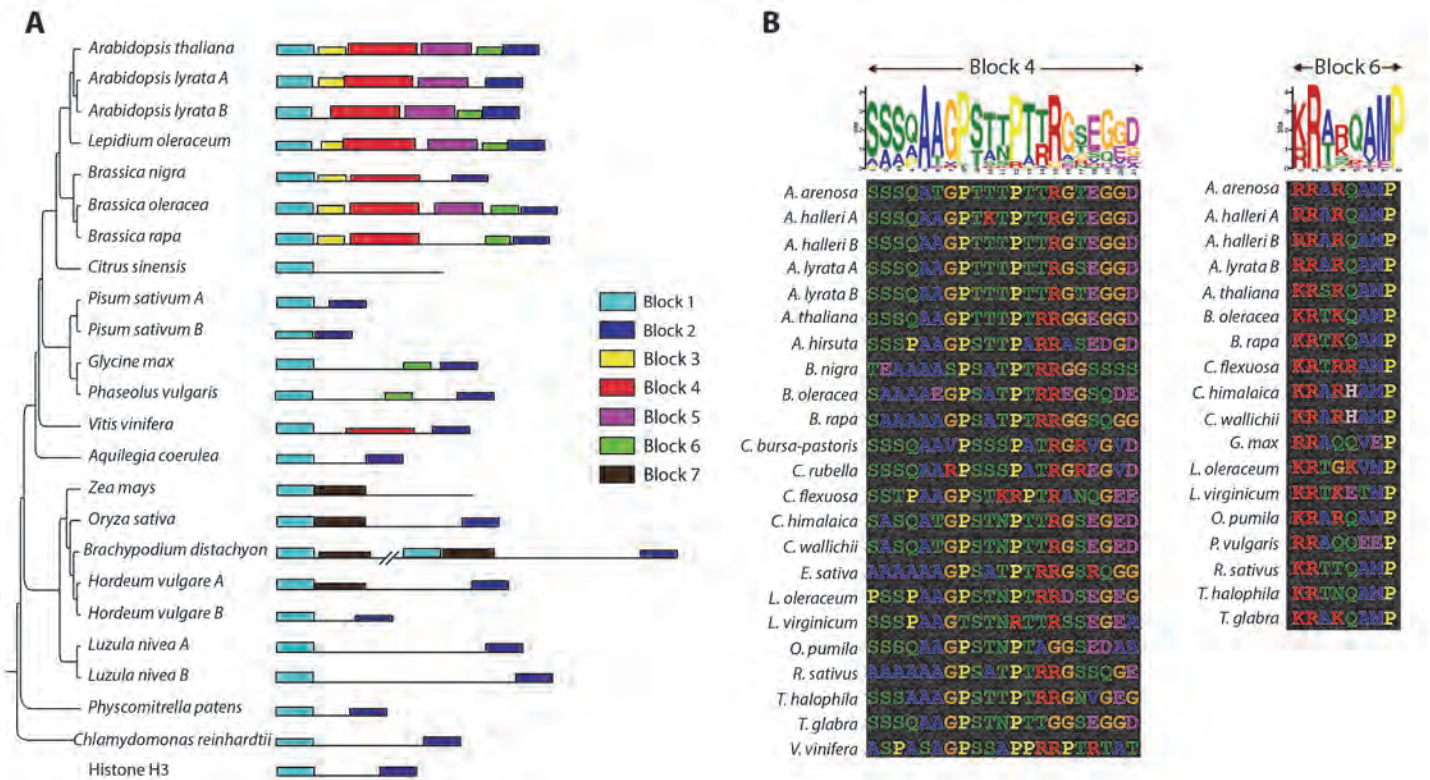


Figure 5. Identification of sequence motifs in plant CENH3 N-terminal tails. (A) Schematic representation of CENH3 N-terminal tails from a subset of plant species, in the context of their known phylogenetic relationships. Motifs identified by MEME [51] are represented as different colored blocks. N-terminal tails are drawn to scale with the relative locations of each motif identified. The height of the motif block is proportional to $-\log(p\text{-value})$. (B) Motif blocks 4 and 6 in Logos format. All instances where the motifs were identified are included below for comparison.

doi:10.1371/journal.pgen.1004970.g005

identified in *H. sapiens* CENH3. Second, in several instances where a species' genome carries two copies of CENH3, there was differential retention of Blocks between the two copies, a situation analogous to sub-functionalization post gene duplication. For example, copy A of CENH3 in *Arabidopsis lyrata* is missing Block 6 but retained Block 3, while copy B is missing Block 3 but has retained Block 6. In *Hordeum vulgare*, the monocot-specific Block 7 is retained in copy A, but lost in copy B. Third, isolated Blocks were identified across long evolutionary distances (Fig. 5B). For example, *Brassicaceae*-specific Block 4 was absent in all other lineages but present in *V. vinifera*, a basal rosid. Similarly, Block 6 that is present in most, but not all, *Brassicaceae* species, was also identified in two distant rosid species, *Phaseolus vulgaris* and *Glycine max*. The most parsimonious explanation for this pattern is that sequences homologous to Block 4 and Block 6 were present in the N-terminal tail of the ancestral CENH3 and were selectively retained or lost in the different rosid species. These observations suggest a modular evolutionary pattern where the constraints on individual Blocks are independent of one another. An outcome of this might be that the N-terminal tails acquire lineage-specific configuration of Blocks, thereby generating combinatorial sequence diversity.

Discussion

The results obtained in this study provide new and dramatically different information about CENH3 function and evolution from that previously available [21]. We observed wide complementation of a *CENH3* loss-of-function mutation, while previous studies failed to obtain

complementation except in the case of CENH3 from a very close relative. The difference lies quite simply in the use of untagged versus GFP-tagged CENH3 proteins in functional complementation assays. Furthermore, a recent study of CENH3^{CSE4} dynamics in yeast found that fusion of the GFP-tag to the CENH3^{CSE4} protein altered its function [27]. Taken together, it is apparent that presence of the GFP-tag significantly interferes with centromere function and protein modified with this fusion has limited use as a proxy for wild-type CENH3 activity.

The role of CENH3 in centromere determination is thought to have originated in an early eukaryotic ancestor [28]. Functional homologs of CENH3 have been identified in plants, animals, fungi and protists [29,30]. This essential gene exists as a single copy in nearly all species. Given the absence of gene duplicates and opportunities for sub-functionalization, this diversity in CENH3 protein sequences is puzzling and begs the question: how conserved are the functional requirements for making a centromere? This question has been asked in at least four different model organisms using primarily two assays: localization of evolutionarily distant CENH3s to the endogenous centromere and functional complementation of the endogenous CENH3 with evolutionary variants [18,21,31–33].

Two contrasting patterns of CENH3 functional conservation are apparent from the literature and this study. The first pattern is one of shared constraint over long evolutionary distances and the second is that of extreme lineage-specificity. In mammalian cells, GFP-tagged CENH3s from *C. elegans* and *S. cerevisiae* localized to centromeres. In addition, *S. cerevisiae* CENH3 rescued mammalian cells from mitotic arrest induced by depletion of the endogenous CENH3 [18]. In *Arabidopsis*, centromeric localization of complementing CENH3 does not extend as far as yeast [21] but CENH3 from *Z. mays*, a distant monocot species, can functionally substitute for the endogenous CENH3 (Fig. 4B and S6). In contrast, in *D. melanogaster*, GFP-tagged CENH3 from a species within the same genus failed to localize to centromeres [31]. In budding yeast, functional complementation of CENH3 is limited to the closely related hemiascomycetes [33]. Hemiascomycetes are unique in having ‘point centromeres’ that are genetically defined by a 125-bp sequence. Point centromeres are a derived evolutionary characteristic [28,34] and a plausible argument is that this specialized centromeric structure places severe lineage-specific constraints on CENH3 function, thereby restricting the limits of functional complementation. The results presented here argue that functional conservation despite sequence divergence is the norm, while stringent functional constraints might be symptomatic of a derived idiosyncratic centromere.

In this study we have asked not only whether a divergent CENH3 can functionally complement the endogenous *A. thaliana* allele, but also how well it complements those functions by providing a quantitative measure of the effect of CENH3 divergence on segregation fidelity. This measure has been possible because *A. thaliana*, like most plants, has a high tolerance for genomic dosage imbalance [35–37], thereby allowing recovery of the products of missegregation. Strikingly, complemented lines that had no fertility issues when fertilized by pollen of the same genotype, displayed large-scale segregation errors when crossed to wild type. Significant fractions of the recovered F1 progeny were either aneuploid or haploid (Table 1). In all cases the missegregated chromosomes originated from the parent expressing the divergent CENH3 (Fig. 3, S4 and S5). This clearly implies that centromeres built on the divergent CENH3, while able to complement essential functions, are deficient in comparison to the endogenous *A. thaliana* CENH3. What is the molecular basis of this functional deficiency? Answering this question constitutes an exciting next challenge since it will uncover species-specific adaptations to centromere function and shed light on what is driving the rapid evolution of this ancient biological structure.

Genome elimination as a barrier to interspecies hybridization has been observed in several taxa [38]. It had been previously shown that engineering modifications to CENH3, namely

fusing an N-terminal GFP-tag and swapping the N-terminal domain with one from Histone H3.3 (GFP-tailswap), causes segregation errors and genome elimination. Our results now show that naturally occurring divergence in CENH3 has the same effect. The most parsimonious explanation is that the underlying mechanistic basis of genome elimination in these different systems is shared while differing quantitatively in its outcome. In contrast to the male-sterile GFP-tailswap construct, CENH3 evolutionary variants are perfectly fertile when selfed, imposing no obvious fitness cost per se (Fig. 1 and 2). This highlights the fact that unlike the artificial GFP-tailswap construct, the naturally occurring mutations in CENH3 have evolved under functional constraint and can fulfill the conserved, essential functions even in the context of a non-native centromere, at least under standard growth conditions. However, in crosses to gametes with wild-type centromeres, the difference in parental CENH3s produces inviable (aborted seeds) and sterile (aneuploid and haploid) F1 progeny. In addition to these fitness penalties, the cross creates genetic novelty including instances of chromosomal breakage and shuffling of the resulting segments (Fig. 3B-D).

Aneuploidy and elimination of the haploid inducer genome are likely a linked phenomenon. Interestingly, fragmented chromosomes have been observed in other systems where genome elimination follows from an interspecific hybridization event [39,40]. In the natural barley wide crosses and in wheat and pearl millet hybrids, micronuclei formation is observed during the process of genome elimination [39,41]. Chromosomes within micronuclei could be targeted for elimination or be rescued by the cell, resulting in potential aneuploid progeny. While most aneuploid karyotypes have a deleterious fitness effect, recent studies have shown that aneuploidy is able to confer adaptive phenotypes under various stress conditions [42,43]. In summary, our data strongly supports a role for CENH3 divergence in speciation, not only as a means for creating a postzygotic reproductive barrier but also as a driver of genetic novelty.

A major finding from our work is that it is divergence in the *L. oleraceum* N-terminal tail that is critical for the missegregation phenotype. Fusing *A. thaliana* N-terminal tail to a divergent HFD improved its function, while fusing a divergent N-terminal tail to the *A. thaliana* HFD corrupts its function. In fact this second chimera showed a more severe missegregation phenotype than the full-length divergent CENH3 (Table 1). This suggests that the two domains of CENH3 might be co-evolving with one another, thus in some cases a chimera between two non-adapted domains could create an allele that is worse than the sum of its individual parts. Nevertheless, our results show that, despite sequence divergence, the HFD of CENH3 from a distant species can be functionally interchanged. Domain-swap experiments have revealed that regions within the HFD are required for centromere localization [31,44]. A plausible hypothesis is that the structural and functional constraints on the HFD are essentially unchanging, while the N-terminal tail is evolving to accommodate lineage-specific differences in centromeric environment.

Our examination of N-terminal tail sequences across the plant kingdom suggests a pattern where blocks of sequence homology are being lost and gained in a lineage-specific manner (Fig. 5A). A tempting conjecture is that these blocks of homology represent functional modules, such as interactions with other centromere-associated proteins. If this was the case we could expect lineage-specific diversity in centromeric machinery, with the integration (or subtraction) of lineage-specific interactions into the ancestral centromere network. Consistent with this expectation, a recent study recently delineated the evolutionary trajectory of Umbrea, a neogene that has gained essential centromeric functions in specific *Drosophila* lineages [45]. While this is in no way conclusive, we propose that the idiosyncratic rewiring of centromeric chromatin constitutes a potential driving force for the evolution of the N-terminal tail of CENH3.

In summary, our results argue that while CENH3 from all species perform conserved functions, each CENH3 is adapted to its own unique cellular, most likely centromeric, environment.

Why there should exist so many diverse solutions to the problem of packaging centromeric chromatin remains enigmatic. However, we demonstrate that this lineage-specific diversification of CENH3 has the potential to contribute to the genetic diversification and reproductive isolation of populations.

Materials and Methods

Plant materials and crossing procedure

Plants were transformed by the *Agrobacterium* floral dip method using standard protocols. Plants were grown under 16 hr of light/8 hr of dark at 20°C. For each cross, at least five flowers from an early inflorescence were emasculated and pollinated one day later with wild type pollen. F1 seeds were first sown in 0.5X MS plates containing 1% sucrose to maximize germination efficiency and then transplanted to soil.

Cloning of CENH3 transgenes

The *L. oleracea* CENH3 coding region including introns was PCR amplified from genomic DNA with the addition of *SalI* and *XbaI* sites at the ends. This PCR product was then cloned using standard restriction enzyme cloning into CP225, a cassette vector generated by Ravi *et al.* (2010) [21]. This vector is based on pCAMBIA1300 and carries the endogenous *A. thaliana* CENH3 promoter region i.e. 1489 bp upstream of the ATG, followed by a small linker region containing *SalI* and *XbaI* sites and finally the CENH3 transcriptional terminator i.e. 585 bp downstream of the STOP codon.

All other constructs were cloned into a new Gateway-compatible cassette vector SM2 that was derived from the above CP225. To construct this vector, we used three-fragment multi-site gateway technology (Life technologies, cat# 12537–023) that allows simultaneous assembly of three DNA fragments in a defined order into a destination vector. The first and third fragments are the endogenous *A. thaliana* CENH3 promoter and terminator respectively, while the second fragment can be any CENH3 variant being tested. We PCR amplified the promoter and terminator sequences from CP225 flanked by the appropriate attB sites and recombined them via the BP reaction into pDONR 221 P1-P4 and pDONR 221 P3-P2 respectively, generating the following entry clones: pENTR L1-promoter-L4 and pENTR L3-terminator-L2. Next, we integrated these two along with pENTR R4-pLac-Spec-R3, the control entry clone for the second fragment, into the destination vector through a single LR reaction. The destination vector was a generous gift from the Pikaard Lab and was a modified pEARLEYGATE302 binary vector that has an additional ampicillin resistance gene for bacterial selection. We then did a reverse BP reaction with this intermediate expression plasmid and pDONR 221 P4r-P3r to replace the placeholder in the second fragment with the Gateway negative selection cassette [Cm^{R} -*ccdB*] generating the final cassette vector, SM2 = CENH3 promoter-attL4- Cm^{R} -*ccdB*-attL3-terminator in pEARLEYGATE302.

The *B. rapa* CENH3 genomic sequence was PCR amplified from the GFP-tagged *B. rapa* CENH3 plasmid generated in Ravi *et al.* (2010) [21]. A chimeric transgene combining the *A. thaliana* N-terminal tail domain with *L. oleraceum* HFD was constructed by overlapping PCR. The N-terminal domain included genomic sequence coding for CENH3 starting from the “ATG” up to but not including the “PGTVAL” motif and the HFD extended from the “PGTVAL” motif to the STOP codon. The reciprocal construct with *L. oleraceum* N-terminal tail domain and *A. thaliana* HFD was similarly constructed. Transgenic variants outside the Brassicaceae were generated using CENH3 cDNA. *Z. mays* CENH3 was PCR amplified from plasmid generated in Ravi *et al.* (2010) [21]. CENH3 cDNA from *V. vinifera* was synthesized by GenScript USA Inc. Piscataway, NJ based on the Genbank sequence, 225454488.

DNA extraction and genotyping

Genomic DNA preparation and PCR genotyping were performed using standard methods. *cenh3-1* was genotyped with dCAPS primers. To genotype the *cenh3-1* mutation in lines with the construct *A. thaliana* N-terminal tail domain fused to *L. oleraceum* HFD, we first performed a PCR reaction with one primer outside the CENH3 promoter genomic DNA fragment present in the transgene. This PCR product was then used as the template in the dCAPS genotyping reaction. For each construct transgene-specific PCR primers were designed and used to confirm the genotype of each transgenic line. Primer sequences are available on request.

Vegetative growth and fertility assays

Representative images of rosettes were taken 25 to 30 days after germination. The percentage of normal seeds was determined by visual inspection using a dissecting microscope. On average, seeds from five individual siliques were pooled and counted for one individual from each T1 family identified as CENH3 transgene *+/+ cenh3 -/-*. Alexander staining of anthers was done according to published protocols [46].

Meiotic chromosome spreads

DAPI stained male meiotic chromosome spreads were prepared as described in Ross et al. [47], and imaged using an Olympus BX61 epifluorescence microscope and Digital Scientific Smart-Capture 3 software

Characterization of haploids and aneuploids

Flow cytometric determination of genome content was performed on floral buds using published protocols [48]. 0.1g leaf tissue from aneuploid plants were collected and purified using DNA Phytopure Kit (GE). Genomic DNA libraries were prepared using the standard NEB Next DNA Library Prep with NEXTFlex-96 Adapters from BIOO Scientific, pooled and sequenced on Illumina HiSeq 2000 for 50bp single reads. The resulting reads were mapped to TAIR10 using BWA followed by chromosome dosage analysis using the protocol described in Henry et al (2010) [23]. All the individuals that were sequenced and analyzed are identified with a unique FRAG identifier and are described in [S2 Table](#).

Phylogenetic analysis

Reference IDs for all sequences used in this study are available in [S1 Table](#). Multiple alignments of protein sequences encoding the histone fold domain of CENH3s was generated using MUSCLE and refined manually [49]. Evolutionary analyses were conducted in MEGA6 [50]. Phylogenetic history was inferred using the Maximum Likelihood method. The analysis involved 71 protein sequences. All positions containing gaps and missing data were eliminated. There were a total of 85 positions in the final dataset.

Motif identification

MEME [51] with default parameters was used to identify statistically significant blocks of sequence homology in N-terminal tails extracted from 67 plant CENH3 sequences available from public databases.

Supporting Information

S1 Fig. (A) Meiotic prophase I in *L. oleraceum* CENH3 complemented lines. Meiotic prophase I is divided into 5 cytologically distinct sub-stages. Chromosomes are associated with a proteinaceous axis during leptotene. Axes of homologous chromosomes juxtapose together during zygotene, as a protein structure called the synaptonemal complex polymerizes between them. Synapsis is complete at pachytene, where homologues are fully paired. Homologues begin to separate during diplotene, but remain associated by chiasmata, marking the points of genetic crossover generated by homologous recombination. Chromosomes are condensed further at diakinesis, where chiasmata are more readily visible. In LoCENH3 (-/-), prophase I is cytologically indistinguishable from wild type, indicating that the complementation does not affect meiotic recombination. Scale bar = 10 μ m. (B) Chromosome fragmentation was observed in a single anaphase II pollen mother cell. Chromosome fragments are indicated by arrows. Scale bar = 10 μ m (PDF)

S2 Fig. Confirmation of haploid genome content in phenotypic haploids. (A) Representative haploid plant. Note absence of silique elongation and trichomeless leaves associated with recessive *gl1-1* glabrous mutation. (B) Comparison of nuclear DNA content of flower buds from 4 wild-type diploids and 11 phenotypic haploids as determined by flow cytometry. (TIF)

S3 Fig. Absence of phenotypic abnormalities in selfed populations of CENH3 complemented lines. Selfed progeny of CENH3 complemented lines are phenotypically similar to WT Col-0 plants, in contrast to the selfed triploid population that exhibits phenotypic diversity due to expected aneuploidy. LoCENH3 is *L. oleraceum* CENH3 and BrCENH3 is *B. rapa* CENH3. The genotype of the endogenous *CENH3* locus is indicated in parentheses. (TIF)

S4 Fig. Dosage plots and SNP analysis using whole genome sequencing of diploids and aneuploids from *L. oleraceum* CENH3 genome elimination crosses. (A) Dosage plots with 100kb bins across all five chromosomes. (B) Percent Col-0 SNPs across a 1Mb region across all five chromosomes. (TIF)

S5 Fig. Dosage plots and SNP analysis using whole genome sequencing of diploids and aneuploids from *B. rapa* CENH3 genome elimination crosses. (A) Dosage plots with 100kb bins across all five chromosomes. (B) Percent Col-0 SNPs across a 1Mb region across all five chromosomes. (TIF)

S6 Fig. Phenotype of CENH3 complemented lines. (A) Shown here are plants of the same age. (B) Confirmation of genotype by PCR. The genotype of the endogenous *CENH3* locus is indicated in parentheses. LoCENH3 is *L. oleraceum* CENH3, BrCENH3 is *B. rapa* CENH3, VvCENH3 is *V. vinifera* CENH3 and ZmCENH3 is *Z. mays* CENH3. AtNTT-LoHFD is a chimeric CENH3 where the *A. thaliana* N-terminal tail is fused to the *L. oleraceum* HFD and LoNTT-AtHFD is the reciprocal construct. (TIF)

S7 Fig. Alignment of CENH3 Histone Fold Domain protein sequences. Positions identical to *A. thaliana* are represented as (.) and positions different from *A. thaliana* are indicated by the corresponding amino-acid substitution. (TIFF)

S1 Table. List of all gene sequences and their database IDs used in this study.
(DOCX)

S2 Table. Characteristics of all aneuploids analyzed by whole genome sequencing in this study.
(XLS)

S3 Table. List of all sequences identified by MEME as motifs.
(XLSX)

Acknowledgments

We are grateful to Dr. Isabelle Henry for assistance with flow cytometry, Dr. Jessica Budke for advice on phylogenetic analysis and Dr. Craig Pikaard for the gift of a plasmid. We thank Dr. Gregory Smaldone, Dr. Anne Britt and Dr. Isabelle Henry for discussions and critical reading of the manuscript. We would also like to acknowledge the assistance of undergraduate students Joel Valencia, William Keenan, Nikki La and Hadley Sheppard.

Author Contributions

Conceived and designed the experiments: SM SWLC. Performed the experiments: SM EHT AW FCHF. Analyzed the data: SM EHT LC AW FCHF. Contributed reagents/materials/analysis tools: SM EHT LC SWLC. Wrote the paper: SM EHT AW LC.

References

1. Allshire RC, Karpen GH (2008) Epigenetic regulation of centromeric chromatin: old dogs, new tricks? *Nat Rev Genet* 9: 923–937. doi: [10.1038/nrg2466](https://doi.org/10.1038/nrg2466) PMID: [19002142](https://pubmed.ncbi.nlm.nih.gov/19002142/)
2. Birchler JA, Gao Z, Sharma A, Presting GG, Han F (2011) Epigenetic aspects of centromere function in plants. *Curr Opin Plant Biol* 14: 217–222. doi: [10.1016/j.pbi.2011.02.004](https://doi.org/10.1016/j.pbi.2011.02.004) PMID: [21411364](https://pubmed.ncbi.nlm.nih.gov/21411364/)
3. Melters DP, Bradnam KR, Young HA, Telis N, May MR, et al. (2013) Comparative analysis of tandem repeats from hundreds of species reveals unique insights into centromere evolution. *Genome Biol* 14: R10. doi: [10.1186/gb-2013-14-1-r10](https://doi.org/10.1186/gb-2013-14-1-r10) PMID: [23363705](https://pubmed.ncbi.nlm.nih.gov/23363705/)
4. Fu S, Lv Z, Gao Z, Wu H, Pang J, et al. (2013) De novo centromere formation on a chromosome fragment in maize. *Proceedings of the National Academy of Sciences of the United States of America* 110: 6033–6036. doi: [10.1073/pnas.1303944110](https://doi.org/10.1073/pnas.1303944110) PMID: [23530217](https://pubmed.ncbi.nlm.nih.gov/23530217/)
5. du Sart D, Cancilla MR, Earle E, Mao JI, Saffery R, et al. (1997) A functional neo-centromere formed through activation of a latent human centromere and consisting of non-alpha-satellite DNA. *Nat Genet* 16: 144–153. PMID: [9171825](https://pubmed.ncbi.nlm.nih.gov/9171825/)
6. Williams BC, Murphy TD, Goldberg ML, Karpen GH (1998) Neocentromere activity of structurally acentric mini-chromosomes in *Drosophila*. *Nat Genet* 18: 30–37. PMID: [9425896](https://pubmed.ncbi.nlm.nih.gov/9425896/)
7. Black BE, Cleveland DW (2011) Epigenetic centromere propagation and the nature of CENP-a nucleosomes. *Cell* 144: 471–479. doi: [10.1016/j.cell.2011.02.002](https://doi.org/10.1016/j.cell.2011.02.002) PMID: [21335232](https://pubmed.ncbi.nlm.nih.gov/21335232/)
8. Gong Z, Wu Y, Koblizkova A, Torres GA, Wang K, et al. (2012) Repeatless and repeat-based centromeres in potato: implications for centromere evolution. *Plant Cell* 24: 3559–3574. doi: [10.1105/tpc.112.100511](https://doi.org/10.1105/tpc.112.100511) PMID: [22968715](https://pubmed.ncbi.nlm.nih.gov/22968715/)
9. Han F, Lamb JC, Birchler JA (2006) High frequency of centromere inactivation resulting in stable dicentric chromosomes of maize. *Proc Natl Acad Sci U S A* 103: 3238–3243. PMID: [16492777](https://pubmed.ncbi.nlm.nih.gov/16492777/)
10. Mendiburo MJ, Padeken J, Fulop S, Schepers A, Heun P (2011) *Drosophila* CENH3 is sufficient for centromere formation. *Science* 334: 686–690. doi: [10.1126/science.1206880](https://doi.org/10.1126/science.1206880) PMID: [22053052](https://pubmed.ncbi.nlm.nih.gov/22053052/)
11. Cooper JL, Henikoff S (2004) Adaptive evolution of the histone fold domain in centromeric histones. *Molecular biology and evolution* 21: 1712–1718. PMID: [15175412](https://pubmed.ncbi.nlm.nih.gov/15175412/)
12. Malik HS, Henikoff S (2001) Adaptive evolution of Cid, a centromere-specific histone in *Drosophila*. *Genetics* 157: 1293–1298. PMID: [11238413](https://pubmed.ncbi.nlm.nih.gov/11238413/)
13. Henikoff S, Ahmad K, Malik HS (2001) The centromere paradox: stable inheritance with rapidly evolving DNA. *Science (New York, NY)* 293: 1098–1102. PMID: [11498581](https://pubmed.ncbi.nlm.nih.gov/11498581/)

14. Zwick ME, Salstrom JL, Langley CH (1999) Genetic variation in rates of nondisjunction: association of two naturally occurring polymorphisms in the chromokinesin nod with increased rates of nondisjunction in *Drosophila melanogaster*. *Genetics* 152: 1605–1614. PMID: [10430586](#)
15. Dawe RK, Hiatt EN (2004) Plant neocentromeres: fast, focused, and driven. *Chromosome Res* 12: 655–669. PMID: [15289670](#)
16. Fishman L, Saunders A (2008) Centromere-associated female meiotic drive entails male fitness costs in monkeyflowers. *Science (New York, NY)* 322: 1559–1562. doi: [10.1126/science.1161406](#) PMID: [19056989](#)
17. Blower MD, Karpen GH (2001) The role of *Drosophila* CID in kinetochore formation, cell-cycle progression and heterochromatin interactions. *Nat Cell Biol* 3: 730–739. PMID: [11483958](#)
18. Wieland G, Orthaus S, Ohndorf S, Diekmann S, Hemmerich P (2004) Functional Complementation of Human Centromere Protein A (CENP-A) by Cse4p from *Saccharomyces cerevisiae*. *Molecular and cellular Biology* 24: 6620–6630. PMID: [15254229](#)
19. Round EK, Flowers SK, Richards EJ (1997) *Arabidopsis thaliana* centromere regions: genetic map positions and repetitive DNA structure. *Genome Res* 7: 1045–1053. PMID: [9371740](#)
20. Ravi M, Chan SW (2010) Haploid plants produced by centromere-mediated genome elimination. *Nature* 464: 615–618. doi: [10.1038/nature08842](#) PMID: [20336146](#)
21. Ravi M, Kwong PN, Menorca RM, Valencia JT, Ramahi JS, et al. (2010) The rapidly evolving centromere-specific histone has stringent functional requirements in *Arabidopsis thaliana*. *Genetics* 186: 461–471. doi: [10.1534/genetics.110.120337](#) PMID: [20628040](#)
22. Franzke A, Lysak MA, Al-Shehbaz IA, Koch MA, Mummenhoff K (2011) Cabbage family affairs: the evolutionary history of Brassicaceae. *Trends Plant Sci* 16: 108–116. doi: [10.1016/j.tplants.2010.11.005](#) PMID: [21177137](#)
23. Henry IM, Dilkes BP, Miller ES, Burkart-Waco D, Comai L (2010) Phenotypic consequences of aneuploidy in *Arabidopsis thaliana*. *Genetics* 186: 1231–1245. doi: [10.1534/genetics.110.121079](#) PMID: [20876566](#)
24. Chen G, Rubinstein B, Li R (2012) Whole chromosome aneuploidy: big mutations drive adaptation by phenotypic leap. *BioEssays: news and reviews in molecular, cellular and developmental biology* 34: 893–900. doi: [10.1002/bies.201200069](#) PMID: [22926916](#)
25. Wang H, Moore MJ, Soltis PS, Bell CD, Brockington SF, et al. (2009) Rosid radiation and the rapid rise of angiosperm-dominated forests. *Proceedings of the National Academy of Sciences of the United States of America* 106: 3853–3858. doi: [10.1073/pnas.0813376106](#) PMID: [19223592](#)
26. Malik HS, Vermaak D, Henikoff S (2002) Recurrent evolution of DNA-binding motifs in the *Drosophila* centromeric histone. *Proc Natl Acad Sci U S A* 99: 1449–1454. PMID: [11805302](#)
27. Wisniewski J, Hajj B, Chen J, Mizuguchi G, Xiao H, et al. (2014) Imaging the fate of histone Cse4 reveals de novo replacement in S phase and subsequent stable residence at centromeres. *eLife* 3: e02203. doi: [10.7554/eLife.02203](#) PMID: [24844245](#)
28. Malik HS, Henikoff S (2009) Major evolutionary transitions in centromere complexity. *Cell* 138: 1067–1082. doi: [10.1016/j.cell.2009.08.036](#) PMID: [19766562](#)
29. Westermann S, Schleiffer A (2013) Family matters: structural and functional conservation of centromere-associated proteins from yeast to humans. *Trends Cell Biol* 23: 260–269. doi: [10.1016/j.tcb.2013.01.010](#) PMID: [23481674](#)
30. Dubin M, Fuchs J, Graf R, Schubert I, Nellen W (2010) Dynamics of a novel centromeric histone variant CenH3 reveals the evolutionary ancestral timing of centromere biogenesis. *Nucleic Acids Res* 38: 7526–7537. doi: [10.1093/nar/gkq664](#) PMID: [20675719](#)
31. Vermaak D, Hayden HS, Henikoff S (2002) Centromere Targeting Element within the Histone Fold Domain of Cid. 22: 7553–7561. PMID: [12370302](#)
32. Moraes IC, Lermontova I, Schubert I (2011) Recognition of *A. thaliana* centromeres by heterologous CENH3 requires high similarity to the endogenous protein. *Plant Mol Biol* 75: 253–261. doi: [10.1007/s11103-010-9723-3](#) PMID: [21190064](#)
33. Baker RE, Rogers K (2006) Phylogenetic analysis of fungal centromere H3 proteins. *Genetics* 174: 1481–1492. PMID: [17028330](#)
34. Meraldi P, McAinsh AD, Rheinbay E, Sorger PK (2006) Phylogenetic and structural analysis of centromeric DNA and kinetochore proteins. *Genome Biol* 7: R23. PMID: [16563186](#)
35. Henry IM, Dilkes BP, Tyagi AP, Lin HY, Comai L (2009) Dosage and parent-of-origin effects shaping aneuploid swarms in *A. thaliana*. *Heredity (Edinb)* 103: 458–468. doi: [10.1038/hdy.2009.81](#) PMID: [19603060](#)

36. Meyers LA, Levin DA (2006) ON THE ABUNDANCE OF POLYPLOIDS IN FLOWERING PLANTS. *Evolution* 60: 1198–1206. PMID: [16892970](#)
37. Ramsey J, Schemske DW (2002) NEOPOLYPLOIDY IN FLOWERING PLANTS. *Annual Review of Ecology and Systematics* 33: 589–639.
38. Houben A, Sanei M, Pickering R (2011) Barley doubled-haploid production by uniparental chromosome elimination. *Plant Cell, Tissue and Organ Culture (PCTOC)* 104: 321–327.
39. Gernand D, Rutten T, Varshney A, Rubtsova M, Prodanovic S, et al. (2005) Uniparental chromosome elimination at mitosis and interphase in wheat and pearl millet crosses involves micronucleus formation, progressive heterochromatinization, and DNA fragmentation. *Plant Cell* 17: 2431–2438. PMID: [16055632](#)
40. Ishii T, Ueda T, Tanaka H, Tsujimoto H (2010) Chromosome elimination by wide hybridization between Triticeae or oat plant and pearl millet: pearl millet chromosome dynamics in hybrid embryo cells. *Chromosome Res* 18: 821–831. doi: [10.1007/s10577-010-9158-3](#) PMID: [20953694](#)
41. Sanei M, Pickering R, Kumke K, Nasuda S, Houben A (2011) Loss of centromeric histone H3 (CENH3) from centromeres precedes uniparental chromosome elimination in interspecific barley hybrids. *Proc Natl Acad Sci U S A* 108: E498–505. doi: [10.1073/pnas.1103190108](#) PMID: [21746892](#)
42. Yona AH, Manor YS, Herbst RH, Romano GH, Mitchell A, et al. (2012) Chromosomal duplication is a transient evolutionary solution to stress. *Proceedings of the National Academy of Sciences* 109: 21010–21015. doi: [10.1073/pnas.1211150109](#) PMID: [23197825](#)
43. Chen G, Bradford WD, Seidel CW, Li R (2012) Hsp90 stress potentiates rapid cellular adaptation through induction of aneuploidy. *Nature* 482: 246–250. doi: [10.1038/nature10795](#) PMID: [22286062](#)
44. Black BE, Jansen LET, Maddox PS, Foltz DR, Desai AB, et al. (2007) Centromere identity maintained by nucleosomes assembled with histone H3 containing the CENP-A targeting domain. *Molecular cell* 25: 309–322. PMID: [17244537](#)
45. Ross BD, Rosin L, Thomae AW, Hiatt MA, Vermaak D, et al. (2013) Stepwise evolution of essential centromere function in a *Drosophila* neogene. *Science (New York, NY)* 340: 1211–1214. doi: [10.1126/science.1234393](#) PMID: [23744945](#)
46. Peterson R, Slovin JP, Chen C (2010) A simplified method for differential staining of aborted and non-aborted pollen grains. *International Journal of Plant Biology* 1.
47. Ross KJ, Fransz P, Jones GH (1996) A light microscopic atlas of meiosis in *Arabidopsis thaliana*. *Chromosome Res* 4: 507–516. PMID: [8939362](#)
48. Henry IM, Dilkes BP, Young K, Watson B, Wu H, et al. (2005) Aneuploidy and genetic variation in the *Arabidopsis thaliana* triploid response. *Genetics* 170: 1979–1988. PMID: [15944363](#)
49. Edgar RC (2004) MUSCLE: multiple sequence alignment with high accuracy and high throughput. *Nucleic Acids Res* 32: 1792–1797. PMID: [15034147](#)
50. Tamura K, Stecher G, Peterson D, Filipinski A, Kumar S (2013) MEGA6: Molecular Evolutionary Genetics Analysis version 6.0. *Mol Biol Evol* 30: 2725–2729. doi: [10.1093/molbev/mst197](#) PMID: [24132122](#)
51. Bailey TL, Elkan C (1994) Fitting a mixture model by expectation maximization to discover motifs in biopolymers. *Proc Int Conf Intell Syst Mol Biol* 2: 28–36. PMID: [7584402](#)
52. Jones DT, Taylor WR, Thornton JM (1992) The rapid generation of mutation data matrices from protein sequences. *Comput Appl Biosci* 8: 275–282. PMID: [1633570](#)